

Molecular Recognition in Water Using Macrocyclic Synthetic Receptors

Luis Escobar and Pablo Ballester*

Cite This: *Chem. Rev.* 2021, 121, 2445–2514

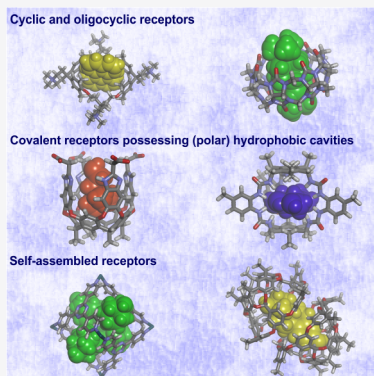
Read Online

ACCESS |

Metrics & More

Article Recommendations

ABSTRACT: Molecular recognition in water using macrocyclic synthetic receptors constitutes a vibrant and timely research area of supramolecular chemistry. Pioneering examples on the topic date back to the 1980s. The investigated model systems and the results derived from them are key for furthering our understanding of the remarkable properties exhibited by proteins: high binding affinity, superior binding selectivity, and extreme catalytic performance. Dissecting the different effects contributing to the proteins' properties is severely limited owing to its complex nature. Molecular recognition in water is also involved in other appreciated areas such as self-assembly, drug discovery, and supramolecular catalysis. The development of all these research areas entails a deep understanding of the molecular recognition events occurring in aqueous media. In this review, we cover the past three decades of molecular recognition studies of neutral and charged, polar and nonpolar organic substrates and ions using selected artificial receptors soluble in water. We briefly discuss the intermolecular forces involved in the reversible binding of the substrates, as well as the hydrophobic and Hofmeister effects operating in aqueous solution. We examine, from an interdisciplinary perspective, the design and development of effective water-soluble synthetic receptors based on cyclic, oligo-cyclic, and concave-shaped architectures. We also include selected examples of self-assembled water-soluble synthetic receptors. The catalytic performance of some of the presented receptors is also described. The latter process also deals with molecular recognition and energetic stabilization, but instead of binding ground-state species, the targets become elusive counterparts: transition states and other high-energy intermediates.



CONTENTS

1. Introduction	2445
2. Electrostatic and Dispersion Intermolecular Interactions	2447
2.1. Hydrophobic Effect	2449
2.2. Hofmeister Effect	2451
3. Cyclic and Oligocyclic Covalent Receptors Featuring a Hydrophobic Cavity	2452
3.1. Cyclophanes	2452
3.2. Pillar[n]arenes	2459
3.3. Cucurbit[n]urils	2463
3.4. Bambus[6]urils	2469
4. Covalent Receptors Possessing a Concave Hydrophobic Cavity	2470
4.1. Calix[n]arenes	2470
4.2. Resorcin[4]arenes	2474
5. Covalent Receptors Possessing a Polar Hydrophobic Cavity	2481
5.1. Temple Receptors	2482
5.2. Naphthotubes	2485
5.3. Calix[4]pyrroles	2488
6. Self-Assembled Water-Soluble Receptors	2492
6.1. Metal Coordination Cages	2492

6.2. Noncovalent Capsules	2499
7. Comparison of the Binding Properties of Different Macrocycles with Some Selected Guests	2501
8. Overview and Outlook	2504
Author Information	2505
Corresponding Author	2505
Author	2505
Notes	2505
Biographies	2505
Acknowledgments	2505
References	2505

1. INTRODUCTION

Molecular recognition in water using macrocyclic synthetic receptors constitutes a research area that can be traced back to

Received: May 27, 2020

Published: January 20, 2021



the early 1980s. The investigated model systems and the results derived from them provided answers to our understanding of the large values observed for proteins' binding affinity, selectivity, and catalytic performance.^{1,2} Nevertheless, the aim of these investigations was and still is the desire to fully understand noncovalent interactions in water, both in ground-state (molecular recognition) and transition-state (catalysis) complexes.

Protein binding pockets are constructed by aliphatic and/or aromatic groups of amino acid residues, which build up a hydrophobic environment having cleft or cavity-like shape. The polar and charged groups of other amino acid residues are buried in these proteins' hydrophobic cavities. This arrangement minimizes the solvation of the latter with water molecules of the bulk solution. The solvation of polar groups with a discrete number of water molecules seems to be key for their involvement in supramolecular functions like molecular recognition, reactivity modulation, and reaction catalysis.³ The use of synthetic receptors in molecular recognition studies in water overcomes some limitations encountered in the direct study of biological counterparts. For example, the study of the binding processes by spectroscopic techniques becomes simplified and can be performed in a wider range of temperatures to allow a detailed thermodynamic analysis of complexation.⁴

Molecular recognition in water is also appreciated in areas of research not directly involving synthetic receptors, such as molecular self-assembly, drug discovery, and supramolecular catalysis taking place also in water. Furthermore, the applications of water-soluble supramolecular systems in nanotechnology and biomedicine¹ are realizing the importance of understanding the noncovalent interactions at play and in particular the role exerted by the hydrophobic effect (HE).

The physical and chemical properties of water^{5–10} offer both opportunities and challenges for molecular recognition. The free energy gain that produces the formation of stable host–guest complexes in water results from the contribution of two main components: First, the favorable and newly formed intermolecular interactions established between host and guest upon complex formation. This component is akin to gas phase binding. Second are the advantageous intermolecular interactions of the interfacial water molecules solvating the complex compared to those for the separate binding partners. The second energy component is referred as the HE.¹¹ The different intermolecular interactions involved in the two energy components share in common their electrostatic (*e.g.*, hydrogen bonds) and dispersive (van der Waals, London forces, *etc.*) origins. The HE is important in regulating binding affinity, especially for binding sites with nonpolar cavities and/or substrates having hydrophobic residues. On the other hand, the intermolecular interactions between host and guest that are established in the complex, especially the ones that are electrostatic in nature, play important roles in dictating binding selectivity and complex geometry.¹² The thermodynamic characterization and the physical nature of the noncovalent intermolecular forces driving complexation both in solution and in the gas phase will be discussed in some detail in section 2. In this section, we include two subsections to briefly discuss the properties of the HE and the Hofmeister effect, aka the salting effect. Both phenomena are strongly rooted on energy differences of noncovalent interactions established by the interfacial layer of solvating water molecules in different states of a binding system.

The solvation of ions and neutral molecules depends on the properties of liquid water.^{8,9} Ions are strongly solvated by water molecules. Cations are solvated through cation–dipole interactions involving the electron density of the lone pairs of the oxygen atom of water, whereas anions interact with the partially positively charged hydrogen atoms of water molecules. As a result, the charge of the ions is significantly screened by the aqueous medium.¹⁰ Water also interacts with polar neutral molecules by establishing a network of hydrogen bonds. In contrast, nonpolar molecules are poorly solvated and tend to aggregate.

Synthetic molecular receptors must meet common requirements to efficiently bind molecules and ions in water.¹³ The receptors must be soluble in water at concentrations that allow spectroscopic and/or calorimetric studies. This limits the number of building blocks available for their syntheses. In general, ionizable or charged groups are incorporated at the periphery of the receptor's scaffold to ensure water solubility and prevent aggregation.¹⁴ The architecture of the receptor must be relatively rigid, from a conformational point of view, in order to avoid the hydrophobic collapse of the binding pocket, which translates into the loss of binding properties. The binding site of the receptor must be complementary in terms of size, shape, and function to the substrate characteristics in order to ensure optimal intermolecular interactions, high affinity, and selectivity.¹⁵ The fulfillment of these requirements demands special considerations when polar groups are involved. The binding event must also compensate the high dielectric constant ($\epsilon = 78.5$ at 278 K) and the strong hydrogen-bonding ability of water. The main features of synthetic and biological receptors (*i.e.*, proteins) are summarized in Table 1.¹⁶

Table 1. Main Features of Discrete, Synthetic Receptors, and Globular Natural Proteins

	synthetic receptors	proteins
building blocks	aromatic/aliphatic and heterocyclic scaffolds	amino acids
challenges	water solubility, preorganization	geometry (angles/vertices)
typical length dimensions	1–10 nm	10–100 nm
cavity environment	hydrophobic WPFG ^a	hydrophobic WPFG ^a

^aHydrophobic with/without polar functional groups.

Molecules may exhibit unusual chemical and physical properties when confined in small spaces. In water, the modification of chemical reactivity of guests bound in well-defined, hydrophobic cavities of synthetic receptors has been amply demonstrated.^{17,18} Therefore, synthetic receptors might mimic enzymatic cavities and function as molecular vessels to perform chemical reactions.

The accuracy of theoretical calculations in predicting binding affinity values of small molecular weight molecules to biological receptors is of great interest for rational drug design and fast hit-to-lead optimization. However, biological systems pose multiple challenges (slow binding dynamics, ionization changes, *etc.*), limiting a direct comparison of experimental data to the theoretical estimates. The water-soluble host–guest systems developed by the groups of Isaacs (section 3.3) and Gibb (section 4.2) have emerged as a practical and effective alternative providing experimental

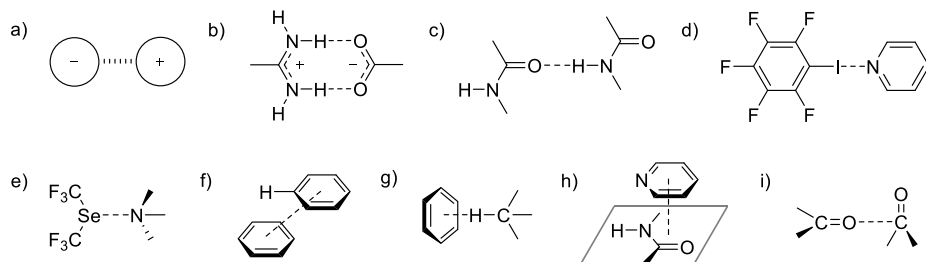


Figure 1. Examples of intermolecular interactions: (a) ion-pairing, (b) salt-bridge, (c) hydrogen bond, (d) halogen bond, (e) chalcogen bond, (f) offset stacked π - π , (g) CH- π , (h) amide- π , and (i) orthogonal C=O...C=O.

binding data for comparing and benchmarking different theoretical methods within the series of blind predictive challenges of the Statistical Assessment of Modeling of Proteins and Ligands (SAMPL) exercise.^{19,20}

Unfortunately, the agreement between the experimentally determined kinetic and thermodynamic data for the complexation processes involving synthetic receptors in water with those obtained from quantum chemical methods or molecular dynamic calculations is, to say the least, suboptimal.^{6,19–21} This fact is somewhat surprising owing to the huge development experienced in the last decades in computational methods and hardware. Nevertheless, this limitation is a clear indication of the difficulties encountered in modeling binding processes in water, which relate to the important role played by the solvent molecules in the solvation/desolvation processes that are concomitant to the binding event.^{11,22,23}

We are aware of the difficulties encountered in calculating accurate energy minimized structures for the supramolecular complexes formed in water, as well as the limitations associated with related calculations performed in the gas phase. Thus, the energy minimized structures (MM3) of the simplified/pruned supramolecular complexes that are included throughout the review simply aim at illustrating its three-dimensional nature and the existence of a size and shape complementarity between host and guest. We consider that the provided representation offers a superior visualization of the complexes than the corresponding line-drawing structures. We refrain to disclose energy values or draw conclusions in relation to their thermodynamic stabilities. We know that the provided structures might not correspond exactly with those calculated in solution using either first-principles or MD empirical calculations. Nevertheless, we consider them to be illustrative of reality.

In this review, we overview the past three decades of molecular recognition studies in water using macrocyclic synthetic receptors. We restrain ourselves to the use of discrete and homogeneous synthetic receptors and the complexation of polar and nonpolar organic molecules, as well as small ions. We briefly comment on the nature and strength of the intermolecular forces (section 2) driving the reversible formation of host–guest complexes in gas phase and in solution. We mention the hydrophobic (section 2.1) and Hofmeister effects (section 2.2) owing to their important roles in nonpolar binding in water solution. Both effects are based on energy differences between intermolecular interactions. Recently, the topics mentioned in sections 2.1 and 2.2 were covered in more detail in the book “Supramolecular Chemistry in Water”, edited by Kubik, and we refer the readers to the corresponding chapter.¹¹ We review the developments achieved in the design of effective receptors in water, using

cyclic, oligocyclic, and concave-shaped unimolecular architectures (covalent receptors) (sections 3–5). Self-assembled water-soluble receptors (section 6), *i.e.*, metal coordination cages and noncovalent capsules, are also mentioned. We highlight selected examples of synthetic hosts capable of mediating/catalyzing chemical transformations. We are aware that we have not included all relevant examples, and we want to apologize to the authors for our biased selection. Noncyclic (clips and tweezers), planar (porphyrins), and boronic acid-based receptors are out of the scope of this review, and the reader is addressed to other literature references that cover the topics.^{4,13,15,24–26} Likewise, we will not dwell in synthetic water-soluble receptors based exclusively on molecular units derived from nature, *i.e.*, saccharides for cyclodextrins^{13,27,28} and amino acids for cyclopeptides.^{13,29} However, we will briefly mention cyclodextrins by comparing their binding affinities with those of the synthetic receptors explicitly described in the text.

2. ELECTROSTATIC AND DISPERSION INTERMOLECULAR INTERACTIONS

The magnitude of the binding constants determined for 1:1 complexes of synthetic receptors in water lies in the range of 1–10¹⁷ M⁻¹.³ The binding affinity values are typically enhanced by increasing the nonpolar contacts (*i.e.*, number and surface area) between the cavity and the bound guest. Moreover, the combination of additional host–guest intermolecular interactions¹⁰ with those inducing the hydrophobic effect has evolved as a sensible approach in the design of synthetic receptors able to efficiently bind polar substrates in water solution^{30,31} (see section 5).

The nature of the intermolecular interactions can be mainly electrostatic, meaning that their establishment does not require a reorganization of charges or electron density in the interacting atoms or molecules. Alternatively, intermolecular interactions may have a significant dispersive character, which do require a temporary reorganization of at least one of the electron densities of the interacting partners. Polarizability greatly influences dispersive interactions. In any case, the dissection of intermolecular interactions in their electrostatic and dispersive terms is not trivial, neither from an experimental nor a theoretical approximation.

Different binding motifs or intermolecular forces work synergistically in the establishment of a host–guest complex in order to produce high levels of affinity and selectivity.^{32,33} Owing to the reduced polarizability of water, dispersion forces are supposed to be more important between two organic substrates forming a complex than in the separate water-solvated counterparts.³⁴ However, this dogma has been recently challenged in the case of “soft” liquid–vapor like

interfaces of water molecules. These are the type of interfaces present in the first water solvation layer of large molecules (see Hydrophobic Effect in section 2.1).

Coulombic or ionic interactions are one type of electrostatic forces. They relate to the attractive or repulsive interaction established between two charged species (charge–charge) (Figure 1a). Because of the high dielectric constant of water and its superior abilities for charge solvation (charge–dipole interaction), ion-pairing of ions featuring large ionic charge density tends to be quite weak in this solvent (*i.e.*, just considering the ϵ value of water, the interaction between two oppositely monocharged particles is 1% of that in the gas phase). A salt-bridge is defined by a combination of two interactions: hydrogen-bonding reinforced with ionic-bonding (Figure 1b). The free energy of a water-solvated salt-bridge was estimated to be *ca.* 4.2 kJ·mol⁻¹.³⁵ In water, a salt-bridge or ion-pair interaction is mainly driven by entropy ($\Delta S > 0$) and opposed by enthalpy ($\Delta H > 0$).³⁶ This interaction type was successfully applied by Schmuck in the binding of oxoanions (*e.g.*, carboxylates, phosphates, *etc.*) in water using acyclic acyl guanidinium receptors.^{4,10,37}

As additional example of the above, the complexation of anions and anionic molecules in water using synthetic receptors was first approached by the use of positively charged receptors (ionic interaction). For example, Schmidtchen *et al.* reported tetrahedral hosts bearing quaternary ammonium groups at their vertices for the recognition of halide anions.^{38,39} The host's counteranions were properly selected (large and polarizable) in order to minimize interferences with the binding of the targeted anionic guest.^{40,41}

Unfortunately, positively charged anion receptors tend to be poorly selective because they rely mainly on ionic interactions, which are nondirectional. The inclusion of hydrogen bond donor groups in the cationic scaffolds of the anion receptors improved their selectivity. More recently, Kubik *et al.* reported neutral receptors (cyclopeptides) exclusively based on hydrogen-bonding interactions in order to overcome the limitations of charged hosts.^{29,42}

However, complexes stabilized exclusively by solvent-exposed hydrogen-bonding interactions display a reduced thermodynamic stability in water owing to the competitive hydrogen-bonding nature of the latter (Figure 1c). Therefore, the efficient formation of hydrogen-bonding complexes in water requires the protection of the polar groups in deep and hydrophobic binding sites that limit the access of bulk water molecules⁴³ (see section 5). Hydrophobic concave binding pockets can be obtained by designing unimolecular receptors, *i.e.* cavitands (see section 4), or by self-assembly processes of multiple copies of nonpolar molecules, *i.e.* metallo-cages and hydrogen-bonded capsules (see section 6). The extensive use of aromatic panels in shaping the hydrophobic and concave cavities of the receptors creates difficulties for the placement of converging polar groups in them. In nature, polar peptide residues converge in the hydrophobic interior of the protein binding sites and are able to establish efficient hydrogen-bonding interactions with the bound substrates.^{32,33}

In contrast to hydrogen bonds, halogen bonds (XB) are not significantly affected by solvent polarity.⁴ This characteristic hints to the existence of additional forces than electrostatics in their formation (*i.e.*, dispersive, charge-transfer, *etc.*). However, halogen bonds are relatively weak in both polar and nonpolar solvents (Figure 1d). The XB donor contains a halogen atom featuring an electrophilic region (σ -hole), whereas the XB

acceptor is an electron-donating group in another or the same molecule. The strength of a XB depends on the properties of both binding partners. For example, iodinated compounds form stronger halogen bonds than brominated counterparts, and those are better than chlorinated derivatives. Additionally, electron-withdrawing substituents on the XB donor increases the σ -hole potential, reinforcing the halogen-bonding interaction. Likewise, electron-donating groups in the XB acceptor assist the thermodynamic stabilization of the halogen bond. Formation of efficient halogen bonds requires an angle close to linearity (165–180°) along the R–X···A interactions. The XB donor–acceptor distance in a strong interaction is below the sum of the van der Waals radii of the atoms involved. Halogen-bonding interactions are driven by enthalpy and opposed by entropy.⁴⁴

In analogy to halogen-bonding interactions, chalcogen bonding is defined as the interaction between a nucleophile (lone-pair), such as an oxygen or nitrogen atom, and an electron-deficient chalcogen atom (σ -hole), such as sulfur, selenium, or tellurium (Figure 1e). Chalcogen bonds are directional, *i.e.*, they require angles close to 180°, and are not significantly affected by solvent polarity.^{45,46}

Aromatic interactions are widely encountered in nature.^{47,48} Cations are attracted by aromatic rings due to the negative electrostatic potential of the π -surface of the planar aromatic component.⁴⁹ The cation– π interaction (see section 3.1) can contribute to enhance the free energy of binding in more than 8.4 kJ·mol⁻¹, both in synthetic and natural complexes.⁴ For example, *ca.* 25% of L-tryptophan amino acids in nature establish cation– π interactions with positively charged L-arginine or L-lysine residues. The cation– π interaction is formed primarily by an electrostatic component, even though dispersion interactions might be also involved.⁵⁰

On the contrary, anion– π interactions are usually repulsive owing to the unfavorable interaction of the negatively charged ion and the π -electron cloud of the aromatic ring. Attractive anion– π interactions can be established when the aromatic component features a positive quadrupole or is polarizable. For example, the free energy of anion– π interactions was quantified to be *ca.* 10 kJ·mol⁻¹ in the binding of oxoanions (*e.g.*, sulfate and selenate) with a nitroso-amine-pyrimidine receptor in water solution, containing 0.1 M ammonium chloride.⁵¹ In this particular example, the anion– π interaction was entropically favorable, probably due to the required water desolvation of the nonpolar aromatic surface and the anion on complex formation. Examples of enthalpically driven anion– π interactions were reported, but they involved the use of organic solvents.⁵²

Aromatic π – π stacking and CH– π interactions have both electrostatic and dispersion contributions.³⁴ On the one hand, the binding geometry of two aromatic groups can be edge-to-face, offset stacked, or face–face stacked⁴⁴ (Figure 1f). On the other hand, CH– π interactions are directional, featuring an angle between 140° and 180° (center ring···H–C) and a distance of 2.3–2.9 Å. The strength of the CH– π interaction increases with the acidity of the CH bond and the increase in the electron density of the aromatic ring⁴ (Figure 1g). In general, CH– π interactions contribute less than 10.5 kJ·mol⁻¹ to the binding free energy.⁵³ These interactions are particularly interesting in carbohydrate binding,^{54,55} in which the association constants of the complexes between monosaccharides and proteins are in the order of 10³–10⁴ M⁻¹ (three CH groups face the aromatic ring).⁵⁶

Amide groups are widely present in nature, and they form the backbone of proteins. They establish $\pi-\pi$ and NH– π interactions with aromatic groups. Interestingly, the $\pi-\pi$ binding geometry between amides and aromatic heterocycles involves the antiparallel alignment of their dipole moments⁴⁴ (Figure 1h). Furthermore, the oxygen atom of the carbonyl group of amides can be involved in hydrogen bonds with hydroxyl groups, among other hydrogen bond donors, in water.⁵⁷ Most likely, the NHCO···HO interaction is mainly driven by entropy due to the desolvation of the binding polar groups. Other heteroatoms, such as sulfur, interact favorably with π -systems through dispersion interactions. The sulfur– π interaction accounts for up to 2.1 kJ·mol⁻¹ in the stability of folded proteins.³⁴

Finally, orthogonal dipolar interactions, such as C=O···C=O and C–X···C=O (C=O/X···C=O, 90° angle), were involved in the stabilization of protein's secondary structure⁴⁴ (Figure 1i). These interaction modes can be considered as examples of the currently fashionable π -hole bonding.⁵⁸

2.1. Hydrophobic Effect

The hydrophobic effect (HE) is mainly present in nonpolar binding processes occurring in water, such as protein folding, ligand–protein complex formation, and membrane self-assembly, as well as in those involving synthetic host–guest and self-assembly systems.^{59,60} Although the basic properties defining the HE are qualitatively understood, there are many features of this ubiquitous phenomenon that remain to be fully explained and quantified.^{11,61} The HE favors apolar binding (aggregation) and results from the free energy difference between: (1) the combination of the strong hydrogen-bonding of the water molecules in the solvating layer, the weak dispersion interactions that they establish with the aggregating nonpolar molecules and other noncovalent forces present in the aggregate, versus (2) the weaker hydrogen-bonding and dispersion interactions of the interfacial water molecules solvating the separate free species (*vide infra*). Thus, the HE should not be considered a separate intermolecular interaction (see above for a classification of intermolecular interactions) but a consequence of the energy difference in the intermolecular interactions established during the water solvation of the free and the aggregated species. Compared to polar and protic organic solvents, water has the highest cohesive intermolecular interactions (stronger hydrogen bonds) and possesses the lowest molecular polarizability. Taken together, these two effects make water the best solvent to promote apolar complexation, however, not beyond the expected level based on its physical properties.^{62,63}

The first attempt of a detailed theory explaining the low affinity of nonpolar groups for water was provided by Frank and Evans.⁶⁴ The authors described the clustering of water molecules into microscopic “icebergs” around nonpolar molecules and discussed the entropic consequences of the arrangements. A few years later, Kauzmann coined the term “hydrophobic bonding” to describe the water-mediated process that induces the spontaneous tendency to aggregation of nonpolar groups of proteins in order to minimize their exposed surface area.⁶⁵ These forays into the origins of the HE revealed a perplexing aspect of the phenomenon: the strength of the interaction between the nonpolar groups seemed not to be related to their physicochemical properties but to those of the aqueous media.⁶⁶ Back then and even now, scientists are used to thinking that interactions between residues and groups are

due to their own physicochemical properties rather than those established with the solvent medium. However, and as mentioned above, the cohesive nature of the intermolecular interactions of water molecules is believed to be the main one responsible for the HE. In addition, as pointed out by Chandler,⁶¹ the dispersion interactions established between the solutes and the water molecules of the interfacial layer,^{3,14} which were considered not to be very important owing to the reduced polarizability of water molecules, are gaining considerable importance in recent years. The HE provides an impetus to nonpolar binding in water but lacks of specific and directional characteristics.¹⁰ Studies on simple synthetic models are necessary to further gain understanding of the HE operating in more complex synthetic systems and in biology.⁶ Hydrophobicity is a multifaceted phenomenon that reveals different characteristics depending on the solutes' size, shape, and strength of the direct attractive interactions established between them.⁶¹ Water-mediated hydrophobic interactions are directly linked to hydrophobic hydration.⁶⁷ To a first approximation, the free energy for assembling a hydrophobic complex in water is the difference between the hydration free energy of each component in their free state and the hydration free energy of the assembled state.

Chandler pointed out that the physics that govern hydrophobicity at macroscopic and molecular size scales are fundamentally different.⁶¹ At the molecular scale, the hydration of a large solute or aggregate (>1 nm of girth) makes it impossible for adjacent water molecules to maintain a complete hydrogen-bonding network as those in the bulk. In response to this loss of hydrogen bonds, water molecules tend to move away from the large solute and form an interface akin to that between liquid and vapor. In this case, the solute is said to be “dry” or “dewetted”, and the density of the water interface is reduced compared to that of the bulk.

On the contrary, for small hydrophobic solutes, the water density immediately adjacent to the solute's surface is larger than that of the bulk. Solvating water molecules adopt a similar hydrogen-bonding pattern than that of the liquid but experiencing significant reordering. Under these circumstances, the small solute is said to be “wet”. The consideration on water solvation based on solutes' size adds to the growing evidence indicating that the HE only becomes significant if the nonpolar area buried in the complex or aggregate is larger than ~1 nm².

On the basis of all the above, the tendency of hydrophobic aggregation can be traced down, to a first instance, to the dependence of hydrophobic solvation on solute's size. Thus, when small solutes aggregate to form a hydrophobic unit with a volume to surface ratio large enough, the overall free energy of the aggregate's solvation might be lower than that of the individual solutes. This effect constitutes a favorable driving force for aggregation.

The driving forces of hydrophobic aggregation increase with temperature. This observation is used to imply that the process is entropically driven. However, in reality and as indicated by Chandler, the process is driven by the difference in free energies of the entropically dominated solvation of small molecules and the enthalpically controlled hydration of larger ones.⁶¹ It is worth mentioning here, as already anticipated above, that dispersion (van der Waals and London forces), being negligible on the structure of dense fluids, might become rather important in “soft” liquid–vapor like interfaces of water molecules. As briefly mentioned above, hydrophobic interactions can be driven either by entropy, enthalpy, or both. A

temperature-dependent enthalpy–entropy crossover has been observed in the hydration processes of nonpolar solutes as well as in protein folding and binding processes in water.

At ambient temperature, an increase in entropy and a reduced or nonexistent enthalpy gain are distinctive attributes associated with binding processes driven by the so-called “classical” HE. This thermodynamic signature is related to water desolvation of small nonpolar surfaces and concomitant assembly of aggregates with poorly defined structures in terms of size (polydisperse aggregates) and/or binding geometry. On the contrary, the so-called “nonclassical” HE is associated with an enthalpically driven binding process (see examples by Diederich *et al.* and Dougherty *et al.* in section 3.1). Also in this regard, the presence of “high-energy” water molecules in the cucurbit[*n*]uril’s cavity (see section 3.3) has been used as an alternative concept to explain the high enthalpic contribution observed in the hydrophobic host–guest binding processes.^{68,69} In literature, the term “high-energy” has been used indistinctly to refer to the free energy or to the enthalpy component of the water molecules included in nonpolar binding sites. Nevertheless, at equilibrium, the free energies of all water molecules, either present in interfacial solvation layers or in the bulk solution are identical.⁶⁷ Thus, the thermodynamic signature of the “nonclassical” hydrophobic effect should not be assigned to nonexistent differences in free energy between interfacial and bulk water molecules. Instead, it should be explained by the gain in free energy for the intermolecular interactions of the interfacial water molecules solvating the complex, *i.e.*, favored hydrogen-bonding network and superior dispersion (van der Waals forces) compared to those for the free solvated counterparts.⁴ Also, the temperature-dependent changes of enthalpy and entropy for binding processes occurring in water reduce the utility of the classification of the event as driven by the “classical” and “nonclassical” HE.¹¹

Independently of the thermodynamic signatures of binding processes in water, if hydrophobic interactions are involved, one typically observes large changes in heat capacity with temperature. The heat capacity change for a binding process (ΔC_p^b) is a thermodynamic measure that quantifies the dependence of the enthalpy with the temperature at constant pressure (see examples of Diederich *et al.* and Dougherty *et al.* in section 3.1 and section 7). The molecular HE relies on shielding areas of nonpolar surfaces from directly interacting with water molecules. Thus, the magnitude of ΔC_p^b has been related to the amount of involved surface area, while its negative sign has been assigned to the preferential burial of nonpolar surfaces on complex formation.⁷⁰ Nevertheless, the foundation of the burial of nonpolar surfaces, which occurs on complex formation, and the water reorganization processes is not universally accepted.⁷¹ This physical interpretation of the molecular HE indirectly assigns a larger heat capacity value to the water molecules in the bulk with respect to those interacting with nonpolar surfaces. Although the magnitude of ΔC_p^b should not be used to identify the role of the HE in the binding process, its sizable temperature dependence may be considered a more convincing evidence.¹¹ With some exceptions, including cyclodextrins⁷² and cyclophanes, the effect of the temperature in the thermodynamics of the binding processes of synthetic receptors in water has not been extensively studied.⁴⁹

In water, the temperature dependence of enthalpy is typically reflected in parallel changes of entropy, owing to the almost temperature invariable magnitude of the free

energies of binding and protein folding processes in water.⁷³ This trade-off of enthalpy and entropy results in the well-known phenomenon of enthalpy–entropy compensation (EEC) effect,^{6,74} which might be simply due to the basic thermodynamic laws.⁷⁵ Although enthalpy–entropy compensation effects were assigned as a general property of weak molecular interactions, *i.e.*, $\Delta G \sim 0$,⁷⁶ they are also observed in binding processes having large free energy magnitudes, *i.e.*, protein–substrate binding or host–guest complexes in water.

The molecular basis of the different thermodynamic signatures determined for binding processes in water driven by the HE is rather complex. It combines the noncovalent interactions present in the host–guest complex with the significant reorganization of the water molecules. This reorganization is caused by the desolvation of the free components and the solvation of the resulting complex.^{77–79} The enthalpy–entropy compensation (EEC) effect is also responsible for the temperature-dependent enthalpy–entropy crossovers referred above, which is characteristic of certain folding and binding processes occurring in water.

The water desolvation energy of a solute’s surface depends not only on its size (surface and volume) (*vide supra*) but also on its shape. On the one hand, the desolvation of small convex surfaces is accompanied by favorable entropy change at room temperature. On the other hand, the desolvation of concave surfaces is associated with favorable enthalpy change.⁸ Note that concave surfaces are more hydrophobic than their flat counterparts owing to the significant reduction in the number of hydrogen bonds experienced by the included water molecule/s compared to the bulk counterparts⁷ (Figure 2).

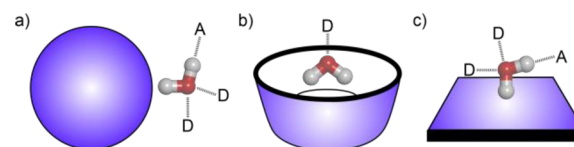


Figure 2. Surfaces of solutes being desolvated upon complexation: (a) convex, (b) concave, and (c) flat shapes. For each case, a water molecule is shown along with the hydrogen bonds to donor (D) or acceptor (A) water molecules in the solvation shell or the bulk.

Consequently, when the included water molecules are released to the bulk, in response to the complexation of a nonpolar substrate, its reorganization is expected to provide a gain in enthalpy.⁴⁰ This enthalpy gain is expected to reduce as the number of water molecules included in the cavity increases.^{44,69} This process has been related to a reduction in binding affinity. Nevertheless, differences in binding free energies should not be exclusively assigned to energy differences between interfacial and bulk water molecules.⁸⁰ Most likely, the interaction energy of the interfacial water molecules in the complex compared to that of the free substrates is also significantly modified.

It is worthy to note here that very similar nonpolar concave binding sites of synthetic cavitands, only differing in the presence and position of methyl groups encircling their open portal, showed a diverse range of water solvation.⁸⁰ Remarkably, the adequate orientation of the methyl groups induced the “drying” of the receptor’s nonpolar binding pocket. This result demonstrated that the receptor’s apolar binding site can serve to template water cavitation. It also offered an alternative to control the complexation strength of

nonpolar guests in water, which is not related to the release of water molecules included in the receptor's cavity. As the authors pointed out, whether a nonpolar binding pocket is preferentially "wet" or "dry" depends on the subtle balance between weak attractive dispersion interactions and the limited number of hydrogen bonds of the included water molecules compared with the formation of a water–air interface at the receptor's binding site. Guest complexation was enhanced in the "dry" state of the receptor owing to the lack of competition with water solvation. In any case and owing to the small size of water, the solvation of nonpolar binding pockets is better considered as a matter of extent: weakly or strongly hydrated.

As mentioned above, the term "high-energy" when referring to the water molecules included in concave nonpolar binding sites, *i.e.*, cucurbit[n]urils,^{68,69} is arguable. First, and as already stated above, the thermodynamic signature of binding events in water must not be rationalized based on nonexistent differences in *free energy* between interfacial/included water molecules and its bulk counterparts.⁶⁷ Second, as discussed in the previous paragraphs, the fact that "dry" or "weakly hydrated" nonpolar cavities exist in liquid water demonstrates that water solvation occurs only if it is energetically favorable.^{80,81} Third, water molecules included in nonpolar binding pockets are simply very bad guests and their substitution by an organic substrate might produce a free energy of binding as favorable as in the gas phase. Nevertheless, this controversy found in literature shows that additional work is needed to fully understand solvation effects.

The shape of the receptor's binding site is also very important to minimize hydrogen-bonding interactions of the included polar groups with water molecules in the bulk. *In silico* calculations of nonpolar cavities featuring a radius lower than 1 nm revealed that they are expected to be empty ("dry" or "weakly hydrated") most of the time.⁸² Nevertheless, water molecules can be found in small nonpolar cavities if polar groups able to get involved in hydrogen-bonding interactions are present. In contrast, large hydrophobic cavities lacking of polar groups are generally occupied by water molecules ("wet").⁴ Exceptions to the rule are known. Computational studies revealed the existence of large "dry" or "weakly hydrated" regions in protein binding sites.³³ Large nonpolar aromatic cavities of synthetic receptors displaying a "reduced hydration" were also recently described and mentioned above.⁸⁰ Water molecules included in aromatic cavities may be stabilized by favorable OH–π interactions. The type and arrangement of the buried functional groups need to be specially considered when designing water-soluble synthetic receptors featuring polar binding sites.^{69,83,84}

2.2. Hofmeister Effect

The addition of salts (ion-pairs) to aqueous solutions, aka salting, is known to influence solute's properties. In this sense, more than 125 years ago, the Hofmeister effect provided very early evidence on how salts influenced the solubility of solutes. For reasons that are still not entirely clear but may be related to their different modes of solvation by water molecules (see section 1), the Hofmeister effect is much more prominent with anions than with cations. Anions and cations are traditionally sorted in Hofmeister series according to their effect on "salting-out" and "salting-in" solutes, *i.e.*, increase in salt concentration induces solute precipitation and solute's solubility is increased with salt addition. The implication of the salting phenomenon is more general than solubility modulation of solutes in water.

The salting problem is also of significance in altering binding/aggregation processes occurring in water, *i.e.*, recognition between proteins, stability of their secondary and tertiary structures, phase boundaries of micellar solutions and lipid layer, affinity values for host–guest systems, *etc.*⁸

The salting phenomenon was described to be not solute-dependent, leading to the classification and ordering of anions/cations in the well-known "Hofmeister series". Even today, the mechanism of the Hofmeister effect (salting effect) is not entirely clear. The original explanations invoked changes in the structure of water. This led to the naming of some ions as kosmotropes (induce order in the structure of water) and others as chaotropes (induce disorder in the structure of water). More recent studies and theories consider alternative explanations that involve the existence of specific interactions of solutes with the anions as well as their impact on the water structure of their first or second solvation shells, but not beyond, because in water electrostatic interactions are strongly shielded.^{6,77} These findings made that within the water sciences community the terms "kosmotrope" and "chaotrope" are rapidly becoming archaic. Moreover, the terms "kosmotrope" and "chaotrope" are associated not only to the salting effect produced by the ions but also to the original and misleading explanation of the observed effect. We advocate for the use of the terms "salting-in" and "salting-out" in naming the ions properties.

"Salting-out" anions feature small sizes and high charge densities such as fluoride and sulfate. They are strongly hydrated, increase solvent surface tension, and decrease solubility of nonpolar molecules (strengthen the HE). In contrast, "salting-in" anions are large and charge-delocalized such as iodide and perchlorate. They display reduced hydration energies, are more prone to interact with other solutes and increase the solubility of nonpolar molecules in water (weaken the HE) (Figure 3).^{43,77,85}

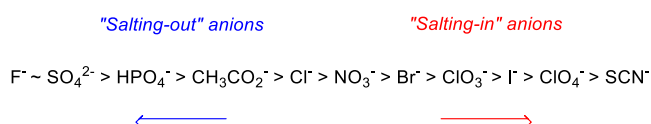


Figure 3. Hofmeister series for anions: ranking of anions to induce the precipitation of solutes from water.

Reports on the interactions of certain "salting-in" anions with hydrophobic surfaces and cavities of synthetic and natural receptors in water resulted in the coining of the term "chaotropic effect". This term was considered as a driving force being orthogonal to the HE itself. That is, the difference between the hydration free energies of the complex and the free binding partners. The "chaotropic effect" is particularly efficient for very large anions with low ionic charge density, which are not well solvated by water and extend the classical Hofmeister scale at the "salting-in" side (Figure 3). These anions are designated as "super chaotropic" species (*e.g.*, borate clusters and polyoxometalates) corresponding to "salting-in" anions displaying a diffuse charge.⁸⁵ We consider that the coining of the term "chaotropic effect" adds confusion to the already complex area of host–guest binding in water and we suggest that it should be considered simply as the "salting-in" effect exerted by anions featuring a large charge diffusion owing to its extended surface.

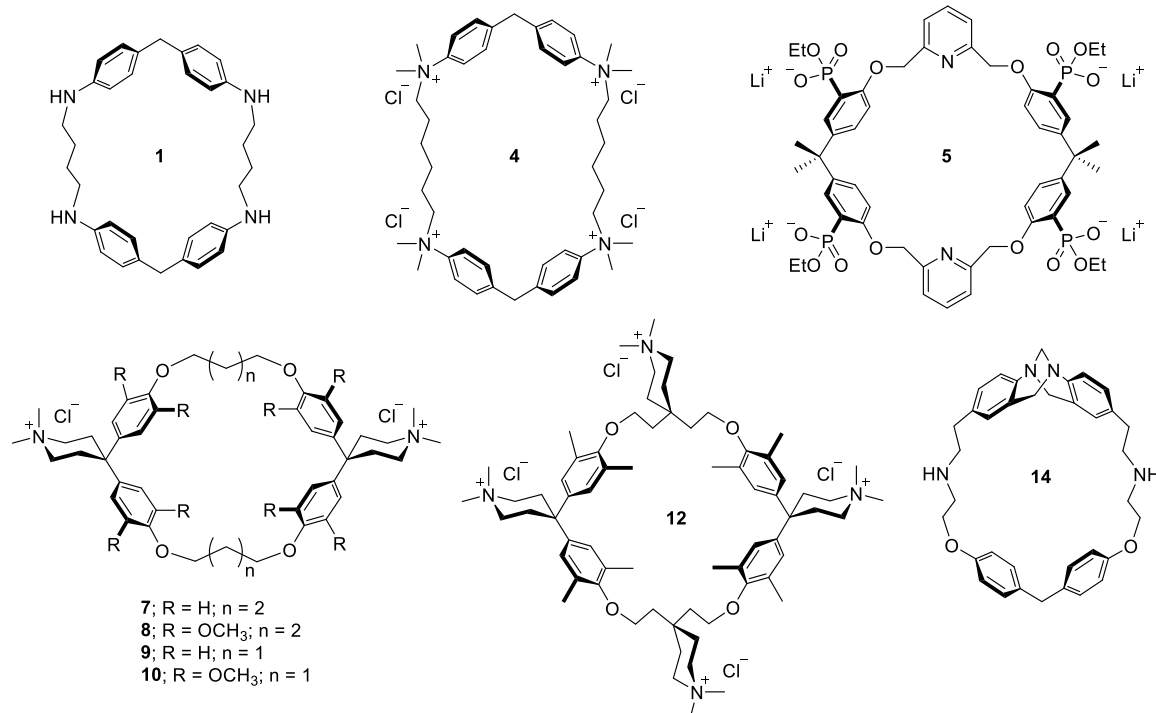


Figure 4. Line-drawing structures of cyclophanes based on diphenylmethane units.

Using synthetic host–guest systems, Gibb's group has put a lot of effort in understanding the Hofmeister effect (salting effect) on binding affinity.⁷⁷ To this end, a water-soluble deep-cavity cavitand bearing external carboxylic acid groups was used as model system (see section 4.2). The binding of adamantane carboxylic acid to the receptor's cavity involved the deep inclusion of the adamantane residue (nonpolar section). The addition of “salting-out” anions favored binding, whereas “salting-in” anions had the opposite effect. These results were rationalized in terms of the Hofmeister effect and the competitive binding of the “salting-in” anions in the hydrophobic cavity. Further studies evidenced that the observed Hofmeister effect was not only related to the inclusion of the “salting-in” anions into the receptor's cavity but also to the concomitant binding of salt cations to the peripheral carboxylate groups.⁴ Other examples of salting effects are described in the studies of Schneider *et al.* with a positively charged cyclophane (section 3.1) and those of Davis *et al.* using a “temple” receptor (section 5.1).

In the same vein, the binding of large “salting-in” anions featuring a diffuse charge was studied by Nau and co-workers using γ -cyclodextrin.⁸⁵ The association constants of the resulting complexes were in the order of 10^3 – 10^6 M^{−1}. Interestingly, the binding processes were thermodynamically characterized as enthalpically driven and opposed by entropy. In agreement with Gibb's findings, the obtained results confirmed that “salting-in” anions, which are weakly solvated by water, bind efficiently in the hydrophobic cavities of cyclodextrins that are also badly solvated by water.⁴⁰

The fact that “salting-in” anions are poorly solvated by water may also be responsible of the “reverse” Hofmeister effect.¹¹ Typically, the interaction of “salting-in” anions with nonpolar groups or solutes induces an increase in solubility (*vide supra*). However, in certain cases, the same “salting-in” anions can induce the precipitation of the solute. On the one hand, this dual behavior presents a problem to the theory explaining the

Hofmeister effect simply based on the modification of water structure. On the other hand, it provides strong support to the idea that the Hofmeister effect for “salting-in” anions involves a direct interaction of the anion with the solute. In this case, the unexpected reduction of solubility is related to the ion-pairing of the anion with positively charged groups of the solute. It seems that the “reverse” Hofmeister effect is at the heart of the chloride selection as countercation of small ammonium groups soluble in water. The corresponding perchlorate salt displays a reduced water solubility owing to stronger ion-pairing.

3. CYCLIC AND OLIGOCYCLIC COVALENT RECEPTORS FEATURING A HYDROPHOBIC CAVITY

In this section, we discuss water-soluble synthetic receptors featuring monocyclic or bicyclic architectures having a covalent connectivity of aromatic units. The binding site provided by these cyclic covalent hosts (aka unimolecular hosts) is mainly hydrophobic.

3.1. Cyclophanes

Cyclophanes are synthetic molecular receptors formed by aromatic units linked together with alkyl or aryl spacers. The structure of cyclophanes offers a hydrophobic cavity commonly open to the bulk solution at its two opposite ends. Ionizable or charged groups (e.g., carboxylic acids, amines, ammonium cations, etc.) are appended to the cyclophanes' scaffolds to impart their solubility in water and minimize aggregation tendency.^{15,86} On the basis of these features, cyclophanes are good candidates to study the binding of nonpolar molecules or residues in water. Cyclophanes incorporating polar groups in the interior of their hydrophobic cavities, *i.e.*, inwardly directed toward them, are rare.⁶⁹

The first examples of molecular recognition in water using cyclophane receptors were reported by Koga *et al.* in 1980.⁸⁷ Cyclophane 1 is based on two rigid diphenylmethane units connected by two butane-1,4-diamine spacers (Figure 4).

Cyclophane **1** is soluble in water at pH < 2 owing to the protonation of its secondary amines. The authors demonstrated that, in the solid state, **1** formed a 1:1 inclusion complex with 1,2,4,5-tetra-methylbenzene. The receptor adopted a rhomboid-like conformation (*ca.* 7.9 × 6.5 Å²) to accommodate the benzene derivative in its aromatic cavity. The authors also investigated the binding properties of **1** in acidic aqueous solution. For example, 1-anilinonaphthalene-8-sulfonate potassium salt **2** (Figure 5) was used as guest.

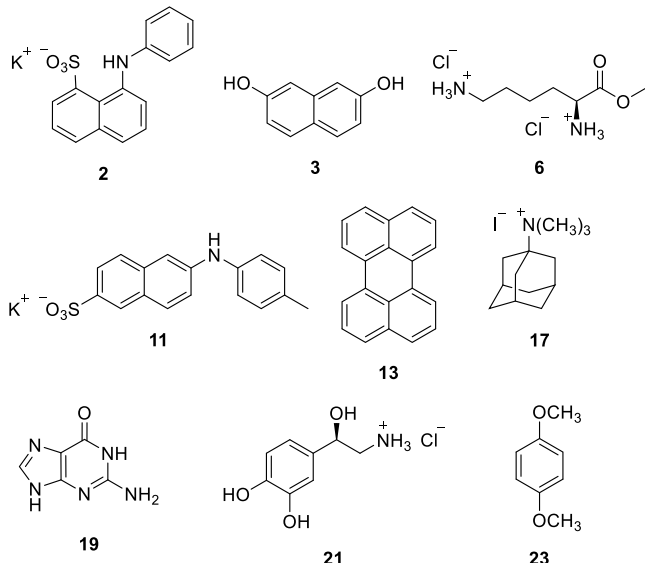


Figure 5. Guest molecules studied with cyclophane receptors.

Compound **2** featured emission properties and, therefore, titration experiments were performed using fluorescence spectroscopy. The incremental addition of tetra-ammonium cyclophane [1+4H]⁴⁺ in acidic water to a solution of sulfonate **2**⁻, also in acidic water, induced the gradual enhancement of the guest's emission band intensity. The fit of the obtained titration data to a 1:1 binding model using a linear regression (Benesi–Hildebrand plot) returned a remarkable binding constant value of K_a ($2^- \subset [1+4H]^{4+}$) = 6.3×10^3 M⁻¹. However, the geometry of the $2^- \subset [1+4H]^{4+}$ complex was not determined in solution by ¹H NMR spectroscopy.

After these initial studies, Koga *et al.* reported the binding studies of 2,7-dihydroxynaphthalene **3** (Figure 5) with cyclophane **1** in DCl/D₂O solution (pD = 1.2) using ¹H NMR spectroscopy.⁸⁸ The incremental addition of receptor [1+4H]⁴⁺ to a water solution of **3** induced upfield shifts to the proton signals of the guest. Simultaneously, the proton signals of the butyl spacers of [1+4H]⁴⁺ also moved upfield, whereas the protons of the methylene bridges of the two *para*-phenyl units did not experience appreciable chemical shift changes. Taken together, these observations supported the inclusion of **3** in the aromatic cavity of [1+4H]⁴⁺ in acidic water solution. The protons of bound **3** and those of the aliphatic chains of bound [1+4H]⁴⁺ moved upfield owing to the shielding effect exerted by the aromatic rings present in the respective binding partners. The chemical exchange process between the free and the bound components of the $3 \subset [1+4H]^{4+}$ complex showed fast exchange dynamics on the ¹H NMR chemical shift time scale. This fast chemical exchange is related to the existence of two opposite open portals in the cyclophane's structure, allowing the rapid formation and dissociation of the inclusion

complex. The association constant of the $3 \subset [1+4H]^{4+}$ complex was estimated to be 2.8×10^3 M⁻¹. Interestingly, a sensible binding geometry for the complex was derived from the analysis of the chemical shift changes experienced by the protons of both host and guest. The naphthalene derivative **3** was bound in a pseudoaxial orientation in the aromatic cavity of [1+4H]⁴⁺. In this binding geometry, the two hydroxyl groups of guest **3** were exposed to the bulk aqueous solution (Figure 6).

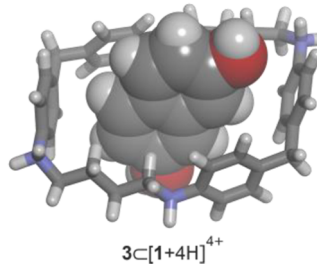


Figure 6. Energy minimized structure (MM3) of the putative $3 \subset [1+4H]^{4+}$ inclusion complex. Host is depicted in stick representation and guest is shown as CPK model.

Cyclophane **1** and its octa-N-methylammonium analogue were used in the binding studies of a series of charged aromatic guests.^{89–91} The obtained results revealed that the anionic guests were bound more strongly than the cationic derivatives, K_a (anionic guest \subset cyclophane) > $10 \times K_a$ (cationic guest \subset cyclophane). This finding indicated that the formation of 1:1 inclusion complexes derived from cyclophane [1+4H]⁴⁺ did not only follow the size and shape complementary principles, but it also took into account the charge complementarity between binding partners.

The length and conformational rigidity of the spacers in **1** were also modified to tune the dimensions and hydrophobicity of the cyclophane's cavity.^{89,92} Thus, the incorporation of cyclohexyl units in the spacers boosted the binding constant of 1-anilinonaphthalene-8-sulfonate **2**⁻ to 5.0×10^5 M⁻¹ (increase of 2 orders of magnitude with respect to the parent receptor [1+4H]⁴⁺). In the latter complex, bound **2**⁻ adopted an equatorial orientation, burying completely the naphthalene group in the receptor's cavity.

Additional water-solubilizing groups were appended to the spacers of the *bis*-(diphenylmethane) cyclophane **1** aiming at improving receptor's solubility. Kikuchi, Murakami, and co-workers incorporated four L-aspartate residues to the four nitrogen atoms of **1**.^{93,94} The attached amino acids allowed the modulation of the overall charge of the receptor at will. The carboxylic acids of the aspartate residues were ionized at basic pH, leading to anionic cyclophanes. On the contrary, protonation of the primary amines of the aspartates at acidic pH gave the cationic counterparts. Using this cyclophane derivative, the authors observed that depending on the overall charge of the host ($z = +4$ or $z = -4$), the electrostatic interactions impacted by 1 or 2 orders of magnitude on the thermodynamic stabilities determined for the 1:1 complexes with mono- and dicharged guests (anionic and cationic).

On the basis of the above, Schneider *et al.* synthesized the *bis*-(diphenylmethane) cyclophane receptor **4** bearing hexyl chains as spacers and four quaternary ammonium groups⁹⁵ (Figure 4). The cavity size of tetra-cationic **4**⁴⁺ could accommodate purine bases, such as adenine and their

corresponding nucleosides and nucleotides, establishing 1:1 complexes. For example, the energy minimized structure of the complex of adenosine monophosphate, $\text{AMP}^{2-}\text{C4}^{4+}$, shows the adenine fragment included in the aromatic cavity of C4^{4+} and the ribose unit placed near one of the portals of the macrocyclic binding site (Figure 7 and Table 3). The phosphate group of

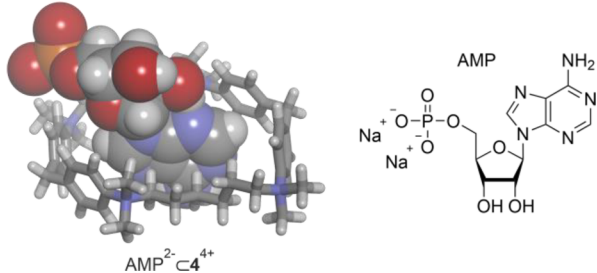


Figure 7. (left) Energy minimized structure (MM3) of the $\text{AMP}^{2-}\text{C4}^{4+}$ complex and (right) line-drawing structure of AMP disodium salt. The host is depicted in stick representation and the guest is shown as CPK model.

the guest is exposed to the bulk aqueous solution, even though it can establish electrostatic interactions with the cationic ammonium groups of the receptor. Cyclophane C4^{4+} displayed high binding selectivity for adenine derivatives in water.

Cyclophane C4^{4+} was also employed as model system to study the effect of salt addition (salting effect) in the binding of naphthalene 2-carboxylate.^{96,97} An increase in the concentration of NaCl resulted in a moderate reduction of binding affinity (from $K_a = 5.97 \times 10^3 \text{ M}^{-1}$, $I = 0.09$, to $1.96 \times 10^3 \text{ M}^{-1}$, $I = 0.48$) and in the observation of a linear relationship between $\log K_a$ and the Debye–Hückel term $f(I)$ ($\log K_a = \log K_a^\circ + mI^{1/2}/(1 + I^{1/2})$, where I is the ionic strength). The calculated slope of the linear regression (m) was -1.45 . This value was significantly lower than the one expected ($m = -4.07$) if the host ($z = +4$), guest ($z = -1$) and 1:1 complex ($z = +3$) were treated as normal ions. The addition of NaCl, in the range of concentrations used, had a reduced impact on the HE toward binding as could be expected for an anion located in the middle of the Hofmeister series (see section 2.2). In any case, the authors concluded that the surprising linear Debye–Hückel correlation may be used as an approximate, empirical indicator of the level of the importance of the Coulombic interactions for the stabilization of the supramolecular host–guest complexes in water. Thus, for complexes in which Coulombic or charge–charge interactions dominate binding (see electrostatic interactions in section 2), slope values (m) of the corresponding linear Debye–Hückel correlations in the range of -4 to -3 should be expected.

Water-solubilizing groups were also attached as substituents in the diphenylmethane walls of the cyclophanes. For example, Schrader, Finocchiaro, and co-workers designed cyclophane **5** having four monoethyl phosphonic acid groups, as lithium salts, and bearing two *ortho*-substituted pyridines as spacers⁹⁸ (Figure 4). This receptor bound the methyl ester of diprotonated L-lysine 6^{2+} (Figure 5) through the formation of charge-assisted hydrogen bonds (see section 2) between the ammonium groups of the guest and the negatively charged monoethyl phosphonates of the receptor 5^{4-} . The two protonated ammonium groups of 6^{2+} could be also involved in hydrogen-bonding interactions with the nitrogen atom of the pyridine residues of receptor 5^{4-} . The binding constant for

the $\text{6}^{2+}\text{C5}^{4-}$ complex was determined to be $K_a = 1.2 \times 10^3 \text{ M}^{-1}$ in water. This is a remarkable value considering that the complex is mainly stabilized through electrostatic interactions.

Diederich *et al.* functionalized the methylene bridges of *bis*(diphenylmethane) cyclophanes with spiro-piperidinium units and replaced the amino groups of the spacers by ether functions,⁹⁹ **7–10** (Figure 4). These structural modifications allowed the placement of the quaternary ammonium groups far from the receptor's cavity, minimizing their possible effects on the binding event. It is worth mentioning that, in the solid state, the cavity of spiro-piperidinium cyclophanes was occupied by two water molecules. In water solution, the *bis*-piperidinium cyclophane 7^{2+} featured a critical micellar concentration (cmc) of $1.6 \times 10^{-4} \text{ M}$, which limited the implementation of ^1H NMR spectroscopy titrations. Nevertheless, the binding constants of the complexes derived from 7^{2+} were determined by solid–liquid and liquid–liquid extraction methods as well as fluorescence spectroscopy titrations. Dicationic cyclophane 7^{2+} formed 1:1 inclusion complexes with aromatic guests. As in the previous examples reported by Koga and co-workers, the cyclophane complexes were stabilized by the HE, and the establishment of $\pi-\pi$, $\text{CH}-\pi$, and long-range Coulombic and dispersion interactions (*i.e.*, van der Waals) (see section 2). For example, the complex of 6-[*(4-methylphenyl)-amino*]-2-naphthalenesulfonate **11**⁻ (Figure 5) and cyclophane 7^{2+} featured an association constant value of $K_a = 4.3 \times 10^3 \text{ M}^{-1}$ in water.¹⁰⁰ The binding constant of the $\text{11}^-\text{C7}^{2+}$ complex was similar to that of the same guest with β -cyclodextrin, a neutral noncharged receptor.

On the other hand, cyclophane **8** displayed a more polarizable and deeper aromatic cavity than **7** owing to the presence of *ortho*-methoxy substituents in the phenyl rings^{99,101} (Figure 4). This structural modification also produced an increase of the cmc value to 10^{-2} M . Cyclophane 8^{2+} complexed neutral, aromatic molecules, forming 1:1 inclusion complexes having stability constant values in the order of $K_a = 10^3\text{--}10^4 \text{ M}^{-1}$.

The complexation process of aromatic guests with cyclophanes was mainly driven by the HE, which made it difficult to dissect the contribution of $\pi-\pi$ interactions to the binding. In this regard, Diederich *et al.* applied cyclophanes **8**, **9**, and **10** (Figure 4) to examine the electronic complementarity between receptors and guests.¹⁰² The main aim of these studies was to derive the contribution of donor–acceptor interactions to binding. 1,4-Disubstituted benzene derivatives were chosen as guests because they displayed an axial binding geometry, *i.e.*, the phenyl group was included in the cavity of the cyclophane receptors and the polar groups in *para*-position were exposed to the aqueous solution. The electronic properties of the π -systems of the phenyl group in the guests can be tuned by the electron-donor or electron-withdrawing characteristics of the *para*-substituents. In turn, the change in the electrostatic surface potential (ESP) of the guest's π -systems was expected to influence the thermodynamic stability of the inclusion complexes. In this regard, the stabilities of the inclusion complexes of cyclophane **9**²⁺ followed the expected trend with respect to the electron donor–acceptor properties of the guest substituents: acceptor–acceptor > donor–acceptor > donor–donor. In contrast, cyclophanes **8**²⁺ and **10**²⁺ did not follow a similar relationship. The difference in the obtained results was attributed to the *ortho*-methoxy substituents in the phenyl rings of cyclophanes **8**²⁺ and **10**²⁺. The authors indicated that solvation effects of the guests, as well as of the latter

Table 2. Molecular Electrostatic Potentials (MEP Values, $\text{kJ}\cdot\text{mol}^{-1}$) of *para*-Substituted Benzenes and Their Binding Constants (K_a , M^{-1}) with cyclophanes 8^{2+} , 9^{2+} , and 10^{2+} in D_2O at 293 K

Guest	Electronic nature	MEP ($\text{kJ}\cdot\text{mol}^{-1}$) ^a	K_a (receptor 8^{2+})	K_a (receptor 9^{2+})	K_a (receptor 10^{2+})
	Donor-donor	-98.7	3.6×10^2	< 10	21
	Donor-acceptor	+2.5	2.3×10^4	6.0×10^2	2.1×10^3
	Acceptor-acceptor	+69.4	7.8×10^3	1.3×10^3	not determined

^aMEP values at the center of the phenyl ring (DFT level, B3LYP/6-31G*, Spartan version 7.2.7).

cyclophanes, governed the relative association strengths (Table 2).

Hunter *et al.* changed the ether linkages of the *bis*-(diphenylmethane) cyclophanes to pyridyl 2,6-dicarboxamide groups.¹⁰³ The resulting receptor proved to be effective for the binding of cyclic dipeptides (K_a ca. 100 M^{-1}). This receptor constitutes one of the scarce examples of cyclophanes bearing inwardly oriented polar binding functions (see section 5 for three-dimensional receptors featuring polar hydrophobic cavities).

The incorporation of two additional spiro-dimethyl-piperidinium units in the spacers of the *bis*-(diphenylmethane) cyclophane scaffold afforded compound 12¹⁰⁰ (Figure 4). Cyclophane 12 was characterized by a cmc value of $7.5 \times 10^{-3} \text{ M}$, which is 50-fold larger than that of cyclophane 7 ($1.6 \times 10^{-4} \text{ M}$). Furthermore, the *ortho*-methyl substituents of the phenyl groups of 12 yielded a deeper and more hydrophobic aromatic cavity enhancing the HE.⁶⁹ Tetra-piperidinium 12⁴⁺ was an efficient receptor for the binding in water of neutral polyaromatic guests, such as pyrene, perylene, and fluoranthene, and anionic naphthalene derivatives, featuring dissociation constants in the micromolar range. For example, the binding constant value of 1-anilinonaphthalene-8-sulfonate 2⁻ with receptor 12⁴⁺ was almost 1 order of magnitude larger than that with the simple tetra-cationic cyclohexyl-substituted derivative of [1+4H]⁴⁺ (Table 3). Perylene 13 (Figure 5) showed a perfect fit for the aromatic cavity of 12⁴⁺.¹⁰⁰ The 13C12⁴⁺ complex was highly stable in water featuring a binding constant value of $K_a = 1.6 \times 10^7 \text{ M}^{-1}$ (Figure 8).

The thermodynamic signatures experimentally measured by Diederich *et al.* served to introduce the concept of the “nonclassical” hydrophobic effect (see section 2.1) for the binding of aromatic guests with cyclophanes in water.^{4,101} The binding processes were thermodynamically characterized by a strong enthalpy gain, $\Delta H = -33.5$ to $-50.2 \text{ kJ}\cdot\text{mol}^{-1}$, and an entropic penalty, $T\Delta S = -8.4$ to $-20.9 \text{ kJ}\cdot\text{mol}^{-1}$. Note that these thermodynamic signatures are in sharp contrast with the ones expected for processes driven by the so-called “classical” hydrophobic effect ($\Delta H \sim 0$ and $T\Delta S > 0$). It was then proposed that the large and negative enthalpic term derived from the release of water molecules included in the receptor’s cavity to the bulk solution. The included water molecules were

expected to have a higher enthalpy than those in the bulk owing to the limited number of hydrogen bonds that they could establish. Some of the enthalpy gained upon binding could also derive from the more favorable enthalpic dispersion interactions present in the complex compared to those in the hydrated free binding partners. We commented above (section 2.1 dedicated to the HE) that the assignment of the thermodynamic signatures of binding processes occurring in water exclusively to energy differences between bound and bulk-released water molecules is not recommended. Examples of binding processes showing the characteristics of the “nonclassical” HE and involving weakly hydrated nonpolar binding sites are known.⁸⁰

The thermodynamic stabilities (K_a) of the complexes formed between cyclophane 8^{2+} and *para*-substituted benzenes were determined by ¹H NMR spectroscopy titrations in a range of 20 K.¹⁰⁴ The van’t Hoff analyses of the titrations data returned enthalpic terms that were qualitatively in good agreement with those directly measured by calorimetry. The observed changes in heat capacity (ΔC_p) produced larger uncertainty in the values calculated from the van’t Hoff analyses. The determined ΔC_p values were in the order of *ca.* $-420 \text{ J}\cdot\text{mol}^{-1}\cdot\text{K}^{-1}$ for those guests having a strong dipole moment and hydroxyl substituents. This magnitude of ΔC_p was in the same range of that determined for the binding of nonpolar substrates with cyclodextrins.¹⁰⁵

One of the issues with the diphenylmethane-based cyclophane receptors is the easy rotation of their aromatic rings leading to multiple conformations. In an effort to reduce conformational flexibility, Wilcox *et al.* used molecular units derived from Tröger’s base in the construction of cyclophanes.¹⁰⁶ The change of one of the diphenylmethane components by a dibenzodiazocine scaffold afforded a relatively more rigid receptor, 14 (Figure 4). Cyclophane 14 is soluble at concentrations up to $5 \times 10^{-2} \text{ M}$ in 0.1 M KCl/DCl buffer, $\text{pD} = 1.9$. In this acidic solution, three of the four nitrogen atoms of 14 are protonated (one of the diazocine nitrogen atoms remained unprotonated). The interaction of [14+3H]³⁺ with a series of *para*-methyl-substituted benzenes was probed by ¹H NMR spectroscopy titrations. In all cases, the signal corresponding to the *para*-methyl substituent of the guests experienced the largest upfield shift upon addition of the

Table 3. Binding Constant Values (K_a , M⁻¹) of Selected Cyclophane Complexes in Water Solution^a

Guests	Cyclophanes based on diphenylmethane units						Other cyclophanes			
	[1+4H] ⁴⁺	4 ⁴⁺	5 ⁴⁻	7 ²⁺	12 ⁴⁺	[14+3H] ³⁺	15 ⁴⁻	16 ⁴⁻	[18+4H] ⁴⁺	24
2 ^{87,100}	6.3 × 10 ³				3.6 × 10 ⁶					
3 ⁸⁸	2.8 × 10 ³									
AMP ^{2+,95}		1.9 × 10 ³								
6 ^{2+,98}			1.2 × 10 ³							
11 ^{-,100}				4.3 × 10 ³						
13 ¹⁰⁰					1.6 × 10 ⁷					
4-methylphenol ¹⁰⁶						53				
4-cyanophenol ¹⁰⁶						1.7 × 10 ²				
4-toluenesulfonate ¹⁰⁶						3.3 × 10 ²				
17 ^{+,107}							8.2 × 10 ⁴	9.2 × 10 ³		
19 ¹¹⁹									2.0 × 10 ³	
pyrene ¹²⁷										6.0 × 10 ⁶

^aSee Figure 4 and Figure 9 for the line-drawing structures of the compounds and the text for details.

receptor [14+3H]³⁺. This indicated the deep inclusion of the *para*-methyl group of the guests into the cyclophane's cavity. The fit of the chemical shift changes to a 1:1 binding model, using a nonlinear least-squares method, returned binding

constant values in the range of 40–400 M⁻¹. Neutral electron-rich aromatic guests, such as 4-methylphenol, were weakly bound by [14+3H]³⁺, $K_a = 53$ M⁻¹. However, acceptor–donor phenyl-substituted guests, such as 4-cyanophenol, showed an

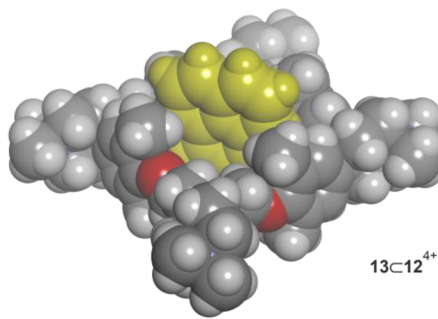


Figure 8. Energy minimized structure (MM3) of the $13\subset_{\text{C}}12^{4+}$ inclusion complex. Host and guest (in yellow) are shown as CPK models.

increase in binding affinity, $K_a = 1.7 \times 10^2 \text{ M}^{-1}$. In the case of anionic aromatic molecules, they were bound by $[14+3\text{H}]^{3+}$ featuring K_a values in the order of $10^2\text{--}10^3 \text{ M}^{-1}$. For example, the binding constant of the 4-toluenesulfonate $\subset[14+3\text{H}]^{3+}$ complex was $3.3 \times 10^2 \text{ M}^{-1}$. Probably, Coulombic interactions were also at play. These latter association constant values were in line with those reported by Diederich and co-workers using cyclophanes 7^{2+} and 8^{2+} (Figure 4).

Dougherty *et al.* designed cyclophanes based on the ethenoanthracene scaffold,¹⁰⁷ **15** and **16** (Figure 9). The ethenoanthracene scaffold is rigid, concave, and delivers an electron-rich aromatic surface area to the cyclophane's cavity. The phenyl and cyclohexyl spacers of **15** and **16**, respectively, also aid the cyclophanes to adopt a preorganized structure. Carboxylate groups were anchored to the ethenoanthracene units in the faces exposed to the bulk solution. In borate buffer at $\text{pD} = 9$, cyclophanes **15** and **16** were soluble in water and featured large cmc values in the range of $2\text{--}8 \times 10^{-4} \text{ M}$.

The ethenoanthracene-based cyclophanes adopted two possible conformations for binding: a rhomboid-shaped conformation was preferred for planar guests, such as iminium ions, whereas a toroid-shaped conformation was suitable for the binding of spherical guests, such as tetra-alkylammonium substrates. Neutral electron-deficient aromatic molecules and tetra-carboxylates of ethenoanthracene cyclophanes, **15**⁴⁻ and **16**⁴⁻, formed 1:1 inclusion complexes featuring association constant values in the range of $K_a = 10^3\text{--}10^6 \text{ M}^{-1}$. These guests were preferentially bound to **15**⁴⁻ and **16**⁴⁻ than electron-rich counterparts owing to the superior donor-

acceptor complementarity of the binding partners. Cyclophanes **15**⁴⁻ and **16**⁴⁻ also showed high binding affinity for ammonium guests, such as *N*-methylquinolinium and *N*-methylisoquinolinium. The binding studies assigned a gain of $12.5 \text{ kJ}\cdot\text{mol}^{-1}$ for the complexation free energy deriving from the combination of donor–acceptor interactions and cation– π interactions.¹⁰⁷ The cation– π interaction accounted for at least $4.2 \text{ kJ}\cdot\text{mol}^{-1}$ or more to the thermodynamic stability of these complexes.⁵⁰ Long-range Coulombic interactions between the external carboxylates of the receptors and the ammonium group of the quinolinium unit of the guests contributed to a lesser extent ($<1.3 \text{ kJ}\cdot\text{mol}^{-1}$ per carboxylate group).^{107,108}

Adamantane trimethylammonium **17**⁺ (Figure 5) was a perfect fit for the cavity of the cyclophanes reported by Dougherty and co-workers.¹⁰⁷ The binding free energy of the $17^+\subset15^{4-}$ complex was $-28.0 \text{ kJ}\cdot\text{mol}^{-1}$. The $17^+\subset15^{4-}$ complex was $5.4 \text{ kJ}\cdot\text{mol}^{-1}$ thermodynamically more stable than the $17^+\subset16^{4-}$ (phenyl spacer substituted by cyclohexyl) counterpart in borate buffer solution ($\text{pD} = 9$) (Table 3). Interestingly, the complexation-induced chemical shifts determined from the ^1H NMR titration spectra indicated that the trimethylammonium cation of guest **17**⁺ was included deeper in the hydrophobic aromatic cavity of the **15**⁴⁻ receptor than the adamantane unit (Figure 10).

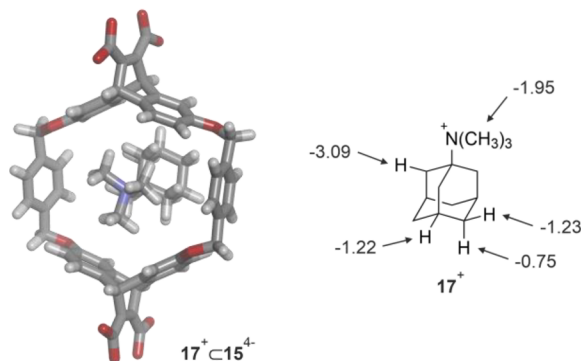


Figure 10. (left) Energy minimized structure (MM3) of the $17^+\subset15^{4-}$ complex (receptor in the toroid conformation) and (right) complexation-induced chemical shifts ($\Delta\delta = \delta_{\text{bound}} - \delta_{\text{free}}$, ppm) of proton signals of bound 17^+ .

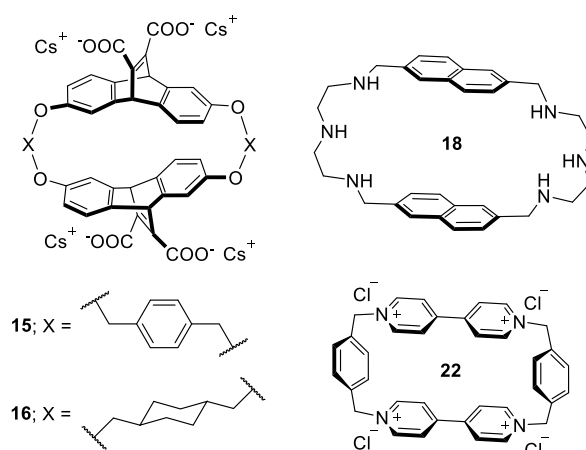


Figure 9. Line-drawing structures of additional cyclophane receptors discussed in the text.

The complexation of the ammonium organic guests by cyclophane tetra-carboxylates **15⁴⁺** and **16⁴⁺** in water was driven by enthalpy. The determined heat capacity values (ΔC_p) for these binding processes were large and negative¹⁰⁹ (see section 2.1), and their magnitude coincided with those determined by Diederich *et al.* for the binding of their cyclophane receptors with polar *para*-substituted benzene derivatives.

The existence and importance of the cation–π interaction in synthetic and natural host–guest complexes was not obvious at the time that Dougherty and co-workers introduced the ethenoanthracene-based cyclophanes. In this regard, his group conducted host–guest binding studies using a series of cyclophane receptors, including tetra-carboxylates **15⁴⁺** and **16⁴⁺** and a library of cationic guests: alkyliminium, tetraalkylammonium, sulfonium, and guanidinium substrates.¹¹⁰ The results demonstrated that the cation–π interaction had a significant effect in the stability of the host–guest complexes. For example, the complexation of *N*-methylquinolinium was 10.5 kJ·mol^{−1} more favorable than that of the neutral closely related derivative, 4-methylquinoline.

Dougherty *et al.* also investigated the influence on binding of the negatively ionized carboxylate groups using modified ethenoanthracene-based cyclophanes. For example, the phenyl spacers of **15⁴⁺** were decorated with additional carboxylate groups at their *ortho*-positions, providing extra electrostatic interactions and, therefore, enhancing the binding affinity toward cationic organic guests.¹⁰⁸ Conversely, the added carboxylate groups impacted negatively on the recognition of neutral molecules, presumably, owing to the reduction of the hydrophobicity of the binding pocket. Interestingly, the modified octa-carboxylate cyclophane receptor was highly effective for the binding of L-arginine. The complex was stabilized by Coulombic, π–π and cation–π interactions between the guanidinium group of the guest and the highly ionized ($z = -8$) aromatic scaffold of the receptor ($K_a = 4.7 \times 10^3$ M^{−1}). The binding geometry and affinity toward the guanidinium cation of L-arginine residues allowed the recognition of dipeptides containing an L-arginine residue as C-terminal amide. The second residue of the dipeptides featured different length side chains connecting to the terminal ammonium group. The ammonium group could make a tight salt-bridge with a carboxylate of the host. The authors demonstrated that the precise position of the terminal protonated amine was important and significantly affected the binding energy. Other modifications at the spacers of ethenoanthracene-based cyclophanes were reported in literature.^{110–113}

Inspired by the cyclophane receptors reported by the group of Dougherty, Otto, Sanders, and co-workers replaced the two oxygen atoms at the aromatic rings of the ethenoanthracene scaffold by thiol groups.^{114,115} The reaction of the dithiol ethenoanthracene building block and a *meta*-dithiol phenyl derivative led to a mixture of cyclophanes (dynamic combinatorial library, DCL) by the formation of reversible disulfide bonds (dynamic combinatorial chemistry, DCC). Interestingly, the addition of cationic guests (e.g., quaternary amines and imines) produced the amplification of certain cyclophanes of the DCL. Thus, the size and shape of the templating guest determined the structure (type and number of building blocks) of the major cyclophane present in the DCL.

The results obtained in the binding of L-arginine with tetra-carboxylate cyclophane **15⁴⁺** and other derivatives served for the discovery by Waters *et al.*, also using DCC studies, of an efficient and selective chiral receptor bearing two ethenoanthracene units and one naphthalene spacer linked by disulfide bonds.¹¹⁶ This cyclophane was able to bind nonsymmetric dimethyl L-arginine (Me₂N–CNH₂–NH-alkyl), which is a post-translational modification in proteins, with significant selectivity over symmetric dimethyl L-arginine (MeHN–CNHMe–NH-alkyl, aka sRMe₂, R = arginine in one letter code) and the monomethylated counterpart (MeHN–CNH₂–NH-alkyl). The synthetic receptor displayed affinities and selectivity for the different L-arginine methylation states that are comparable to the native methyl L-arginine binding sites. The dissociation constant of sRMe₂ was in the low micromolar range, which is remarkable owing to the fact that the main driving force for binding was the interaction with the methylated side chain. The observed higher selectivity for sRMe₂ over the monomethylated state was attributed to differences in dispersion (van der Waals contacts), cation–π interactions, and desolvation penalties. Waters *et al.* also applied DCC studies to the identification of ethenoanthracene-based cyclophane receptors displaying high binding affinity and selectivity for ζ-trimethylammonium L-lysine (KMe₃⁺, K = lysine in one letter code) over di-, mono-, and nonmethylated states of the L-lysine side-chain (KMe_n⁺; $n = 2–0$).^{117,118}

Lehn *et al.* used naphthalene units for the construction of water-soluble cyclophanes. Receptor **18** featured two parallel naphthalene units linked together by two polyamine linkers¹¹⁹ (Figure 9). At pH = 6 (pyridine/trifluoroacetic acid buffer), four of the six amine nitrogen atoms of **18** were protonated (Figure 11). The central nitrogen atoms remained unproto-

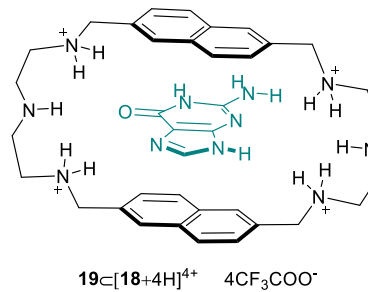


Figure 11. Line-drawing structure of the complex between guanine **19** and cyclophane $[18+4H]^{4+}$ at pH = 6.

nated because, as a result of being flanked by two ammonium groups, their pK_a values were relatively low. The existence of four ammonium groups in $[18+4H]^{4+}$ was expected to induce a repulsion between them, thus circumventing the hydrophobic collapse of the cavity by stacking of its two aromatic sections, “roof” and “floor”. ¹H NMR and fluorescence titration experiments demonstrated that $[18+4H]^{4+}$ was able to bind aromatic carboxylates and nucleotides. Contrary to the binding selectivity displayed by cyclophane **4⁴⁺** (Figure 4) toward adenine, receptor $[18+4H]^{4+}$ selectively bound guanine **19** (Figure 5), K_a (guanine $\subset [18+4H]^{4+}$)/ K_a (adenine $\subset [18+4H]^{4+}$) ~ 10 , probably due to superior π–π interactions and solvation processes (Figure 11 and Table 3). However, the binding constant ratio diminished to *ca.* 4 in the complexation of the corresponding monophosphate nucleotides, GMP²⁻ and AMP²⁻. Most likely, this result was

a direct consequence of the relevance of the Coulombic interactions in the binding of the nucleotides.⁸⁶

Cyclophanes with larger aromatic cavities were constructed using *para*-phenyl–ethynyl–phenyl units as building blocks. For example, Schrader *et al.* reported the construction of cyclophane **20** (Figure 9) based on the latter scaffold being both the “roof” and “floor”.¹²⁰ The ionized phosphonic acid groups of the *para*-phenyl substituted spacers imparted water solubility to **20**, which featured a cmc value of 3×10^{-4} M. The overall charge and its distribution were not ideal to avoid aggregation at millimolar concentrations. Tetra-anionic receptor **20**⁴⁻ complexed protonated noradrenaline **21**⁺ (Figure 5), among other catecholamines, forming 1:1 and 2:1 guest/host complexes. The stepwise binding constants were in the order of 10^3 M⁻¹.

On the other hand, structurally simple cyclophanes bearing *para*-benzene derivatives at the “roof” and “floor” were designed.^{121–123} As discussed above for cyclophane [18+4H]⁴⁺, ammonium groups were incorporated to deliver water solubility. The cationic nature of these simple cyclophanes was applied in the binding of organic and inorganic anions such as carboxylate and sulfate, respectively.

Paraquat units were also used as building blocks for the synthesis of cyclophanes. The resulting cyclophanes featured an electron-deficient cavity, which was ideal for the complexation of electron-rich aromatic molecules. The cationic paraquat scaffolds also imparted water solubility. The cyclo-bis-(paraquat-*para*-phenylene) cyclophane **22** was introduced by Stoddart *et al.* in the late 1980s¹²⁴ (Figure 9). The tetracationic receptor **22**⁴⁺ featured a rectangular cavity with dimensions of 10.3×6.8 Å². In the presence of electron-rich aromatic substrates, such as 1,4-dimethoxybenzene **23** (Figure 5), 1:1 inclusion complexes were formed in D₂O solution. The aromatic rings of host and guest established charge-transfer π–π interactions. ¹H NMR binding studies showed that the aromatic protons of **23** experienced an upfield shift of $\Delta\delta \sim -3$ ppm, whereas the protons of the methoxy groups moved upfield only $\Delta\delta \sim -0.5$ ppm upon complexation. These chemical shift changes indicated that the guest was bound in an axial orientation. The *para*-methoxy substituents were located at the portals of the receptor’s cavity (Figure 12). It is interesting to note that the *bis*-paraquat cyclophane **22**⁴⁺ was able to bind amino acids containing electron-rich aromatic substituents, such as L-tryptophan.⁸⁶

The axial binding geometry featured by certain aromatic guests with receptor **22**⁴⁺ suggested that 1,4-dialkoxy-phenyl and 1,5-dialkoxy-naphthalene derivatives would produce inclusion complexes with pseudorotaxane topology.^{125,126} The binding constant values of the corresponding 1:1 inclusion complexes were in the range between 10^4 and 10^6 M⁻¹.

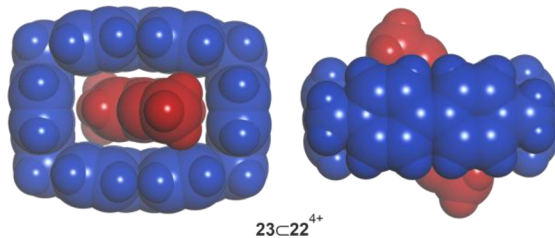


Figure 12. Energy minimized structure (MM3) of the **23**<**22**⁴⁺ inclusion complex: side and top views (receptor in blue and guest in red).

Note that the cyclophanes discussed above are monocyclic, featuring shallow cavities open at both ends. The construction of hydrophobic binding pockets shielded from solvation by bulk water molecules requires preorganized, three-dimensional structures (see section 2.1). This issue was addressed by Diederich and co-workers using bicyclic cyclophanes. Cyclophane **24** (Figure 13) bears five tertiary amines which, upon

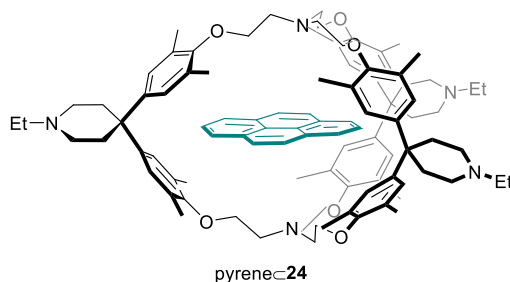


Figure 13. Line-drawing structure of the pyrene²⁴ complex.

partial protonation, delivered water solubility to the corresponding multicationic receptor. The binding pocket of multicationic **24** accommodated polycyclic aromatic hydrocarbons.¹⁰¹ The aromatic guests resided in the plane defined by the three spiro-carbon atoms of the receptor. The pyrene²⁴ inclusion complex was highly stable in water,¹²⁷ $K_a = 6.0 \times 10^6$ M⁻¹ (Figure 13). The HE, dispersion, and dipole-induced-dipole interactions (van der Waals forces) played key roles in achieving the high levels of binding affinity for the inclusion complexes of **24**.

3.2. Pillar[n]arenes

Pillar[n]arenes ($n = 5–10$) are synthesized by the acid-catalyzed condensation of 1,4-dialkoxy-substituted benzenes and paraformaldehyde. The *para*-benzene units are connected at their 2- and 5-positions by methylene bridges in a cyclic fashion (Figure 14a). Therefore, the aromatic panels of pillar[n]arenes having suitable sized substituents can freely rotate around the methylene bridges. This motion is fast on the ¹H NMR chemical shift time scale. The cavity of pillar[n]arenes is electron-rich and hydrophobic, and it is open at two opposite ends to the bulk solution.^{15,17} Pillar[n]arenes are able to accommodate size and shape complementary electron-deficient guests.

Pillar[5]arenes were introduced by Ogoshi, Nakamoto, and co-workers in 2008.¹²⁸ The structure of pillar[5]arene resembles a pentagon featuring a cavity diameter of *ca.* 5 Å (Figure 14a), similar to that of α -cyclodextrin. Pillar[5]arenes **25a** and **25b**, bearing methoxy and hydroxyl substituents, respectively, were soluble in most common organic solvents. Nevertheless, the functionalization of the phenolic OHs with ionizable or charged groups rendered water-soluble pillar[5]arenes.

Water-soluble pillar[5]arenes **26** and **27** were decorated with carboxylate^{129–131} and ammonium¹³² residues, respectively (Figure 14a). These pillar[5]arenes and bigger analogues (pillar[n]arenes, $n = 6–10$)^{131,133} bound charged organic guests in water, giving rise to 1:1 inclusion complexes in most cases. The complexes were stabilized by a combination of the HE, π–π, CH–π, charge-transfer, and Coulombic interactions (see section 2).^{4,69} The charged groups at the portals of the receptor’s cavity were the ones establishing Coulombic interactions with the charged residues of bound guests. For

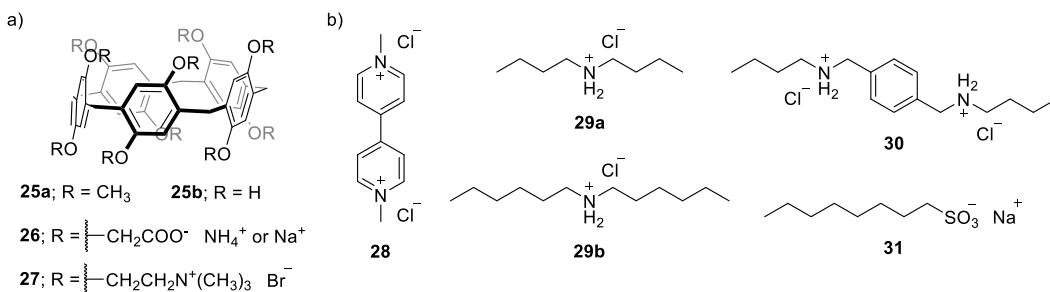


Figure 14. Line-drawing structures of: (a) pillar[5]arenes 25–27 and (b) guest molecules studied with these receptors.

example, the deca-carboxylate pillar[5]arene receptor 26¹⁰⁻ and dimethyl viologen 28²⁺ (Figure 14b) formed a 1:1 inclusion complex featuring a binding constant value $K_a = 8.2 \times 10^4 \text{ M}^{-1}$ in water¹²⁹ (Figure 15). Interestingly, the dicationic

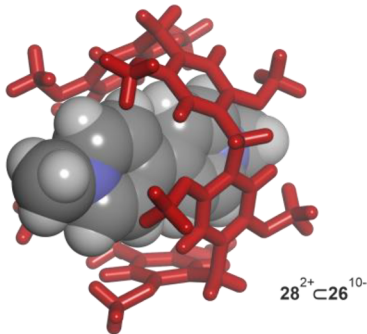


Figure 15. Energy minimized structure (MM3) of the simplified 28²⁺ C 26¹⁰⁻ complex. Pillar[5]arene (in red) is depicted in stick representation. Bound guest is shown as CPK model. The alkyl substituents of the receptor are pruned to methyl groups to simplify the calculation.

guest 28²⁺ threaded the cavity of pillar[5]arene 26¹⁰⁻, featuring a pseudorotaxane-like topology. The inclusion complexes of pillar[5]arenes and 1,4-bis-(pyridinium)butane guests displayed a similar binding geometry.¹³⁰

Dasgupta, Mukherjee, and co-workers investigated the association process of secondary dialkyl ammonium guests 29a,b (Figure 14b) with the deca-carboxylate pillar[5]arene 26¹⁰⁻ in D₂O solution without buffering the solution for pH control.¹³⁴ The analysis of the ¹H NMR titration spectra indicated that the binding process of the receptor, with any of the two guests, experienced fast exchange dynamics on the chemical shift time scale. This is a common feature of cyclic receptors with cavities wide-open at its two ends and featuring stability constants in the range of 10³–10⁵ M⁻¹. One of the N-alkyl substituents of protonated 29a⁺ or 29b⁺ was included in the deca-carboxylate pillar[5]arene's cavity, whereas the other substituent was exposed to the bulk aqueous solution. The ammonium group of the guest was involved in multiple Coulombic interactions with the carboxylate residues at one of the portals of the cavity. The determined association constant values were 5.9 × 10³ M⁻¹ and 2.8 × 10⁴ M⁻¹ for the 29a⁺ C 26¹⁰⁻ and 29b⁺ C 26¹⁰⁻ complexes, respectively.

The larger diammonium guest 30²⁺ (Figure 14b) and deca-carboxylate pillar[5]arene 26¹⁰⁻ formed a 1:2 guest/host complex¹³⁴ (Figure 16). The para-xylene spacer located between the two ammonium cations of 30²⁺ was optimal for the formation of the ternary complex in water. The calculated binding constant values for the first and second binding events,

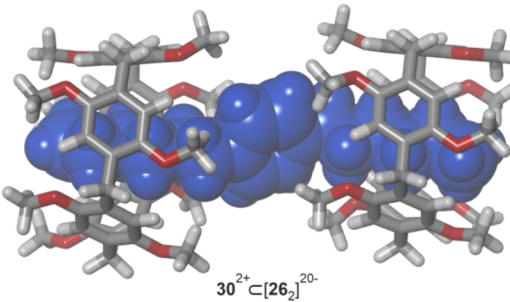


Figure 16. Energy minimized structure (MM3) of the simplified 30²⁺ C [26]²⁰⁻ complex. The pillar[5]arene are depicted in stick representation, and the bound guest (in blue) is shown as CPK model. Terminal carboxylate groups are pruned to hydrogen atoms to simplify the calculations.

$K_{1:1}$ (30^{2+} C 26^{10-}) = $6.2 \times 10^2 \text{ M}^{-1}$ and $K_{1:2}$ (30^{2+} C $26^{10-} \rightleftharpoons 30^{2+}$ C $[26]^{20-}$) = $1.7 \times 10^2 \text{ M}^{-1}$, indicated that the binding process did not show signs of cooperativity ($\alpha = [4 \times K_{1:2}] / K_{1:1} \sim 1$). The lack of binding cooperativity shows that water molecules solvating charged groups may exert large screening effects in their Coulombic interactions. In short, the two copies of receptor 26¹⁰⁻ involved in the 1:2 complex did not display significant repulsive intermolecular Coulombic interactions between the terminal carboxylate groups.

Li, Jia, and co-workers showed that the deca-carboxylate pillar[5]arene 26¹⁰⁻ also bound cationic L-arginine, L-lysine, and L-histidine, forming 1:1 inclusion complexes with moderate-binding affinities ($K_a \sim 10^3 \text{ M}^{-1}$).¹³⁵ The binding selectivity toward these amino acids was remarkable in comparison with other α -amino acids (K_a ca. 20 M⁻¹). The guanidinium, ammonium, and imidazolium cationic groups of the former amino acids established additional Coulombic interactions with the carboxylate residues at the receptor's portal opposite to the one involved in the complexation of the α -ammonium group (see also ethenoanthracene-based cyclophane complexes in section 3.1). This ditopic binding mode was used to explain the observed binding selectivity in favor of the dicationic amino acids.¹³⁶

As discussed above, deca-carboxylate pillar[5]arene 26¹⁰⁻ was a good receptor for positively charged guests, but it did not bind negatively charged counterparts. On the contrary, the deca-trimethylammonium pillar[5]arene 27¹⁰⁺ (Figure 14a) recognized negatively charged guests, such as carboxylic acids and sulfonates. Huang *et al.* reported binding studies of 1-octylsulfonate sodium salt 31 (Figure 14b) with receptor 27.¹³² The 31⁻ C 27¹⁰⁺ complex formed in solution featured an inclusion binding geometry in which the octyl chain of the bound guest was included in the receptor's cavity (Figure 17). The sulfonate group of 31⁻ was then involved in electrostatic

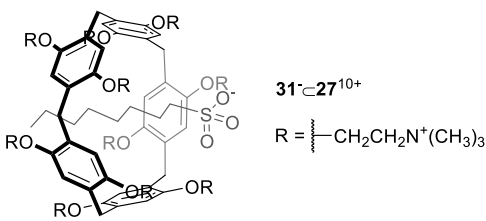


Figure 17. Line-drawing structure of the $31^- \subset 27^{10+}$ inclusion complex.

interactions with the ammonium groups at one of the receptor's portals. The combination of the host–guest interactions involved in $31^- \subset 27^{10+}$ translates into a $K_a = 1.3 \times 10^4 \text{ M}^{-1}$. The magnitude of this constant value was in line with the affinities displayed by the deca-carboxylate receptor 26^{10-} toward cationic guests.^{132,136} Francisco, García-Río and co-workers reported similar examples on the binding properties of 27^{10+} (used as tetrafluoroborate salt instead of bromide) using aromatic sulfonates as guests.^{137,138}

A deca-amine pillar[5]arene acted as a wheel or cyclic component in the formation of 1:1 complexes with long-chain α,ω -diacids in water, as shown by Yu, Hou, and co-workers.¹³⁹ The aliphatic chain of the bis-carboxylates threaded the aromatic cavity of the pillar[5]arene. The complex formation was driven by the HE and the establishment of multiple CH– π interactions. In addition, the ionized carboxylic acids (carboxylates) of the guests and the cationic primary ammonium groups at the portals of the host were involved in Coulombic interactions. In general, the binding constants of the dicarboxylate \subset [pillar[5]arene+nH] $^{n+}$ complexes were in the order of 10^4 M^{-1} .

Huang *et al.* also investigated the binding properties of the deca-trimethylammonium receptor 27^{10+} using a series of neutral guests (alkanes, aliphatic alcohols, xylenes, etc.) in water.¹⁴⁰ The complexation of neutral substrates by the pillar[5]arenes is driven by the HE, π – π , CH– π , and dispersion (*i.e.*, van der Waals) interactions. The binding constant values of the latter complexes were in the order of 10 – 10^2 M^{-1} . Most likely, the reduction in binding constant values resulted from the lack of Coulombic interactions between host and guest. As expected for the HE being the main component driving the binding process, the association constant values for aliphatic alcohols increased with the length of the alkyl chain: *n*-pentanol > *n*-butanol > *n*-propanol.

Pillar[6]arene possesses an hexagonal cavity with a diameter of *ca.* 6.7 Å. The cavity size is slightly larger than that of β -cyclodextrin. Water-soluble pillar[6]arenes **32**–**35** were functionalized with carboxylate, pyridinium, trimethylammonium, and 1-methyl-1*H*-imidazolium groups,¹⁷ respectively (Figure 18a). Huang *et al.* reported pillar[6]arene **32** featuring a cmc value of *ca.* 10^{-4} M .¹⁴¹ The binding studies of receptor **32** were performed in dilute water solutions and monitored using UV/vis and fluorescence spectroscopies. Dodeca-carboxylate pillar[6]arene **32**¹²⁻ bound pyridinium cations, in agreement with the previous results discussed for the deca-carboxylate pillar[5]arene **26**¹⁰⁻ having a reduced cavity size. The binding constant value of the $36^+ \subset 32^{12-}$ inclusion complex between 1-octylpyridinium **36**⁺ (Figure 18c) and pillar[6]arene **32**¹²⁻ was determined to be $3.3 \times 10^5 \text{ M}^{-1}$ in aqueous solution (Table 4). The high binding constant value displayed by the latter complex is derived from the Coulombic interactions established between the pyridinium cation of the guest and the carboxylate residues at one of the host's portals as well as the establishment of multiple host–guest CH– π and π – π interactions (see section 2). Pillar[6]arene **32**¹²⁻ also formed thermodynamically highly stable 1:1 inclusion complexes with α,ω -long-chain aliphatic guests bearing a pyridinium cation at one end and a pyrene unit at the opposite one ($K_a \sim 10^5 \text{ M}^{-1}$). The bound guests were threaded through the cavity of **32**¹²⁻. As described above, the terminal pyridinium cation established Coulombic interactions with the carboxylate residues of one of the host's portals, whereas the terminal pyrene unit remained exposed to the bulk solution through the opposite host's portal.

The cationic *trans*-azobenzene **37**⁺ (Figure 18b) was nicely included in the aromatic cavity of pillar[6]arene **32**¹²⁻ (Figure 19). In contrast, pillar[6]arene **32**¹²⁻ was not able to accommodate the *cis*-conformation of the diphenyl-azo group of **37**⁺.¹⁴² Alternatively, *cis*-**37**⁺ formed an inclusion complex with **32**¹²⁻ by including its trimethylammonium group in the receptor's cavity (Figure 19). The *cis*-**37**⁺ \subset **32**¹²⁻ complex was stabilized mainly by establishing cation– π and CH– π interactions between the ammonium group of the guest and the electron-rich aromatic panels of the receptor. The different binding modes of the two complexes, *trans*-**37**⁺ \subset **32**¹²⁻ and *cis*-**37**⁺ \subset **32**¹²⁻, translated in 1 order of magnitude difference between their corresponding stability constant values, favoring the complexation of *trans*-**37**⁺ (Table 4).

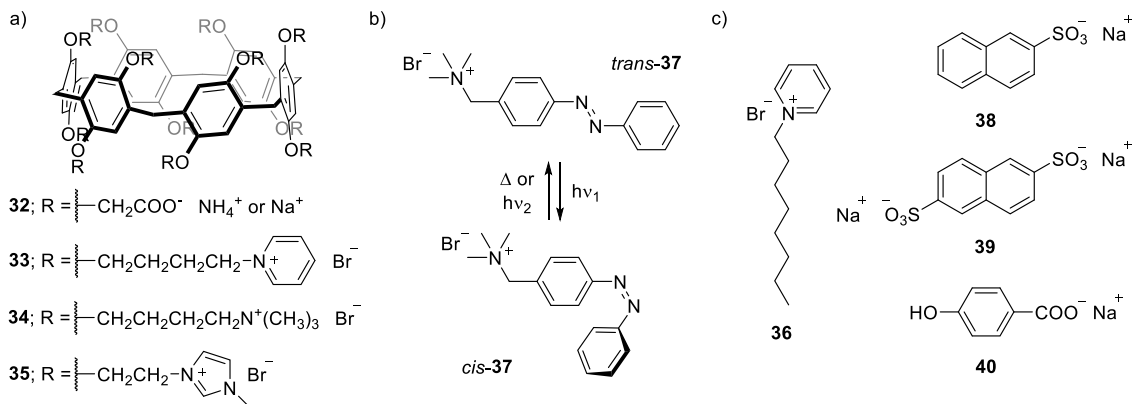


Figure 18. Line-drawing structures of: (a) pillar[6]arenes **32**–**35**, (b) *trans*/*cis* isomers of azobenzene **37**, and (c) compounds **36** and **38**–**40** used as guest molecules for the pillar[6]arene receptors.

Table 4. Binding Constant Values (K_a , M $^{-1}$) of Selected Pillar[n]arene Complexes Formed in Water Solution^a

	Pillar[5]arenes		Pillar[6]arenes			
	26 ¹⁰⁻	27 ¹⁰⁺	32 ¹²⁻	33 ¹²⁺	34 ¹²⁺	35 ¹²⁺
Guests	Binding constant, K_a					
	8.2×10^4					
	5.9×10^3					
	2.8×10^4					
		1.3×10^4				
			3.3×10^5			
			4.1×10^5			
			5.9×10^4			
				3.8×10^4	2.5×10^4	
				2.1×10^5		
						3.2×10^6
			1.9×10^7			

^aSee Figure 14 and Figure 18 for the line-drawing structures of the receptors and the text for details.

Jia, Li and co-workers reported pillar[6]arene 33 decorated with 12 pyridinium cations (Figure 18a), which imparted receptor's water solubility.¹⁴³ The authors investigated the binding of dodeca-pyridinium 33¹²⁺ with naphthalenesulfonates, 38⁻ and 39²⁻ (Figure 18c), in phosphate buffer at pH = 7.2. The upfield complexation-induced shifts ($\Delta\delta$) experienced by the aromatic protons of the bound guests were in the range of -0.3 to -0.5 ppm. This indicated that the naphthalene group of the guests was included in the aromatic cavity of the receptor. The binding constant values of the 38⁻ C 33¹²⁺ and 39²⁻ C 33¹²⁺ inclusion complexes were calculated as 3.8×10^4 and 2.1×10^5 M $^{-1}$, respectively, by means of fluorescence titration experiments. The binding constant of 39²⁻ C 33¹²⁺ was

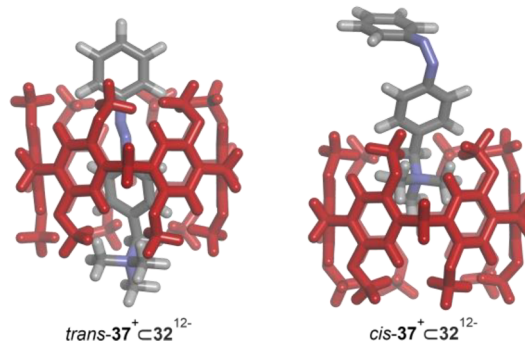


Figure 19. Energy minimized structures (PM3, water COSMO model as implemented in SCIGRESS version FJ2.4x) of the simplified *trans*-37⁺ C 32¹²⁻ and *cis*-37⁺ C 32¹²⁻ complexes. The host (in red) and the guest are depicted in stick representation. Alkyl substituents of 32¹²⁻ are pruned to methyl groups to simplify the calculations.

almost 1 order of magnitude larger than that of 38⁻ C 33¹²⁺. This result was explained considering the additional Coulombic interactions (ditopic interaction) established between the extra sulfonate group present in 39²⁻ and the cationic pyridinium groups at the receptor's portals (Figure 20). As could be expected, the analogous dodeca-trimethyl-

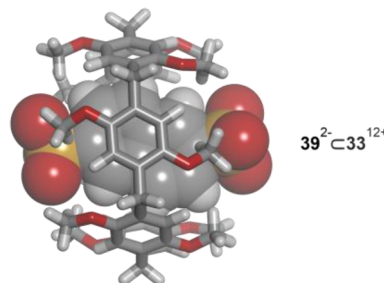


Figure 20. Energy minimized structure (MM3) of the simplified 39²⁻ C 33¹²⁺ complex. The host is depicted in stick representation and the guest is shown as CPK model. The alkyl substituents of the receptor are pruned to methyl groups to simplify the calculations.

lammonium pillar[6]arene 34¹²⁺ (Figure 18a) reported by Xue *et al.* complexed the naphthalenesulfonate 38⁻ featuring a binding constant value similar to that of the 38⁻ C 33¹²⁺ complex.¹⁴⁴

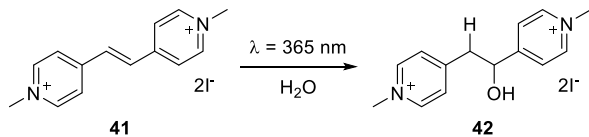
Xue *et al.* also reported binding studies between the sodium salt of 4-hydroxybenzoate 40 (Figure 18c) and dodeca-bromide dodeca-imidazolium pillar[6]arene 35 (Figure 18a) using fluorescence spectroscopy.¹⁴⁵ The binding constant value of the 40⁻ C 35¹²⁺ complex was determined to be 3.2×10^6 M $^{-1}$ (Table 4). The authors suggested that, in the 40⁻ C 35¹²⁺ inclusion complex, ionic hydrogen-bonding interactions (see salt-bridges in section 2) were established between the carboxylate group of the bound guest and the hydrogen atom of the imidazolium cations, NCHN⁺, at one of the two portals of the receptor's cavity.

Recently, Isaacs *et al.* reported the synthesis and binding properties of a family of sulfated pillar[n]arenes ($n = 5-7$).¹⁴⁶ The design of these pillar[n]arenes consisted on the elimination of the methylene groups between the oxygen atoms of the *para*-benzene rings and the carboxylate groups, as well as the replacement of the latter to give sulfate groups. The sulfate groups provided a highly charge density around the portals of the receptors. The sulfated pillar[n]arenes ($n = 5-6$)

demonstrated to be more efficient, in most of the cases, toward the binding of quaternary ammonium guests than the carboxylate pillar[*n*]arenes **26**¹⁰⁻ and **32**¹²⁻ discussed above.

Pillar[6]arenes have potential applications in many fields.¹³⁶ For example, Xia, Shi, and co-workers applied the dodeca-carboxylate pillar[6]arene **32**¹²⁻ (Figure 18a) for the protection of azastilbene **41**²⁺ in water solution¹⁴⁷ (Scheme 1). Azastilbene **41**²⁺ underwent hydration upon photo-

Scheme 1. Photohydration Reaction of Azastilbene **41** to give **42**



irradiation at 365 nm in water, producing adduct **42**²⁺. Nevertheless, in the presence of receptor **32**¹²⁻, the concentration of azastilbene **41**²⁺ free in water solution was significantly reduced, K_a (**41**²⁺||**32**¹²⁻) = 1.9×10^7 M⁻¹. This provoked a dramatic decrease of the photohydration reaction rate. Thus, the pillar[6]arene **32**¹²⁻ functioned as a supramolecular protecting group for the photolabile guest **41**²⁺, presumably absorbing the high-energy photons from the light source or increasing the energy of the hydration-reaction transition state of the included guest.

3.3. Cucurbit[n]urils

The condensation reaction of glycoluril and its derivatives with formaldehyde in acidic media produces cyclic and acyclic cucurbit[*n*]urils.^{148–150} The cyclic cucurbit[*n*]urils (*n* = 5–8, **43**–**46**) feature a pumpkin-like structure, in which the glycoluril units are linked together by 2 × *n* methylene bridges (Figure 21). In contrast to the pillar[*n*]arenes (section 3.2), the glycoluril units cannot freely rotate around the methylene junctions of the cucurbit[*n*]urils, leading to conformationally rigid receptors' structures. All cyclic cucurbit[*n*]urils display a cavity depth of *ca.* 9.1 Å, but they have different cavity diameters. The cavity volume of the cyclic cucurbit[*n*]urils

varies from 82 (**43**, *n* = 5, CB5) to 479 Å³ (**46**, *n* = 8, CB8) (Figure 21).

There are also many examples of acyclic glycoluril-based receptors reported by Isaacs, Wang, and co-workers. However, these tweezer-like receptors are outside of the scope of this review and the interested reader is referred to other literature references.^{15,151–156}

The cyclic cucurbit[*n*]urils feature a hydrophobic cavity with two polar and open ends. The two portals of the cavity are defined by the carbonyl groups of the glycoluril components.¹⁴⁸ The carbonyl groups of these receptors are keen to be involved in dipole-mediated interactions with complementary functional groups of the bound guests.^{69,150} The interior of the cucurbit[*n*]uril receptors is suitable for the inclusion of nonpolar residues. The internal surface of the cucurbit[*n*]urils' cavity displays a reduced polarizability. In this sense, the molecules included in the cavity experience an environment that is comparable to the gas phase.² Owing to their symmetry, cucurbit[*n*]urils possess a large quadrupole moment, which may be relevant for the arrangement of included dipolar and quadrupolar molecules as well as for the packing that they adopt in the solid state.¹⁵⁷

The solubility of the cucurbit[*n*]uril derivatives **43**–**46** in pure water is different.¹⁴⁹ Cucurbit[6]uril **44** and cucurbit[8]-uril **46** are poorly soluble (<10⁻⁴ M), whereas cucurbit[5]uril **43** and cucurbit[7]uril **45** possess good solubility in water (2–3 × 10⁻³ M) (Figure 21). Studies in the solid state showed that cucurbit[6]uril **44** and cucurbit[8]uril **46** self-associated more efficiently than cucurbit[5]uril **43** or cucurbit[7]uril **45** by intermolecular CH···O interactions (methylene and methine hydrogen atoms and carbonyl oxygen atoms).¹⁵⁸ This may explain the more favorable solvation of CB5 **43** and CB7 **45** compared to that of CB6 **44** and CB8 **46**. It is worth mentioning that the referred cucurbit[*n*]uril derivatives are neutral receptors and their water solubility is mainly imparted by the polar ureido groups at the portals. The protonation or coordination with alkali ions of their carbonyl oxygen atoms increases the solubility of cucurbit[*n*]urils in water.^{136,148}

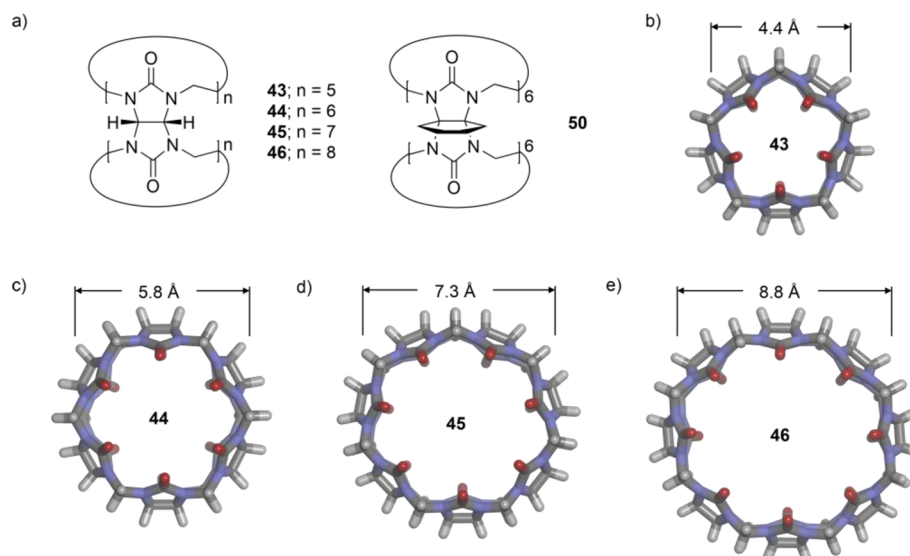


Figure 21. (a) Line-drawing structures of cucurbit[*n*]urils (*n* = 5–8) **43**–**46** and **50**; energy minimized structures (MM3) of: (b) **43**, (c) **44**, (d) **45**, and (e) **46**. The structures are depicted in stick representation and the diameter of the cavities is indicated.

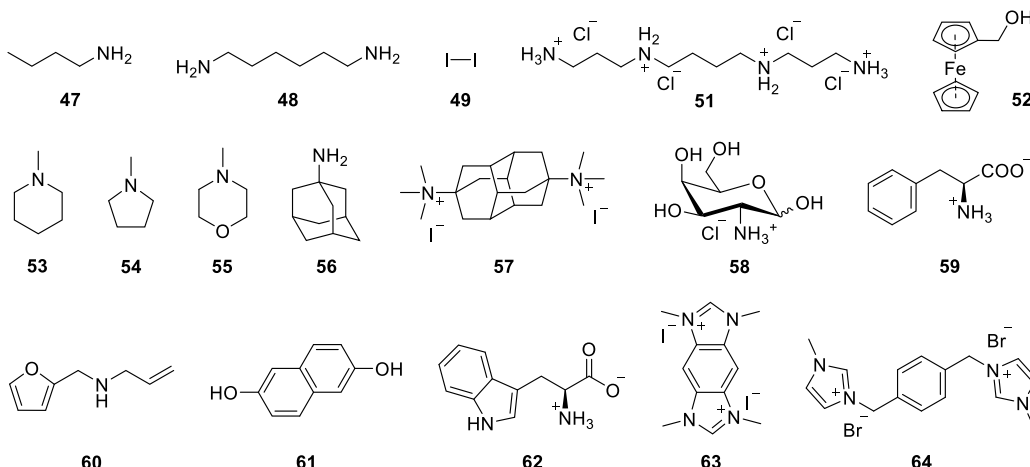


Figure 22. Line-drawing structures of a series of compounds studied as guest molecules for the binding with cucurbit[*n*]urils (*n* = 6–8) receptors.

In general, the inclusion complexes of cucurbit[*n*]urils 43–46 with nonpolar or positively charged guests are kinetically stable (*i.e.*, chemical exchange between free and bound components is slow on the ^1H NMR chemical shift time scale). Most likely, their kinetic stability is derived from the small diameter of the portals (*ca.* 2 Å less) with respect to that of the internal cavity.^{136,148} The in/out exchange processes of the guests display high-energy barriers even for complexes not thermodynamically highly stable.

The complexes of cucurbit[n]urils with cationic guests are characterized by association constant values that are 3 orders of magnitude larger than those with structurally related neutral guests.⁶⁹ This increase in thermodynamic stability results from the additional stabilization of the charged complexes by means of cation–dipole interactions.¹⁵⁹ The complexation process of size and shape complementary guests with cucurbit[n]urils (CBs) is driven by the “nonclassical” hydrophobic effect (*i.e.*, enthalpically driven binding process) and the difference in dispersion interactions of the complex (polarizable bound guest in the nonpolarizable interior of the cyclic host) with those present in the hydrated partners free in solution.⁶⁹ The origin of the binding enthalpy using cucurbit[n]uril receptors was attributed to the release of “high-energy” water molecules from the receptor’s cavity to the bulk solution upon complexation.^{68,69} The “nonclassical” hydrophobic effect is maximized in the case of cucurbit[7]uril 45, for which the number of bound water molecules in the cavity that cannot satisfy their hydrogen-bonding characteristics is supposed to be modest.^{68,69} Despite the fact that the cavity featured by cucurbit[n]urils is open at its two ends, their inclusion complexes seem to obey the 55% packing coefficient rule introduced by Rebek and co-workers.¹⁶⁰

In general, cucurbit[5]uril 43 binds small molecules and noble gases, whereas cucurbit[6]uril 44 is able to accommodate aliphatic residues. The larger cavities provided by cucurbit[7]uril 45 and cucurbit[8]uril 46 can accommodate even aromatic guests.¹⁵⁰

In particular, cucurbit[5]uril **43** displays a small cavity volume (83 \AA^3) limiting the number of complementary guests. For example, **43** bound neutral small molecules, such as methanol and acetonitrile, diatomic gases (e.g., N_2 , O_2 , CO and CO_2) and noble gas atoms (e.g., Ar).^{149,150} Owing to the polar character of the cavity portals, **43** also formed *endo*-complexes with either inorganic or organic cations, such as Pb^{2+} or

ammonium salts, respectively. The bound cationic guests served to seal the hydrophobic cavity of cucurbit[5]uril 43. Recently, Biedermann, Vankova, Heine, Duignan, Nau, and co-workers demonstrated that the binding process of noble gases to cucurbit[5]uril 43 was driven by differences in cavitation energies,⁸¹ *i.e.*, the recovery of the formed void cavities in the bulk aqueous solution by inclusion of the solvated guest in the receptor's binding site (see section 2.1).

Cucurbit[6]uril **44** features a cavity diameter of 5.8 \AA ¹⁴⁸ (Figure 21). In the solid state, three water molecules are included in the cavity of **44**.¹⁴⁹ Most likely, the cavity of the receptor is also solvated in water solution. The bound water molecules are released to the bulk solution upon guest binding. Aliphatic mono- and diammonium cations were bound by **44**, producing 1:1 inclusion complexes.^{148–150} For example, Mock and Shih showed that the alkyl chain of protonated *n*-butyl amine, $[47+\text{H}]^+$ (Figure 22), was a perfect fit for the cavity volume of **44** and, therefore, it formed the most stable complex of the *n*-alkyl ammonium series, $K_a([47+\text{H}]^+ \cap \text{C}44) = 1.0 \times 10^5 \text{ M}^{-1}$.^{161,162} For alkyl diammonium salts, hexane-1,6-diammonium $[48+2\text{H}]^{2+}$ (Figure 22) was also a good fit for receptor **44**.¹⁶¹ Thus, $[48+2\text{H}]^{2+}$ threaded through the cavity of the cucurbit[6]uril. This binding geometry placed the two ammonium groups of the guest near the two opposite polar portals of the receptor rendering a 1:1 host/guest ditopic binding with a stability constant of $K_a([48+2\text{H}]^{2+} \cap \text{C}44) = 2.8 \times 10^6 \text{ M}^{-1}$ (Figure 23). The 1:1 inclusion complexes were stabilized by the combination of the HE, ion–dipole, and hydrogen-bonding (dipole–dipole) interactions (see section

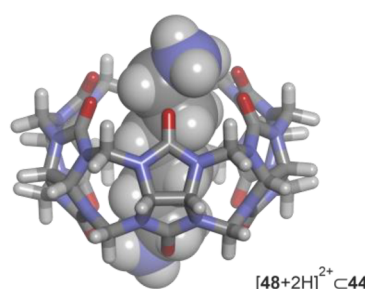


Figure 23. Energy minimized structure (MM3) of the $[48+2H]^{2+} \subset C44$ inclusion complex. The cucurbit[6]uril is depicted in stick representation, and the bound guest is shown as CPK model.

Table 5. Binding Constant Values (K_a , M⁻¹) of Selected Inclusion Complexes of Cucurbit[n]uril Receptors (CBn; n = 6–8) Formed in Water Solution^a

Cucurbit[n]urils			Cucurbit[n]urils				
	CB6 44	CB7 45	CB8 46		CB6 44	CB7 45	CB8 46
Guests	Binding constant, K_a			Guests	Binding constant, K_a		
 17 ^{+,163,175}		1.7×10^{12}		 [56+H] ^{+,175}		4.2×10^{12}	
 28 ^{2+,182,191}		1.0×10^5	8.5×10^5	 57 ^{2+,176}		7.2×10^{17}	
 [47+H] ^{+,163}	9.1×10^5			 58 ^{+,177}		1.6×10^4	
 THF ¹⁶⁵	1.7×10^3			 [59+H] ^{+,178}		1.2×10^6	
 I-I	1.4×10^6			 Tyr-Leu-Ala ¹⁸⁷			1.4×10^8
 52 ¹⁷³		3.0×10^9		 53 ^{2+,188}			2.9×10^4
 [53+H] ^{+,174}		5.0×10^7		 63 ^{2+,188}			5.7×10^5
 [54+H] ^{+,174}		7.8×10^6		 64 ^{2+,189}			1.9×10^6
 [55+H] ^{+,174}		2.3×10^6					

^aSee Figure 21 for the line-drawing structures of the receptors. Details on the pH used in the binding experiments are provided in the text.

2). It is worth mentioning that, owing to the low solubility of **44** in pure water, the above-described inclusion complexes were formed in a 1:1 formic acid/water solution mixture. Remarkably, Inoue, Kim, and co-workers showed that the binding constant value of the $[47+\text{H}]^+ \leftarrow \text{C}44$ complex determined in a 5×10^{-2} M aqueous NaOAc buffer at pH ~ 4.7 displayed an analogous magnitude¹⁶³ (Table 5). Cucurbit[6]uril **44** also complexed neutral molecules with good binding affinities. For example, Kim *et al.* and Bartik *et al.* independently reported the complexation of tetrahydrofuran by **44** featuring a binding constant value of $K_a = 1.7 \times 10^3 \text{ M}^{-1}$ in water.^{164,165}

Recently, Nau *et al.* reported the binding of di-iodine 49 (Figure 22) with cucurbit[6]uril 44.¹⁶⁶ The corresponding 1:1 inclusion complex, 49 \subset 44, featured a large association constant value, $K_a = 1.4 \times 10^6 \text{ M}^{-1}$. The complex was

stabilized mainly by the HE. Interestingly, halogen-bonding interactions (see section 2) between the iodine atoms of bound **49** and the π -system of the carbonyl groups of **44** were also claimed to be important and responsible of the tilted orientation observed for the bound guest (Figure 24).

As mentioned above for cucurbit[5]uril 43, inorganic cations were also bound to the polar C=O groups at the cavity portals of 44.¹⁴⁹ The binding constant value of the latter complexes were determined to be in the order of $10^2\text{--}10^3\text{ M}^{-1}$. This result suggested that inorganic cations could interfere in the formation of the inclusion complexes.

Cucurbit[6]uril 44 was applied in the self-assembly of (pseudo)rotaxanes¹⁶⁷ and in the assistance of chemical transformations, yielding rotaxanes.¹⁶⁸ For example, 44 catalyzed the 1,3-dipolar cycloaddition of alkynes and azides, aka “click” reaction, in water¹⁶⁹ (Scheme 2). Both terminal

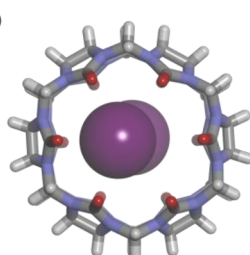
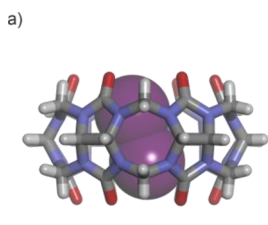


Figure 24. X-ray structure of the **49C44** complex (CCDC 869027): (a) side and (b) top views. The receptor is depicted in stick representation, and I_2 guest is shown as CPK model.

alkyne and azide guests, bearing ammonium groups at the distal ends of their short alkyl chains, formed inclusion complexes with **44**. The use of **44** in catalytic amounts induced an acceleration in the formation of the corresponding triazole and rendered the reaction regioselective (1,4-isomer exclusively formed). Mock *et al.* rationalized the obtained results by the transient formation of a 2:1 ternary heterocomplex.¹⁶⁹ In this complex, the reacting groups of the two guests were included in the hydrophobic cavity of the receptor, leading to an increase in local concentration and a putative compression of reactants.¹⁷⁰ The latter effect might destabilize the ground-state energy with respect to that of the transition state, thus reducing the reaction's energy barrier.¹⁷¹ Unfortunately, the use of cucurbit[6]uril **44**, as catalyst suffered of product inhibition. This issue is very common in the use of supramolecular containers for the acceleration of chemical reactions.

One of the main limitations of the use of cucurbit[6]uril **44** is its low solubility in water. To overcome it, Inoue, Kim, and co-workers designed the cyclohexyl-substituted cucurbit[6]uril **50**, whose solubility is 0.2 M in water¹⁶³ (Figure 21a). The cavity size of **50** was analogous to that of **44**. However, the binding constant values of the inclusion complexes of **50** in pure water were 2–5 orders of magnitude larger than those reported for **44**, either in a 1:1 formic acid/water mixture or salt solution. For example, the complexes between aliphatic monoammonium guests and **50** featured binding constant values in the range of $K_a = 10^4\text{--}10^8\text{ M}^{-1}$. In the same vein, the binding constants of α,ω -aliphatic diammonium salts increased up to $10^7\text{--}10^{10}\text{ M}^{-1}$. For example, the tetra-protonated spermine **51**⁴⁺ (Figure 22) formed a thermodynamically highly stable complex with **50** featuring a binding constant value of $3.4 \times 10^{12}\text{ M}^{-1}$ in pure water (Figure 25).

Cucurbit[7]uril **45**, featuring a cavity volume of 279 \AA^3 (Figure 21), constitutes a paradigmatic example of the “nonclassical” HE for binding owing to the large magnitudes of the enthalpic term measured for its complexation.^{2,149,172} The association constant values of the 1:1 inclusion complexes derived from **45** were in the range of $10^7\text{--}10^{17}\text{ M}^{-1}$. Cucurbit[7]uril **45** complexed neutral and charged guests, such as aromatic, adamantane, and ferrocene derivatives.

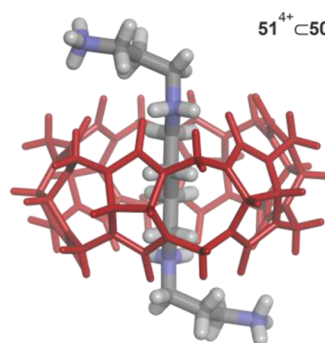


Figure 25. Energy minimized structure (MM3) of the simplified **51**⁴⁺**50** complex. The host (in red) and the guest are depicted in stick representation. The cyclohexane groups of **50** are pruned to hydrogen atoms to simplify the calculation.

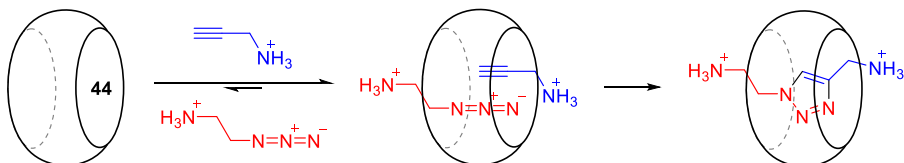
Inoue, Kaifer, Kim, and co-workers showed that neutral ferrocene **52** (Figure 22) was bound by cucurbit[7]uril **45** with high affinity, $K_a = 3.0 \times 10^9\text{ M}^{-1}$ in water at neutral pH.¹⁷³ The ferrocene guest **52** nicely filled the cavity volume of the receptor. Additionally, the binding constants of complexes of **45** with ferrocene derivatives decorated with ammonium groups were boosted up to values of $10^{12}\text{--}10^{15}\text{ M}^{-1}$.^{2,136} These results evidenced the significant role played by the cation–dipole interactions in the formation of supramolecular complexes derived from cucurbit[n]uril receptors.

Gamal-Eldin and Macartney investigated the complexation of the protonated tertiary amines *N*-methyl piperidine [**53**^{+H}]⁺, *N*-methyl pyrrolidine [**54**^{+H}]⁺, and *N*-methyl morpholine [**55**^{+H}]⁺ (Figure 22), to cucurbit[7]uril **45** in $5 \times 10^{-2}\text{ M}$ NaOAc buffer at pH ~ 4.7 .¹⁷⁴ The binding constant values of these 1:1 complexes were in the order of $10^6\text{--}10^7\text{ M}^{-1}$ (Table 5). Interestingly, the analysis of the ¹H NMR spectra of equimolar mixtures of host and guest supported the inclusion of the bound ammonium cation in the hydrophobic cavity of receptor **45**.

Cucurbit[7]uril **45** also included protonated amino-adamantane derivatives featuring $K_a = 10^{12}\text{--}10^{14}\text{ M}^{-1}$ in water.¹⁷⁵ The adamantane group was a perfect fit for the cavity of receptor **45**. In these cases, the adamantane group was buried in the receptor's cavity while the ammonium group remained exposed to the bulk solution¹⁵ (see ethenoanthracene-based cyclophanes in section 3.1 for a different binding geometry). The latter was involved in cation–dipole interactions with the carbonyl groups at one of the two polar portals of the receptor.⁴ Isaacs *et al.* reported the accurate binding constant values of the complexes of adamantane trimethylammonium **17**⁺ (Figure 5) and protonated amino-adamantane [**56**^{+H}]⁺ (Figure 22) with **45** as $1.7 \times 10^{12}\text{ M}^{-1}$ and $4.2 \times 10^{12}\text{ M}^{-1}$, respectively, in aqueous buffer solution at pH ~ 4.7 .

The understanding of the driving forces involved in the binding equilibria of cucurbit[7]uril **45** was key in the design

Scheme 2. “Click” Reaction Catalyzed by Cucurbit[6]uril **44**



of efficient guests. Mlinarić-Majerski, Glaser, Isaacs, and co-workers measured a binding constant value of $K_a = 7.2 \times 10^{17} \text{ M}^{-1}$ in pure water, and $K_a = 1.9 \times 10^{15} \text{ M}^{-1}$ in $5 \times 10^{-2} \text{ M}$ NaOAc buffer for the 1:1 inclusion complex between diamantane diammonium 57^{2+} (Figure 22) and cucurbit[7]uril 45.¹⁷⁶ It is important to remember here that ions, *i.e.*, Na^+ , compete with guest binding to the dipoles of the carbonyl groups at the portals of cucurbit[n]urils. The crystal structure of the $57^{2+}\subset 45$ complex showed that the two ammonium cations of 57^{2+} established a total of 14 cation–dipole interactions with the carbonyl groups of the receptor (Figure 26). Furthermore, dicationic diamantane derivative 57^{2+} and

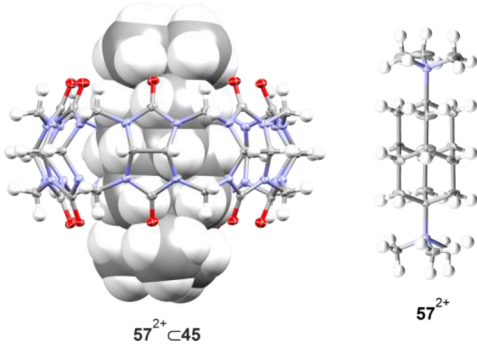


Figure 26. X-ray crystal structures of $57^{2+}\subset 45$ (left, CCDC 969769) and 57^{2+} (right). The structures are shown in ORTEP view with thermal ellipsoids set at 50% probability. Hydrogen atoms are shown as fixed-size spheres of 0.3 Å radius. Bound guest is shown as CPK model.

cucurbit[7]uril 45 were size and shape complementary, maximizing nonpolar contacts. The inclusion of the nonpolar section of 57^{2+} into the hydrophobic cavity of 45 was an enthalpically driven process. On the contrary, the interaction of ammonium cations with the carbonyl groups of the receptor was mainly favored by entropy.^{2,136}

The thermodynamic data, described by several research groups, for the complexation processes of cucurbit[7]uril 45, suggested that the increase in the number of cationic groups attached to the guest's scaffold did not impact on the enthalpic contribution to complex formation (*ca.* $-88 \text{ kJ}\cdot\text{mol}^{-1}$). In contrast, the overall charge ($z = +1$, *e.g.*, monoammonium ferrocene) of the guest had a significant influence on the entropic component by favoring the binding process (change of *ca.* $17 \text{ kJ}\cdot\text{mol}^{-1}$).² Thus, some inclusion complexes with cucurbit[7]uril 45 seemed to overcome the typically observed enthalpy–entropy compensation effect, as shown by Kaifer, Isaacs, Gilson, Kim, Inoue, and co-workers.¹⁷²

Furthermore, Natarajan, Kim, and co-workers demonstrated that receptor 45 was able to bind protonated amino-saccharides, such as D-galactosamine hydrochloride 58^+ (Figure 22), with good binding affinity (Table 5).¹⁷⁷ It is worth mentioning here that the α/β -mutarotation of saccharides is slow on the ^1H NMR chemical shift time scale and the α/β ratio at equilibrium in water solution is *ca.* 63:37 for protonated 58^+ . The results of 2D NMR experiments demonstrated that the α -anomer of the monosaccharide 58^+ was preferentially bound by 45. Most likely, the α -anomer was involved in energetically more favorable cation–dipole interactions⁴ when bound in the cavity of cucurbit[7]uril (Figure 27a).

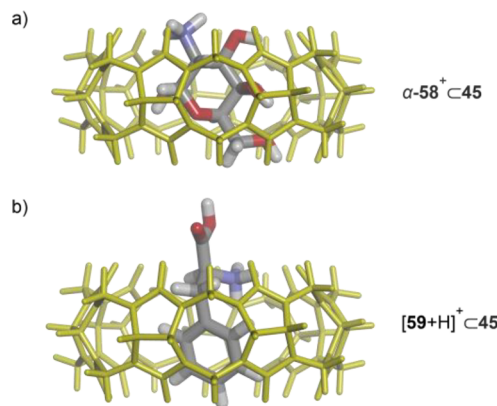


Figure 27. Energy minimized structures (MM3) of: (a) $\alpha-58^+\subset 45$ and (b) $[59+\text{H}]^+\subset 45$. The cucurbit[7]uril 45 (in yellow) and the guests are depicted in stick representation.

Owing to the excellent binding performance of cucurbit[7]uril 45 toward ammonium guests, the binding properties of the receptor were also investigated in the recognition of aromatic amino acids in acidic aqueous solution. In this respect, the aromatic residue of the amino acid was included in the hydrophobic cavity of 45, and the ammonium group interacted electrostatically with the carbonyl groups of one of the receptor's polar portals. The binding constant of the amino acid complexes were high. For example, L-phenylalanine 59 (Figure 22) and cucurbit[7]uril 45 formed a 1:1 complex, $[59+\text{H}]^+\subset 45$, featuring a stability constant of $K_a = 1.2 \times 10^6 \text{ M}^{-1}$ in phosphoric acid buffer at pH = 2¹⁷⁸ (Figure 27b). More interestingly, cucurbit[7]uril 45 displayed a modest binding selectivity for L-phenylalanine over other aromatic amino acids.

Cucurbit[7]uril 45 was also applied in supramolecular catalysis. Masson, Scherman, and co-workers investigated the effect of 45 in the intramolecular Diels–Alder reaction of *N*-allyl-2-furfurylamines,¹⁷⁹ such as **60** (Figure 22 and Figure 28a). In the absence of the receptor, **60** reacted to produce the corresponding Diels–Alder product in less than 10% yield after 25 days. In contrast, the yield of the reaction increased up to 90% in only 6 h when cucurbit[7]uril 45 was added to the solution in catalytic amounts. The cucurbit[7]uril 45 complexed the protonated reactant, $[60+\text{H}]^+$, in a hairpin-like conformation. In this conformation, the diene and the

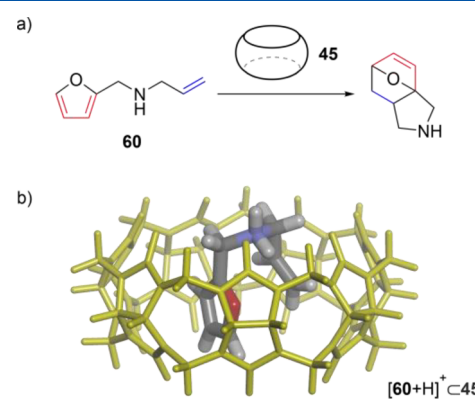


Figure 28. (a) Diels–Alder reaction of *N*-allyl-2-furfurylamine **60** and (b) energy minimized structure (MM3) of $[60+\text{H}]^+\subset 45$. The host (in yellow) and the guest are depicted in stick representation.

dienophile groups were in close proximity (Figure 28b). The stabilization of the bound reactant in this high-energy conformation decreased the energy barrier of the intramolecular Diels–Alder reaction.

Cucurbit[*n*]urils 43–45 (CB5, CB6, CB7) do not form inclusion complexes of stoichiometry larger than 1:1 due to the limited dimensions of their cavities, with a few exceptions. On the other hand, cucurbit[8]uril 46 with a cavity diameter of 8.8 Å (Figure 21) enables the formation of homoternary, 2:1, and heteroternary, 1:1:1, inclusion complexes.¹⁵

Cucurbit[8]uril 46 and the electron-deficient dimethyl viologen 28^{2+} (Figure 14b) formed a 1:1 inclusion complex stabilized by the HE and cation–dipole interactions, as shown by Kim and co-workers.¹⁸⁰ Kim *et al.*¹⁸¹ and Urbach *et al.*¹⁸² independently reported that the binding constant value of the $28^{2+}\subset 46$ complex was in the order of 10^5 M^{-1} in phosphate buffer at pH = 7 ($K_a = 1.1 \times 10^5\text{ M}^{-1}$ in 0.5 M phosphate buffer by UV–vis spectroscopy titrations and $K_a = 8.5 \times 10^5\text{ M}^{-1}$ in 10^{-2} M phosphate buffer by ITC experiments). Dimethyl viologen 28^{2+} filled approximately half of the cavity of 46 and, therefore, the remaining free space was similar to the cavity size of cucurbit[7]uril 45. Most likely, repulsive Coulombic interactions disfavored the binding of a second viologen molecule in the cavity of the $28^{2+}\subset 46$ complex. Conversely, the addition of the neutral, electron-rich 2,6-dihydroxynaphthalene 61 (Figure 22) to the $28^{2+}\subset 46$ complex provoked the quantitative formation of the heteroternary $[61\cdot28^{2+}]\subset 46$ complex¹⁸⁰ (Figure 29). The coinclusion of 28^{2+}

cavity of $28^{2+}\subset 46$ was calculated as K_a ($28^{2+}\subset 46 \rightleftharpoons [62\cdot28^{2+}]\subset 46$) = $4.3 \times 10^4\text{ M}^{-1}$ in 10^{-2} M sodium phosphate buffer at pH = 7. The binding process was enthalpically driven, $\Delta H = -44.3\text{ kJ}\cdot\text{mol}^{-1}$, and opposed by entropy, $T\Delta S = -17.6\text{ kJ}\cdot\text{mol}^{-1}$. At r.t., the thermodynamic parameters were consistent with the so-called “nonclassical” hydrophobic effect operating in the formation of this and other structurally related inclusion complexes (see HE in section 2.1). The preassembled $28^{2+}\subset 46$ complex also recognized with high affinity and selectively the L-tryptophan residue at the N-terminal position of L-tryptophan-containing tripeptides over those incorporated at the internal position or the C-terminus.¹⁸² Interestingly, in the absence of dimethyl viologen 28^{2+} , the tripeptide Trp-Gly-Gly (Gly = glycine) dimerized in the cavity of cucurbit[8]uril 46 by the inclusion of two N-terminal L-tryptophan residues.^{182,186} The binding process of Trp-Gly-Gly with 46 displayed noncooperativity ($\alpha = 4 \times K_{2,1}/K_{1,1} = 1$), whereas it showed positive cooperativity ($\alpha > 1$) for the dimerization of Phe-Gly-Gly (Phe = phenylalanine) within 46. More recently, Urbach *et al.* reported that the tripeptide Tyr-Leu-Ala (Tyr = tyrosine; Leu = leucine, and Ala = alanine) bound to cucurbit[8]uril 46 featuring a binding constant value of $K_a = 1.4 \times 10^8\text{ M}^{-1}$ in 10^{-2} M sodium phosphate buffer at pH = 7. The latter complex also displayed high sequence specificity (e.g., the sequence isomer Tyr-Ala-Leu featured a much lower association constant, $K_a = 2.9 \times 10^4\text{ M}^{-1}$).¹⁸⁷ The Tyr and Leu residues of the tripeptide Tyr-Leu-Ala were included in the hydrophobic cavity of cucurbit[8]uril 46, whereas the C-terminal alanine residue was placed near the CB8’s portals.

Urbach, Bielawski, Scherman, and co-workers replaced the viologen paraquat 28^{2+} in the $28^{2+}\subset 46$ complex by the tetramethyl benzo-*bis*-imidazolium 63^{2+} ¹⁸⁸ (Figure 22). The benzo-*bis*-imidazolium 63^{2+} and cucurbit[8]uril 46 also formed a 1:1 inclusion complex ($K_a = 5.7 \times 10^5\text{ M}^{-1}$ in 10^{-2} M sodium phosphate buffer at pH = 7). In this case, the formation of the heteroternary inclusion complex with 61 induced the quenching of the fluorescence emission of bound 63^{2+} . The association constant of $63^{2+}\subset 46$ with 61 to give the $[61\cdot63^{2+}]\subset 46$ complex was determined to be K_a ($63^{2+}\subset 46 \rightleftharpoons [61\cdot63^{2+}]\subset 46$) = $7.2 \times 10^4\text{ M}^{-1}$.

Interestingly, the 1:1 inclusion complex formed between *bis*-imidazolium 64^{2+} (Figure 22) and cucurbit[8]uril 46, reported by Scherman *et al.*, featured a cage-like structure¹⁸⁹ (Figure 30). The two terminal imidazolium cations of 64^{2+} sealed the openings of the two opposite portals of the bound receptor 46. A binding constant value of K_a ($64^{2+}\subset 46$) = $1.9 \times 10^6\text{ M}^{-1}$ was

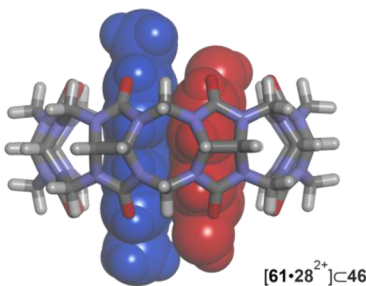


Figure 29. Energy minimized structure (MM3) of the $[61\cdot28^{2+}]\subset 46$ heteroternary complex. The host is depicted in stick representation and the guest molecules are shown as CPK models (28^{2+} in blue and 61 in red).

and 61 in the cavity of cucurbit[8]uril 46 was mainly driven by the HE. Biedermann, Scherman, and co-workers demonstrated that the binding strength in the 1:1:1 heteroternary complex depended on the solvation/desolvation energies of the free guests, 28^{2+} and 61.^{183–185} On the other hand, the binding selectivity was controlled by the establishment of $\pi\cdots\pi$ and charge-transfer interactions between the two electronic complementary aromatic surfaces of the included guests. The charge-transfer excited-state was also stabilized by the coinclusion of 28^{2+} and 61 within the cucurbit[8]uril 46.¹⁸⁴

Urbach *et al.* applied the preassembled $28^{2+}\subset 46$ inclusion complex for the recognition of L-tryptophan residues (Trp).¹⁸² The formation of the corresponding 1:1:1 heteroternary complex, $[62\cdot28^{2+}]\subset 46$, induced the observation of the expected charge-transfer band between the bound viologen 28^{2+} and the indole group of L-tryptophan 62 (Figure 22). The complex formation also provoked the quenching of the fluorescence emission of the indole group. The stepwise binding constant for the inclusion of L-tryptophan 62 into the

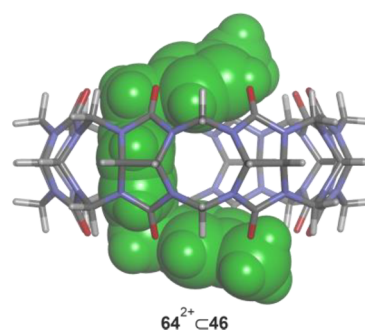


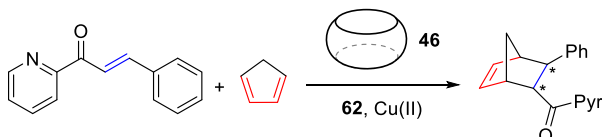
Figure 30. Energy minimized structure (MM3) of the $64^{2+}\subset 46$ complex. The receptor is depicted in stick representation and the guest (in green) is shown as CPK model.

determined for the 1:1 complex in water using ITC experiments. The $\text{64}^{2+}\text{C}46$ complex was able to accommodate small guest molecules (*G*) in the free available space of the cavity, leading to 1:1:1 heteroternary complexes. The stepwise stability constant value for the second binding event of the $[\text{G}\cdot\text{64}^{2+}]\text{C}46$ complex was in the order of 10^3 M^{-1} . Note that the structure of the cage-like complex $\text{64}^{2+}\text{C}46$ imposes a severe size selective binding in the co-inclusion of a second guest (Figure 30). This requirement precluded the co-inclusion of the large 2,6-dihydroxynaphthalene guest **61** in the preformed $\text{64}^{2+}\text{C}46$ complex.

Further investigations by Biedermann *et al.* suggested that the binding of an auxiliary guest into the cavity of cucurbit[8]uril **46** produced “high-energy” water molecules to be present in the interior of the preformed 1:1 complex. The included “high-energy” water molecules are supposed to be ejected to the bulk solution upon formation of the ternary complex. This binding scenario was used by the authors to explain the favorable enthalpy ($\Delta H < 0$) and unfavorable entropy ($T\Delta S < 0$) characterizing the inclusion processes of the second guest.

Cucurbit[8]uril **46** was applied as nanoreactor in asymmetric catalysis by Scherman, Herrmann, and co-workers.¹⁹⁰ Thus, the Diels–Alder reaction of azachalcone and cyclopentadiene using a simple amino acid as chiral source (L-tryptophan **62**), Cu(II) as Lewis acid, and cucurbit[8]uril **46** produced high enantioselectivities (up to 92% ee) (Scheme 3).

Scheme 3. Diels–Alder Reaction of Azachalcone and Cyclopentadiene (Asterisks Denote Stereogenic Carbon Atoms)



Likewise, the reactions experienced modest rate accelerations (9.5-fold) when compared to the outcomes using larger bioinspired catalysts (DNA and protein scaffolds). During catalysis, the aromatic side chain of the amino acid, *i.e.*, L-tryptophan **62**, and the pyridine ring of the dienophile were included in the cavity of cucurbit[8]uril **46** forming a ternary complex. Most likely, both included residues were also complexed to Cu(II) and the vinylbenzene unit of the dienophile was protruding out of the cavity and exposed to the solvent and the incoming diene. The overall concept relies on a supramolecular catalytic system based on a chiral transition-metal complex included in a nonchiral macrocycle.

3.4. Bambus[6]urils

Bambus[6]urils feature a relatively hydrophobic cavity with 12 converging CH-groups that is open at two opposite ends.¹⁹² Their name derives from the resemblance of their structure to that of a bamboo plant (Figure 31a). Bambus[6]urils are synthesized from the acid-catalyzed condensation of 2,4-disubstituted-glycoluril unit with paraformaldehyde. In general, the conjugate base of the halogen acid, *i.e.*, chloride, acts as a templating agent for the cyclization process. The X-ray structure of the chloride complex, $\text{Cl}^-\text{C}65$, supported the potential templating effect of the chloride and suggested the application of bambus[6]urils as receptors for anions in water solution (Figure 31b).

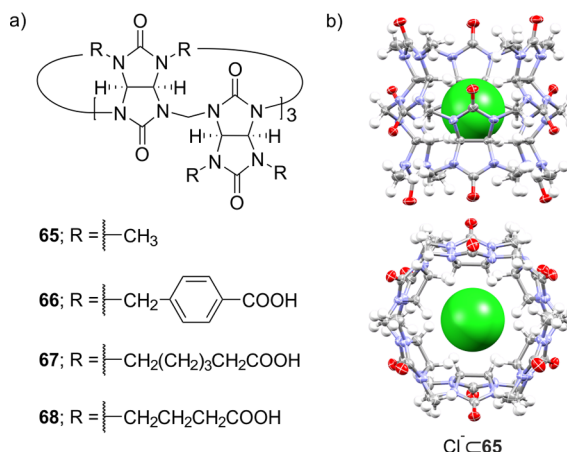


Figure 31. (a) Line-drawing structures of bambus[6]urils **65–68** and (b) X-ray crystal structure of $\text{Cl}^-\text{C}65$ (CCDC 761932). The structure is shown in ORTEP view with thermal ellipsoids set at 50% probability, and hydrogen atoms are shown as fixed-size spheres of 0.3 Å radius. Chloride anion is shown as CPK model.

Glycoluril precursor units that are not soluble in water can also be condensed with formaldehyde and induced to cyclize in organic solvents using organic acids (*i.e.*, toluene solvent and *para*-toluenesulfonic acid catalyst).¹⁹² Under these conditions, tetra-butylammonium bromide was added as templating agent. Bambus[6]urils possess some structural features that are related to those of cucurbit[*n*]urils and hemicucurbit[*n*]urils (not discussed in this review). The bambus[6]urils, like cucurbit[*n*]urils, offer a hydrophobic cavity. However, the cavity of the former is conformationally and structurally more flexible than that of the latter. The methine hydrogen atoms of the glycoluril panels in bambus[6]urils are slightly acidic and oriented toward the interior of the hydrophobic cavity. This characteristic makes bambus[6]urils efficient receptors for anions. The bound anion is included in the cavity being stabilized by 12 weak C–H…X[−] hydrogen bonds (see section 2). The electrostatic surface potential map of bambus[6]urils shows a positive region in the interior of the cavity and a negative region at the portals.¹⁹³ Moreover, the conformational flexibility of the cavity of bambus[6]uril allows its adaptation to anions of different sizes and shapes.

Sindelar *et al.* reported the first bambus[6]uril, **65** (Figure 31a), in 2010.¹⁹³ The bambus[6]uril **65** featuring *N*-methyl substituents at the glycoluril panels was not soluble in pure water. The cavity of **65** had a diameter of 6.4 Å and a depth of 12.7 Å, approximately 4 Å deeper than that of the cucurbit[6]uril analogue. Titration experiments of receptor **65** with halide anions in a 1:1 water/acetonitrile solvent mixture showed that the binding constants of the complexes followed the order: $\text{Cl}^- (K_a = 7.8 \times 10^2 \text{ M}^{-1}) < \text{Br}^- (K_a = 4.8 \times 10^4 \text{ M}^{-1}) < \text{I}^- (K_a = 8.9 \times 10^5 \text{ M}^{-1})$.^{193,194}

The functionalization of the available nitrogen atoms of the structure of bambus[6]urils with carboxylic acid groups produced the water-soluble receptors **66–68** (Figure 31a) reported by Sindelar and co-workers.^{195,196} The cavity of bambus[6]urils accommodated a water molecule in the solid state. Hence, it was expected the release of the bound molecule upon anion binding in water solution.⁴ The bound anion was then shielded from the bulk aqueous solution. These considerations suggested that solvation/desolvation processes

of free and bound species are important in the stabilization of these complexes.^{40,197}

Bambus[6]uril **66**, bearing 12 benzoic acid groups, was soluble in water (1 mM, pD = 7.1).¹⁹⁵ Note that at this pD, some of the carboxylic acids of **66** are ionized as carboxylates. To accurately determine the anion binding constants of **66**, 2×10^{-2} M K₂DPO₄ were added to the solution to control ionic strength. Binding studies showed the following order of binding affinities: F⁻ < Cl⁻ < CN⁻ < Br⁻ < NO₃⁻ < BF₄⁻ < I⁻ < ClO₄⁻. This trend clearly pointed out that anion desolvation must play an important role in the binding. The anions featuring a modest binding affinity, K_a (F⁻, Cl⁻, CN⁻ \subset **66**) = 10^2 – 10^3 M⁻¹, formed kinetically labile complexes, *i.e.*, chemical exchange was fast on the ¹H NMR chemical shift time scale. On the contrary, anions that bound strongly to the bambus[6]uril receptor **66**, K_a (Br⁻, NO₃⁻, BF₄⁻, I⁻ \subset **66**) = 10^5 – 10^7 M⁻¹, produced kinetically stable complexes on the ¹H NMR chemical shift time scale (Table 6). For example, the

Table 6. Binding Constant Values (K_a , M⁻¹) of Selected Complexes of Bambus[6]uril Receptors in Water Solution^a

anions	bambus[6]urils		
	binding constant (K_a)		
	66 ¹⁹⁵	67 ¹⁹⁶	68 ¹⁹⁶
F ⁻	1.1×10^2		
Cl ⁻	9.1×10^2		
Br ⁻	1.4×10^5	1.7×10^3	2.4×10^2
I ⁻	1.0×10^7	1.1×10^6	2.1×10^5
ClO ₄ ⁻	5.5×10^7		

^aSee Figure 31 for the line-drawing structures of bambus[6]uril receptors and text for details.

highest association constant was measured for ClO₄⁻ anion, K_a (ClO₄⁻ \subset **66**) = 5.5×10^7 M⁻¹.¹⁹⁵ The negatively ionized benzoic acids of **66** did not seem to compete with the inorganic anions for the binding pocket of the bambus[6]uril receptor (*vide infra*). The modification of the pD (7.1–11.3) did not have a significant influence on the association constant value determined for the Cl⁻ \subset **66** complex. Likewise, the modification of the ionic strength (0.2–0.8 M NaCl) of the aqueous solutions produced small changes in the stability constant value of the ClO₄⁻ \subset **66** complex. With this finding, the authors concluded that the binding strength seemed to prevail over the “salting-out” effect of the salt^{195,196} (see Hofmeister effect in section 2.2). In addition, ITC experiments revealed that anion binding to **66** was driven by enthalpy and opposed by entropy (*e.g.*, K_a (I⁻ \subset **66**) = 2.0×10^6 M⁻¹; $\Delta H = -84.1$ kJ·mol⁻¹ and $T\Delta S = -47.5$ kJ·mol⁻¹ in water at pH = 7.1).¹⁹⁵

The bambus[6]urils **67** and **68** (Figure 31a) had pentyl and propyl substituents, respectively, which were functionalized with terminal carboxylic acids.¹⁹⁶ Receptors **67** and **68** were soluble in phosphate aqueous buffer at pD = 7.5. As indicated above for **66**, some of the carboxylic acids of **67** and **68** are ionized as carboxylates. The binding constant values of the receptor’s series for Br⁻ and I⁻ decreased in the same order: **66** > **67** > **68** (Table 6). The observed trend was explained by considering a competitive intramolecular binding of the carboxylate groups for the receptor’s cavity and the establishment of repulsive Coulombic interactions between the carboxylate groups and the bound anion. Remarkably, the

crystal structure of **67** showed the inclusion of two of its carboxylate arms in the receptor’s cavity. A water molecule bridged the two carboxylate groups (Figure 32). In addition,

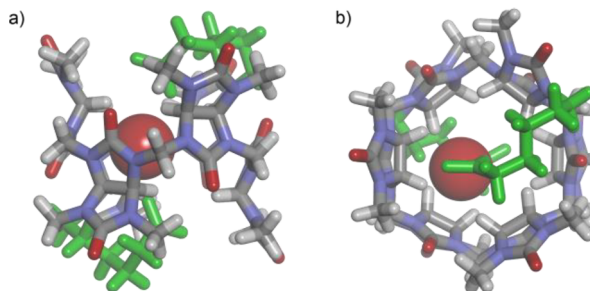


Figure 32. X-ray crystal structure of **67** (CCDC 1511981): (a) side and (b) top views. Bambus[6]uril is depicted in stick representation, and introverted carboxylates are highlighted in green. External carboxylates are pruned to methyl groups for clarity. The oxygen atom of the bound water molecule is shown as CPK model with the hydrogen atoms omitted for clarity.

the authors suggested that the aliphatic carboxylates of **67** and **68** were able to establish more effective electrostatic repulsions with bound anions than the rigid benzoates present in **66**. For example, the binding constant values determined for I⁻ were K_a (I⁻ \subset **67**) = 1.1×10^6 M⁻¹ and K_a (I⁻ \subset **68**) = 2.1×10^5 M⁻¹.¹⁹⁶ This result was rationalized assuming that the short propyl substituents of **68** brought the carboxylate groups close to the portals of the receptor disfavoring anion binding.

Finally, it is worth mentioning that biotin[6]uril, *i.e.*, a macrocycle formed by the condensation of six units of D-biotin and formaldehyde, developed by the group of Pittelkow,¹⁹⁸ resembles the structure of a bambus[6]uril. Biotin[6]uril bears six carboxylic acid groups providing water solubility. The binding constants of biotin[6]uril with the halide anions followed the same order observed for bambus[6]urils, *i.e.*, Cl⁻ < Br⁻ < I⁻.¹⁹⁸ For example, the binding constant value of the I⁻ \subset biotin[6]uril complex was determined to be 2.5×10^3 M⁻¹ in phosphate buffer at pD ~ 7.5.¹⁹⁹ The binding process was driven by enthalpy, $\Delta H = -42.8$ kJ·mol⁻¹, and opposed by entropy, $T\Delta S = -23.0$ kJ·mol⁻¹. Note that the binding constant of I⁻ decreased almost 3 orders of magnitude with respect to that determined for bambus[6]uril **67** (K_a (I⁻ \subset **67**) = 1.1×10^6 M⁻¹). The difference in binding affinity between biotin[6]uril and bambus[6]uril toward halide anions may be related to the different solvation modes of the corresponding receptor’s cavities. In the solid state, two water molecules occupied the cavity of biotin[6]uril,¹⁹⁹ whereas the cavity of bambus[6]uril **67** showed one bound water molecule.¹⁹⁶

4. COVALENT RECEPTORS POSSESSING A CONCAVE HYDROPHOBIC CAVITY

In this section, we discuss covalent receptors displaying a concave hydrophobic cavity closed at one end and open at the opposite end. The concave and aromatic cavity is shallow in the case of calix[n]arenes and resorcin[4]arenes but becomes deeper for cavitands derived from resorcin[4]arene scaffolds.

4.1. Calix[n]arenes

Calix[n]arenes **69**–**75** ($n = 4$ – 7) (Figure 33a) are comprised of phenol units linked together by methylene bridges at their *meta*-position.^{15,49} The calix[n]arene scaffold adopts multiple conformations in solution, *i.e.*, cone, pinched cone, and

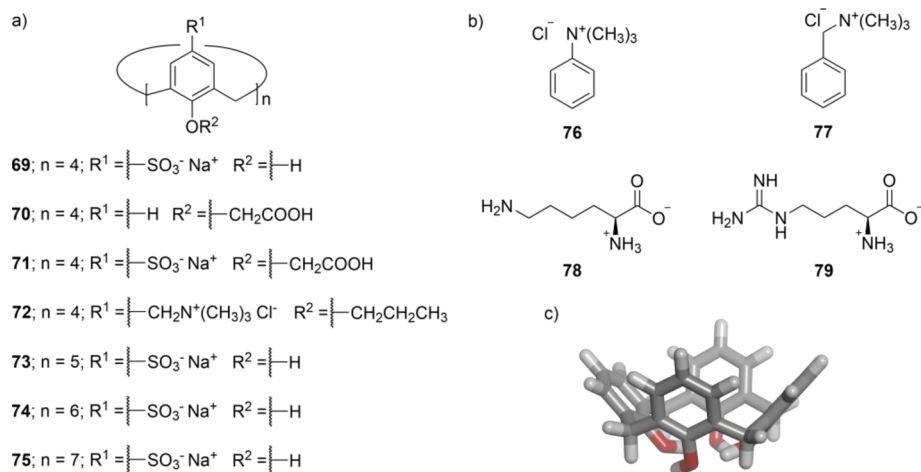


Figure 33. Line-drawing structures of: (a) calix[n]arenes **69–75** and (b) some molecules investigated as guests for these receptors. (c) Energy minimized structure (MM3) of a calix[4]arene in the cone conformation. The calix[4]arene is depicted in stick representation.

alternate, owing in some cases, to the rotation of the aromatic panels around the methylene bridges. The interconversion rate between conformers depends on the size of the substituents attached to the aromatic panels. The calix[4]arenes in cone conformation display a shallow aromatic cavity widely open at one end and closed at the opposite⁸ (Figure 33c).

The structure of calix[n]arenes can be modified at either the lower and/or the upper rim. In this regard, water-soluble calix[n]arenes have been prepared by appending carboxylic acid, phosphonate, sulfonate, or ammonium groups at their rims.^{15,49} The shallow hydrophobic cavity of calix[n]arenes do not isolate bound water molecules from the bulk solution, *i.e.*, they are able to establish hydrogen bonds with water molecules in the bulk. Accordingly, there is not expected to be a large and favorable enthalpic contribution to guest binding from the release of bound water molecules. X-ray crystallographic studies performed by Atwood *et al.*²⁰⁰ and later by Steed *et al.*²⁰¹ showed that calix[4]arenes can bind one water molecule, which is stabilized by OH- π and dispersion interactions. On the contrary, calix[5]arenes can accommodate up to three water molecules in their cavity, as reported by Steed, Atwood, Clark, and co-workers²⁰² (see hydration of cavities in section 2.1).

Calix[4]arenes, such as **69** (Figure 33a), were found to bind inorganic cations in water.¹⁵ For example, Morel and Morel-Desrosiers showed that monocharged cations and tetrasulfonate calix[4]arene **69**⁴⁻ formed 1:1 complexes featuring an inclusion binding geometry in water at pH = 2.²⁰³ The binding process was found to be enthalpically driven, in part, owing to the establishment of cation- π interactions (see sections 2 and 3.1). However, doubly charged cations also interacted with the sulfonate groups at the upper rim of the receptor **69**⁴⁻, as shown by Morel and Morel-Desrosiers²⁰³ and Bonal *et al.*²⁰⁴ As might be expected for ion-pairing interactions in water, the binding processes of the dicationic guests were mainly driven by entropy.

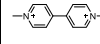
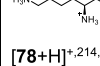
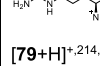
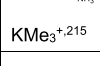
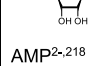
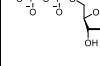
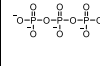
Calix[4]arene receptors also bind neutral and charged organic substrates leading to 1:1 inclusion complexes in water.¹⁵ Typically, the guest is included in the shallow hydrophobic cavity of the calix[4]arene.⁶⁹ The binding process induces the receptor to adopt the cone conformation (Figure 33c). Furthermore, the formation of the inclusion complex produces the maximization of the host-guest intermolecular

interactions and a reduction in the overall solvent accessible surface area. The cone (or pinched cone) conformer of calix[4]arenes can be identified by the observation of two separate signals for the hydrogen atoms of the methylene bridges in the ¹H NMR spectrum.²⁰⁵ At the same time, the proton signals of the bound guests experience upfield shifts owing to the shielding effect exerted by the aromatic cavity of the receptor. For example, a hydrogen nucleus in the deepest region of the calix[4]arene's cavity displays a complexation-induced shift of $\Delta\delta \sim -2$ ppm.¹⁵ In most calix[4]arene complexes, the chemical exchange between free and bound components is fast on the ¹H NMR chemical shift time scale.

The inclusion complexes of sulfonate calix[4]arenes and positively charged organic guests, such as organic ammonium cations, were stabilized by the HE, CH- π , cation- π , and Coulombic interactions. For example, Shinkai *et al.* reported that the adamantane trimethylammonium **17**⁺ (added as chloride salt, Figure 5) and tetra-sulfonate calix[4]arene **69**⁴⁻ formed a 1:1 complex featuring a binding constant of K_a ($\text{17}^+ \subset \text{69}^{4-}$) = $2.1 \times 10^4 \text{ M}^{-1}$ in 0.1 M phosphate buffer at pD = 7.3.^{206–208} In the $\text{17}^+ \subset \text{69}^{4-}$ complex, either the adamantane residue or the trimethylammonium group could be buried in the cavity of the receptor. Indeed, the two binding geometries of the $\text{17}^+ \subset \text{69}^{4-}$ complex were present in solution and were involved in a chemical exchange process that was fast on the ¹H NMR chemical shift time scale. The existence in solution of the two binding modes served to explain the chemical shift changes observed in the ¹H NMR spectra of the 1:1 complexes formed between calix[4]arene **69**⁴⁻ with phenyl trimethylammonium **76**⁺ and benzyl trimethylammonium **77**⁺ as guests²⁰⁶ (Figure 33b and Table 7). That is, the observed upfield shifts experienced by the signals of the aromatic protons and the trimethylammonium groups supported the two possible orientations of the bound guests. Liu *et al.* reported the binding constant value of 1-methylpyridinium with calix[4]-arene **69**⁴⁻ as $K_a = 6.4 \times 10^5 \text{ M}^{-1}$ in water.²⁰⁹ In this case, the pyridinium cation was selectively included in the calix[4]-arene's cavity. Liu *et al.* also investigated the complexation process of bipyridinium^{209,210} and biguanidinium²¹¹ guests with calix[4]arene **69**⁴⁻ in water solution.

Arena, Sciotto, Ungaro, and co-workers studied the binding properties of calix[4]arenes **70** and **71** toward organic ammonium cations²¹² (Figure 33a). The calix[4]arenes **70**

Table 7. Binding Constant Values (K_a , M⁻¹) of Selected Calix[*n*]arene Complexes Formed in Water Solution^a

Guests	Calix[4]arenes				Bigger calix[<i>n</i>]arenes (<i>n</i> = 5 - 7)		
	[69] ⁴⁻	[70-4H] ⁴⁻	[71-4H] ⁸⁻	[72] ⁴⁺	[73-H] ⁶⁻	[74-2H] ⁸⁻	[75-2H] ⁹⁻
 17 ^{+,207}	2.1 × 10 ⁴					1.0 × 10 ³	
 28 ^{2+,223}							3.2 × 10 ⁴
 52 ²²²						3.7 × 10 ³	
 76 ^{+,207,212}	5.6 × 10 ³	1.6 × 10 ²	2.0 × 10 ³				
 77 ^{+,212,219}		50	2.0 × 10 ³		1.0 × 10 ⁴		
 [78+H] ^{+,214,220}	8.0 × 10 ²				62		
 [79+H] ^{+,214,220}	1.5 × 10 ³				1.1 × 10 ²		
 KMe₃ ^{+,215}	3.6 × 10 ⁴						
 AMP ^{2-,218}				1.3 × 10 ³			
 ADP ^{3-,218}				2.7 × 10 ³			
 ATP ^{4-,218}				1.1 × 10 ⁴			

^aSee Figure 33a for the line-drawing structures of the receptors. Details on the pH used in the binding experiments are provided in the text.

and **71** were soluble at millimolar concentrations in 0.1 M phosphate buffer solution at pD = 7.3 owing to the ionization of the carboxylic groups installed at their lower rims. The incorporated lower rim functions were also useful in locking

the receptors' cone conformation. The number and placement (upper and lower rim) of the charged substituents in the calix[4]arenes had a significant effect in the binding modes and association constant values of their complexes with the

alkylammonium cations. For example, in the $76^+ \subset [70\text{-}4\text{H}]^{4-}$ complex, the trimethylammonium group of 76^+ (phenyl trimethylammonium) was exclusively included in the aromatic cavity of the lower rim tetra-carboxylate calix[4]arene $[70\text{-}4\text{H}]^{4-}$ establishing cation- π and CH- π interactions. In striking contrast, for the $76^+ \subset [71\text{-}4\text{H}]^{8-}$ complex, the guest was exclusively bound to the tetra-sulfonate tetra-carboxylate calix[4]arene $[71\text{-}4\text{H}]^{8-}$ through the inclusion of its phenyl ring and the establishment of π - π and CH- π interactions. Simultaneously, the trimethylammonium group of bound 76^+ in the $76^+ \subset [71\text{-}4\text{H}]^{8-}$ complex interacted through Coulombic interactions with the upper rim sulfonate substituents of the host. The different binding modes and intermolecular interactions present in complexes $76^+ \subset [70\text{-}4\text{H}]^{4-}$ and $76^+ \subset [71\text{-}4\text{H}]^{8-}$ translated into a difference of just 1 order of magnitude between their association constant values in favor of the ditopic $76^+ \subset [71\text{-}4\text{H}]^{8-}$ complex (Table 7).

The 1:1 inclusion complex of benzyl trimethylammonium 77^+ (Figure 33b) with the lower rim substituted tetra-carboxylate calix[4]arene $[70\text{-}4\text{H}]^{4-}$ displayed a binding geometry similar to that discussed above for the $76^+ \subset [70\text{-}4\text{H}]^{4-}$ counterpart²¹² that was selective inclusion of the trimethylammonium knob. However, the binding constant value of the latter complex, $77^+ \subset [70\text{-}4\text{H}]^{4-}$, suffered a 3-fold drop in binding affinity (K_a ($77^+ \subset [70\text{-}4\text{H}]^{4-}$) = 50 M^{-1}) compared to that of the former. In striking contrast and quite surprisingly to us, the $77^+ \subset [71\text{-}4\text{H}]^{8-}$ complex displayed, in solution, two binding geometries that were rapidly interconverting on the ^1H NMR chemical shift time scale (Figure 34). The binding constant values determined for the $76^+ \subset [71\text{-}4\text{H}]^{8-}$

$[79\text{-H}]^+ \subset 69^{4-}$, featured binding constant values in the order of 10^3 M^{-1} in phosphate buffer at pH = 8 (Table 7). Furthermore, di- and tripeptides containing L-lysine and L-arginine residues were also bound to the sulfonate receptor 69^{4-} . On the basis of the results obtained by 1D and 2D NMR experiments, the protonated terminal amine of L-lysine [$78\text{-H}]^+$ and the guanidinium group of L-arginine [$79\text{-H}]^+$ were selectively included in the shallow hydrophobic cavity of calix[4]arene 69^{4-} . Hof *et al.* investigated the binding of L-lysine at different methylation states (KMe_n^+ , $n = 3 - 1$) to calix[4]arene 69^{4-} in $4 \times 10^{-2} \text{ M}$ phosphate buffer at pH = 7.4.²¹⁵ The complex between ζ -trimethylammonium L-lysine (KMe_3^+) and calix[4]arene 69^{4-} featured the largest binding constant value of the methylated L-lysine series, K_a ($\text{KMe}_3^+ \subset 69^{4-}$) = $3.6 \times 10^4 \text{ M}^{-1}$. The $\text{KMe}_3^+ \subset 69^{4-}$ complex was stabilized by the HE, Coulombic, and cation- π interactions, in part, owing to the inclusion of the trimethylammonium knob of the guest in the receptor's cavity. Later, Hof *et al.* developed trisulfonate calix[4]arene receptors in order to improve the binding selectivity toward KMe_3^+ .²¹⁶ The replacement of a phenyl sulfonate panel of calix[4]arene 69^{4-} by a biphenyl group boosted the binding constant of KMe_3^+ up to $8.0 \times 10^4 \text{ M}^{-1}$ (see ethenoanthracene-based cyclophanes for the selective binding of KMe_3^+ in section 3.1). Calix[4]arene receptors decorated with phosphonic acids at their upper rims were also used by Rachon *et al.* for the binding of amino acid methyl esters in water.²¹⁷

Calix[4]arene receptors bearing alkylammonium substituents at their upper rims were efficient receptors for the complexation of nucleotides in water. For example, the upper rim substituted tetra-trimethylammonium calix[4]arene tetrachloride salt 72 (Figure 33a), reported by Shi and Schneider, was soluble in water.²¹⁸ Calix[4]arene 72 adopted a fixed cone conformation owing to the appended propyl substituents at its lower rim, *i.e.*, the energy barrier for the rotation of the aromatic panels around the methylene bridges increased significantly. The tetra-ammonium receptor 72^{4+} recognized adenosine monophosphate (AMP^{2-}), diphosphate (ADP^{3-}), and triphosphate (ATP^{4-}) derivatives in water at $\text{pD} \sim 7$. The ammonium cations of 72^{4+} were involved in Coulombic interactions with the phosphate residues of the bound nucleotide. The proposed binding geometry of the complexes placed the saccharide residue of the bound nucleotide partially included in the aromatic cavity of the receptor and the adenine unit totally exposed to the bulk solvent. The magnitude of the binding constant values for these complexes were in line with the thermodynamic stability for the formation of two salt-bridges in water, $K_a = 10^3 - 10^4 \text{ M}^{-1}$ (see section 2). An increasing trend in the K_a magnitude with the overall charge of the guest was observed (Table 7).

Steed, Atwood, Clark, and co-workers reported that the calix[5]arene 73 (Figure 33a) possessed five to seven negative charges, depending on the pH of the aqueous solution, owing to the presence of five sulfonate groups at its upper rim and the potential ionization of one or two phenolic OHs at its lower rim.²⁰² Later, Sciotto *et al.* reported the molecular recognition properties of the penta-sodium salt of penta-sulfonate calix[5]arene 73 in water (0.1 M phosphate buffer at $\text{pD} = 7.3$) using a series of organic ammonium guests²¹⁹ and amino acids.²²⁰ For example, benzyl trimethylammonium 77^+ and the hexa-anionic form of calix[5]arene $[73\text{-H}]^{6-}$ formed a 1:1 inclusion complex featuring an association constant $K_a = 1.0 \times 10^4 \text{ M}^{-1}$. NMR and molecular modeling studies (MM3) of the

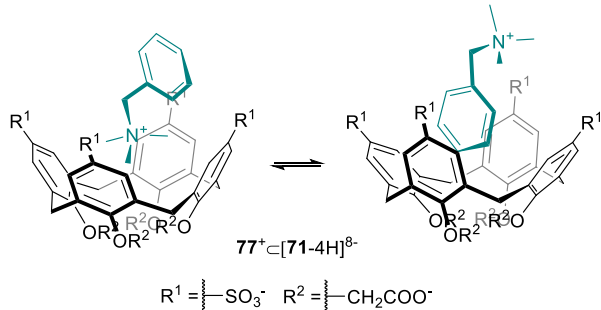


Figure 34. Equilibrium between the two binding geometries featured by the $77^+ \subset [71\text{-}4\text{H}]^{8-}$ complex.

$4\text{H}]^{8-}$ and $77^+ \subset [71\text{-}4\text{H}]^{8-}$ complexes turned out to be identical (Table 7). It is worth mentioning that the tetra-sulfonate tetra-carboxylate calix[4]arene $[71\text{-}4\text{H}]^{8-}$ included the phenyl trimethylammonium guest, 76^+ , in a single binding geometry due to a preferred ditopic interaction with the guest.²¹³ A subtle change in the structure of the guest (addition of a methylene group in 77^+) had a significant but difficult to predict impact either on the thermodynamic stabilities or the binding modes of the complexes with the two studied hosts, $[70\text{-}4\text{H}]^{4-}$ and $[71\text{-}4\text{H}]^{8-}$.

The binding of amino acids and short peptides in water has been investigated using tetra-sulfonate receptor 69^{4-} and larger calix[n]arene homologues (*vide infra*). For example, Morel-Desrosiers *et al.* reported the formation of 1:1 inclusion complexes between protonated L-lysine [$78\text{-H}]^+$ and L-arginine [$79\text{-H}]^+$ (Figure 33b) with tetra-sulfonate calix[4]-arene 69^{4-} .²¹⁴ The amino acid complexes, $[78\text{-H}]^+ \subset 69^{4-}$ and

$77^+C[73\text{-H}]^{6-}$ complex suggested that the guest was included in the electron-rich aromatic cavity of the receptor with a tilted orientation (Figure 35). The binding constants of amino acids,

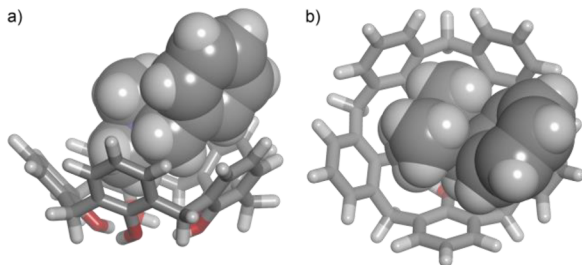


Figure 35. Energy minimized structure (MM3) of the simplified $77^+C[73\text{-H}]^{6-}$ complex: (a) side and (b) top views. The calix[5]-arene is depicted in stick representation, and the bound benzyl trimethylammonium guest is shown as CPK model. The five upper-rim sulfonate groups are removed for clarity.

such as monocationic L-lysine $[78\text{+H}]^+$ and L-arginine $[79\text{+H}]^+$ (Figure 33b), with the hexa-anionic calix[5]-arene $[73\text{-H}]^{6-}$ were 1 order of magnitude lower than those of the same guests with analogous tetra-sulfonate calix[4]arenes (Table 7). Nevertheless, similar binding modes were proposed for the different complexes.

The hexa-sodium salt of hexa-sulfonate calix[6]arene 74 (Figure 33a) featured eight negative charges in neutral water solution: six sulfonates at the upper rim and two ionized phenolic OHs at the lower rim, $[74\text{-}2\text{H}]^{8-}$. In the solid state, Atwood, Clark, and co-workers showed that the ionized calix[6]arene $[74\text{-}2\text{H}]^{8-}$ adopted a double partial cone conformation stabilized by four intramolecular hydrogen bonds²²¹ (Figure 36). Most likely, this conformation is also present in water solution. The octa-anionic calix[6]arene $[74\text{-}2\text{H}]^{8-}$ formed a 1:1 inclusion complex with trimethylammonium adamantine guest 17^+ (added as chloride salt) featuring a binding constant value of $K_a = 1.0 \times 10^3 \text{ M}^{-1}$.²⁰⁷ This binding constant was 1 order of magnitude lower than the one

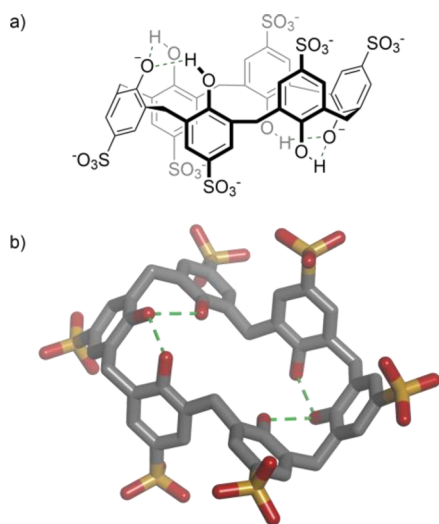


Figure 36. Octa-anionic calix[6]arene $[74\text{-}2\text{H}]^{8-}$: (a) line-drawing and (b) X-ray crystal structure (CCDC 1288096). The calix[6]arene is depicted in stick representation, and hydrogen atoms are omitted. Intramolecular hydrogen-bonding interactions are represented with dashed lines (in green).

determined for the $17^+C[69]^{4-}$ complex (*i.e.*, calix[4]arene receptor). The host–guest intermolecular interactions (non-polar contacts and Coulombic forces) were not optimal in the $17^+C[74\text{-}2\text{H}]^{8-}$ complex, producing a decrease in the expected binding affinity based on the overall charge of the receptor.

The interaction of ferrocene derivatives with octa-anionic calix[6]arene receptor $[74\text{-}2\text{H}]^{8-}$ was also investigated in aqueous solution by Gokel, Kaifer, and co-workers.²²² Neutral ferrocene 52 (Figure 22) and octa-anionic calix[6]arene $[74\text{-}2\text{H}]^{8-}$ formed a 1:1 inclusion complex. The inclusion geometry of the complex was supported by the observed chemical shift changes in the ^1H NMR spectra of titration experiments. The binding constant value of the $52C[74\text{-}2\text{H}]^{8-}$ complex was determined as $K_a = 3.7 \times 10^3 \text{ M}^{-1}$ in water solution. As expected, the use of cationic ferrocene guests produced an increase in binding affinity up to 10^4 M^{-1} .

In the same vein, the hepta-sodium salt of hepta-sulfonate calix[7]arene 75 (Figure 33a), reported by Vasca, Neri, and co-workers, possessed nine negatively charged groups, *i.e.*, $[75\text{-}2\text{H}]^{9-}$, in aqueous solution at $\text{pD} = 7.3$.²²³ The structure of calix[7]arene was conformationally flexible. Therefore, $[75\text{-}2\text{H}]^{9-}$ adopted multiple conformations in aqueous solution. The X-ray crystal structure of 75 and *in silico* calculations indicated that a double cone pinched conformation was energetically favored. Calix[7]arene $[75\text{-}2\text{H}]^{9-}$ also featured a large aromatic surface area enabling the binding of aromatic guests. For example, this receptor bound dimethyl viologen 28^{2+} (Figure 14b) in water, forming a thermodynamically highly stable 1:1 complex (Table 7). The preferred binding geometry of the $28^{2+}C[75\text{-}2\text{H}]^{9-}$ complex was difficult to elucidate experimentally. Most likely, the $28^{2+}C[75\text{-}2\text{H}]^{9-}$ complex was present in multiple binding geometries that were involved in fast chemical exchange processes on the NMR chemical shift time scale.

Finally, chiral groups were also incorporated at the upper rim of water-soluble sulfonate²²⁴ and carboxylate²²⁵ calix[n]-arenes. These calix[n]arenes were applied for the chiral recognition of α -amino acids and their methyl ester derivatives. They showed modest levels of binding selectivity for methyl esters of D-tryptophan and D-phenylalanine versus the L-counterparts.²²⁵ Deep-cavity calix[n]arenes were also introduced in the literature, providing association constant values in the order of $10^4\text{--}10^5 \text{ M}^{-1}$ for aromatic cationic guests, such as 76^+ and 77^+ .^{226,227}

4.2. Resorcin[4]arenes

The cyclic covalent arrangement of four electron-rich resorcinol units provides the resorcin[4]arene scaffold. The resorcinol aromatic panels are connected by methine bridges bearing alkyl substituents (aka “feet”). The OH phenol functions of the resorcin[4]arene scaffold form a cyclic seam of hydrogen bonds, which can be reinforced by hydrogen-bonded water molecules.²²⁸ These inter- and intramolecular hydrogen-bonding interactions stabilize the cone conformation of resorcin[4]arene (C_4 symmetry) in close analogy to that of calix[4]arenes unsubstituted at their lower rim (Figure 37 and Figure 33, respectively). The resorcin[4]arene in the cone conformation displays a shallow concave hydrophobic cavity.

An included atomic nucleus in the deepest region of the aromatic cavity of resorcin[4]arenes experiences a strong upfield shift of $\Delta\delta \sim -2.5 \text{ ppm}$.²²⁹ The dynamics of the chemical exchange processes between free and bound components of complexes derived from resorcin[4]arenes are

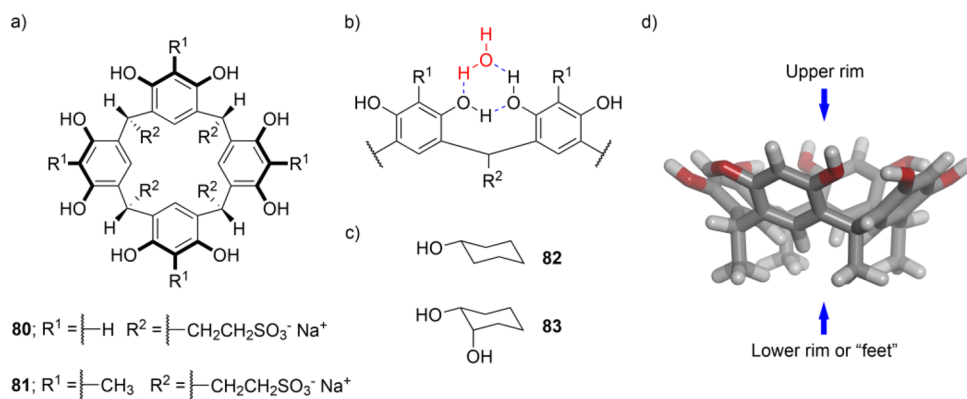


Figure 37. Line-drawing structures of: (a) resorcin[4]arenes **80** and **81**; (b) section of a resorcin[4]arene scaffold showing the hydrogen-bonding network between the resorcinol OHs and a water molecule and (c) guest molecules studied with these receptors. (d) Energy minimized structure (MM3) of the cone conformation of a resorcin[4]arene scaffold. The resorcin[4]arene is depicted in stick representation. Upper and lower rims are indicated with arrows (in blue).

fast on the ^1H NMR chemical shift time scale. We will show below (end of this section) that resorcin[4]arenes featuring a deep aromatic cavity, aka deep cavitands, show remarkably different binding exchange dynamics compared to the shallow parent derivatives.

As described for calix[4]arenes, ionizable or charged groups, e.g., carboxylic acids, sulfonates, phosphates, and ammonium,¹⁵ were attached at either the upper and lower rims of the resorcin[4]arene scaffold with the aim to impart water solubility to their derivatives. For example, the resorcin[4]arene bearing four terminal sulfonate groups at its lower rim alkyl substituents, **80** (Figure 37a), was highly soluble in water. Aoyama *et al.* demonstrated that tetra-anionic sulfonate resorcin[4]arene **80⁴⁻** formed 1:1 inclusion complexes with cyclic and acyclic alcohols.²²⁹ These complexes showed the nonpolar section of the cyclic alcohol, *i.e.*, **82** and **83** (Figure 37c), buried in the cavity of the receptor and the hydroxyl group of the bound guest remained exposed to the bulk aqueous solution (Figure 38). The binding constant values of

It is worth mentioning that the installation of charged groups at the lower rim of the resorcin[4]arene receptors did not interfere with the kinetic and thermodynamic characteristics of the binding processes with charged guests.²²⁹ On the contrary, when the same charged groups were implemented at the upper rim of the receptors, the resulting inclusion complexes experienced noticeable differences in thermodynamic and kinetic stabilities in response to the sign of the guest's charge (*vide infra*).

Diederich *et al.* elaborated the aromatic cavity of the resorcin[4]arene scaffold by functionalizing the resorcinol units at their *para*-position with phenyl substituents,²³⁰ **84** (Figure 39). In addition, the authors used ethylene chains to bridge the resorcinol OHs of the receptor's scaffold. The incorporation of the ethylene bridges produced a conformationally more rigid and preorganized receptor structure, aka cavitand.²³¹ These structural modifications were expected to enhance the HE (see section 2.1) for the binding of nonpolar residues or substrates. Cavitand **84** was further decorated with four amidinium groups at its upper rim and four tri(ethylene glycol) monomethyl ether chains at its "feet". The upper and lower rim substituents warranted water solubility to **84**. The cationic amidinium groups also assisted the binding of guests having negatively charged complementary functions.

The tetra-cationic cavitand **84⁴⁺** was used for the binding of carboxylate anions in water.²³⁰ Isophthalates, such as **85²⁻** (Figure 40), formed 1:1 and 2:1 guest/host complexes with receptor **84⁴⁺** in pure D_2O (K_a (**85²⁻** \subset **84⁴⁺**) = $8.6 \times 10^4 \text{ M}^{-1}$ and K_a (**85²⁻** \subset **84⁴⁺** \rightleftharpoons [**85₂**⁴⁻] \subset **84⁴⁺**) = $7.7 \times 10^3 \text{ M}^{-1}$). In striking contrast, 1:1 complexes were exclusively formed in $5 \times 10^{-3} \text{ M}$ aqueous borate buffer solution at pH = 9.2 (Figure 41). The binding constant value of the 1:1 inclusion complex, **85²⁻** \subset **84⁴⁺**, in buffer solution was in line with that determined in pure water (Table 8). The deep inclusion of isophthalate **85²⁻** in the cavity of receptor **84⁴⁺** was driven by the HE with the assistance of electrostatic interactions: ion-pairing and hydrogen-bonding (see section 2). These results demonstrated that the formation of high stoichiometry complexes mainly stabilized by means of electrostatic interactions could be suppressed in certain buffer solutions.^{15,136,232}

Following a different approach, Rebek and co-workers bridged the resorcinol OHs of the resorcin[4]arene scaffold with aromatic panels.²³² These resorcin[4]arene derivatives are known as deep cavitands. Deep cavitands soluble in organic

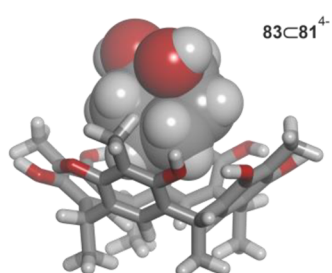


Figure 38. Energy minimized structure (MM3) of the simplified $83 \subset 81^{4+}$ complex. The resorcin[4]arene is depicted in stick representation and the guest is shown as CPK model. Water-solubilizing groups were pruned to methyl groups to simplify the calculation.

the latter complexes were determined to be lower than 20 M^{-1} in D_2O (Table 8). Nevertheless, the analogous *para*-methyl-substituted tetra-sulfonate resorcin[4]arene **81⁴⁻** (Figure 37a) featured binding constants up to 10^2 M^{-1} with the same alcohols (Table 8). The increase in binding affinity resulted from the deeper hydrophobic cavity featured by **81⁴⁻** in comparison to that of **80⁴⁻** lacking the *para*-methyl substituents.⁵⁶

Table 8. Binding Constant Values (K_a , M⁻¹) of Selected Complexes of Resorcin[4]arene and Cavitand Receptors Formed in Water Solution^a

	Resorcin[4]arenes		Cavitands			
	80⁴⁻	81⁴⁻	84⁴⁺	86⁴⁺	[95-8H]^{B-}	98⁴⁺
Guests	Binding constant, K_a					
 82²²⁹	16	1.3×10^2				
 83²²⁹	14	80				
 85^{2,230}			9.7×10^4			
 87²³⁵				1.4×10^2		
 [97-H]⁻²⁴⁸					4.7×10^6	
<chem>ClO4-</chem> ⁻²⁴⁸					95	
 99^{+,249}						3.4×10^3

^aSee Figure 37 and Figure 39 for the line-drawing structures of the hosts and text for details.

solvents were originally introduced by Cram *et al.*^{233,234} Water-soluble deep cavitands are present in solution mainly as D_{2d} “velcrand” dimers. In turn, “velcrand” dimers are in equilibrium with monomeric C_{2v} “kite” conformers. Moreover, “kite” conformers are also in equilibrium with C_{4v} “vase” counterparts.²³⁵ The two monomeric free conformers are present in low abundance in water solution (Figure 42). The dimerization of resorcin[4]arene cavitands into “velcrands” is driven by the HE (see section 2.1). Interestingly, the “kite” conformer features a shallow aromatic cavity, whereas the “vase” counterpart displays a deep hydrophobic cavity. Neither the “velcrand” dimer nor the “kite” conformer are able to establish highly thermodynamically and kinetically stable host–guest inclusion complexes. Nevertheless, the binding of size and shape complementary guests with the monomeric “vase” conformer induces the resorcin[4]arene dimer to dissociate. The bound receptor in “vase” conformation maximizes nonpolar contacts and minimizes the solvent accessible surface area. It is worth mentioning that the ^1H NMR spectrum of the “vase” conformer displays the hydrogen atom of the alkyl substituted methine as a triplet resonating at $\delta \sim 5.5$ ppm.^{235,236} This signal is significantly shielded in the “kite” conformer owing to the equatorial orientation of the aromatic bridging panels. The chemical exchange between the free conformers of the monomeric cavitands (“kite” and “vase”) is slow on the ^1H NMR chemical shift time scale. Moreover, the

high-energy barrier for the conformational exchange is the main contributor in controlling the guest in/out slow exchange kinetics of the “vase” complexes.²³⁷ Thus, it is expected for resorcin[4]arene deep cavitands to produce “vase” inclusion complexes that are kinetically stable on the ^1H NMR chemical shift time scale.

Water-solubilizing groups were appended at the “feet” of resorcin[4]arene deep cavitands: amine,²³⁵ oligo(ethylene glycol),²³⁸ pyridinium,²³⁹ imidazolium,²⁴⁰ and guanidinium groups.²⁴¹ Cavitand **86** possessed four ammonium groups at the lower rim and eight amide functions at its upper rim²³⁵ (Figure 39). Both amides and ammonium groups imparted water solubility. In the “vase”, the upper rim amides formed a belt of eight hydrogen bonds that stabilized the conformation (aka self-folding cavitand). The upper rim amide groups could also assist the binding of guests bearing complementary polar functions. Tetra-ammonium deep cavitand **86⁴⁺** included size complementary neutral guests. The formed 1:1 complexes featured stability constant values of the order of 10^2 M⁻¹. For example, **86⁴⁺** formed a thermodynamically and kinetically stable 1:1 inclusion complex with adamantanone **87** (Figure 40) in water²³⁵ (Table 8). The adamantanone residue of bound **87** was buried in the deep aromatic binding pocket of **86⁴⁺** in the “vase” conformation. The carbonyl group of the bound guest was located close to the open end of the cavity remaining partially exposed to the bulk aqueous solution (Figure 43).

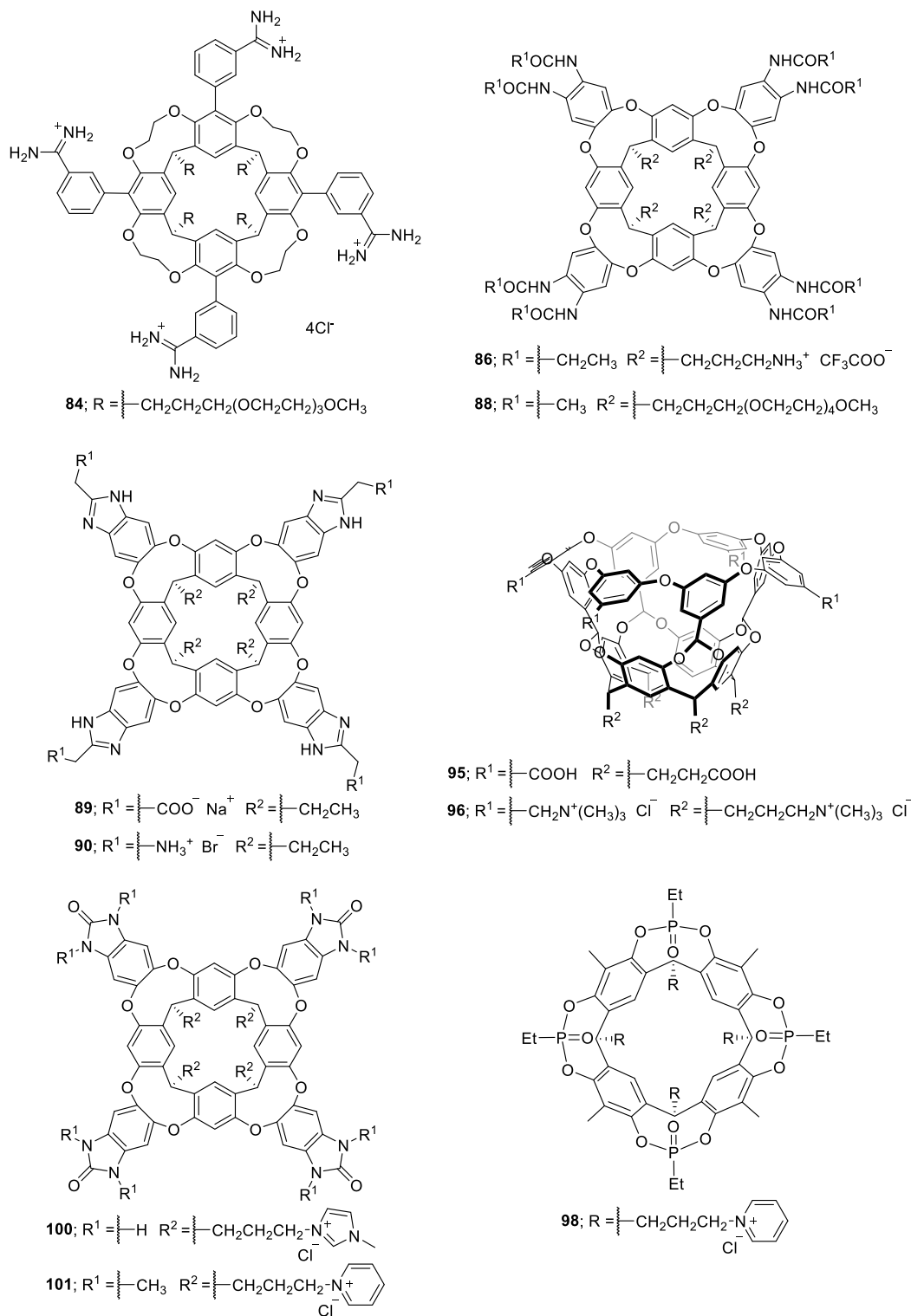


Figure 39. Line-drawing structures of resorcin[4]arene cavitands and deep cavitands.

The replacement of the cationic ammonium groups at the lower rim of 86^{4+} with oligo(ethylene glycol) chains produced the neutral deep cavitand 88^{238} (Figure 39). The oligo(ethylene glycol) chains provided water solubility of 88 over a wide pH range. Receptor 88 complexed protonated adamantane amines and methyl-quinuclidinium guests featuring K_a values up to 10^2 M^{-1} . The complexation process of the cationic guests with the neutral deep cavitand was driven by entropy. This thermodynamic signature was assigned to the

partial desolvation of the charged group of the guest upon inclusion in the deep aromatic cavity of the host.

The Rebek group also used as aromatic panels of the resorcin[4]arene deep cavitands benzimidazole units with anionic and cationic substituents, 89^{237} and 90^{242} (Figure 39). The charged groups at the upper rim of the receptors induced their solubility in water. For example, the tetra-carboxylate resorcin[4]arene cavitand 89^{4-} displayed solubility in water *ca.* 10^{-2} M^{237} . The tetra-carboxylate 89^{4-} adopted the “vase”

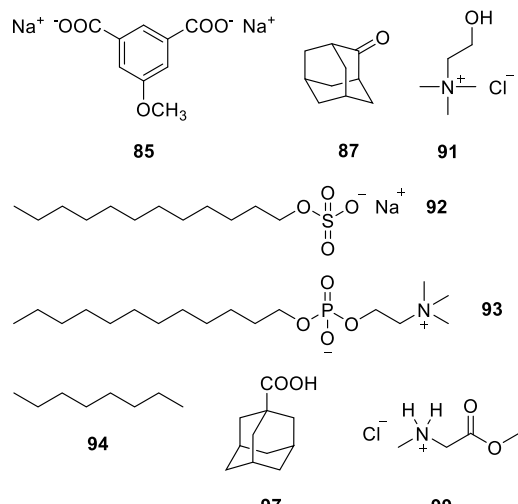


Figure 40. Line-drawing structures of guest molecules studied with resorcin[4]arene cavitands and deep cavitands.

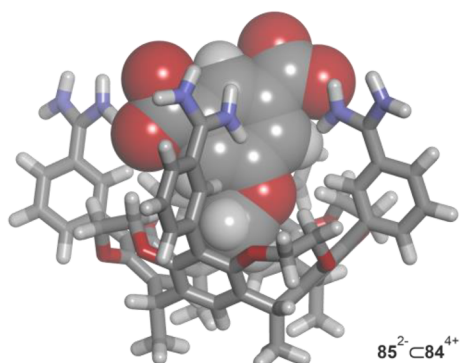


Figure 41. Energy minimized structure (MM3) of the simplified $85^{2-} \subset 84^{4+}$ complex. Resorcin[4]arene 84^{4+} is depicted in stick representation, the guest is shown as CPK model and the substituents at the lower rim pruned to methyl groups.

conformation in water solution owing to an included THF molecule captured during the last synthetic step. Hydrogen-bonded bridging water molecules located between adjacent benzimidazole units of 89^{4-} further stabilized the “vase” conformation (Figure 44). The binding of a complementary guest for the cavity of 89^{4-} provoked the release of the included THF molecule to the bulk aqueous solution. Interestingly, the protons of the guests that were included in the deep cavity of the benzimidazole deep cavitands experienced a strong magnetic shielding effect owing to the

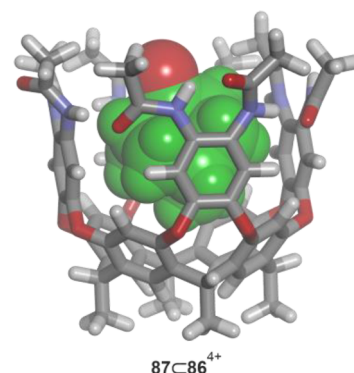


Figure 43. Energy minimized structure (MM3) of the simplified $87 \subset 86^{4+}$ complex. The cavitand is depicted in stick representation, and the guest (in green) is shown as CPK model. The oxygen atom (in red) of bound 87 is highlighted. Water-solubilizing groups were pruned to methyl groups to simplify the calculation.

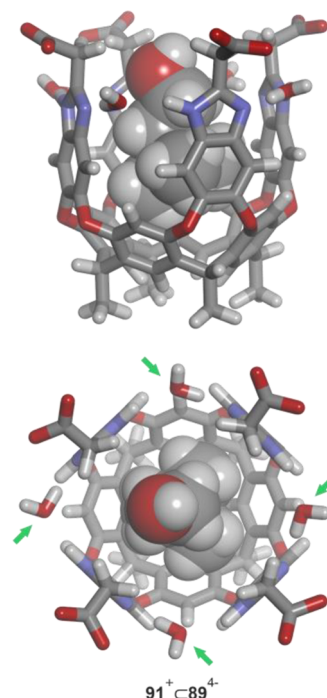


Figure 44. Energy minimized structure (MM3) of the simplified $91^+ \subset 89^{4-}$ complex: side and top views. The cavitand is depicted in stick representation and the guest is shown as CPK model. Hydrogen-bonded water molecules at the upper rim are indicated with arrows (in green). Substituents at the lower rim were pruned to methyl groups to simplify the calculations.

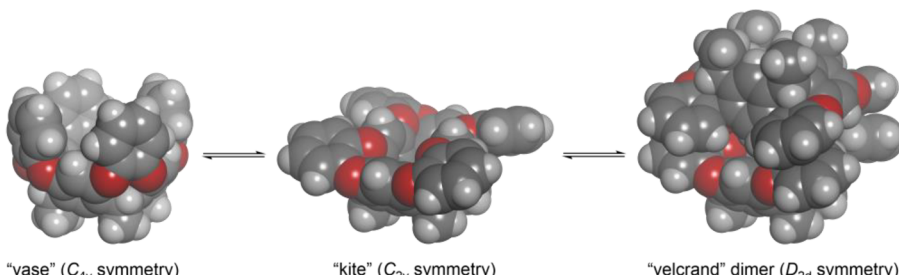


Figure 42. Conformational equilibria of resorcin[4]arene cavitands. The cavitands are shown as CPK models with the upper rim functions removed for clarity. Water-solubilizing groups at the cavitand’s “feet” were pruned to methyl groups to simplify the calculation.

eight aromatic panels that surround them.²³² For example, a nucleus of an atom located in the deepest region of the cavity displayed an upfield shift of $\Delta\delta = -4.4$ to -4.9 ppm. The tetra-carboxylate cavitand 89^{4-} and the tetra-methylammonium cation formed a 1:1 inclusion complex featuring a binding constant of $K_a = 4.3 \times 10^3 \text{ M}^{-1}$.²³⁷ On the other hand, cationic guests featuring nonpolar alkyl residues displayed binding constant values larger than 10^4 M^{-1} . In this regard, choline 91^+ (Figure 40) and acetylcholine formed thermodynamically and kinetically highly stable 1:1 inclusion complexes with 89^{4-} in water (Figure 44). In general, the binding processes of these cavitands were mainly enthalpically driven.

Deep cavitands 89 and 90 were structurally closely related (Figure 39). They only differed in the type of substituents present at their upper rims: carboxylates in 89^{4-} and alkylammonium cations in 90^{4+} . The two cavitands were applied by Rebek *et al.* to investigate the effect of the charge complementarity between host and guest on the binding affinity in water.²⁴² The obtained results indicated that the difference in binding affinities (K_a) of a pair of complexes of the two hosts with the same charged guest, *e.g.*, adamantane bearing a carboxylate or ammonium group, was around 1 order of magnitude. This finding evidenced that charge complementarity is also required for efficient binding between charged partners even in water. A similar result was disclosed previously in the section dedicated to cyclophane receptors (section 3.1). Not surprisingly, neutral adamantane guests displayed similar binding affinities for both cavitands.

Long-alkyl chain guests were bound with unusual conformations in the hydrophobic cavity of benzimidazole deep cavitands.²³² Trembleau and Rebek observed that surfactants, such as dodecyl sulfate 92 (SDS) and dodecyl phosphocholine 93 (DPC) (Figure 40), adopted a helical conformation when included in the deep cavity of tetra-carboxylate 89^{4-} in water.²⁴³ The terminal methyl group of the bound guest was located in the deepest region of the receptor's cavity, whereas the polar head protruded from the cavity and remained exposed to the bulk aqueous solution. Interestingly, the buried section of the aliphatic chain of 92^- and 93 featured a condensed coiled conformation which filled better the cavity volume and established a larger number of CH- π interactions (see section 2) with the aromatic walls of the receptor 89^{4-} (Figure 45). Note that the helical arrangement of the alkyl chain of the bound surfactant was *ca.* $13 \text{ kJ}\cdot\text{mol}^{-1}$ higher in energy than the extended counterpart (2.1 – $2.5 \text{ kJ}\cdot\text{mol}^{-1}$ per gauche interaction). Nevertheless, the gain in free energy of binding overcame the energetic cost of the guest to adopt the coiled structure owing to the existence of a larger number of intermolecular interactions than in a fully extended conformation of the guest.

The coiled helical arrangement adopted by polar guests with long-alkyl chains when included in the cavity of 89^{4-} was also observed for linear hydrocarbons.²⁴⁴ Interestingly, the ^1H NMR spectrum of the 1:1 inclusion complex of *n*-octane 94 (Figure 40) with deep cavitand 89^{4-} showed a set of upfield shifted signals for the protons of the bound guest displaying an unexpected symmetrical pattern (only four methylene signals were observed). The comparison of the ^1H NMR spectrum for the complex of *n*-octane, $94\subset 89^{4-}$ with that of the bound surfactant 92^- (SDS) suggested that the chemical shift of the four signals assigned to the methyl and methylene protons of bound *n*-octane 94 were, in fact, the average of the two different magnetic environments experienced by the α - and ω -

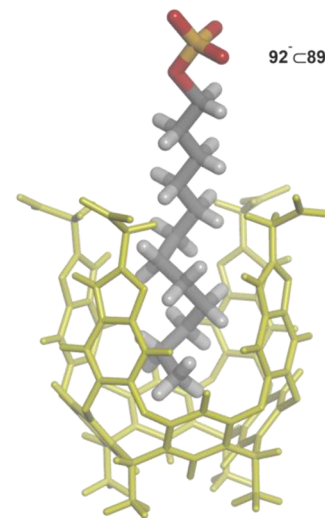


Figure 45. Energy minimized structure (MM3) of $92^- \subset 89^{4-}$. The resorcin[4]arene (in yellow) and the guest are depicted in stick representation. Note that the buried section of 92^- in the cavity of 89^{4-} adopts a helical conformation.

methyl moieties, the $\alpha + 1$ and $\omega - 1$ methylenes, and so on. The signal pattern and the chemical shift values of the protons of bound 94 were in agreement with a compact, coiled structure experiencing a fast tumbling motion on the chemical shift time scale (Figure 46). In contrast, shorter *n*-alkanes, such as *n*-pentane, featured fully extended carbon-chain conformations in the bound form.²⁴⁵

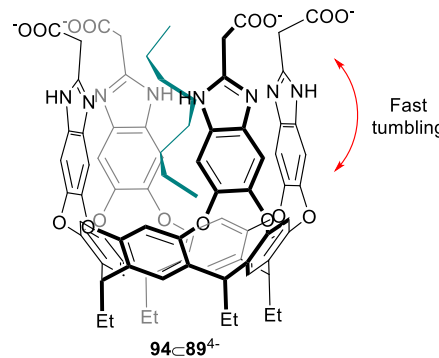


Figure 46. Line-drawing structure of the $94 \subset 89^{4-}$ complex. Bound guest (in green) adopts a coiled conformation and experiences a fast tumbling motion (red double arrow) on the ^1H NMR chemical shift time scale.

Alternative water-soluble resorcin[4]arene cavitands displaying deep hydrophobic cavities were designed by Gibb *et al.*, 95^{246} and 96^{247} (Figure 39). Gibb's deep-cavity cavitands incorporated four water-solubilizing groups at the upper and four more at the lower rim. Gibb's cavitands featured a conformationally rigid "vase" conformation in water. In particular, the octa-acid cavitand 95 was soluble in neutral water at micromolar concentrations. The solubilization of 95 in water at millimolar concentrations required a pH increase >9 . The cavitand 96 bearing eight peripheral quaternary ammonium groups was structurally analogous to the octa-acid 95 . The open-end of the cavity in the Gibb's cavitands was surrounded by a large hydrophobic section suggesting that

these cavitands could have a tendency to self-associate into high-order aggregates¹⁴ (see section 6.2).

Gibb and Gibb applied the octa-acid **95** to investigate the Hofmeister effect (see section 2.2) in its binding processes with nonpolar residues.²⁴⁸ The use of synthetic model systems is of great importance for our further understanding of the Hofmeister effect in natural complexes. In a 10⁻² M phosphate water-buffered solution at pH = 11.3, the interaction between the adamantane carboxylic acid **97** (Figure 40) and the octa-acid **95** produced a 1:1 inclusion complex. At pH = 11.3, all carboxylic acid groups of the host **95** and the guest **97** were ionized as carboxylates: octa-acid **95** was converted into the octa-carboxylate [95-8H]⁸⁻ and **97** was converted into the carboxylate [97-H]⁻. In the inclusion complex [97-H]⁻⊂[95-8H]⁸⁻, the adamantane group of [97-H]⁻ was deeply included in the hydrophobic cavity of [95-8H]⁸⁻. On the other hand, the carboxylate group of bound [97-H]⁻ protruded out of the cavity and remained exposed to the bulk aqueous solution. The protrusion of the guest's carboxylate prevented the dimerization of the bound cavitand octa-carboxylate [95-8H]⁸⁻. The binding constant value for the [97-H]⁻⊂[95-8H]⁸⁻ complex was determined to be $K_a = 4.7 \times 10^6 \text{ M}^{-1}$ ($\Delta G = -38.1 \text{ kJ}\cdot\text{mol}^{-1}$). In the presence of "salting-out" anions (F⁻ and SO₄²⁻), the free energy of binding for the [97-H]⁻⊂[95-8H]⁸⁻ complex was favored by *ca.* 2.1 kJ·mol⁻¹. This result was in agreement with the enhancement of the HE exerted by "salting-out" anions. In contrast, the presence of "salting-in" anions (I⁻, SCN⁻, and ClO₄⁻) were detrimental for the binding process. For example, the reduction in the binding free energy of the [97-H]⁻⊂[95-8H]⁸⁻ complex was notable in the presence of perchlorate, *ca.* 4.2 kJ·mol⁻¹.

The binding of the adamantane carboxylate [97-H]⁻ to the hydrophobic cavity of [95-8H]⁸⁻ in phosphate buffer solution was driven by enthalpy. In striking contrast, the same complexation process in the presence of 0.1 M NaClO₄ was driven by entropy. Interestingly, the detailed analysis of the ¹H NMR titration spectra of ClO₄⁻ with octa-carboxylate cavitand [95-8H]⁸⁻ revealed that the "salting-in" anion interacted with the receptor forming a 1:1 host/guest inclusion complex. The binding constant value determined for the ClO₄⁻⊂[95-8H]⁸⁻ complex was 95 M⁻¹. Therefore, at high NaClO₄ concentrations, the "salting-in" anion effectively competed with the binding of a convex hydrophobe, *i.e.*, the adamantane residue of [97-H]⁻, for the hydrophobic binding pocket of [95-8H]⁸⁻. A further-reaching conclusion of this work was that the interaction of "salting-in" anions with concave nonpolar aromatic regions might be the basis of the mechanism of the "salting-in" effect that they produce on protein solutions. The correct location of four methyl groups at the portal of a slightly more lipophilic version of receptor [95-8H]⁸⁻ induced the spontaneous drying of its nonpolar binding site (see section 2.1).⁸⁰

Geremia, Dalcanale, and co-workers introduced tetraphosphonate resorcin[4]arene cavitands with pyridinium "feet". For example, the tetra-phosphonate cavitand **98** bear four P=O groups inwardly directed with respect to the cavity of the receptor²⁴⁹ (Figure 39). The X-ray crystal structures of structurally related tetra-phosphonate cavitands showed that water molecules interacted with the polar functions, but the cavity of the receptors was "dry". This observation suggested that the cavity of the resorcin[4]arene **98** was poorly solvated also in aqueous solution.

The tetra-phosphonate tetra-pyridinium cavitand **98**⁴⁺ was shown to be an efficient receptor for N-methylated amino acids in water.²⁴⁹ The stability constants for the 1:1 inclusion complexes were calculated to be in the range of $K_a = 10^3$ – 10^4 M^{-1} . The binding processes were characterized by a favorable enthalpy term and opposed entropy. For example, the 1:1 inclusion complex of the methyl ester of N-methyl glycine, **99**⁺ (Figure 40), and the tetra-phosphonate receptor **98**⁴⁺ displayed the N-methyl group of the guest buried in the cavity of the receptor (Table 8). Therefore, the binding of the ammonium cation residue of **99**⁺ was stabilized through cation–dipole and hydrogen-bonding interactions with the P=O groups of the receptor (Figure 47). Amino acids lacking N-methylation were not bound by the tetra-phosphonate cavitand **98**⁴⁺ in water.

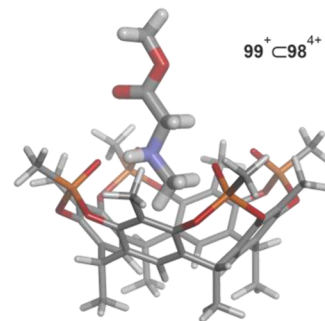


Figure 47. Energy minimized structure (MM3) of the simplified **99**⁺⊂**98**⁴⁺ complex. The cavitand and the guest are depicted in stick representation. Phosphonate substituents and water-solubilizing groups were pruned to methyl groups to simplify the calculation.

Yu, Rebek, and co-workers applied benzimidazolone resorcin[4]arene cavitands **100** and **101** (Figure 39) to mediate/catalyze chemical transformations in water.²⁵⁰ For example, the tetra-cationic cavitand **100**⁴⁺ was able to bind long-chain α,ω -amino acids in a folded conformation.²⁴⁰ The binding geometry of the complex brought in close proximity the terminal amino and acid groups of the guest. In this arrangement, the intramolecular cyclization reaction of the bound amino acid to produce the corresponding lactam was favored. Therefore, the cyclization of α,ω -amino acid **102** gave the 12-membered ring lactam **103** with a 4-fold yield improvement in the presence of the cavitand **100**⁴⁺ (Figure 48) compared to the same reaction in the bulk. Most likely, the yield of the lactam was higher in the presence of the cavitand because the competitive intermolecular reactions leading to oligomeric products were not favored.

The mediation of intramolecular cyclization reactions of long-chain substrates required the use of cavitand **100** in stoichiometric amounts. This limitation was somehow alleviated by the fact that the chaperone cavitand **100** could be reused after product extraction with an organic solvent. The Rebek group reported other examples of mediated cyclization reactions using benzimidazolone resorcin[4]arene deep cavitands as synthetic chaperones.^{251,252}

Another application of benzimidazolone cavitands consisted of the monofunctionalization of dissymmetric compounds (*i.e.*, desymmetrization). When two functional groups present in the same molecule are totally independent, they exhibit equal reaction rate constants leading to a mixture of products. For example, consider the reaction of a difunctional symmetric compound, A, to give the monofunctionalized product, B, with

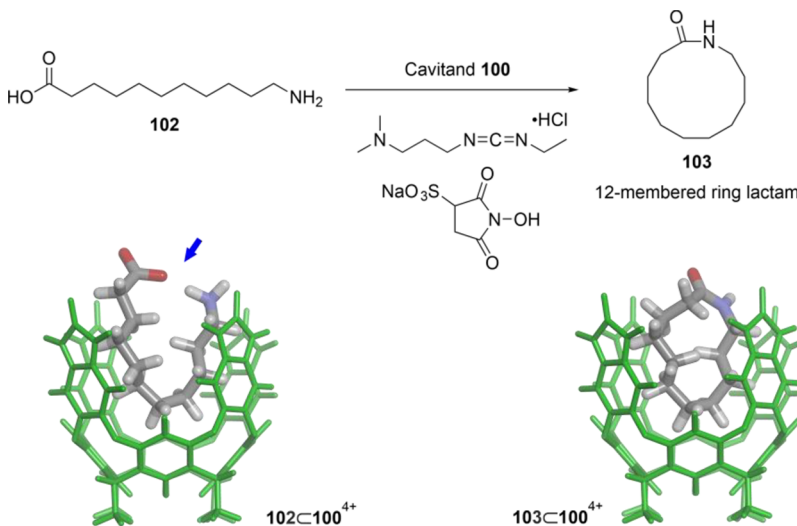


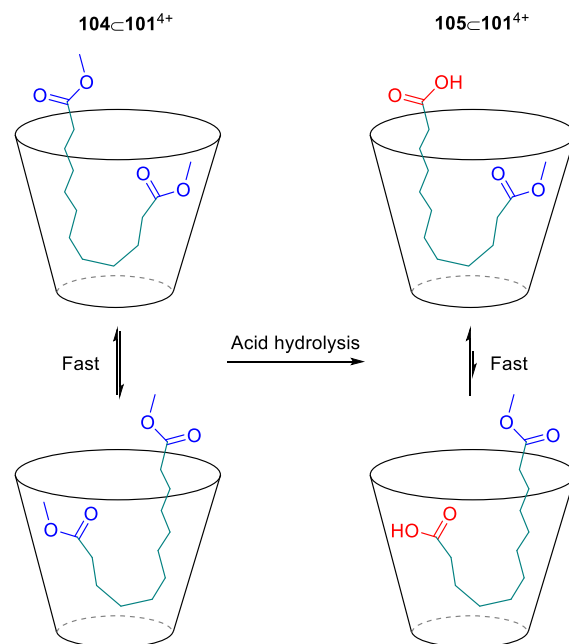
Figure 48. (top) Intramolecular cyclization reaction of the α,ω -amino acid **102** to give lactam **103**; (bottom) energy minimized structures (MM3) of the simplified inclusion complexes of **102** and **103** with cavitand **100**⁴⁺. The cavitand (in green) and the guests are depicted in stick representation. Arrow (in blue) indicates the proximity of the two reacting groups in the $102 \subset 100^{4+}$ complex.

a rate constant k_1 ($A \rightarrow B$), followed by the reaction of B to yield the direacted compound, C , with a rate constant k_2 ($B \rightarrow C$). In the case that $k_1 = k_2$, the upper limit for the yield of the monoreacted compound B is 36.8%.²⁵³ This outcome complicates the purification and isolation of the synthetically valuable monoreacted (nonsymmetric) product. Using the deep cavitand **101**, long-chain α,ω -difunctional substrates were quantitatively bound in water solution at millimolar concentration to form 1:1 inclusion complexes.

For example, the long-chain diester **104** included in the tetra-cationic cavitand **101**⁴⁺ experienced a chemical exchange process that was fast on the chemical shift time scale between two *J*-conformations, most likely through a “yo-yo” motion²⁵³ (Scheme 4). This motion provoked the preferential exposure of one of the two terminal ester groups to the bulk aqueous medium, while the other remained buried in the hydrophobic cavity of the receptor. In this case, because of the low solubility of the diester **104** in water, the acid hydrolysis of the ester function occurred at the water/cavitand interface. Thus, the exposed ester group of **104** produced the monoester monoacid product **105**. The increase in solubility of the diester **104** produced by complex formation accelerated the rate of the hydrolysis in comparison to the same reaction in the absence of the cavitand **101**⁴⁺. In contrast, the rate of the hydrolysis reaction of the terminal ester group of monofunctionalized **105** was reduced because the bound guest adopted a biased *J*-conformation. The bound monofunctionalized product **105** showed the terminal ester group buried in the receptor’s cavity, where the reaction did not take place and the polar carboxylic acid exposed to the bulk aqueous solution. In other words, the ester group of **105** spent more time buried in the cavity of the receptor, which explained the decrease in the rate of the hydrolysis of **105** to give the diacid product. Under basic conditions, the monoester monoacid product **105** was produced in more than 90% yield because the $[105\text{-H}]\text{-}\subset\text{C}101^{4+}$ inclusion complex precipitated from the solution.

Other applications of water-soluble resorcin[4]arene deep cavitands were recently reported by Blackmond, Yu, Rebek, and co-workers.^{250,254–256}

Scheme 4. Cartoon Representation of the Hydrolysis Reaction of Diester **104 to Yield Monoester Monoacid **105** in the Presence of Cavitand **101**⁴⁺ (Represented as a Vase)^a**



^aExchange dynamics between *J*-conformations of bound guests are indicated. Note that both bound guests, **104** and **105**, experience “yo-yo” motions that are fast on the ¹H NMR chemical shift time scale. In the case of bound **105**, the exposure of the terminal carboxylic acid group to the bulk solution is favored.

5. COVALENT RECEPTORS POSSESSING A POLAR HYDROPHOBIC CAVITY

The incorporation of converging polar groups in the receptor’s cavity expands its binding selectivity beyond the size and shape complementary criteria. Moreover, the *endo*-functionalized receptor’s cavity becomes suitable for the inclusion of polar substrates. The complexes of polar hosts with polar guests establish complementary polar interactions compensating, to some extent, the energy required for the dehydration of the

functional groups before binding.⁸⁴ In this section, we discuss the properties of receptors possessing functionalized cavities, which were designed for the selective and efficient binding of small polar guests in water solution.

5.1. Temple Receptors

A general approach used to rationally design polar hydrophobic cavities has been the use of two aromatic panels and a number of conformationally rigid and polar spacer groups.²⁵⁷ As shown in Figure 49, the resulting arrangement resembles a

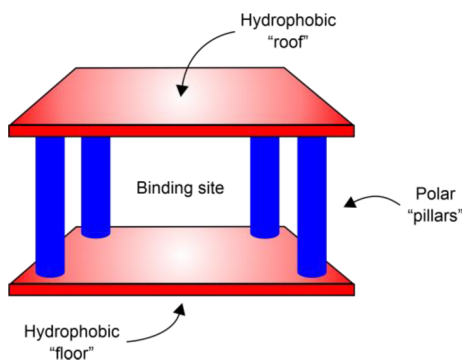


Figure 49. Cartoon of the construction of “temple” receptors.

classical “temple”, featuring hydrophobic “roof” and “floor” and polar functionalities as “pillars” that avoid the hydrophobic collapse of the cavity.⁵⁶ “Pillars” have also been functionalized with ionizable and charged groups to impart water solubility to the final construct.

The polar/functionalized hydrophobic cavity of the “temple” receptors can accommodate polar guests, such as carbohydrates.²⁵⁸ In nature, lectins are protein receptors that recognize carbohydrates in aqueous solution. Lectins display a preorganized aromatic cleft or cavity in which polar groups converge.⁵⁶ Therefore, carbohydrate recognition is driven by the HE (section 2.1) and the establishment of hydrogen-bonding and CH–π interactions (section 2). The stability constant values for monosaccharidelectin complexes are in the range of 10^3 – 10^4 M^{-1} . Carbohydrate families and even more monosaccharides are structurally very similar. This fact implies that in order to achieve high levels of affinity and binding selectivity in their recognition process, multiple hydrogen bonds and CH–π contacts⁵³ must be present in the formed complexes.^{258,259}

All-equatorial mono- and disaccharides are ideal guests for the synthetic “temple” receptors, aka synthetic lectins.^{56,258} All-equatorial saccharide derivatives feature the larger number of axial CH groups, which are suitable to interact with the aromatic panels at the “roof” and “floor” of the receptor. In turn, the equatorially oriented OH functions can establish hydrogen-bonding interactions with the polar groups from the “pillars” inwardly directed to the cavity. The group of Davis designed efficient “temple” receptors for the recognition of carbohydrates in water.²⁶⁰ Different aromatic scaffolds (*e.g.*, biphenyl, *tert*-phenyl, pyrene, *etc.*) were used for the construction of the “roof” and “floor” of the “temple” structures. The used “pillars” usually contained isophthalamide units. The amide groups provided polar functions for the establishment of hydrogen-bonding interactions with the included guest. It is worth mentioning here that there are receptor’s conformations locating most of the amide NH

protons of the “pillars” inwardly oriented with respect to the cavity of the “temple” receptor.

One of the earliest versions of the water-soluble “temple” receptors reported by Davis *et al.* was based on biphenyl units. The biphenyl structure was slightly twisted owing to the steric clashes arising from the opposite *ortho*-protons of the connected aromatic units in a planar conformation. Nevertheless, the biphenyl unit was a good aromatic platform to establish CH–π interactions with the axially oriented CHs of the bound saccharides. For example, the tricyclic receptor **106** contained two biphenyl units (“floor” and “roof”) linked together by four isophthalamide groups (“pillars”)²⁶¹ (Figure 50). The polar “pillars” could offer a total of eight hydrogen bond donors directed toward the aromatic binding site. The phenyl components of the “pillars” were equipped with small dendrons terminated with carboxylate groups to ensure receptor’s water solubility. In general, the “temple” receptors formed 1:1 inclusion complexes with mono- and disaccharides in water solution.²⁶⁰ For example, freshly dissolved D-glucose **107** (Figure 51) in water exists as a mixture of α- and β-anomers in a 72:28 ratio. The apparent binding constant value determined for the $\text{107}\subset\text{106}^{12-}$ complex was 4.6 M^{-1} (weighted average of K_a values for putative $\alpha\text{-107}\subset\text{106}^{12-}$ and $\beta\text{-107}\subset\text{106}^{12-}$ complexes). The apparent binding constant value increased up to 9.2 M^{-1} when equilibrated D-glucose (40:60 α/β ratio) was used as guest²⁶¹ (Table 9). This result suggested that “temple” receptor **106**¹²⁻ displayed selectivity for the binding of the β-anomer of D-glucose **107**. Interestingly, 2D NMR experiments revealed that, in solution, the β-D-glucose isomer, **β-107**, was included almost exclusively in the cavity of **106**¹²⁻. Thus, the minimum value for the binding constant of the $\beta\text{-107}\subset\text{106}^{12-}$ complex was estimated as 9.2 M^{-1} . Glycosides do not undergo mutarotation in water solution. The pure methyl β-D-glucoside **108** (Figure 51) formed a 1:1 inclusion complex with “temple” receptor **106**¹²⁻, for which a binding constant value of $K_a = 27.3\text{ M}^{-1}$ was calculated. Receptor **106**¹²⁻ also bound disaccharides in water, such as D-cellobiose **109** (Figure 51). However, the interaction between the “temple” receptor **106**¹²⁻ and D-cellobiose **109** was weaker ($K_{app} = 16.6\text{ M}^{-1}$) than with the methyl β-D-glucoside **108**.²⁶¹

The biphenyl “temple” receptor **106**¹²⁻ displayed good binding selectivity toward certain monosaccharides, despite the low magnitude of their binding constants. The apparent binding constant value for the complex of the equilibrated D-glucose, $\text{107}\subset\text{106}^{12-}$, was 5-fold larger than that of the D-galactose counterpart (32:68 α/β ratio), **110**¹²⁻²⁶¹ (Table 9). This binding difference is notable if one considers that the two monosaccharides, **107** and **110**, are epimers only at C4-position (Figure 51).

To improve the binding affinity of “temple” receptor **106**, alkoxy substituents were incorporated at *para*-positions of the biphenyl units.²⁶² This structural modification was expected to produce an increase in the hydrophobicity of the receptor’s cavity and reduce the access of bulk water molecules for the solvation of the amide groups. The obtained results demonstrated a moderate increase in the thermodynamic stabilities of the all-equatorial monosaccharides complexes (*i.e.*, 2–4 times). In addition, the incorporation of the *para*-substituents in the biphenyl scaffold also affected the electron density of its π-systems and, thereby, the strength of the CH–π interactions (see section 2) established with the bound carbohydrates. The use of biphenyl scaffolds functionalized

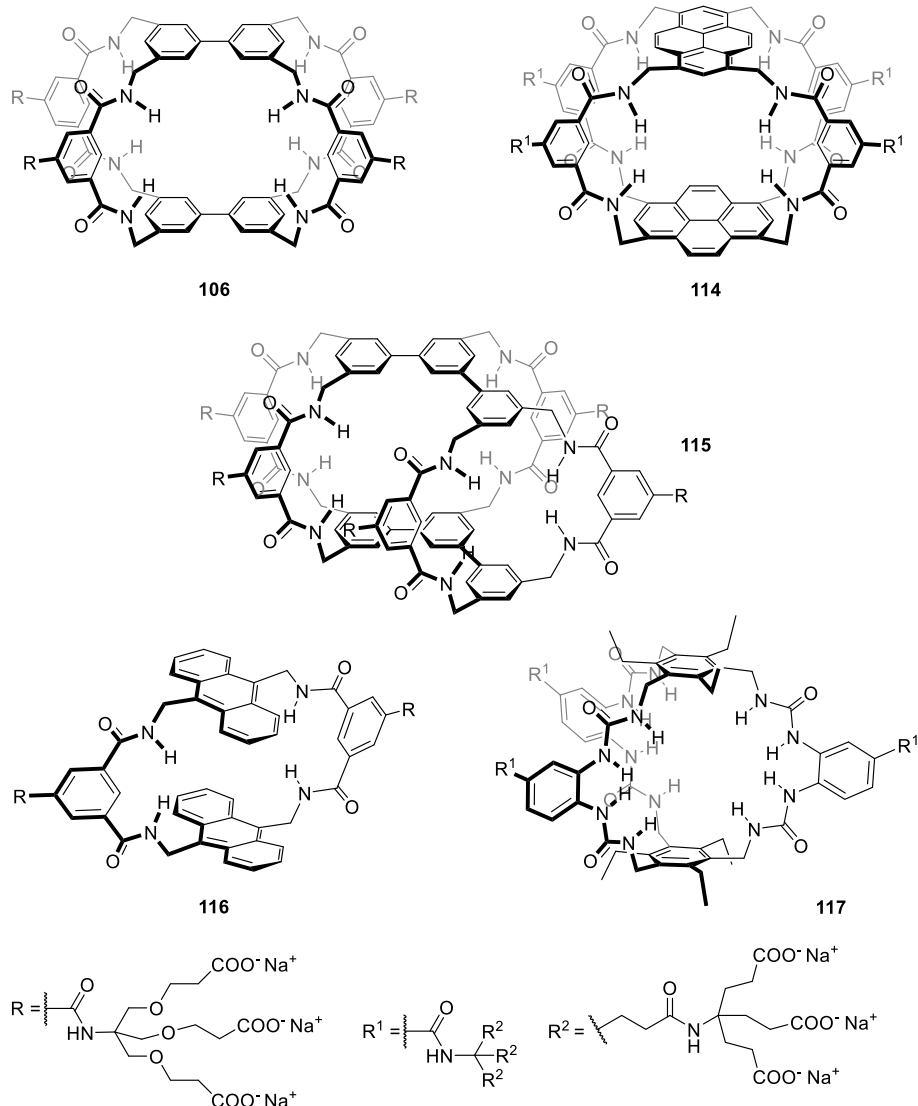


Figure 50. Line-drawing structures of “temple” receptors.

with OH and F groups produced a small increase in the binding constant values.²⁶³ The contribution of the CH–π interactions to the overall thermodynamic stability of the complex was likely masked by other factors such as changes in the hydrophobicity of the cavity and the receptor’s conformation. Additionally, the structure of the “pillar” components of the receptor were also modified. For example, two of the isophthalamide linkers in the “pillars” of **106** were replaced by *bis*-aminomethyl pyrrole units in the structure of the “temple” receptor.²⁶⁴ This structural modification did not induce significant changes in binding affinity but slightly improved selectivity.

N-Acetyl-monosaccharides interacted with tricyclic receptor **106**¹²⁻ featuring binding constant values larger than that of the parent compounds.²⁶⁵ The β-anomer of *N*-acetyl D-glucosamine **111** (α/β ratio = 64:36 in water, Figure 51) was exclusively bound by receptor **106**¹²⁻ featuring an apparent binding constant value of $K_{app} = 56\text{ M}^{-1}$. The anomers of the methyl-glycoside derivative of *N*-acetyl D-glucosamine **111**, **112** α-anomer and **113** β-anomer (Figure 51), displayed significantly different affinities for the “temple” receptor **106**¹²⁻. The determined binding constant for the

112 C **106**¹²⁻ complex was 24 M^{-1} , whereas the value increased to $6.3 \times 10^2\text{ M}^{-1}$ for the complex formation with the β-anomeric guest, **113** C **106**¹²⁻. Receptor **106**¹²⁻ showed a binding affinity for methyl β-N-acetyl D-glucosamine **113** that was 23-fold larger than for the methyl β-D-glucoside **108** (Table 9). Moreover, the affinity of receptor **106**¹²⁻ for methyl β-N-acetyl D-glucosamine **113** was similar to that of the natural wheat germ agglutinin. Even more interesting, receptor **106**¹²⁻ featured an anomer binding selectivity for the methyl β-N-acetyl D-glucosamine **113** higher than that of the natural lectin.

The binding geometry of the **113** C **106**¹²⁻ complex was investigated using 2D NMR spectroscopy experiments and molecular modeling studies²⁶⁵ (Figure 52). The energy minimized structure (MM3) of the **113** C **106**¹²⁻ complex showed the β-N-acetyl D-glycoside, **113**, fully included in the polar hydrophobic cavity of the “temple” receptor **106**¹²⁻. The *N*-acetyl amino group protruded partially outside of the cavity throughout one of its portals. The amide NH of the guest was involved in NH–π interactions with the biphenyl units of the receptor.²⁵⁸ The hydroxymethyl group of included **113** was located in the portal of the cavity, which was opposite to the one threaded by the *N*-acetyl amino substituent. The molecular

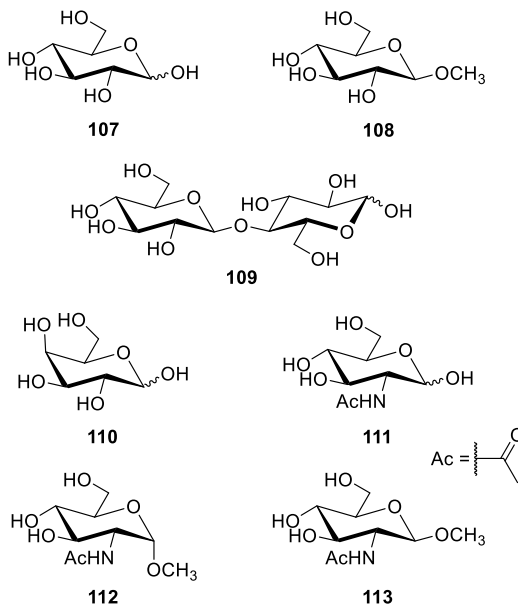


Figure S1. Line-drawing structures of the carbohydrates used as guests for the “temple” receptors.

modeling structure of the $113 \subset 106^{12-}$ complex confirmed that all polar substituents of the monosaccharide were equatorially oriented in order to minimize steric clashes with the aromatic panels of the receptor and, at the time, maximize host–guest interactions. The preferred equatorial orientation of all substituents served to explain the lower binding affinities displayed by receptor 106^{12-} on binding the α -N-acetyl D-glycoside, 112, as well as the α -anomeric isomers of other monosaccharides.

The binding performance of the Davis’s “temple” receptors was improved by replacing the biphenyl units in 106 with pyrene derivatives in 114²⁶⁶ (Figure 50). The pyrene scaffold was completely planar and offered a larger aromatic surface area. Therefore, the HE and the nonpolar contacts with the axial CHs of bound carbohydrates were expected to be enhanced. For example, the β -N-acetyl D-glycoside 113 and the pyrene-based receptor 114³⁶⁻ formed a thermodynamically and kinetically stable 1:1 inclusion complex in water featuring a binding constant value of $K_a = 1.8 \times 10^4 \text{ M}^{-1}$. This value represented almost a 30-fold increase on binding affinity with respect to the $113 \subset 106^{12-}$ complex (Table 9). In contrast, the binding selectivity for the two anomers $K_a(113 \subset \text{receptor})/K_a(112 \subset \text{receptor})$ dropped from a value ratio of 23 for receptor 106^{12-} to 11 for the pyrene-based counterpart 114³⁶⁻.

Davis *et al.* showed that larger “temple” receptors efficiently bound disaccharides in water solution.^{267,268} The authors synthesized the tetra-cyclic receptor 115 bearing *tert*-phenyl units at the “roof” and “floor” of its “temple” structure and five isophthalamide derivatives as “pillars”²⁶⁷ (Figure 50). The “pillar” units were equipped with carboxylate-terminated dendrons. An overall 15 negative charge ensured the solubility of “temple” 115¹⁵⁻ in water. “Temple” receptor 115¹⁵⁻ complexed disaccharide D-cellulobiose 109 (Figure 51) in water, forming a 1:1 inclusion complex with an apparent stability constant of $K_{app} = 6.0 \times 10^2 \text{ M}^{-1}$. The detailed analyses of a series of 2D NMR spectra acquired for the $109 \subset 115^{15-}$ complex indicated that the glycosidic bond of the bound disaccharide adopted a *cis*-conformation. In this conformation, the bound guest fit nicely in the polar

Table 9. Binding Constant or Apparent Binding Constant Values (K_a or K_{app} , M^{-1}) of Selected Complexes of “Temple” Receptors Formed in Water Solution^a

Guests	“Temple” receptors				
	106^{12-}	114^{36-}	115^{15-}	116^{6-}	117^{27-}
$107^{261,270,271}$	9.2			56	1.8×10^4
$108^{261,270}$	27.3			96	
$109^{261,267}$	16.6		6.0×10^2		
110^{261}	2.1				
111^{265}	56				
$112^{265,266}$	24	1.6×10^3			
$113^{265,266}$	6.3×10^2	1.8×10^4			

^aSee Figure 50 for the line-drawing structures of the receptors. Details on the pH used in the binding experiments are provided in the text.

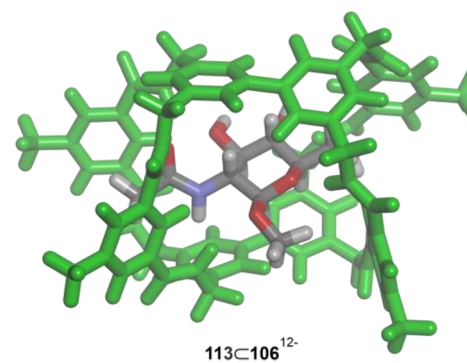


Figure 52. Energy minimized structure (MM3) of the simplified $113 \subset 106^{12-}$ complex. “Temple” receptor (in green) and bound guest are depicted in stick representation. Water-solubilizing groups were pruned to methyl groups to simplify the calculation.

hydrophobic cavity of the “temple” receptor and satisfied the shape, size, and function complementarity principles of complex formation (Figure 53).

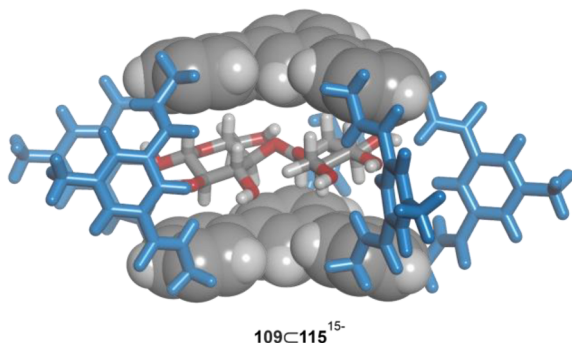


Figure 53. Energy minimized structure (MM3) of the simplified cellobiose complex, $109\subset 115^{15-}$. The “roof” and “floor” of the “temple” receptor are shown as CPK models, and the “pillars” (in blue) are depicted in stick representation. The bound disaccharide is depicted in stick representation. Water-solubilizing groups were pruned to methyl groups to simplify the calculation.

The results of ITC experiments indicated that the binding process leading to the $109\subset 115^{15-}$ complex was enthalpically driven ($\Delta H = -13.4 \text{ kJ}\cdot\text{mol}^{-1}$) and accompanied by a small favorable entropy ($T\Delta S = +2.6 \text{ kJ}\cdot\text{mol}^{-1}$).²⁶⁷ The favorable enthalpic gain on complex formation was assigned to the hydrogen-bonding and CH–π interactions that were established between the host and the guest upon complex formation.^{56,259}

The effect of “salting-in” anions, such as thiocyanate (SCN^-), on carbohydrate binding was investigated using the synthetic “temple” receptors **106** and **115**.²⁶⁹ In the presence of 0.3 M KSCN, the association constant values for the saccharide complexes experienced a decrease of more than 3-fold. Most likely, the “salting-in” anion competed with the carbohydrate guests for the binding of the nonpolar regions of the cavity⁸⁵ and, possibly, with the inwardly directed hydrogen bond donors of the “temple” receptor.

The sensing of D-glucose in biological media is a challenging task because it requires the use of synthetic water-soluble receptors displaying high binding affinity and selectivity for a highly polar and hydrophilic guest (see binding of other polar guests in sections 5.2 and 5.3). In recent years, the group of Davis has developed “temple” receptors for the selective binding of D-glucose in water. For example, the “temple” receptor **116** was based on two anthracene panels and two isophthalamide spacer as “pillars”²⁷⁰ (Figure 50). The bis-anthracenyl receptor **116**⁶⁻ complexed D-glucose **107** featuring an apparent binding constant value of $K_{\text{app}} = 56 \text{ M}^{-1}$ in water. A similar value was determined in 0.1 M phosphate buffer at pH = 7.1. The methyl β-D-glucoside, **108**, and the “temple” receptor, **116**⁶⁻, formed a 1:1 inclusion complex featuring a stability constant of $K_a = 96 \text{ M}^{-1}$ in water (Figure 54). The magnitude of these binding constants was adequate for the sensing of D-glucose at the concentration present in human blood. Receptor **116**⁶⁻ displayed significantly lower binding affinities toward other monosaccharides, K_a and $K_{\text{app}} < 1 \text{ M}^{-1}$.

More recently, Davis *et al.* reported a highly efficient receptor, **117** (Figure 50), with improved affinity for the binding of D-glucose, **107**, in water.²⁷¹ The “temple” receptor **117** was based on two tri-1,3,5-ethylmesitylene units linked together by three *ortho*-urea-substituted phenyl linkers. The six urea groups of receptor **117** offered a total of 12 hydrogen bond donor NH groups inwardly oriented toward the three-dimensional cavity of the receptor. The glucose complex,

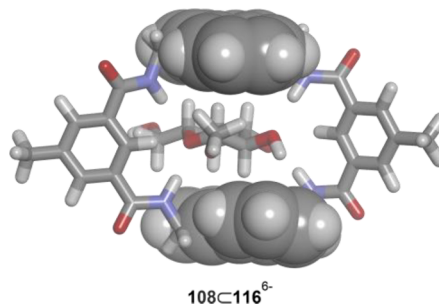


Figure 54. Energy minimized structure (MM3) of the simplified methyl β-D-glucoside complex, $108\subset 116^{6-6}$. The “roof” and “floor” units of the receptor are shown as CPK models, and the “pillars” are depicted in stick representation. The guest is depicted in stick representation. Water-solubilizing groups were pruned to methyl groups to simplify the calculation.

$107\subset 117^{27-}$, featured a remarkable apparent binding constant value of $K_{\text{app}} = 1.8 \times 10^4 \text{ M}^{-1}$ in 10^{-2} M phosphate buffer at pH = 7.4 (Figure 55). Other monosaccharides exhibited

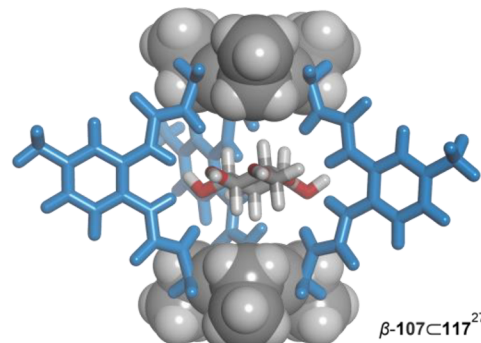


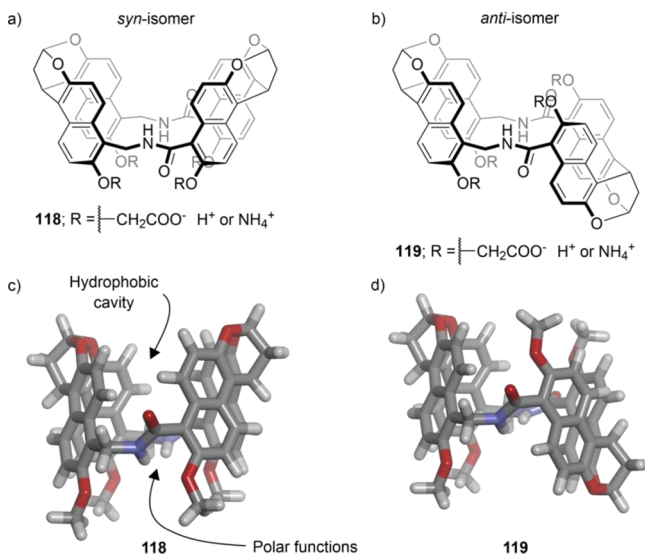
Figure 55. Energy minimized structure (MM3) of the simplified $\beta\text{-}107\subset 117^{27-27}$ complex involving the β-anomer of glucose. The “roof” and “floor” units of the receptor are shown as CPK models, and the “pillars” (in blue) are depicted in stick representation. The guest is depicted in stick representation. Water-solubilizing groups were pruned to methyl groups to simplify the calculation.

binding constant values that were at least 1 order of magnitude lower than that of the $107\subset 117^{27-}$ complex. Additionally, nonsaccharide guests, such as uric acid, adenosine, or paracetamol, were not included in the cavity of 117^{27-} . These results demonstrated that synthetic receptors relying on hydrogen-bonding and CH–π interactions can feature high binding affinity and selectivity for D-glucose recognition and sensing in water solution.

“Temple” receptors, which structurally resemble the ones discussed above, were used to complex polysaccharides.²⁷² Polysaccharides, such as cellulose, display low solubility in water. The “temple” receptors were bound to different regions of the polysaccharide structure. The resulting supramolecular polymer featured a polyrotaxane topology and improved the water solubility of the bound polysaccharide.

5.2. Naphthotubes

Glass *et al.*,²⁷³ as well as Jiang *et al.*,²⁷⁴ used *endo*-functionalized molecular tubes (aka naphthotubes) based on two *bis*-naphthalene cleft-like units linked together by two amide bonds, as receptors of polar guests in water solution.²⁷⁵ The synthesis of these receptors yielded a mixture of two isomers: *syn* and *anti* (Figure 56). The *syn*-isomer displayed the two *bis*-

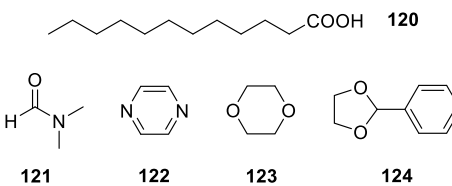


naphthalene units with identical orientation. On the contrary, the *anti*-isomer featured the naphthalene clefts linked in opposite directions.

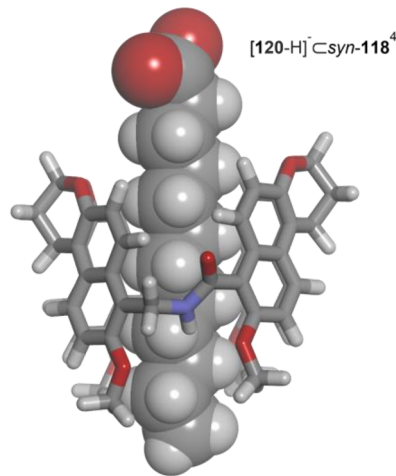
The structure of the *syn*-isomer, *syn*-118, was rather conformationally rigid and presented a deep aromatic cavity (**Figure 56a,c**). However, the *anti*-isomer, *anti*-119, was structurally more flexible, displaying a shallow aromatic cavity (**Figure 56b,d**). The cavities of both isomers were open at two opposite ends. In addition, the molecular tubes, *syn*-118 and *anti*-119, contained two amide linkages, with the NHs inwardly directed with respect to the aromatic cavities. Finally, the structures of the synthesized naphthotubes also had peripheral carboxylate groups, which promoted water solubility.²⁷⁵

The molecular tube *syn*-118 showed a deep hydrophobic cavity with an open polar end defined by the two inwardly directed amide NHs (**Figure 56a,c**). Therefore, the NH amide groups of *syn*-118 were partially shielded from the bulk aqueous solution, but the cavity of the naphthotube was likely solvated by water molecules. Jiang *et al.* pointed out that the release of bound water molecules from the cavity of the molecular tube *syn*-118 to the bulk solution was the main force to drive the inclusion of complementary polar guests.²⁷⁴

The synthesis of the water-soluble naphthotubes *syn*-118 and *anti*-119 was originally reported by Glass *et al.* in 2004.²⁷³ The authors used the *endo*-functionalized tubes to investigate the binding of long-chain carboxylic acids, *i.e.*, fatty acids. The binding experiments were conducted in 2×10^{-2} M HEPES buffer at pH = 8.4. The obtained results showed that the tetra-carboxylate receptors *syn*-118⁴⁻ and *anti*-119⁴⁻ were able to bind the hydrocarbon chain of the fatty acids mainly through the HE and the establishment of hydrogen-bonding interactions worked synergistically to drive the inclusion of the neutral polar molecules in the cavity of the *endo*-functionalized receptors. For example, *anti*-119⁴⁻, produced a 1:1 inclusion complex with dimethylformamide 121 (**Figure 57**) having a binding constant value of K_a ($[120\text{-H}]^-\subset\text{anti-}119^{4-}$) = 3.1×10^2 M⁻¹ in water.²⁷⁴ The complex between tetrahydrofuran and *anti*-119⁴⁻ was characterized with a similar binding constant value (**Table 10**). Note that these two guests, dimethylformamide and tetrahydrofuran, feature just one hydrogen-bonding acceptor group. Surprisingly, *syn*-118⁴⁻ was less efficient in



$[\text{H}]^-\subset\text{anti-}119^{4-}$) $\sim 2 \times 10^4$ M⁻¹ (**Figure 58** and **Table 10**). Note that 120 was deprotonated in basic aqueous buffer



solution leading to dodecanoate $[\text{120}\text{-H}]^-$. *A priori*, the polar hydrophobic cavity of receptor *syn*-118⁴⁻ was suitable for the inclusion of the terminal carboxylate group of the dodecanoate $[\text{120}\text{-H}]^-$. The bound carboxylate was expected to be involved in charge–dipole and hydrogen-bonding interactions with the amide NHs (see **section 2**). However, this binding geometry was not detected in water solution using NMR spectroscopy techniques. Most likely, the high energetic cost required for the desolvation of the carboxylate group in the case of the latter binding geometry was responsible for this result.

A few years later, Jiang *et al.* applied the same *endo*-functionalized molecular tubes, *syn*-118 and *anti*-119, for the recognition of neutral polar guests in water solution.^{275,276} The polar hydrophobic cavity of these receptors was appropriate for binding small molecules having a nonpolar section and one or two hydrogen bond acceptor groups. The HE and the establishment of hydrogen-bonding interactions worked synergistically to drive the inclusion of the neutral polar molecules in the cavity of the *endo*-functionalized receptors. For example, *anti*-119⁴⁻, produced a 1:1 inclusion complex with dimethylformamide 121 (**Figure 57**) having a binding constant value of K_a ($[120\text{-H}]^-\subset\text{anti-}119^{4-}$) = 3.1×10^2 M⁻¹ in water.²⁷⁴ The complex between tetrahydrofuran and *anti*-119⁴⁻ was characterized with a similar binding constant value (**Table 10**). Note that these two guests, dimethylformamide and tetrahydrofuran, feature just one hydrogen-bonding acceptor group. Surprisingly, *syn*-118⁴⁻ was less efficient in

Table 10. Binding Constant Values (K_a , M⁻¹) of Selected Complexes Formed with Naphthotubes Receptors in Water Solution^a

Guests	Naphthotubes	
	<i>syn</i> -118 ⁴⁻	<i>anti</i> -119 ⁴⁻
	Binding constant, K_a	
[120-H] ²⁷³	1.8×10^4	2.7×10^4
121 ²⁷⁴	1.2×10^2	3.1×10^2
THF ²⁷⁴	90	2.3×10^2
122 ²⁷⁷	1.9×10^3	2.2×10^3
123 ²⁷⁴	3.2×10^3	1.4×10^4
124 ²⁷⁷	4.6×10^5	1.4×10^6

^aSee Figure 56 for the line-drawing structure of the hosts. Details of the pH of the water solutions are given in the text.

the binding of the same polar guests.²⁷⁴ Thus, the binding affinity constants for the complexes of *syn*-118⁴⁻ were on the order of 10² M⁻¹ or even lower (Table 10). The authors suggested that the polar hydrophobic cavity of *syn*-118⁴⁻ was better solvated by water molecules than that of *anti*-119⁴⁻.²⁷⁶ Thus, the release of the bound water molecules from the cavity of *syn*-118⁴⁻ to the bulk solution upon guest binding was energetically costlier than that from *anti*-119⁴⁻.

Pyrazine 122 and 1,4-dioxane 123 (Figure 57) possess two heteroatoms that were hydrogen-bonding complementary to the polar NHs defining the polar hydrophobic aromatic cavity of the molecular tubes. In addition, the two latter polar guests were size and shape complementary to the receptor's cavity. The binding constant values of the 1:1 inclusion complexes formed between *syn*-118⁴⁻ and *anti*-119⁴⁻ receptors and the pyrazine 122 were on the order of $K_a \sim 2 \times 10^3$ M⁻¹ (Table 10).²⁷⁷ In contrast, 1,4-dioxane 123 established 1:1 inclusion complexes with the *anti*-119⁴⁻ and *syn*-118⁴⁻ receptors featuring binding constant values that differed by almost 1 order of magnitude, $K_a(123\text{C}^{\text{anti}}\text{-}119^{4-}) = 1.4 \times 10^4$ M⁻¹ and $K_a(123\text{C}^{\text{syn}}\text{-}118^{4-}) = 3.2 \times 10^3$ M⁻¹ (Figure 59).²⁷⁴ As mentioned above, the difference in binding affinities could be related to the different solvation energies of the free receptors in water solution. The heteroatoms (polar groups) of the guests, 122 and 123, established two simultaneous hydrogen-bonding interactions with the two amide NHs of the *anti*-119⁴⁻ and *syn*-118⁴⁻ receptors. ¹H NMR titration experiments

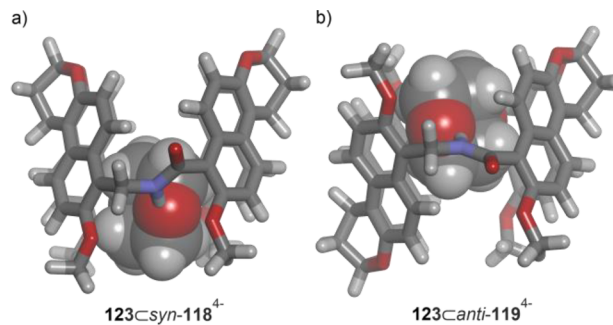


Figure 59. Energy minimized structures (MM3) of the simplified complexes: (a) $123\text{C}^{\text{syn}}\text{-}118^{4-}$ and (b) $123\text{C}^{\text{anti}}\text{-}119^{4-}$. The hosts are depicted in stick representation and the guest is shown as CPK model. Water-solubilizing groups were pruned to methyl groups to simplify the calculation.

performed in 9:1 H₂O/D₂O solution supported the formation of hydrogen-bonding interactions in the inclusion complexes (NH signals moved downfield). The nonpolar section of guests, 122 and 123, was partially shielded from the bulk solution thanks to the *bis*-naphthalene clefts of *syn*-118⁴⁻ and *anti*-119⁴⁻. It is worth mentioning here that the *anti*-receptor 119⁴⁻ displayed a high binding selectivity for 1,4-dioxane, 123, over many other investigated polar guests (*vide infra*).

ITC experiments revealed that the complexation process of 1,4-dioxane, 123, with *anti*-119⁴⁻, was mainly enthalpically driven, $\Delta H = -17.3$ kJ·mol⁻¹ and reinforced by the entropic term, $T\Delta S = +5.6$ kJ·mol⁻¹.²⁷⁴ Taken together, the results derived from the characterization of the $123\text{C}^{\text{anti}}\text{-}119^{4-}$ complex were used to invoke the “nonclassical” hydrophobic effect in the binding process (see HE in section 2.1) and the existence of polar interactions (hydrogen bonds) in water. The binding enthalpy of the $123\text{C}^{\text{syn}}\text{-}118^{4-}$ complex was similar to that of the $123\text{C}^{\text{anti}}\text{-}119^{4-}$ complex, but the entropy of binding was less favorable for the former ($T\Delta S = +2.6$ kJ·mol⁻¹).

More recently, Jiang *et al.* investigated the driving forces and molecular properties involved in the binding of polar guests by the *endo*-functionalized molecular tubes.²⁷⁷ By performing a principal component analysis of the determined binding affinities (*i.e.*, the mathematical correlation between molecular properties of guests and binding constant values of complexes), the authors concluded that the increase in the hydrophobicity, volume, surface area, and polarizability of the guest had a positive effect on the K_a value. On the other hand, the increase of the dipole moment of the guest had a detrimental effect on the K_a value. It is worth mentioning here that these molecular properties are not the only factors to be considered for efficient binding. *In silico* calculations indicated that the binding process of polar guests with *endo*-functionalized molecular tubes was also driven by the HE. In addition, the formation of the intermolecular hydrogen bonds was key in achieving high binding selectivity for polar over nonpolar counterparts. On the basis of all these findings, it was restated that the guest must be size, shape, and function complementary to the polar hydrophobic cavity of the *endo*-functionalized receptors. Furthermore, the ideal guest should form two hydrogen bonds with the amide NHs and fill completely the cavity of the receptor. The adequate filling of the receptor's cavity should provoke the release of the bound water molecules. With all this information at hand, Jiang *et al.* designed guest 124 (Figure 57), which was a perfect fit for the cavity of the *syn*-receptor

118⁴⁻ as well as a good complementarity for the binding pocket of the *anti*-receptor **119⁴⁻** (Figure 60). The **124C_{anti}-119⁴⁻**

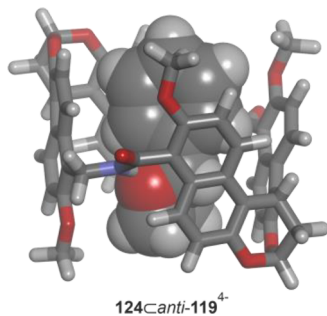


Figure 60. Energy minimized structure (MM3) of the simplified **124C_{anti}-119⁴⁻** complex. The host is depicted in stick representation and the guest is shown as CPK model. Water-solubilizing groups were pruned to methyl groups to simplify the calculation.

119⁴⁻ complex was characterized with a binding constant value of $K_a = 1.4 \times 10^6 \text{ M}^{-1}$ ²⁷⁷ which is one of the largest values reported to date for the complexation of a small polar molecule by a synthetic host bearing endohedral polar groups in water. The binding affinity of the **124C_{syn}-118⁴⁻** was calculated as $K_a = 4.6 \times 10^5 \text{ M}^{-1}$. The thermodynamic characterization of the binding process of the former 1:1 complex, **124C_{anti}-119⁴⁻**, revealed a highly favorable enthalpy term, $\Delta H = -45.1 \text{ kJ}\cdot\text{mol}^{-1}$, and an unfavorable entropy component, $T\Delta S = -9.9 \text{ J}\cdot\text{mol}^{-1}$.

The achiral naphthotubes *syn*-**118** and *anti*-**119** were applied for the sensing of chiral epoxides.²⁷⁸ Chiral epoxides transferred their point chirality to the supramolecular assembly. The circular dichroism spectra of the supramolecular complexes of receptors *syn*-**118⁴⁻** and *anti*-**119⁴⁻** served to quantify the enantiomeric excess of the products derived from asymmetric epoxidation reactions.

Receptors *syn*-**118** and *anti*-**119** were also used for the assembly of poly(pseudorotaxanes).²⁷⁹ These supramolecular polymers were converted into hydrogels upon metal complexation.

5.3. Calix[4]pyrroles

Calix[4]pyrroles are macrocyclic compounds containing four pyrrole units linked together by fully substituted sp^3 -carbon atoms, known as *meso*-carbons. Calix[4]pyrroles are conformationally flexible and adopt different conformations in solution characterized by the relative orientation of their pyrrole units. On the one hand, in nonpolar solvents, such as dichloromethane and chloroform, calix[4]pyrroles adopt an alternate conformation: 1,2- or 1,3-alternate. On the other hand, in polar solvents, such as acetone, acetonitrile, and methanol, calix[4]-pyrroles display a cone or partial-cone conformation. In cone conformation, calix[4]pyrroles establish four convergent hydrogen-bonding interactions between the four pyrrole NHs and a hydrogen bond acceptor group of a solvent molecule or a bound guest.²⁸⁰

The incorporation of aromatic substituents at the *meso*-carbons of calix[4]pyrroles produces aryl-extended derivatives. Aryl-extended calix[4]pyrroles exist as four possible configurational isomers, $\alpha\alpha\beta\beta$, $\alpha\beta\alpha\beta$, $\alpha\alpha\alpha\beta$, and $\alpha\alpha\alpha\alpha$, depending on the relative orientation of their *meso*-aryl substituents. This configurational notation was introduced by Sessler *et al.*²⁸¹ in analogy to the atropoisomerism nomenclature used for tetraphenyl-substituted porphyrins. In cone conformation, the tetra- α or $\alpha\alpha\alpha\alpha$ -isomer of aryl-extended calix[4]pyrroles features a deep aromatic cavity closed at one end by a polar binding site and open at the opposite end^{4,281} (Figure 61b).

In water solution, the conformation adopted by the tetra- α isomer of aryl-extended calix[4]pyrroles remains dynamic. The tetra- α isomer may adopt alternate and cone conformations, which rapidly interconvert on the ¹H NMR chemical shift time scale. The tetra- α isomer of aryl-extended calix[4]pyrroles engage in 1:1 inclusion complexes, with neutral guests possessing electron-rich regions that are suitable hydrogen bond acceptors. The inclusion of the guest in the polar aromatic cavity locks the calix[4]pyrrole receptor in the cone conformation.²⁸⁰ The inclusion of the polar guest in the receptor's cavity isolates the hydrogen-bonding groups of the bound binding partners from solvation with bulk water molecules. This binding arrangement constitutes a unique characteristic of the inclusion complexes derived from aryl-

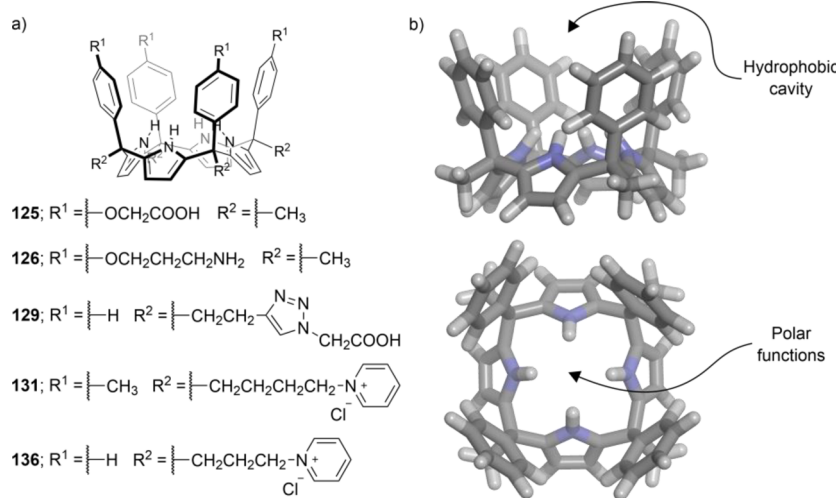


Figure 61. (a) Line-drawing structures of aryl-extended calix[4]pyrroles and (b) energy minimized structure (MM3) of the tetra- α isomer of tetraphenyl-extended calix[4]pyrrole in cone conformation: side and top views. The receptor is depicted in stick representation. Substituents at the upper and lower rims are removed for clarity.

extended calix[4]pyrrole receptors, which is expected to provide a substantial contribution of hydrogen-bonding interactions ([section 2](#)) to the overall gain in binding free energy of the complex. The HE ([section 2.1](#)) also plays an important role in the high levels of binding affinity measured for the complexes of the tetra- α isomer of aryl-extended calix[4]pyrroles with polar guests in water solution.

Tetra- α aryl-extended calix[4]pyrroles equipped with ionizable or charged groups at either the upper or lower rim were reported in the literature. In 2009, our research group introduced two water-soluble aryl-extended calix[4]pyrroles.²⁸² The first series of water-soluble aryl-extended calix[4]pyrroles were functionalized with carboxylic acids, **125**, and amino groups, **126**, at their upper rim ([Figure 61a](#)). Both calix[4]pyrroles were soluble at millimolar concentrations in water solution at pH \sim 7. Interestingly, tetra-carboxylate calix[4]pyrrole [**125**-4H]⁴⁺ and tetra-ammonium calix[4]pyrrole [**126**+4H]⁴⁺ complexed pyridyl N-oxides, **127** and **128** ([Figure 62a](#)), in water forming thermodynamically and kinetically

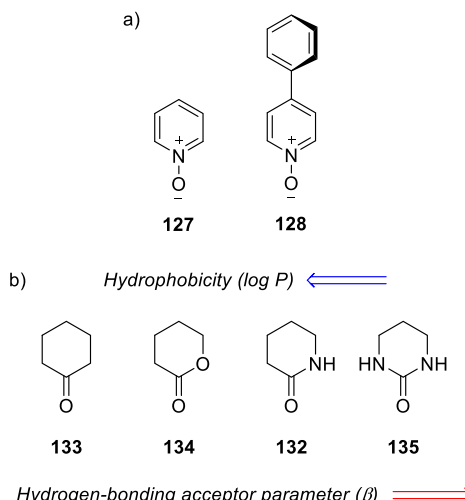


Figure 62. Line-drawing structures of neutral polar guests: (a) pyridyl N-oxides, **127** and **128**, and (b) six-membered cyclic guests, **132**–**135**. Trends of hydrophobicity ($\log P$) and hydrogen-bonding acceptor parameter (β) are indicated for the six-membered ring series.

highly stable 1:1 inclusion complexes.²⁸² The binding constant value of pyridine N-oxide **127** with any of the two hosts was *ca.* $2 \times 10^4 \text{ M}^{-1}$. The binding affinity decreased 1 order of magnitude for the *para*-phenyl pyridyl N-oxide derivative **128** ([Table 11](#)).

The fact that similar binding constant values were determined for pairs of complexes of the same guest with the two receptors, evidenced that the different characteristics of the water-solubilizing groups did not affect their thermodynamic stabilities (see also the studies using cavitand complexes in [section 4.2](#)). This result was in agreement with our expectations, owing to the neutral character of the polar guests. In the inclusion complexes of the N-oxides, the oxygen atom of the bound guest established four simultaneous hydrogen bonds with the four pyrrole NHs of the calix[4]pyrrole unit of the receptor. The four aromatic walls of the receptor were engaged in π – π and CH– π interactions with the aromatic groups of the bound guests.²⁸²

The placement of substituents at the upper rim of aryl-extended calix[4]pyrroles **125** and **126** could have a

deleterious effect on the thermodynamic stability of their inclusion complexes owing to the existence of potential steric clashes with the bound guests. With the aim to evaluate this hypothesis, the water-solubilizing groups were moved to the lower rim of structurally related water-soluble aryl-extended calix[4]pyrroles,²⁸³ *i.e.*, **129** ([Figure 61a](#)). The terminal carboxylic acid groups in **129** were located away from the calix[4]pyrrole's binding pocket. This change prevented the interference of the water-solubilizing groups with the binding process. Nevertheless, the binding constant value of the **127C**[**129**-4H]⁴⁺ complex was very similar to that determined for the **127C**[**125**-4H]⁴⁺ counterpart ([Table 11](#)). This finding indicated that the placement of the water-solubilizing groups, at either the upper or lower rim of the water-soluble aryl-extended calix[4]pyrrole receptors, had a minimum effect on the thermodynamic stability of these inclusion complexes.

The results of ITC experiments determined that the binding process of pyridyl N-oxides with aryl-extended calix[4]pyrrole receptors, in water solution, was strongly driven by the enthalpy.²⁸³ This thermodynamic signature is characteristic of the so-called “nonclassical” hydrophobic effect ([section 2.1](#)) and is also expected for supramolecular complexes formed in water having a well-defined binding geometry. This was clearly the case for the inclusion complexes at hand, in which directional polar interactions ([section 2](#)), such as hydrogen-bonding, π – π , and CH– π were also involved. Unfortunately, dissecting the contributions of polar interactions and the HE to the overall free energy of binding was far from trivial (*vide infra*).

The aryl-extended calix[4]pyrrole receptors discussed above were functionalized at either their upper or lower rims. In 2017, our group reported a synthetic methodology for the preparation of tetra- α isomers of aryl-extended calix[4]pyrroles functionalized at both upper and lower rims.²⁸⁴ The method involved the use of methyltributylammonium chloride as additive and 4 M HCl in dioxane as Lewis acid. The ammonium chloride salt was used as a templating agent to favor the formation of the tetra- α isomer in the reaction mixture. For example, the tetrol precursor of the calix[4]pyrrole cavitands **130a,b**²⁸⁵ ([Figure 63](#)) was obtained following the templating agent synthetic methodology. Calix[4]pyrroles functionalized only at the lower rim were also accessible using this methodology, *i.e.*, **131**²⁸⁵ ([Figure 61a](#)).

Tetra-pyridinium receptors **130a,b**⁴⁺ and **131**⁴⁺ displayed good binding affinities, $K_a > 10^4 \text{ M}^{-1}$, toward size complementary lactams, for example, the six-membered ring **132** ([Figure 62b](#)), in water solution.²⁸⁵ The energy minimized structure (MM3) of the **132C**[**130a**⁴⁺] complex ([Figure 64](#)) showed the oxygen atom of the lactam establishing four hydrogen bonds with the pyrrole NHs of the calix[4]pyrrole core in cone conformation. The nonpolar section of the lactam was buried in the deep cavity of the receptor, where it established multiple CH– π contacts with the *meso*-aromatic walls. The NH of the bound lactam was also engaged in NH– π interactions.

We assessed the importance of intermolecular hydrogen-bonding interactions in the complexes of water-soluble aryl-extended calix[4]pyrroles using a series of cyclic polar guests:²⁸⁵ cyclic ketone **133**, lactone **134**, lactam **132**, and cyclic urea **135** ([Figure 62b](#)). The selected guests have different levels of polarity (basicity of the carbonyl's oxygen atom) and hydrophobicity. The hydrophobicity decreases from

Table 11. Binding Constant Values (K_a , M⁻¹) of Selected Complexes of Calix[4]pyrrole Receptors (C[4]Ps) Formed in Water Solution^a

	Aryl-extended C[4]Ps					Cavitands		Super aryl-extended C[4]Ps	
	[125-4H] ⁴⁺	[126+4H] ⁴⁺	[129-4H] ⁴⁻	131 ⁴⁺	136 ⁴⁺	130a ⁴⁺	130b ⁴⁺	[138-8H] ⁸⁻	139 ⁸⁺
Guests	Binding constant, K_a								
 127 ^{282,283,285,289}	1.6×10^4	2.0×10^4	4.3×10^4				6.9×10^6	8.6×10^5	1.9×10^6
 128 ^{282,283,289}	2.4×10^3	1.5×10^3	2.0×10^5					1.2×10^9	2.6×10^9
 132 ²⁸⁵				7.1×10^4		7.1×10^4	2.3×10^5		
 133 ²⁸⁵							1.4×10^3		
 134 ²⁸⁵							9.5×10^3		
 135 ²⁸⁵							6.9×10^5		
 cis-137 ²⁸⁶					$> 10^4$				

^aSee Figure 61 and Figure 63 for the line-drawing structure of compounds and text for details.

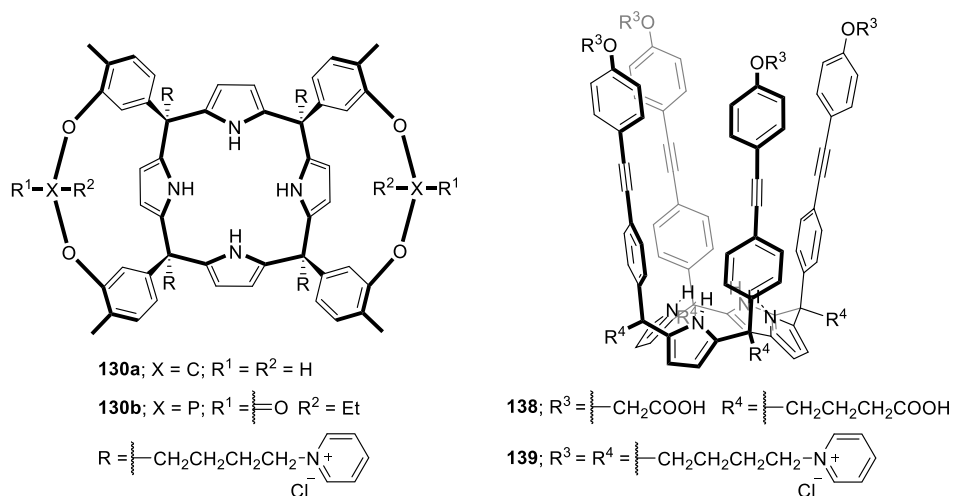


Figure 63. Line-drawing structures of aryl-extended calix[4]pyrrole cavitands 130a,b and super aryl-extended calix[4]pyrroles 138 and 139.

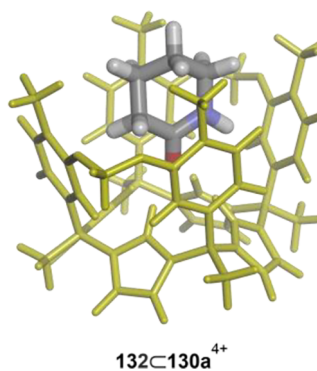


Figure 64. Energy minimized structure (MM3) of the simplified $132\subset 130a^{4+}$ complex. The host (in yellow) and the guest are depicted in stick representation. Water-solubilizing groups were pruned to methyl groups to simplify the calculation.

the cyclic ketone **133** (more hydrophobic) to the cyclic urea **135** (less hydrophobic), as reported by the calculated $\log P$ values (partition coefficient between octanol and water). In water, the binding constant values of supramolecular inclusion complexes were expected to increase in response to the increase of the hydrophobicity of the guests, *i.e.*, K_a (**133** receptor) $> K_a$ (**135** receptor). Surprisingly for us, aryl-extended calix[4]pyrrole receptor **130b⁴⁺** displayed the opposite trend in binding affinities. That is, the water-soluble aryl-extended calix[4]pyrrole bound the less hydrophobic guest, **135**, more strongly than the more hydrophobic counterpart, **133**. Clearly, guest hydrophobicity did not correlate with binding affinity. In contrast, the increase in polarity (basicity) and hydrogen bond acceptor properties of the guests seemed to produce larger binding affinities. Indeed, we observed the existence of a linear relationship between the calculated binding free energies for the inclusion complexes of the cyclic guest's series and the hydrogen-bonding acceptor parameter (β) for their carbonyl's oxygen atom. For example, the 1:1 inclusion complex of the cyclic ketone **133** (less polar guest in the series) featured a binding constant value K_a (**133** \subset **130b⁴⁺**) = $1.4 \times 10^3 \text{ M}^{-1}$. The analogous complex of the cyclic urea **135** (more polar guest in the series) experienced an increase of 2 orders of magnitude in binding constant (Table 11). Taken together, these results supported that hydrogen-bonding interactions contributed to a significant extent to the free energy of binding of the complexes (ΔG). The deep aromatic cavity provided by the aryl-extended calix[4]pyrrole receptors protects the hydrogen-bonded groups of the binding partners from solvation with bulk water molecules, most likely, reinforcing its efficiency. The binding of the cyclic polar guests' series, **132–135**, was characterized by a large enthalpic contribution associated with the “nonclassical” HE.²⁸⁵

Acyclic monoamides were also suitable guests for inclusion in the polar cavity of aryl-extended calix[4]pyrroles.²⁸⁶ Amides exist as a mixture of *trans*- and *cis*-rotamers in solution²⁸⁷ (Figure 65a). The relative population of *trans*- and *cis*-rotamers depends on the amide's substituents and the solvent. In general, the *trans*-rotamer of secondary formamides and acetamides is energetically more favorable than the *cis*-counterpart. The *trans*-to-*cis* interconversion is slow on the NMR chemical shift time scale but fast on the human time scale, precluding the isolation of the pure isomers. The water-soluble aryl-extended calix[4]pyrrole **136** (Figure 61a) was

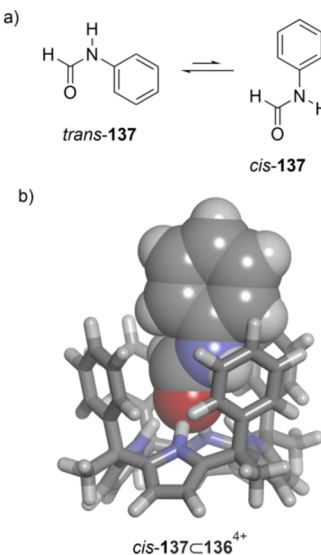


Figure 65. (a) Equilibrium between *trans*- and *cis*-rotamers of **137**; (b) energy minimized structure (MM3) of the simplified *cis*-**137** \subset **136⁴⁺** complex. The host is depicted in stick representation and the bound guest is shown as CPK model. Water-solubilizing groups were pruned to methyl groups to simplify the calculation.

applied for the recognition of secondary and tertiary *N*-phenyl formamides and acetamides in water.²⁸⁶ The deep aromatic cavity of the aryl-extended receptor in the cone conformation showed a good size and shape complementarity for the *cis*-rotamer (Figure 65b). The inclusion of the *trans*-rotamer was expected to energetically destabilize the cone conformation of the receptor due to steric clashes with the *meso*-aryl substituents.

Experimentally, tetra-phenyl tetra-pyridinium receptor **136⁴⁺** showed a high binding affinity ($K_a > 10^3 \text{ M}^{-1}$) and conformational selectivity for the *cis*-rotamer of *N*-phenyl formamides and acetamides.²⁸⁶ For example, although *N*-phenyl formamide **137** (Figure 65a) was present as a 68:32 mixture of *trans/cis* isomers in water, the tetra-phenyl calix[4]pyrrole **136⁴⁺** exclusively bound the *cis*-rotamer of **137** featuring an estimated association constant value K_a (*cis*-**137** \subset **136⁴⁺**) $> 10^4 \text{ M}^{-1}$. Calix[4]pyrrole **136⁴⁺** could be considered as a minimal chaperone selecting the *cis*-rotamer of the formamide and increasing its concentration in the bound form. Using control experiments, the binding constant value for the *trans*-rotamer of *N*-phenyl formamides and acetamides was estimated to be lower than 30 M^{-1} .²⁸⁶ The intermolecular forces involved in the formation of the inclusion complexes of the acyclic monoamides were analogous to those discussed above for the lactam guest.

The elaboration of the aromatic cavity of aryl-extended calix[4]pyrroles with *para*-ethynyl-aryl substituents afforded super aryl-extended derivatives.²⁸⁸ The super aryl-extended calix[4]pyrroles featured a much deeper aromatic cavity than the aryl-extended counterparts (Figure 63). The larger aromatic cavity present in super aryl-extended calix[4]pyrroles was expected to enhance the HE for binding. Moreover, it could also improve the shielding of the intermolecular hydrogen-bonded groups of the inclusion complexes from water solvation. In the previous examples of aryl-extended calix[4]pyrroles, four ionizable or charged groups appended at either their upper or lower rims warranted water solubility. Not surprisingly, super aryl-extended calix[4]pyrroles bearing only

four water-solubilizing groups at their upper rims were not soluble in water at the required concentrations for NMR characterization.²⁸⁸

A significant increase in water solubility for super aryl-extended calix[4]pyrroles was accomplished by appending a total of eight water-solubilizing groups at the periphery of their scaffolds.²⁸⁹ We located four water-solubilizing groups at the upper rim and the other four at the lower rim. The synthesized octa-acid and octa-pyridinium super aryl-extended calix[4]pyrroles, **138** and **139** (Figure 63), respectively, structurally resembled the Gibb's resorcin[4]arene deep-cavity cavitands (Section 4.2). However, the water-soluble super aryl-extended calix[4]pyrroles displayed a functionalized aromatic cavity with four hydrogen bond donors (NHs) at the closed end. The octa-acid **138** was soluble in water at millimolar concentrations at pH \sim 10 owing to the ionization of its carboxylic acids as carboxylates, *i.e.*, $[138\text{-}8\text{H}]^{8-}$, whereas the octa-pyridinium **139⁸⁺** featured similar water solubility independently of the pH of the solution.²⁸⁹

The two water-soluble super aryl-extended calix[4]pyrroles, $[138\text{-}8\text{H}]^{8-}$ and **139⁸⁺**, were used as model systems for the quantification of the HE in the complexation of a series of pyridyl N-oxide derivatives in water.²⁸⁹ The pyridyl N-oxides in the selected series differed in the size of the *para*-substituent: methyl, *tert*-butyl, *n*-butyl, and phenyl. Receptors $[138\text{-}8\text{H}]^{8-}$ and **139⁸⁺** formed 1:1 inclusion complexes with all the pyridyl N-oxides. Not surprisingly and as already mentioned above for other calix[4]pyrrole receptors, the pair of complexes for a given N-oxide featured similar binding constant values. The binding constant values determined for all complexes were larger than 10^5 M^{-1} .

It is worth noting here that the determined binding constant values for the complexes of pyridine N-oxide, **127**, with the two super aryl-extended calix[4]pyrrole receptors, were 1 order of magnitude larger than that of $127\subset[125\text{-}4\text{H}]^{4-}$ complex (**125** is a water-soluble aryl-extended calix[4]pyrrole receptor) (Table 11). The increase in binding affinity was assigned to the enhanced hydrophobic character of the aromatic cavity in the super aryl-extended receptors. In the series of pyridyl N-oxides, the increase in the surface area of the pyridyl's *para*-substituent was translated into an increase in the binding free energy.²⁸⁹ Most likely, the observed intensification in binding affinity was derived from the reduction of the water accessible surface area in the complex and the concomitant increase in the number of nonpolar contacts (mainly van der Waals interactions for the *para*-alkyl chain substituents). Therefore, the gain in free energy could be related to the HE. The determined free energies of binding showed a linear relationship with respect to the surface area of the *para*-alkyl substituents of the N-oxide guest series. The slope of the line defined by the data returned a value of $138\text{--}159 \text{ J}\cdot\text{mol}^{-1}\cdot\text{\AA}^{-2}$.²⁸⁹ The calculated value was assigned to the HE operating in these model systems. The above determined magnitude was in agreement with other values assigned to the HE,³ which were derived from site-directed mutagenesis of protein residues and the transfer of solutes from nonpolar solvents to water.

Interestingly, the inclusion complex of 4-phenylpyridine N-oxide **128** with any of the two super aryl-extended calix[4]pyrrole hosts, $[138\text{-}8\text{H}]^{8-}$ or **139⁸⁺**, featured an additional value of $8.4 \text{ kJ}\cdot\text{mol}^{-1}$ with respect to our estimate based on the reduction of solvent accessible surface area.²⁸⁹ Most likely, this extra energy derived from the formation of a cluster of aromatic interactions in the upper section of the cavity of the

super aryl-extended calix[4]pyrroles (Figure 66). Super aryl-extended calix[4]pyrroles, $[138\text{-}8\text{H}]^{8-}$ and **139⁸⁺**, displayed

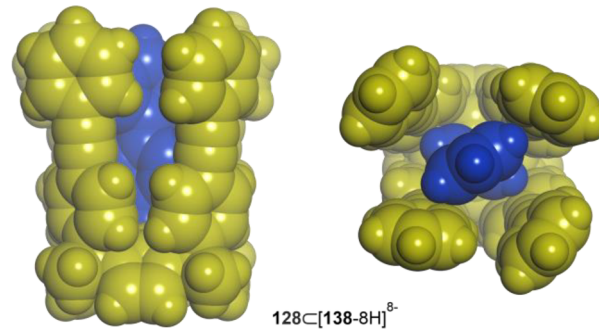


Figure 66. Energy minimized structure of the simplified $128\subset[138\text{-}8\text{H}]^{8-}$ complex: side and top views. The host (in yellow) and the guest (in blue) are shown as CPK models. Water-solubilizing groups are omitted for clarity.

nanomolar dissociation constants for **128** (Table 11), demonstrating that, in water, thermodynamically highly stable complexes can be formed between small polar neutral molecules and synthetic receptors having large functionalized aromatic cavities.

Other applications of water-soluble aryl-extended calix[4]pyrroles were reported in literature. For example, Sessler *et al.* showed that, in aqueous solution, the tetra-acid **125** self-assembled into high-order aggregates in the presence of a ditopic *bis*-N-oxide.²⁹⁰ The morphology of the corresponding supramolecular assembly could be controlled by changing the pH of the solution.

6. SELF-ASSEMBLED WATER-SOLUBLE RECEPTORS

Self-assembly is a supramolecular approach, based on the use of reversible noncovalent interactions,⁴⁴ to hold together multiple copies of molecular components (*i.e.*, building blocks) and produce large, well-defined, and functional architectures¹ under thermodynamic control.¹⁵ The information for the assembly process is encoded in the binding motifs and molecular structures (shape) of the building blocks.²⁹¹ Water-soluble self-assembled receptors were prepared using metal-ligand coordination bonds,¹⁶ and noncovalent electrostatic forces (section 2), like Coulombic²³² and hydrogen-bonding interactions, and the assistance of the HE.¹⁴

In this section, we classify self-assembled molecular containers/receptors in two different categories: cages and capsules. We define cages as self-assembled receptors that feature large portals allowing the reversible passage of guests. They are typically assembled by the combination of flat, rigid multitopic ligands with coordination metal ions (*i.e.*, metal coordination cages). On the other hand, capsules feature an enclosed cavity in which the in/out exchange of the guest requires the partial or total dissociation of the capsular assembly. Capsules are assembled from concave building blocks, such as calix[4]arenes and resorcin[4]arenes (see section 4).

6.1. Metal Coordination Cages

The formation of coordination bonds between metal ions and bespoke multitopic ligands might lead to metal coordination cages. Metal–ligand coordination bonds are thermodynamically highly stable in both nonpolar and polar solvents¹⁵ unless a competitive coordinating solvent is used. In general, the

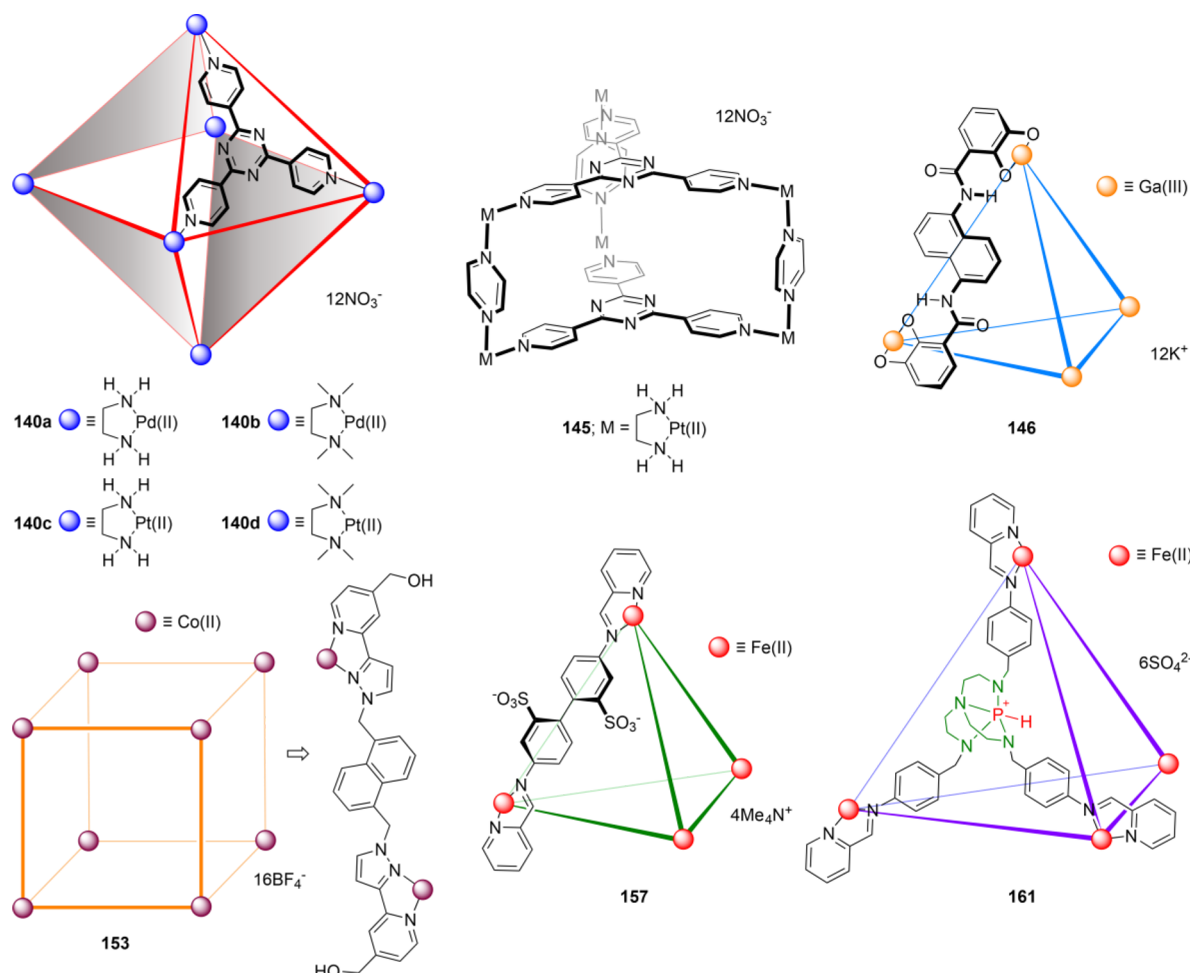


Figure 67. Line-drawing structures of the ligands and the cartoon representations of metal coordination cages.

metallo-cages are soluble in water owing to the use of multiple metal ions for their assembly.²⁹¹ In addition, polar, ionizable, and charged groups can be incorporated in the structures of the ligands to improve the water solubility of the self-assembled metallo-cages and circumvent their aggregation tendency.¹⁶

Most of the examples of metal coordination cages featured a hydrophobic cavity, which could accommodate size and shape complementary neutral or charged guests.^{16,31} The overall charge of the metallo-assembly imposed charge binding selectivity and also affects the stability and reactivity of the bound guests.¹⁸ The main intermolecular interactions for guest binding in self-assembled metallo-cages are the HE and the establishment of host–guest Coulombic interactions (section 2).

Water-soluble octahedral M_6L_4 cages were designed by Fujita *et al.* in the 1990s.²⁹² The designed cages were based on Pd(II) and Pt(II) metal ions in combination with neutral *tri*-pyridyl ligands (Figure 67). The Pd(II)-cages²⁹³ 140a,b and the analogous Pt(II)-cages²⁹⁴ 140c,d were positively charged ($z = +12$). The charged metal ions at the vertices of the octahedron imparted water solubility.¹⁵ The cavity volume of the octahedral cages 140a–d was *ca.* 650 Å³.

In the solid state, an octahedral Pd(II)-cage similar to 140a (ethylenediamine ligands changed by 2,2'-bipyridine ligands) showed 10 water molecules included in its hydrophobic cavity.²⁹⁵ The bound water molecules displayed an ice-like

structure, which was stabilized by water–water hydrogen-bonding interactions and by H₂O–π or OH–π interactions with the aromatic panels of the octahedral cage (see also the inclusion of water in the cavity of calix[4]arenes in section 4.1). Therefore, the formation of the inclusion complexes deriving from the octahedral Pd(II)/Pt(II)-cages was assumed to be mainly driven by the entropy. This entropic gain was assigned to the “melting” of the cluster of water molecules included in the cage’s cavity.²⁹⁵

The binding properties of the dodeca-cationic Pd(II)-cages, 140a,b¹²⁺, and the Pt(II)-counterparts, 140c,d¹²⁺, were very similar. Neutral guests were included in the hydrophobic cavities of the metallo-cages mainly through the HE.²⁹¹ For example, four molecules of 1-adamantanone 141 (Figure 68) were included in the cavity of 140a¹²⁺ forming the 141₄Cl40a¹²⁺ cage complex.²⁹⁶ Interestingly, the inclusion of the four molecules of 1-adamantanone 141 was characterized by a large positive cooperativity. The proton signals of bound 141, in the 141₄Cl40a¹²⁺ cage complex, appeared upfield-shifted in its ¹H NMR spectrum (Figure 68), indicating that the adamantane group was buried in the cage’s cavity (Figure 69). Consequently, the hydroxyl group of the guest remained exposed to the bulk aqueous solution.

The octahedral Pd(II)-cages 140a,b and the analogous Pt(II)-cages 140c,d were also applied to mediate chemical transformations in water solution.^{18,297} For example, the Pd(II)-cage 140b promoted the Diels–Alder reaction of

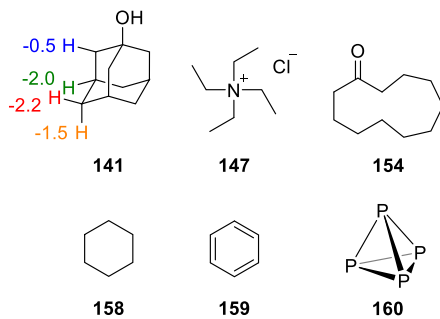


Figure 68. Line-drawing structures of guest molecules studied using metal coordination cages. For 141, complexation-induced chemical shifts ($\Delta\delta = \delta_{\text{bound}} - \delta_{\text{free}}$) are indicated in ppm.

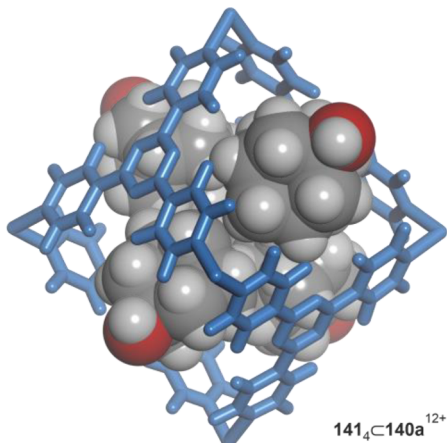
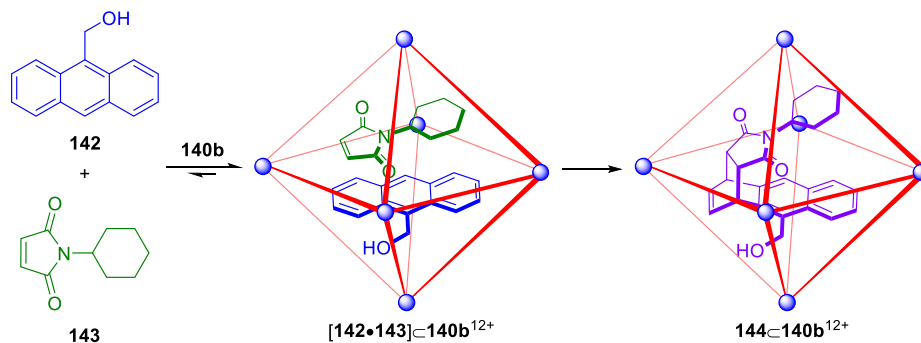


Figure 69. Energy minimized structure (MM3) of the simplified $141_4 \subset 140a^{12+}$ cage complex. The cage (in blue) is depicted in stick representation, and the bound guests are shown as CPK models. Ethylenediamine ligands of the metal centers are removed for clarity.

anthracenes and phthalimides in water solution.²⁹⁸ In the presence of cage 140b, the Diels–Alder reaction between 9-hydroxymethylanthracene, 142, and N-cyclohexylphthalimide, 143, gave the *syn*-isomer, 144, in almost quantitative yield (Scheme 5). This unusual regioselectivity was achieved when using the octahedral metallo-cage as nanoreactor. The two reactants, 142 and 143, were included in the cavity of the Pd(II)-cage 140b¹²⁺, leading to the exclusive formation of the heteroternary $[142 \cdot 143] \subset 140b^{12+}$ cage complex. Most likely, this was the best combination of the potential guests to adequately fill the cavity's volume. The double bond of the

Scheme 5. Diels-Alder Reaction between Diene 142 (in Blue) and Dienophile 143 (in Green) Mediated by the Pd(II)-cage 140b (See Figure 67 for the Structure of 140b)



bound dienophile, 143, was placed in close proximity to the 1,4-position of the anthracene, 142, acting as diene. Therefore, the reaction provided the unusual 1,4-Diels–Alder product 144 (Scheme 5). The reaction required the use of stoichiometric amounts of the Pd(II)-cage 140b.

The metallo-cage 140a was used to catalyze the Knoevenagel condensation of aromatic aldehydes with Meldrum's acid in neutral water.²⁹⁹ Once the aromatic aldehyde was included in the Pd(II)-cage 140a¹²⁺, the cationic environment stabilized the negatively charged reaction intermediate. The reaction product was too large to be fully encapsulated allowing the catalytic turnover of the Pd(II)-cage 140a¹²⁺.

The Pt(II)-cage 145, $M_6L_2L'_3$ (Figure 67), based on two different ligands, featured a trigonal prism structure. The Pt(II)-cage 145 was used to provide a nonpolar environment for the efficient formation of hydrogen-bonded base pairs in water³⁰⁰ (see section 5 for receptors able to bind polar molecules). Separate solutions of AMP²⁻ and UMP²⁻ formed homoternary 2:1 cage complexes with 145¹²⁺: $[\text{AMP}_2]^{4-} \subset 145^{12+}$ and $[\text{UMP}_2]^{4-} \subset 145^{12+}$. On the contrary, an equimolar mixture of the two nucleotides, AMP²⁻ and UMP²⁻, and the Pt(II)-cage 145¹²⁺, led to the exclusive formation in water solution of the heteroternary $[\text{AMP}^{2-} \cdot \text{UMP}^{2-}] \subset 145^{12+}$ cage complex (Figure 70). All 145¹²⁺-cage

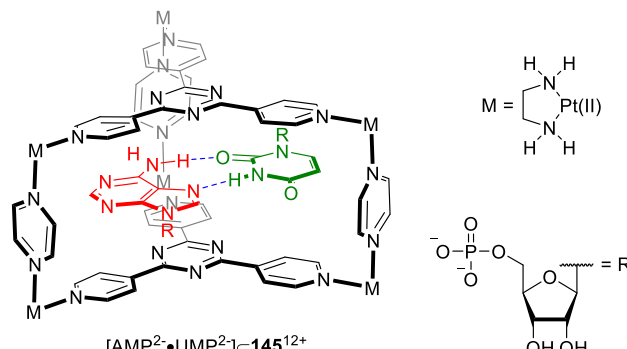


Figure 70. Line-drawing structure of the heteroternary $[\text{AMP}^{2-} \cdot \text{UMP}^{2-}] \subset 145^{12+}$ cage complex. AMP²⁻ and UMP²⁻ are highlighted in red and green colors, respectively.

complexes of the nucleotides were stabilized through the HE, $\pi-\pi$, and Coulombic interactions (section 2). Noteworthy, the heteroternary complex, $[\text{AMP}^{2-} \cdot \text{UMP}^{2-}] \subset 145^{12+}$, was further stabilized by the establishment of two water-shielded hydrogen

bonds between the bases of the two bound nucleotides. Therefore, the hydrophobic cavity of the cage allowed the hydrogen-bonding base-pairing of the two nucleotides in water solution through an anti-Hoogsteen binding geometry.

In 2001, Raymond *et al.* introduced tetrahedral M_4L_6 cages,³⁰¹ e.g., **146** (Figure 67), based on trivalent or tetravalent metal ions, Ga(III), Al(III), Fe(III), Si(IV), or Ti(IV), and a *bis*-catechol-substituted naphthalene ligand. The structures of the M_4L_6 cages assembled with the above-mentioned components were almost identical. We center our discussion on the properties and applications of the Ga(III)-cage, **146**, and refer to other tetrahedral cages, having different metal centers, for comparison. The *bis*-catechol naphthalene ligand was conformationally relatively rigid owing to the formation of intramolecular NH···O hydrogen bonds.³⁰¹ Interestingly, the configuration of a vertex of **146** was mechanically coupled to that of the others owing to the ligand rigidity. This led to the obtention of the Ga(III)-cage **146** as a racemic mixture of two homochiral assemblies, $\Delta\Delta\Delta\Delta$ and $\Lambda\Lambda\Lambda\Lambda$, both displaying T symmetry.^{301,302}

The Ga(III)-cage **146** had 12 negative charges ($z = -12$) imparting water solubility.³⁰¹ The binding pocket of dodeca-anionic **146**¹²⁻, which was surrounded by six naphthalene panels, was hydrophobic. Therefore, neutral and cationic guests were efficiently bound in the cavity of **146**¹²⁻^{15,303} through the HE, Coulombic, cation- π and CH- π interactions (see section 2). Furthermore, the cavity size of **146**¹²⁻ experienced subtle expansions/contractions in order to accommodate to the guests' size (induced fit). The maximum volume displayed by the Ga(III)-cage **146**¹²⁻ was *ca.* 440 \AA^3 .³⁰⁴

The formation of the cage complexes^{17,291} between cationic guests and the Ga(III)-cage **146**¹²⁻ was driven by entropy.^{305,306} This thermodynamic signature mainly derived from the desolvation of the cage's cavity (included water molecules could be stabilized by OH- π interactions) and the charged guest prior to complexation. Cationic guests did also bind to the exterior of the cage through cation- π and Coulombic interactions. The *exo*-binding process of the guests was characterized to be driven by enthalpy.^{305,306}

For example, the binding constant value of the 1:1 cage complex between tetra-ethylammonium, **147**⁺ (Figure 68), and the Ga(III)-cage **146**¹²⁻ was determined to be K_a ($147^+ \subset 146^{12-}$) = $3.5 \times 10^4 \text{ M}^{-1}$ in water containing 0.1 M KCl.³⁰⁵ The binding process was driven by entropy, $T\Delta S = +20.9 \text{ kJ}\cdot\text{mol}^{-1}$, and favored by enthalpy, $\Delta H = -4.1 \text{ kJ}\cdot\text{mol}^{-1}$. The included tetra-ethylammonium guest **147**⁺ was involved in a slow chemical exchange process on the ^1H NMR chemical shift time scale with the free counterpart.³⁰⁷ The guest in/out exchange process involved a slippage mechanism, *i.e.*, deformation of a cage's portal, operating for the entrance/exchange of the guest in the cage complex. On the other hand, the constant value for the binding of the same cationic guest, **147**⁺, to the exterior of the already complexed tetrahedral cage was K_a ($147^+ \subset 146^{12-} \rightleftharpoons 147^+ [147^+ \subset 146^{12-}]$) = 63 M^{-1} . The *exo*-cage binding process displayed fast exchange dynamics between free and bound **147**⁺ on the chemical shift time scale³⁰⁵ (Figure 71). In the latter case, the *exo*-binding process was characterized by $\Delta H = -27.6 \text{ kJ}\cdot\text{mol}^{-1}$ and $T\Delta S = -16.7 \text{ kJ}\cdot\text{mol}^{-1}$.

In the same vein, protonated secondary and tertiary amines were also included in the cavity of the tetrahedral Ga(III)-cage **146**¹²⁻.³⁰⁸ The formed cage complexes were stabilized by

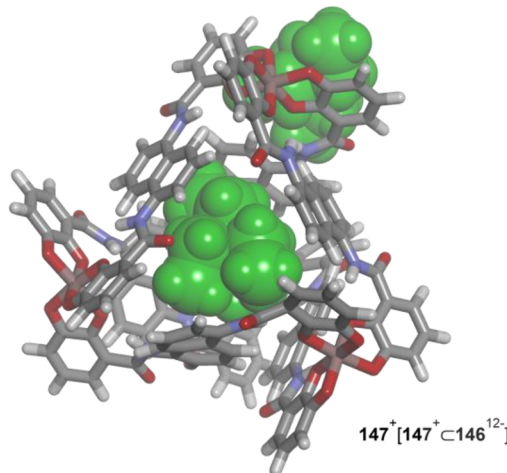


Figure 71. Energy minimized structure (MM3) of the $147^+ [147^+ \subset 146^{12-}]$ cage complex. The cage is depicted in stick representation and the two bound guests (in green) are shown as CPK models.

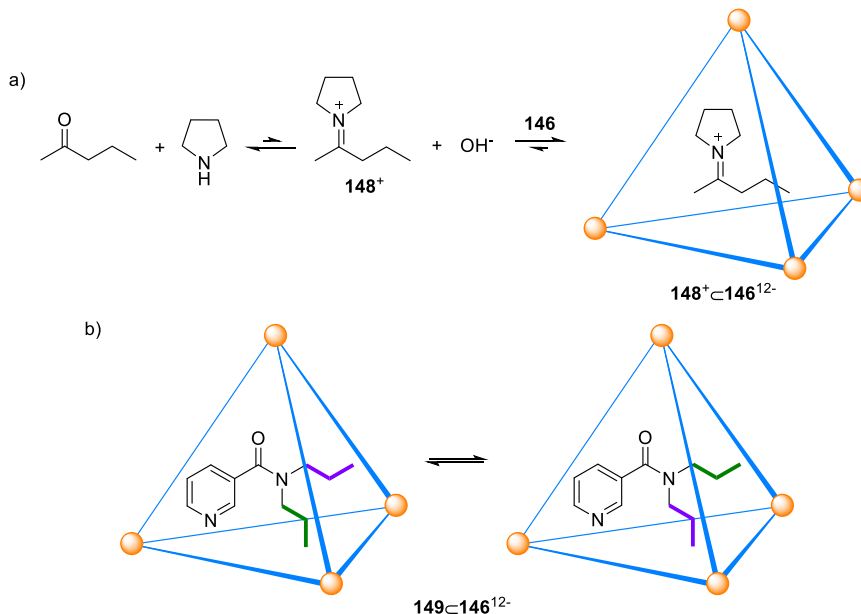
Coulombic and cation- π interactions (section 2). Bergman, Raymond, and co-workers demonstrated that the bound protonated amines experienced an increase of 2.1–4.5 p*K*_a units in basicity.³⁰⁸ Likewise, bound protonated phosphines also displayed an increase in basicity.³⁰⁸ Additionally, proton-bound amine homodimers were stabilized in the hydrophobic cavity of the Ga(III)-cage **146**¹²⁻.³⁰⁹

The stabilization of cationic species in water using the Ga(III)-cage **146**¹²⁻ was applied to the isolation of iminium cations,³¹⁰ such as **148**⁺ (Scheme 6a), which are prone to fast hydrolysis in neutral or basic solution. The iminium cation **148**⁺ was generated *in situ* from the reaction of 2-pentanone with pyrrolidine. Once formed, it was rapidly included and stabilized in the cavity of the Ga(III)-cage **146**¹²⁻ in water at basic pH (Scheme 6a).

Besides cationic species, the hydrophobic character of the cavity of Ga(III)-cage **146**¹²⁻ allowed the inclusion of neutral nonpolar species mainly through the HE.³¹¹ The binding properties of the Ga(III)-cage **146**¹²⁻ and analogues tetrahedral cages were also exploited in the energetic stabilization of transition states and high-energy conformers by Bergman, Raymond, Toste, and co-workers.^{18,303,312} Both stabilization mechanisms might produce rate accelerations for particular processes.

For example, in water solution, the Ga(III)-cage **146**¹²⁻ increased the rate of rotation of the C(O)-N bond for the included, symmetric tertiary amides.³¹³ The planar ground state of the amide group was destabilized in the interior of the cage **146**¹²⁻. The included amide was forced to adopt a twisted conformation. The binding of a high-energy conformer of the amide provoked a decrease of up to 15.1 kJ·mol⁻¹ in the energy barrier of the amide bond rotation. The C(O)-N bond rotation of *N,N*-dipropyl nicotinamide **149** was 450-fold faster in the bound state than free in solution (Scheme 6b). The inversion-rotation process of bound protonated amines was also accelerated by inclusion in the Ga(III)-cage **146**¹²⁻.³¹⁴ It is worth mentioning here that the rate of hydrolysis of secondary amides in basic water was enhanced when the guests were included in the octahedral Pt(II)-cage **140d**¹²⁺, as shown recently by Takezawa, Fujita, and co-workers.²⁹⁷

Scheme 6. (a) Formation and Further Inclusion of the Iminium Cation 148^+ in the Interior of the Ga(III)-Cage 146^{12-} and (b) Amide Bond Rotation of 149 in the $149 \subset 146^{12-}$ Cage Complex (See Figure 67 for the Structure of 146)

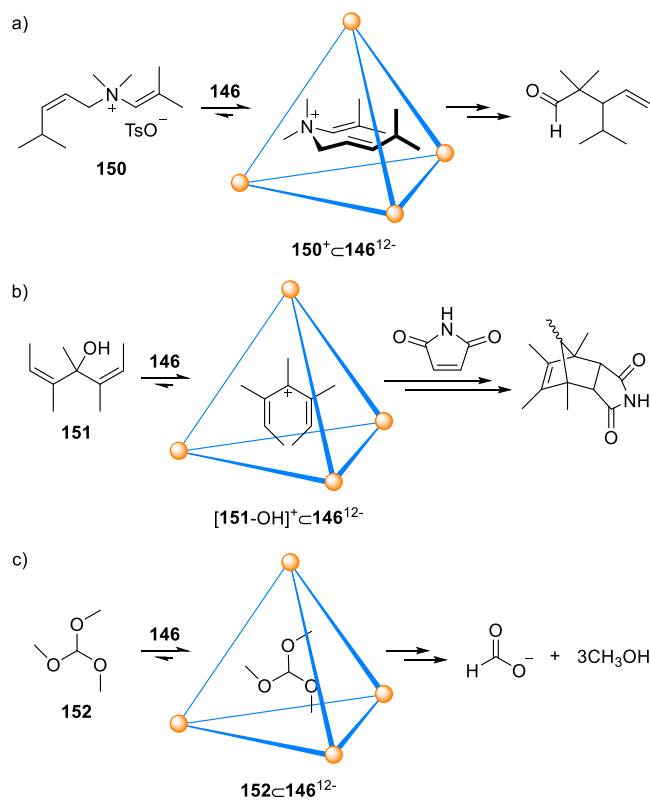


The binding and stabilization of reactive cationic species suggested the application of the Ga(III)-cage 146^{12-} to mediate or catalyze chemical transformations involving cationic substrates or occurring through cationic transition states.^{303,312} The application of the Ga(III)-cage 146^{12-} as catalyst in substoichiometric amounts was required to circumvent the issue of product inhibition. That is, the reaction product must not compete with the substrate for the cage's cavity.

The aza-Cope rearrangement of allylenammonium³¹⁵ and propargylenammonium³¹⁶ cations involves charged starting materials, intermediates, and transition states. A net positive charge of the bound guest is maintained throughout the reaction. The Ga(III)-cage 146^{12-} accelerated the aza-Cope rearrangement of ammonium bound species, such as 150^+ (Scheme 7a), by almost 3 orders of magnitude with respect to the background reaction taking place in water under identical experimental conditions.³¹⁵ The tetrahedral cage 146^{12-} included the allylenammonium cation 150^+ in a chairlike conformation (Scheme 7a), which was suitable to undergo the aza-Cope rearrangement. Most likely, the effect of the cage as catalyst resided on the stabilization of the bound substrate in its high-energy reactive conformation. Interestingly, the reaction product was an iminium cation, which was further hydrolyzed to the corresponding aldehyde, probably by leaking in the bulk aqueous solution. The neutral aldehyde that was produced could not compete with the cationic guest (starting material) for the cavity of the anionic Ga(III)-cage 146^{12-} , thus enabling catalytic turnover.

On the other hand, the Nazarov cyclization of neutral pentamethyl pentadienol 151 (Scheme 7b) involves a positively charged transition state. In this case, the net charge of the bound guest changes throughout the reaction. The Ga(III)-cage 146^{12-} mainly catalyzed the Nazarov cyclization of pentadienol 151 through the stabilization of the positively charged transition state, leading to a remarkable rate acceleration, $k_{\text{catalyzed}}/k_{\text{uncatalyzed}} \sim 10^6$, in water at pH = 11.³¹⁷ In this case, maleimide was used as a trapping agent to

Scheme 7. (a) Aza-Cope Rearrangement of Allylenammonium Tosylate 150 , (b) Nazarov Cyclization of Pentamethyl Pentadienol 151 , and (c) Hydrolysis of Orthoformate 152 Catalyzed by the Ga(III)-cage 146 (See Figure 67 for the Structure of 146)



give the corresponding Diels–Alder product and enable catalytic turnover (Scheme 7b). Otherwise, the Ga(III)-cage 146^{12-} used as catalyst in the Nazarov cyclization suffered of product inhibition.

The effect of the overall charge of the metallo-cage in its catalytic performance was recently investigated by Bergman, Raymond, Toste, and co-workers using two isostructural tetrahedral cages: the Ga(III)-cage **146** and the analogous Si(IV)-cage.³¹⁸ The Si(IV)-cage had eight negative charges, whereas the Ga(III)-cage **146** had 12. As could be expected, the two cages provided similar rate constant values for the aza-Cope rearrangement (Scheme 7a) because the net charge of the bound substrate was maintained constant throughout the reaction. Nevertheless, the Ga(III)-cage **146**¹²⁻ induced an increase in the rate constant of the Nazarov cyclization reaction (Scheme 7b) that was almost 3 orders of magnitude larger than that for the Si(IV)-cage. In this case, the more negatively charged Ga(III)-cage ($z = -12$) stabilized better the cationic transition state, which was generated throughout the reaction, than the Si(IV)-cage ($z = -8$) (see section 6.2 for the effect of the overall charge of noncovalent capsules on chemical transformations in their interiors).

Furthermore, the Ga(III)-cage **146**¹²⁻ also catalyzed the hydrolysis of orthoformate esters,³¹⁹ such as **152** (Scheme 7c), and acetals³²⁰ in basic water. Orthoformates and acetals are stable in neutral or basic water solution but are readily hydrolyzed in acidic media. The Ga(III)-cage **146**¹²⁻ bound the orthoformate ester or acetal and catalyzed their hydrolysis reaction in water at pH > 10. The hydrolysis of orthoformates gave the formate anion as product, which did not compete for binding to the anionic Ga(III)-cage **146**¹²⁻ with the starting material³¹⁹ (Scheme 7c). On the other hand, the hydrolysis of acetals produced the corresponding aldehyde, which was further converted into its hydrate in the bulk aqueous solution.³²⁰ Both products were less hydrophobic guests than the reactants, thus enabling catalytic turnover.

Hunter, Ward, and co-workers designed a cubic M₈L₁₂ cage **153** based on Co(II) metal ions and pyridyl-pyrazolyl ligands³²¹ (Figure 67). The cationic metal centers and the hydroxymethyl substituents of the ligands imparted water solubility to the assembly. The Co(II)-cage **153** was positively charged ($z = +16$), featuring a cavity volume of *ca.* 400 Å³.³²²

In the solid state, the Co(II)-cage **153** showed ten water molecules included in its hydrophobic cavity.³²³ The included water molecules established fewer hydrogen bonds than those in the bulk solution. The release of the bound water molecules led to guest binding processes that were mainly enthalpically driven. This finding was in striking contrast with the entropy driven binding processes described for Pd(II)-cages **140a,b** (*vide supra*). To reconcile both observations, we highlight the fact that the 10 water molecules included in the octahedral Pd(II)-cages **140a,b** were assigned an ice-like structure, which should provide a larger number of hydrogen bonds. In any case, the solvation and desolvation processes, as well as the complexes' stoichiometries, were very different to allow a fair comparison of the two binding metallo-cages.

The Co(II)-cage **153**¹⁶⁺ included preferentially neutral guests over anionic species in water solution.^{321,323–325} Interestingly, the results obtained in the binding studies of a series of cyclic ketones, from cyclopentanone to cycloundecanone, **154** (Figure 68), demonstrated the existence of a linear relationship between the free energy of binding and the surface area of the guests.³²⁴ This relationship quantified in *ca.* 0.3 kJ·mol⁻¹·Å⁻² the HE operating in these cage complexes (see calix[4]pyrroles in section 5.3 for an alternate model system to quantify the HE). The gain in free energy provided by the inclusion of an additional methylene group of the

ketone homologous series in the hydrophobic cavity of the Co(II)-cage **153**¹⁶⁺ was calculated to be *ca.* 5.0 kJ·mol⁻¹.

Cycloundecanone, **154**, formed a thermodynamically highly stable complex with the Co(II)-cage **153**¹⁶⁺ in water³²⁴ (Figure 72). The **154**•**153**¹⁶⁺ cage complex was characterized with a

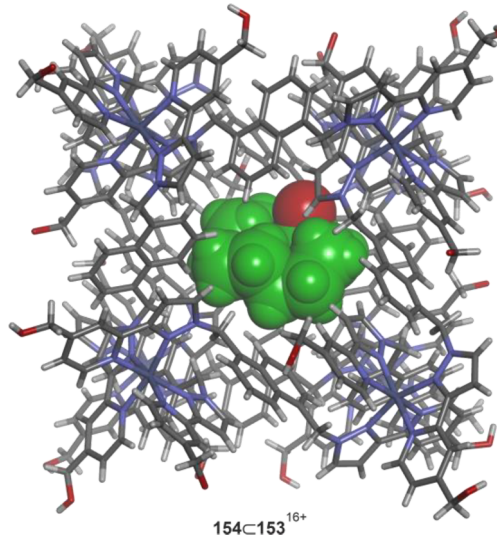


Figure 72. X-ray crystal structure of the **154**•**153**¹⁶⁺ cage complex. Adapted with permission from ref 324. Copyright 2014 American Chemical Society. The cage is depicted in stick representation and the guest (in green) is shown as CPK model. The oxygen atom (in red) of bound guest is highlighted.

binding constant value of $K_a = 1.2 \times 10^6 \text{ M}^{-1}$. More polar cyclic guests with larger β values, such as lactams and pyridine N-oxide, were weakly bound by the Co(II)-cage **153**¹⁶⁺,³²¹ (Table 12). For example, the binding constant value determined for the cage complex of δ -lactam **132** (Figure 62b) was 3 M⁻¹ and 1 M⁻¹ for pyridine N-oxide **127** (Figure 62a). These results, together with the ones obtained in acetonitrile solution, were interpreted by the authors as an indication that the hydrogen-bonding component of guest recognition was switched off in water. In water, the binding of guests to the Co(II)-cage **153**¹⁶⁺ was mainly driven by the HE and assisted with additional dispersion (van der Waals) interactions established in the complex. These results indicated that the important role played by the hydrogen-bonding interactions in the complexation of polar molecules in water using “temple” receptors, aryl-extended calix[4]pyrroles and, to some extent, in the case of naphthotubes (section 5) is not easily translated to other receptor's designs also equipped with polar cavities.

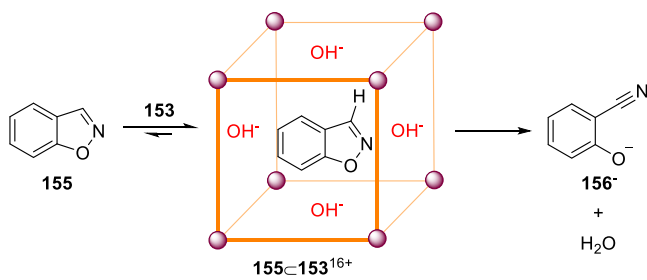
The Co(II)-cage **153**¹⁶⁺ was also used as catalyst in the Kemp elimination reaction of benzisoxazole **155** to give 2-cyanophenolate **156**⁻ in basic water³²⁶ (Scheme 8). Benzisoxazole **155** was included in the cavity of the Co(II)-cage **153**¹⁶⁺, mainly through the HE. The resulting 1:1 cage complex had a significant binding affinity (K_a (**155**•**153**¹⁶⁺) = $4.0 \times 10^3 \text{ M}^{-1}$).³²⁷ At the same time, hydroxide anions were bound to the exterior of the cationic Co(II)-cage via Coulombic interactions, thus producing an increase in local concentration at the periphery of the cage complex **155**•**153**¹⁶⁺. The bound benzisoxazole **155** reacted with the local high concentration of hydroxide to yield the 2-cyanophenolate anion, **156**⁻. The hydrophilicity of the anion **156**⁻ eliminated the competition

Table 12. Binding Constant Values (K_a , M⁻¹) of Selected Cage Complexes Formed in Water Solution with the Co(II)-Cage 153^{16+^a}

Co(II)-cage 153 ¹⁶⁺	
Guests	Binding constant, K_a
 87 ³²⁴	1.9×10^4
 127 ³²¹	1
 132 ³²¹	3
 133 ³²⁴	56
 154 ³²⁴	1.2×10^6
 155 ³²⁷	4.0×10^3

^aSee Figure 67 for the line-drawing structure of the metallo-cage 153 and text for details.

Scheme 8. Kemp Elimination Reaction of Benzisoxazole 155 Catalyzed by the Co(II)-Cage 153 (See Figure 67 for the Structure of 153)



with the reactant 155 for the hydrophobic cavity of the metallo-cage, thus enabling catalytic turnover. The reaction rate constant was significantly enhanced in the presence of the Co(II)-cage 153¹⁶⁺ in water at pD = 8.5, $k_{\text{catalyzed}}/k_{\text{uncatalyzed}} = 2 \times 10^5$ ^{326,328}

Rissanen, Nitschke, and co-workers reported the self-assembly of a tetrahedral M₄L₆ cage 157 using Fe(II) metal ions and biphenyl imine ligands bearing sulfonate groups³²⁹ (Figure 67). Similar metallo-cages were obtained by replacing the Fe(II) metal centers by Co(II) or Ni(II).³³⁰ The Fe(II)-cage 157 was soluble in water owing to the four Fe(II) ions at the vertices and the outwardly directed sulfonate groups at the edges of the tetrahedron (overall charge, $z = -4$). In analogy to

the Raymond's Ga(III)-cage 146, the Fe(II)-cage 157 was obtained as a racemic mixture of two T-symmetric homochiral assemblies, ΔΔΔΔ and ΛΛΛΛ. Metallo-cage 157 featured a cavity volume of ca. 140 Å³.³²⁹

The tetra-anionic Fe(II)-cage 157⁴⁻ preferentially included neutral nonpolar guests over polar and cationic analogues.^{329,331} The inclusion of a suitable neutral guest in the tetrahedral cavity of 157⁴⁻ was driven by the HE. For example, cyclohexane 158 (Figure 68) and 157⁴⁻ formed a 1:1 cage complex in water featuring a binding constant value of $K_a = 7.1 \times 10^4$ M⁻¹.³³¹ In contrast, the cage complex of 1,4-dioxane, 123 (Figure 57), experienced a drop in binding affinity of more than 2 orders of magnitude, $K_a(123\subset 157^{4-}) = 1.5 \times 10^2$ M⁻¹.³³¹ Aromatic guests were also included in the hydrophobic cavity of cage 157⁴⁻. For example, benzene 159 (Figure 68) produced an inclusion complex with Fe(II)-cage 157⁴⁻ in water with a stability constant of $K_a = 3.0 \times 10^3$ M⁻¹.³³¹

Binding studies with the tetrahedral Fe(II)-cage 157⁴⁻ and a series of guests indicated that the binding affinity of the cage complexes were directly related to the hydrophobicity of the guest: the larger the hydrophobicity of the guest, the larger the binding constant.³³¹ The rate constants for the formation of the cage complexes of the Fe(II)-cage 157⁴⁻ were shown to be dependent on the size and shape of the guest. On the basis of this finding, a slippage mechanism was proposed to be operating for the entrance/exchange of guests in the cage complexes of 157⁴⁻,³³² as discussed before for Raymond's metallo-cage.

Building on early work by Cram *et al.* and the entrapment of reactive species, such as cyclobutadiene or benzyne in covalent container molecules,³³³ the tetrahedral Fe(II)-cage 157⁴⁻ also offered a hydrophobic environment to protect reactive species in water.³³⁴ For example, white phosphorus (P₄) 160 (Figure 68) is air sensitive. Nevertheless, white phosphorus 160 could be stored in the cavity of the Fe(II)-cage 157⁴⁻ in water and in the presence of oxygen over 4 months.³³⁵ The stabilization of 160 was rationalized by the constrictive binding of the guest in the cage's cavity (Figure 73), rather than by an unfavorable passage of molecular oxygen through the portals of the cage. Any oxidized product of 160, as well as the corresponding transition state, were not good fits for the cavity of the tetrahedral Fe(II)-cage 157⁴⁻.

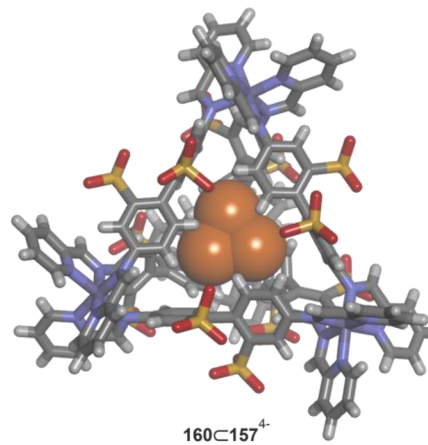


Figure 73. X-ray structure of the 160_C157⁴⁻ cage complex (CCDC 727817). The cage is depicted in stick representation and bound guest is shown as CPK model.

The inwardly directed polar functions of the metallo-cages discussed above had weak hydrogen bond donor properties. To overcome this limitation, Nitschke *et al.* assembled the tetrahedral M_4L_4 Fe(II)-cage **161** using azaphosphatrane ligands and anions as templating agents^{336,337} (Figure 67). The Fe(II)-cage **161** was obtained as a mixture of two isomers. In one of them, the four azaphosphatrane $P^+ \cdot H$ groups converged in the interior of the cavity (T symmetry). In the other isomer, one of the $P^+ \cdot H$ groups pointed outward and the other three were inwardly directed (C_3 symmetry). Both isomeric cages had an overall charge $z = +12$ and their cavities were highly polar.

The anion used as templating agent had a significant role in controlling the symmetry of the major assembled isomer of the Fe(II)-cage **161**¹²⁺. For example, anions having a volume smaller than 53 \AA^3 produced mainly the C_3 -symmetric cage. On the contrary, anions featuring a larger volume ($>53 \text{ \AA}^3$) were more suitable templates for the formation of the T -symmetric cage.³³⁶ One of the isomers of the Fe(II)-cage **161**¹²⁺ could be converted into the other by the simple addition of the corresponding anion in solution. The two isomers of the tetrahedral Fe(II)-cage **161**¹²⁺ were able to include one anion in their cavities even in water solution.³³⁶ That is, the combination of three/four converging ionic hydrogen-bonding interactions, with their associated Coulombic forces (section 2), could overcome the energetic cost associated with anion desolvation in water. Receptor **161**¹²⁺ represents one of the few examples of metal coordination cages featuring endohedral polar functions that are capable of performing efficient recognition of anions in water.³³⁸

Other examples of metal coordination cages and their applications in catalysis were reported in literature.^{339–342}

6.2. Noncovalent Capsules

Noncovalent self-assembled capsules feature an enclosed cavity,³⁴³ which completely isolates the bound guests from water molecules in the bulk solution.¹⁵ Their assembly involves the use of concave molecular scaffolds, such as calix[4]arene and resorcin[4]arene derivatives.²³² The convex shape of the molecular components provided the curvature necessary for the final capsular assembly. The inner volume of the supramolecular capsules might accommodate solvent molecules, complementary guests, or a combination of both of them.³⁴⁴

Crego-Calama, Reinhoudt, and co-workers reported the self-assembly of dimeric capsules based on calix[4]arene scaffolds through ion-pairing interactions (section 2) in water solution.³⁴⁵ Two tetra-charged self-complementary calix[4]-arene derivatives were used for the capsular assembly. One calix[4]arene derivative, **162**, was decorated with carboxylic acids at the upper rim (Figure 74a). The carboxylic acid groups of **162** were ionized in water at basic pH giving $[162 \cdot 4H]^{4-}$. The other calix[4]arene derivative, **163**, was functionalized with amidinium groups also at the upper rim, *i.e.*, 163^{4+} (Figure 74a). The equimolar mixture of the two calix[4]arene derivatives, $[162 \cdot 4H]^{4-}$ and 163^{4+} , in water at $pH = 9$ afforded the heterodimeric capsule $[162 \cdot 4H]^{4-} \cdot 163^{4+}$ (Figure 74a). Interestingly, the propyl substituents of the amidinium groups of 163^{4+} were inwardly directed in the assembled dimeric capsule and filled its internal cavity.³⁴⁵ The subsequent addition of size and shape complementary guests to the capsule's $[162 \cdot 4H]^{4-} \cdot 163^{4+}$ cavity volume, such as 6-amino-2-methyl quinoline **164** (Figure 74b), provoked the protrusion

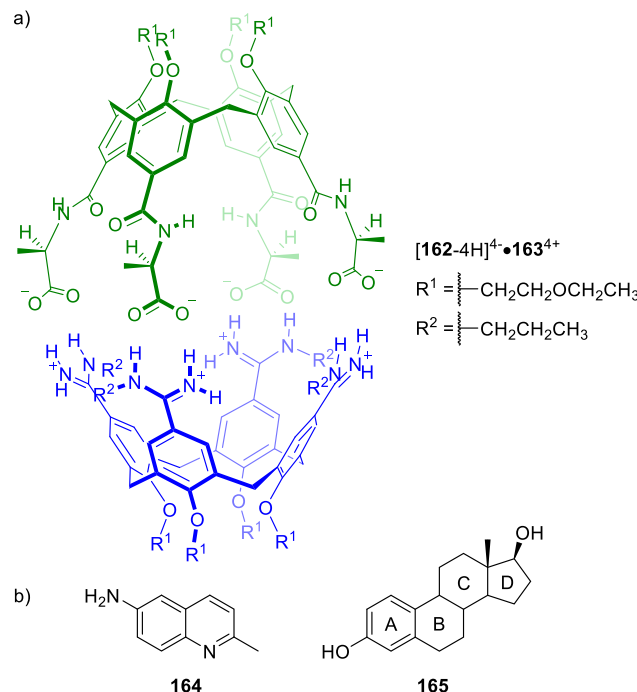


Figure 74. Line-drawing structures of: (a) dimeric capsule $[162 \cdot 4H]^{4-} \cdot 163^{4+}$ ($[162 \cdot 4H]^{4-}$ in green and 163^{4+} in blue) and (b) guest molecules **164** and **165**.

of the propyl groups from the capsule's periphery and the concomitant encapsulation of the guest.³⁴⁶

In section 4.2, we discussed the formation of 1:1 inclusion complexes derived from the octa-acid deep-cavity cavitand **95** (Figure 39). We provided some hints on the tendency to aggregate of the octa-carboxylate and octa-ammonium cavitands, $[95 \cdot 8H]^{8-}$ and 96^{8+} , in water solution. Using this ability and in the presence of suitable guests, Gibb and Gibb demonstrated that the octa-acid **95** self-assembled into a dimeric capsule,²⁴⁶ **95**₂ (Figure 75). The dimerization of **95** was driven by the HE (see section 2.1) owing to the water desolvation of the large aromatic surface area at the cavity portal. In basic water, the peripheral carboxylic acids of **95**₂ were converted into carboxylates warranting water solubility to the dimeric capsule, $[95_2 \cdot 16H]^{16-}$.

The cavity volume of the dimeric capsule $[95_2 \cdot 16H]^{16-}$ was large enough to accommodate steroids, such as estradiol **165** (Figure 74b). The A ring of bound **165** was included in one half, while the D ring occupied the opposite half of the capsule $[95_2 \cdot 16H]^{16-}$ (Figure 75). The quantitative formation of the ternary 1:2 guest/host complex at millimolar concentration, $165 \subset [95_2 \cdot 16H]^{16-}$, indicated that the stability constant value was larger than 10^8 M^{-2} .²⁴⁶

The deep-cavity cavitand $[95 \cdot 8H]^{8-}$ was also assembled into dimeric capsules in the presence of *n*-alkanes, from nonane to heptadecane.³⁴⁷ Alkanes shorter than *n*-decane fit comfortably in the cavity of $[95_2 \cdot 16H]^{16-}$ in extended conformations. On the contrary, longer *n*-alkanes adopted high-energy, compacted-coiled conformations when included in the cavity of the dimeric capsule.³⁴⁸

The stabilization (binding) of high-energy conformers in the cavity of $[95_2 \cdot 16H]^{16-}$ was also investigated using piperidine derivatives by Ramamurthy *et al.*³⁴⁹ For example, in solution, piperidine **166** adopted a conformation in which the O-propyl substituent occupied an equatorial position (Scheme 9). The

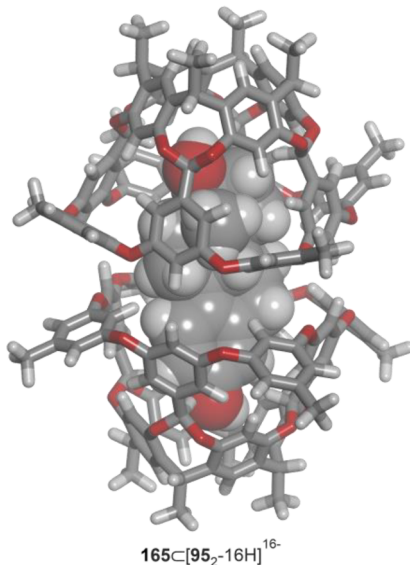
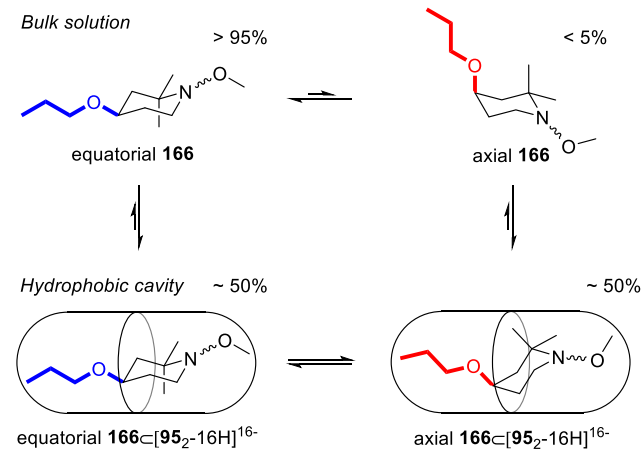


Figure 75. Energy minimized structure (MM3) of the simplified $165\subset[95_2\text{-}16\text{H}]^{16-}$ encapsulation complex. The resorcin[4]arenes are depicted in stick representation, and the guest is shown as CPK model. Water-solubilizing groups were pruned to methyl groups to simplify the calculation.

Scheme 9. Equilibria Experienced by the Piperidine Derivative 166 in the Presence of Capsule $[95_2\text{-}16\text{H}]^{16-}$ in Water (See Figure 39 for the Line-Drawing Structure of 95)



addition of **166** to a millimolar water solution of deep-cavity cavitand $[95\text{-}8\text{H}]^{8-}$ induced the formation of equimolar amounts of two kinetically stable encapsulation complexes on the ^1H NMR chemical shift time scale (Scheme 9). One of the encapsulation complexes corresponded to the equatorial conformer of **166**, equatorial $166\subset[95_2\text{-}16\text{H}]^{16-}$. The other encapsulation isomer included the higher-energy axial conformer of the piperidine derivative **166**, axial $166\subset[95_2\text{-}16\text{H}]^{16-}$.

The homodimeric capsules derived from the self-assembly of $[95\text{-}8\text{H}]^{8-}$ and 96^{8+} (Figure 39) featured the same overall charge of 16 but opposite sign and complementary inner and outer electrostatic potential surfaces. In analogy to the stabilization of charged species exerted by the overall charge of water-soluble metal coordination cages (section 6.1), the signs of the electrostatic potential surfaces and overall charges of the noncovalent dimeric capsules $[95_2\text{-}16\text{H}]^{16-}$ and $[96_2]^{16+}$

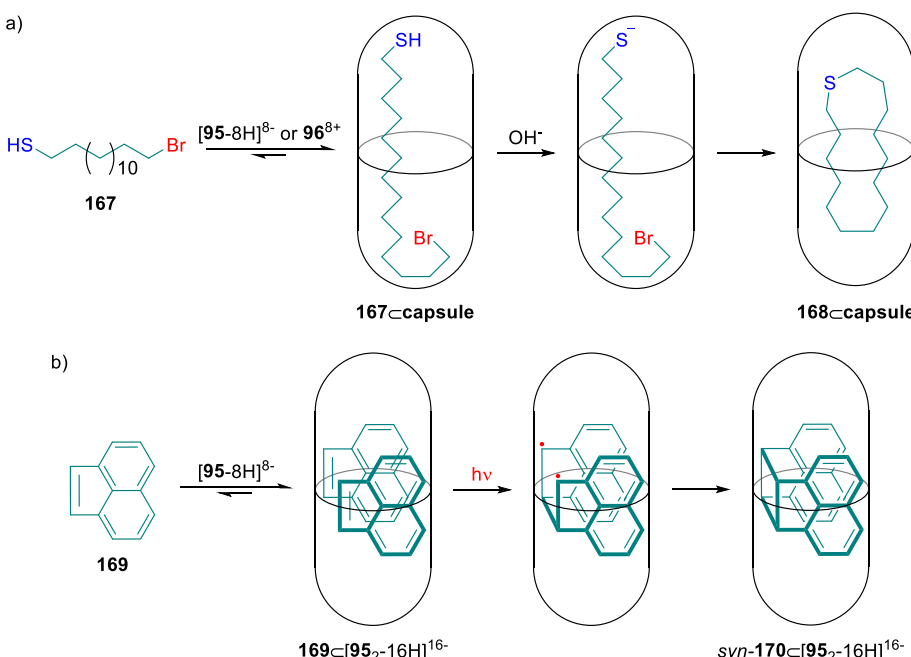
influenced the reactivity of bound guests. Recently, Gibb *et al.* showed the effect exerted by the two dimeric capsules, $[95_2\text{-}16\text{H}]^{16-}$ and $[96_2]^{16+}$, in the intramolecular cyclization reaction of included long-chain α,ω -alkanes bearing terminal thiol and halide groups.³⁵⁰ The cyclization reaction required the deprotonation of the terminal thiol group, at one end of the molecule, with a base to produce the corresponding thiolate. The thiolate then reacted with the halide carbon at the other end of the alkyl chain to render the cyclic product. For example, α,ω -thiol **167** was quantitatively encapsulated in either $[95_2\text{-}16\text{H}]^{16-}$ or $[96_2]^{16+}$ capsules featuring a *J*-binding motif^{350,351} (Scheme 10a). The pK_a value of the bound thiol was larger in the anionic capsule $[95_2\text{-}16\text{H}]^{16-}$ than in the cationic counterpart $[96_2]^{16+}$. This was translated into an energetic stabilization of the thiolate anion upon deprotonation in $[96_2]^{16+}$ or, in other words, the acidity of the bound thiol was enhanced in the cationic dimeric capsule. Therefore, in basic water and in the interior of the anionic capsule $[95_2\text{-}16\text{H}]^{16-}$, **167** underwent an intramolecular cyclization reaction to give the cyclic product **168** in *ca.* 8 h (Scheme 10a). In striking contrast and under identical reaction conditions, the same cyclization reaction took place in *<2* min using the cationic capsule $[96_2]^{16+}$.³⁵⁰

Gibb, Ramamurthy, and co-workers also applied the dimeric capsule $[95_2\text{-}16\text{H}]^{16-}$ to control the excited-state properties of encapsulated guests³⁵² and alter reaction pathways of photochemical processes taking place in its interior.^{353,354} For example, direct irradiation of a suspension of acenaphthylene **169** (Scheme 10b) in water gave a mixture of dimeric products: 40% *syn*-**170** and 60% *anti*-**170**. In striking contrast and under the same irradiation conditions, acenaphthylene **169**, in the presence of $[95\text{-}8\text{H}]^{8-}$, led to the quantitative formation of the *syn*-dimer **170** in borate buffer solution at pH = 9³⁵⁵ (Scheme 10b). The guest **169** and octa-carboxylate $[95\text{-}8\text{H}]^{8-}$ formed a 2:2 host/guest encapsulation complex, $169_2\subset[95_2\text{-}16\text{H}]^{16-}$. The two molecules of **169** were bound in a *syn*-fashion, favoring the formation of *syn*-**170** upon irradiation. The *syn*-dimer **170** nicely fits in the cavity of the capsule $[95_2\text{-}16\text{H}]^{16-}$, but the *anti*-dimer **170** did not. The latter was too large to be accommodated within the capsule's cavity. More recently, Ramamurthy *et al.* coupled the photoisomerization of a neutral spiropyran into its zwitterionic merocyanine form with the reversible disassembly/assembly of the dimeric capsule $[95_2\text{-}16\text{H}]^{16-}$.³⁵⁶

Despite the competitive nature of water for hydrogen-bonding, Rebek *et al.* demonstrated that the tetra-cationic benzimidazolone resorcin[4]arene deep cavitand **171**⁴⁺ self-assembled quantitatively into a cylindrical homodimeric capsule $[171_2]^{8+}$ in the presence of suitable nonpolar guests²³⁹ (Figure 76). The series of guests used as templates included: large aromatic molecules and long *n*-alkanes, such as undecane **172**. The formation of the dimeric capsule, $[171_2]^{8+}$, was mainly driven by the HE owing to the encapsulation of large nonpolar surfaces of the host and the guest, and the formation of a seam of bifurcated hydrogen-bonding interactions at the equator of the assembly.

Recently, Rebek, Yu, and co-workers showed that related dimeric capsules could be assembled in water solution using resorcin[4]arene deep cavitands with 2,1,3-benzoselenadiazole walls.³⁵⁷ In the latter case, the dimeric capsule was held together by the hydrophobic effect and, more interestingly, by chalcogen-bonding interactions (see section 2) between the

Scheme 10. (a) Cyclization Reaction of **167** and (b) Dimerization of **169** in the Interior of the Dimeric Capsule, $[95_2\text{-}16\text{H}]^{16-}$ or $[96_2]^{16+}$



^aNote that only one *J*-conformer of bound **167** is shown for clarity. See Figure 39 for the line-drawing structures of **95** and **96**.

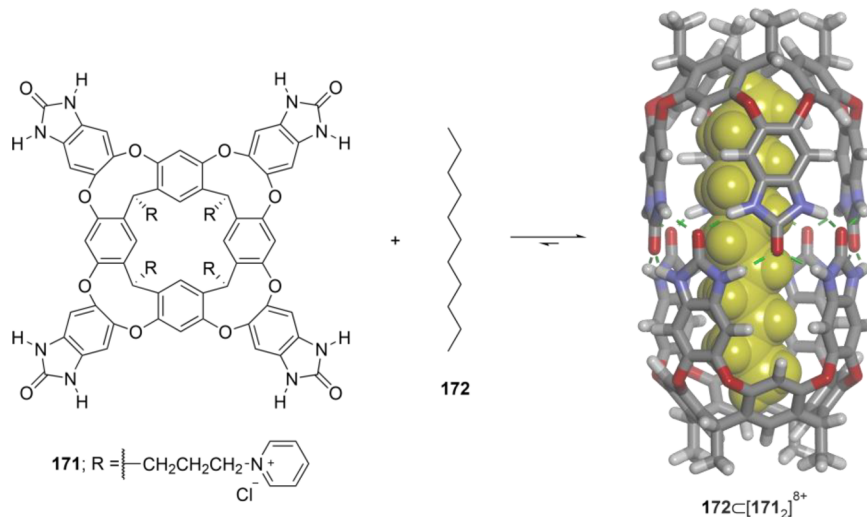


Figure 76. (left) Line-drawing structures of **171** and **172**; (right) energy minimized structure (MM3) of the simplified $172\text{C}[171_2]^{8+}$ encapsulation complex. The cavitand is depicted in stick representation and bound guest (in yellow) is shown as CPK model. Hydrogen bonds are highlighted (green dashed lines).

nitrogen (lone-pair) and the selenium atoms (σ -hole) of the 2,1,3-benzoselenadiazole walls of the deep cavitand.

7. COMPARISON OF THE BINDING PROPERTIES OF DIFFERENT MACROCYCLES WITH SOME SELECTED GUESTS

In this section, we compare the binding mode of selected receptors, corresponding to different families, with a common guest molecule featuring one or multiple binding sites and displaying neutral or charged character.

Dougherty *et al.* investigated the binding of adamantane trimethylammonium iodide salt **17** (Figure 78) with the ethenoanthracene-based cyclophane **15** (Figure 77) bearing *p*-

xylyl spacers in borate buffer at pD = 9.¹⁰⁷ Guest **17** is heteroditopic and possesses two different binding sites: the nonpolar adamantyl residue and the polar trimethylammonium group. Both residues are good fits, in terms of size, shape, and functional complementarity with the receptor's nonpolar aromatic cavity. The calculated complexation-induced shifts (CIS) for the protons of the bound guest suggested that the trimethylammonium cationic residue was deeper in the aromatic cavity than the nonpolar adamantyl counterpart (Figure 10). In addition to the HE, the $17^+\text{C}15^4-$ complex ($K_a = 8.2 \times 10^4 \text{ M}^{-1}$) was stabilized by cation– π interactions and long-range Coulombic interactions between the carboxylates and the alkylammonium group.

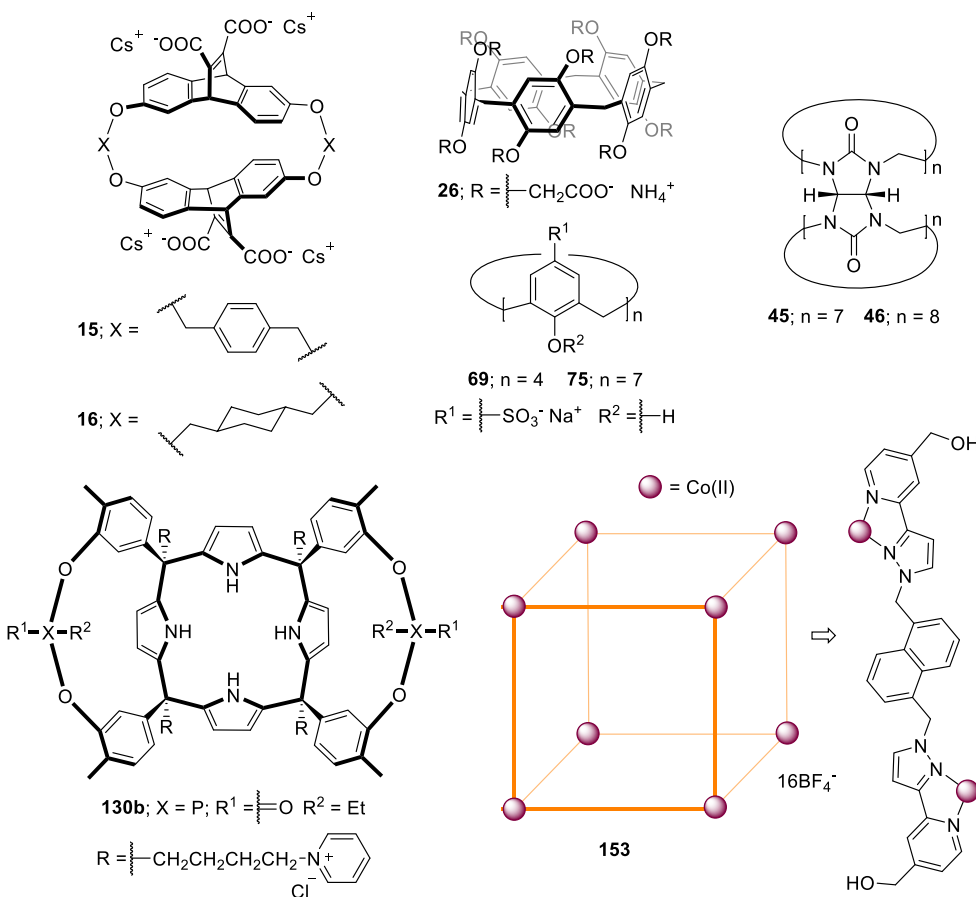


Figure 77. Line-drawing structures of the receptors used for comparison.

Isaacs *et al.* reported the complexation of **17** with cucurbit[7]uril **45** (Figure 77) in buffer solution at pH \sim 4.7.¹⁷⁵ The $\text{17}^+\text{C45}$ complex ($K_a = 1.7 \times 10^{12} \text{ M}^{-1}$) showed an increase in 7 orders of magnitude with respect to the $\text{17}^+\text{C15}^+$ -counterpart. It is known that the adamantane skeleton is complementary to the cavity of CB7 **45**, and its inclusion is mainly driven by the HE. Most likely, the trimethylammonium residue protrudes outside of the cavity and locates in the center of the polar portal defined by the seven C=O groups of the glycoluril units establishing multiple cation–dipole and polar hydrogen-bonding interactions. These extra interactions can be quantified to be in the order of $28.4 \text{ kJ}\cdot\text{mol}^{-1}$. The $\text{17}^+\text{C45}$ complex can be placed among the tightest known to date.

The binding of the adamantane trimethylammonium **17**⁺ (added as chloride salt) was also studied by Shinkai *et al.* with the tetra-sodium salt of tetra-sulfonate calix[4]arene **69** (Figure 77).^{206–208} The authors described the formation of a 1:1 complex, $\text{17}^+\text{C69}^{4-}$, in 0.1 M phosphate buffer at pD = 7.3 ($K_a = 2.1 \times 10^4 \text{ M}^{-1}$). The CIS experienced by the proton atoms of bound **17**⁺ (adamantyl methylene and N-methyl groups moved upfield) indicated that **17**⁺ was not bound in a selective manner. That is, both the adamantyl and ammonium moieties of **17**⁺ were included in the aromatic cavity of **69**⁴⁻. This result was in agreement with the findings of Dougherty *et al.* in the binding of **17**⁺ with water-soluble cyclophanes, *i.e.*, **15**⁴⁻ (*vide supra*). They proposed the existence of cation–π interactions between the guest ⁺NMe₃ residue and the π-systems of the host, which may also be operative in the binding with tetra-sulfonate calix[4]arene **69**⁴⁻. Nevertheless, the sulfonate groups at the upper rim of **69**⁴⁻ provided a strong

anionic field. In addition, the anionic sulfonate groups were involved in Coulombic interactions with the cationic bound **17**⁺.

Dougherty *et al.*¹⁰⁹ and Shinkai *et al.*²⁰⁷ reported the thermodynamic parameters of the complexation processes of **17**⁺ with receptors **15**⁴⁻ and **69**⁴⁻. In both cases and at 298 K, the binding was mainly driven by enthalpy ($\Delta H = -19.6 \text{ kJ}\cdot\text{mol}^{-1}$ for **15**⁴⁻ and $-23.8 \text{ kJ}\cdot\text{mol}^{-1}$ for **69**⁴⁻). The corresponding entropy terms were smaller ($T\Delta S = +10.5 \text{ kJ}\cdot\text{mol}^{-1}$ for **15**⁴⁻ and $+0.8 \text{ kJ}\cdot\text{mol}^{-1}$ for **69**⁴⁻) but also favorable. The thermodynamic signature of both binding processes at 298 K is akin to a “nonclassical” HE. However, while Shinkai *et al.* described a good linear relationship for the plot of $\ln K_a$ vs T^{-1} (25–80 °C), which is indicative of a negligible ΔC_p value, Dougherty *et al.* observed a significant curvature ($\Delta C_p \neq 0$) (25–33 °C). The mathematical analysis of the nonlinear $\ln K_a$ vs T^{-1} data using an adjusted van't Hoff equation allowing for a temperature invariant heat capacity change returned $\Delta C_p = -418 \text{ J}\cdot\text{mol}^{-1}\cdot\text{K}^{-1}$ for the formation of the $\text{17}^+\text{C15}^+$ complex. We commented in the introduction that the existence of a large and negative heat capacity value for binding processes in water could be indicative of the importance of the HE. In turn, large ΔC_p values produce significant enthalpy–entropy compensation (EEC) effects with changes in temperature. This phenomenon makes the interpretation of thermodynamic parameters difficult and may even lead to hydrophobic crossover: the thermodynamic signature of the binding process is modified from “classical” to “nonclassical” HE with temperature. For this reason, we agree with Ernst and Gibb in the reduced utility of the classification of a binding event as

driven by the “classical” or “nonclassical” HE.¹¹ For the formation of the $17^+ \subset 15^{4-}$ complex, the enthalpy–entropy crossover was not observed in the range of studied temperatures. However, at 333 K, the binding became more favored by enthalpy ($\Delta H = -34.3 \text{ kJ}\cdot\text{mol}^{-1}$) and slightly opposed by entropy ($T\Delta S = -3.3 \text{ kJ}\cdot\text{mol}^{-1}$).

In contrast, an enthalpy–entropy crossover was indeed detected at 323 K in the binding of 4-methylquinoline, a neutral guest, with cyclophane **16** featuring a more hydrophobic cavity than **15** (Figure 77). In host **16**, cyclohexyl groups were used instead of the phenyl spacers of **15**. At 298 K, the formation of the 4-methylquinoline \subset **16** $^{4-}$ complex was exclusively driven by entropy but became only favored by enthalpy at 333 K ($\Delta C_p = -794 \text{ J}\cdot\text{mol}^{-1}\cdot\text{K}^{-1}$).

In comparison, the binding of 4-methylquinoline with receptor **15** $^{4-}$ displayed thermodynamic components and changes with temperature ($\Delta H = -41.0 \text{ kJ}\cdot\text{mol}^{-1}$, $T\Delta S = -11.3 \text{ kJ}\cdot\text{mol}^{-1}$ at 298 K, and $\Delta C_p = -543 \text{ J}\cdot\text{mol}^{-1}\cdot\text{K}^{-1}$) that were in line with those determined for the complexation of the cationic trimethylammonium adamantanate guest **17** $^+$ (*vide supra*). The authors commented that the magnitudes of the entropic and enthalpic contributions to binding at 298 K served to identify the role played by electrostatic and hydrophobic interactions. Overall, the described results serve to illustrate the complexity of the binding processes in water that derives from the detailed analysis of the thermodynamic components and its associated changes with temperature. We insist in considering the magnitude and sign of ΔC_p as the most reliable source indicating the role played by the HE in binding.

Dicationic compounds containing a spacer of reduced polarity, like dimethyl viologen **28** $^{2+}$ (Figure 78), are tritopic

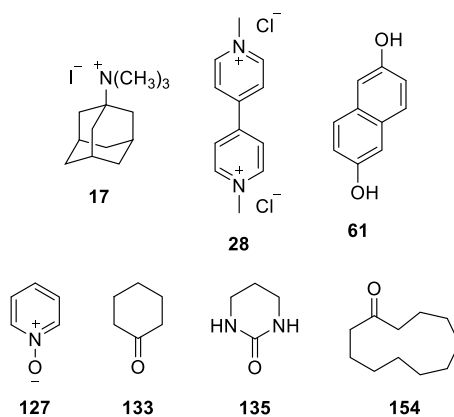


Figure 78. Line-drawing structures of the guests used for the comparison of receptors.

guests. Consequently, its efficient binding in water solution requires multtopic hosts having size, shape, and function complementarity. In water solution, tetra-carboxylate pillar[5]-arene **26** $^{10-}$ (Figure 77) possesses 10 carboxylate groups diverging from its aromatic and nonpolar cavity. The terminal carboxylates are covalently attached through oxy-methylene chains to the 1,4-positions of the phenyl units defining the receptor’s electron-rich aromatic cavity. This substitution renders the rims of the two open portals of **26** $^{10-}$ functionalized with five carboxylate anions each. The aromatic cavity of **26** $^{10-}$ is adequate for the inclusion of the electron-deficient 4,4'-bipyridinium spacer of **28** $^{2+}$. Thus, the interaction of **26** $^{10-}$

with **28** $^{2+}$ produced a 1:1 inclusion complex ($K_a = 8.2 \times 10^4 \text{ M}^{-1}$) stabilized by the HE, donor–acceptor aromatic interactions, charge-transfer, and multiple Coulombic interactions between the negatively charged carboxylate residues located at the host’s portals and the cationic ends of the guest (methylpyridinium) protruding from the receptor’s cavity (Figure 15). The formed **28** $^{2+} \subset$ **26** $^{10-}$ complex featured a pseudorotaxane topology. It also displayed fast exchange dynamics on the chemical shift time scale with the bound counterparts. The inclusion of **28** $^{2+}$ increased significantly the rotation energy barrier of the oxy-methylene units functionalized with the terminal carboxylates that are located at both rims of bound **26** $^{10-}$.¹²⁹

Cucurbit[7]uril **45** (Figure 77) also formed a 1:1 inclusion complex with **28** $^{2+}$ in water solution ($K_a = 1.0 \times 10^5 \text{ M}^{-1}$ in H_2O containing 0.2 M NaCl).¹⁹¹ The β -aromatic protons of bound **28** $^{2+}$ experienced an upfield shift of more than 1.5 ppm, evidencing the inclusion of the guest in the nonpolar cavity of cucurbit[7]uril **45**. The obtained results reflected a good fit between the cavity of **45** and the cross-section of the 4,4'-bipyridinium residue. Likewise, the similarity of distances between the two N-atoms of bipyridinium **28** $^{2+}$ and the centers of the planes defined by the carbonyl oxygen atoms at the portals of **45** maximizes multiple ion–dipole interactions in the **28** $^{2+} \subset$ **45** inclusion complex. The binding affinity of the neutral cucurbit[7]uril **45** receptor for dimethyl viologen **28** $^{2+}$ is similar to that of deca-carboxylate pillar[5]arene **26** $^{10-}$ (Figure 77). Most likely, the HE plays an important role in driving the formation of both complexes. The fact that cucurbit[7]uril **45** is a neutral receptor could maximize this effect.

Cucurbit[8]uril **46** (Figure 77) has a slightly larger cavity than its homologue **45**, lacking one glycoluril bis-methylene unit (cavity diameters of 8.8 and 7.3 Å, respectively). Nevertheless, **46** binds **28** $^{2+}$ and produces a 1:1 inclusion complex ($K_a = 8.5 \times 10^5 \text{ M}^{-1}$).^{180–182} The included dimethyl viologen **28** $^{2+}$ only fills half of the cavity volume of **46**. Probably, the co-inclusion of another molecule of **28** $^{2+}$ is disfavored by repulsive Coulombic interactions. The empty space remaining in the **28** $^{2+} \subset$ **46** complex is similar to the cavity size of **45**. At millimolar concentration, the addition of a size complementary, electron-rich, neutral guest, *i.e.*, 2,6-dihydroxynaphthalene **61** (Figure 78) to the **28** $^{2+} \subset$ **46** complex induced the quantitative formation of the ternary complex [**61** \cdot **28** $^{2+}$] \subset **46** (Figure 29).

Dimethyl viologen **28** was also bound by the hepta-sulfonate calix[7]arene **75** (Figure 77).²²³ At $\text{pD} = 7.3$, $[\text{75-2H}]^{9-}$ presents nine negative charges (seven sulfonate groups and two deprotonated phenols). Receptor $[\text{75-2H}]^{9-}$ is very flexible conformationally and displays a large aromatic cavity suitable for the inclusion of sizable aromatic guests. The **28** $^{2+} \subset$ $[\text{75-2H}]^{9-}$ complex was characterized by a binding constant of $K_a = 3.2 \times 10^4 \text{ M}^{-1}$. The superior binding affinity of dicharged cationic guests compared to monocharged analogues suggested that Coulombic interactions between the sulfonate and the ammonium groups were important for the binding. Molecular modeling studies revealed that **28** $^{2+}$ was sandwiched between the aromatic walls defining the cavity of $[\text{75-2H}]^{9-}$. The positive nitrogen atoms of the ammonium groups were located close to sulfonate substituents.

The examples commented above highlight the importance of charge-based electrostatic interactions (*i.e.*, Coulombic or charge–charge, ion–dipole, and charge-assisted dipole–di-

pole) in combination with the HE for the binding of charged organic guests in water solution. The efficient and selective binding of small molecular weight molecules, featuring polar but neutral character, requests the application of additional principles. The HE is also responsible for the binding strength of the complexes derived from these guests. However, the selectivity in the binding of polar neutral guests is a direct consequence of the establishment of additional neutral electrostatic interactions (dipole–dipole) upon complex formation. The creation of these latter interactions demands the placement of converging polar groups in the nonpolar cavities of the synthetic receptors. This modification is synthetically challenging owing to the widespread use of aromatic panels to shape the nonpolar cavities of the receptors.

The cubic Co(II)-cage **153** (Figure 77) described by Hunter, Ward, and co-workers presents endohedral methylene CH polar groups that are capable to form hydrogen-bonding interactions with the oxygen atoms of encapsulated polar guests.^{321,324} The polar CHs are not accessible to bulk water molecules owing to its deep inclusion in the cage's nonpolar cavity. The authors demonstrated that the binding affinities of the 1:1 cage complexes formed by **153**¹⁶⁺, and a series of homologous aliphatic cyclic ketones increased with guest size (increase in hydrophobic surface area). The peak in binding affinity was reached with cycloundecanone **154** (Figure 78). The corresponding 1:1 cage complex displayed a 50% packing coefficient, which is close to the optimal 55% noted by Rebek and co-workers.¹⁶⁰ The contribution of the polar hydrogen-bonding interactions to the binding of **153**¹⁶⁺ was investigated using a series of six-membered rings containing a polar group with different hydrogen-bonding accepting capabilities (β value), *i.e.*, ketone, lactone, lactam, and *N*-oxide. For this second guest's series, the binding affinities decreased as the β value, and thus guest polarity, increased. For example, pyridine *N*-oxide **127** (Figure 78) was bound by **153**¹⁶⁺ with a low binding affinity of $K_a = 1 \text{ M}^{-1}$. The obtained result indicated that in water, the binding of the metallo-cage **153**¹⁶⁺ to the series of six-membered guest seemed to have the hydrogen-bonding component switched off.

Water-soluble “four-wall” aryl-extended and super aryl-extended calix[4]pyrroles, as well as its cavitand derivatives are good receptors for the binding of small polar molecules (section 5.3). The formed inclusion complexes have 1:1 stoichiometry and are stabilized by a combination of the HE and neutral electrostatic polar interactions: hydrogen-bonds, CH– π , *etc.* Inspired by the work of Hunter, Ward, and co-workers, we used the *bis*-phosphonate cavitand **130b** (Figure 77) to assess the hydrogen-bonding contribution to the binding of small polar guests in water solution.²⁸⁵ To this end, we employed a series of six-membered cyclic polar guest analogous to that employed by Hunter, Ward, and co-workers. Surprisingly for us, the trend in binding affinities displayed by the cavitand **130b**⁴⁺ was opposite to the calculated lipophilicity values of the guests ($\log P$). Conversely, we observed the existence of a linear relationship, displaying a positive slope, between the calculated binding affinity values and the hydrogen-bonding accepting capabilities (β), as well as polarity values of the guests ($\log P$). For example, the complex of **130b**⁴⁺ with cyclohexanone **133** was 2 orders of magnitude less stable than that of the more polar six-membered cyclic urea **135** (Figure 78). We concluded that the polar binding site of **130b**⁴⁺ seemed to provide a better environment for the solvation of the polar guest than water. Interestingly, pyridine

N-oxide **127** (Figure 78) was bound by **130b**⁴⁺ with an affinity value K_a (**127** \subset **130b**⁴⁺) = $6.9 \times 10^6 \text{ M}^{-1}$. This represents a 6 orders of magnitude increase with respect to the metallo-cage **153**¹⁶⁺. The described results support the importance of the placement of converging groups in the nonpolar cavities of synthetic receptors, with large hydrogen-bonding accepting (β) or donating capabilities (α), for the efficient recognition of small polar molecules in water. To improve binding competence, the receptor's polar groups should not be accessible for direct solvation with bulk water molecules (reduced hydration of the binding sites).

This section is used as example in comparing the binding properties of selected receptors with a common guest. Similar comparisons can be drawn from other examples discussed in the text.

8. OVERVIEW AND OUTLOOK

We revised selected families of water-soluble synthetic receptors featuring well-defined internal cavities. The early designs involved cyclophanes featuring 2D hydrophobic cavities open at two opposite ends. These cavities were easily accessible by bulk water molecules. Subsequently, oligocyclic cyclophanes were introduced with the goal of shaping 3D cavities and limiting the access of water molecules to their interiors. The inclusion complexes of cyclophanes with hydrophobic guests displayed acceptable levels of thermodynamic stability ($K_a > 10^3 \text{ M}^{-1}$). However, their kinetic stabilities tended to be low on the ¹H NMR chemical shift time scale.

A further development in the design of 2D receptors consisted on increasing their concavity and/or depth. These modifications aimed at increasing the contact surface area between host and guest and reducing the portal's size in relation to cavity volume. In this endeavor, bent glycoluril units were used to prepare cucurbit[n]urils and bambus[n]urils. Following a related strategy, pillar[n]arenes came to live. The portals of these 2D receptors contain polar groups, but their cavities are rather hydrophobic.

The improvement in host–guest contact surface area reached an initial milestone with the development of calix[n]arenes and resorcin[4]arenes. These receptors were hydrophobic and possessed shallow concave cavities, closed at one end and open at the opposite end. Their upper rims may have attached water-solubilizing groups, which could also interact with polar groups of the bound guest. To minimize interferences with the binding event and allow further elaboration of the receptors' cavity, water-solubilizing groups were moved at the lower rim. At this point, water-soluble cavitands and deep cavitands were developed. They featured a deep and conformationally more rigid cavity than the parent receptors leading to an improvement of the thermodynamic and kinetic stabilities of the resulting inclusion complexes. However, the use of aromatic panels in shaping their cavities created difficulties for the placement of converging polar groups and for their solubilization in water.

This structural limitation has been addressed with the introduction of “temple” receptors, naphthotubes, and aryl- and super aryl-extended calix[4]pyrroles. We are convinced that receptors having functionalized internal cavities are excellent candidates for the efficient and selective recognition of polar guests. We expect to see developments and breakthroughs in this area of research in the next years.

Molecular encapsulation represents the ultimate goal of molecular recognition. We described two strategies, that is, the self-assembly of metallo-cage and capsular containers. Metallo-cages possessed open portals that allowed reversible guest binding. On the other hand, noncovalent capsules, stabilized by weaker interactions, lack of sizable portals. The reversible guest binding in the latter assemblies required their partial dissociation. Most metallo-cages and capsules displayed hydrophobic cavities. Examples of placing convergent functional groups in their interiors are scarce. We also foresee a significant development in this direction in the years to come.

Because catalysis deals with the binding of dynamic targets, we included few applications of water-soluble synthetic receptors in the stabilization of high-energy intermediates and transition states. We expect this area of research to fructify and prosper in the future because catalytic turnover was demonstrated to be more general than initially imagined.

Last but not least, research on water structure and solvation is required to fully understand the hydrophobic and the Hofmeister effects and to elaborate reliable theoretical prediction models for the accurate calculation of host–guest binding properties in water.

We hope that this review will serve as a reference for all those interested in molecular recognition in water. We also expect that the examples included herein will inspire researchers to design new receptors featuring specific properties for their use in other fundamental areas and/or real-world applications.

AUTHOR INFORMATION

Corresponding Author

Pablo Ballester — Institute of Chemical Research of Catalonia (ICIQ), The Barcelona Institute of Science and Technology (BIST), 43007 Tarragona, Spain; ICREA, 08010 Barcelona, Spain;  orcid.org/0000-0001-8377-6610; Email: pballester@iciq.es

Author

Luis Escobar — Institute of Chemical Research of Catalonia (ICIQ), The Barcelona Institute of Science and Technology (BIST), 43007 Tarragona, Spain; Departament de Química Analítica i Química Orgànica, Universitat Rovira i Virgili, 43007 Tarragona, Spain;  orcid.org/0000-0003-0392-8245

Complete contact information is available at:

<https://pubs.acs.org/10.1021/acs.chemrev.0c00522>

Notes

The authors declare no competing financial interest.

Biographies

Luis Escobar was born in 1992 in Albacete, Spain. He received his B.Sc. in Chemistry from the University of Castilla-La Mancha (UCLM) in 2014. After that, he moved to the Institute of Chemical Research of Catalonia (ICIQ) to pursue his Master studies and Doctoral thesis under the supervision of Prof. Pablo Ballester. In 2019, he earned his Ph.D. degree from the University of Rovira and Virgili (URV) and the ICIQ. He is currently a postdoctoral associate in the group of Prof. Thomas Carell at the Ludwig Maximilian University of Munich (LMU), working on prebiotic chemistry and chemical biology. His research interests are in the areas of molecular recognition and self-assembly in aqueous media.

Pablo Ballester was born in 1959 in Palma de Mallorca, Spain. He studied Chemistry at the University of the Balearic Islands (UIB), where he also completed the Ph.D. degree in 1986 under the direction of Prof. Ramón Mestres. He worked as a postdoctoral fellow with Prof. Julius Rebek, Jr. at the University of Pittsburgh and MIT for three years and one year in the UIB with Prof. José M. Saá. In 1990, he joined the Chemistry Department of UIB, where he held the positions of Assistant and Associate Professor. In 2004, he was awarded with an ICREA Research Professorship and moved to the Institute of Chemical Research of Catalonia (ICIQ) to become a group leader. His current research interests are in the areas of molecular self-assembly, molecular recognition, and supramolecular catalysis.

ACKNOWLEDGMENTS

We thank Gobierno de España MCIN/AEI/FEDER, UE (projects CTQ2017-84319-P and CEX2019-000925-S), the CERCA Programme/Generalitat de Catalunya, AGAUR (2017 SGR 1123), and the ICIQ Foundation for financial support. L.E. thanks MECD for a predoctoral fellowship (FPU14/01016). We also thank Dr. Gemma Aragay for proofreading the manuscript prior to submission.

REFERENCES

- (1) Ariga, K.; Ito, H.; Hill, J. P.; Tsukube, H. Molecular Recognition: from Solution Science to Nano/Materials Technology. *Chem. Soc. Rev.* **2012**, *41*, 5800–5835.
- (2) Shetty, D.; Khedkar, J. K.; Park, K. M.; Kim, K. Can We Beat the Biotin-Avidin Pair?: Cucurbit[7]uril-Based Ultrahigh Affinity Host-Guest Complexes and Their Applications. *Chem. Soc. Rev.* **2015**, *44*, 8747–8761.
- (3) Houk, K. N.; Leach, A. G.; Kim, S. P.; Zhang, X. Y. Binding Affinities of Host-Guest, Protein-Ligand, and Protein-Transition-State Complexes. *Angew. Chem., Int. Ed.* **2003**, *42*, 4872–4897.
- (4) Biedermann, F.; Schneider, H.-J. Experimental Binding Energies in Supramolecular Complexes. *Chem. Rev. (Washington, DC, U. S.)* **2016**, *116*, 5216–5300.
- (5) Hunter, C. A. Quantifying Intermolecular Interactions: Guidelines for the Molecular Recognition Toolbox. *Angew. Chem., Int. Ed.* **2004**, *43*, 5310–5324.
- (6) Dill, K. A.; Truskett, T. M.; Vlachy, V.; Hribar-Lee, B. Modeling Water, the Hydrophobic Effect, and Ion Solvation. *Annu. Rev. Biophys. Biomol. Struct.* **2005**, *34*, 173–199.
- (7) Snyder, P. W.; Lockett, M. R.; Moustakas, D. T.; Whitesides, G. M. Is it the Shape of the Cavity, or the Shape of the Water in the Cavity? *Eur. Phys. J.: Spec. Top.* **2014**, *223*, 853–891.
- (8) Hillyer, M. B.; Gibb, B. C. Molecular Shape and the Hydrophobic Effect. *Annu. Rev. Phys. Chem.* **2016**, *67*, 307–329.
- (9) Brini, E.; Fennell, C. J.; Fernandez-Serra, M.; Hribar-Lee, B.; Luksic, M.; Dill, K. A. How Water's Properties Are Encoded in Its Molecular Structure and Energies. *Chem. Rev. (Washington, DC, U. S.)* **2017**, *117*, 12385–12414.
- (10) Rehm, T. H.; Schmuck, C. Ion-Pair Induced Self-Assembly in Aqueous Solvents. *Chem. Soc. Rev.* **2010**, *39*, 3597–3611.
- (11) Ernst, N. E.; Gibb, B. C. Water Runs Deep. In *Supramolecular Chemistry in Water*; Kubik, S., Ed.; Wiley, 2020; pp 1–33.
- (12) Schneider, H. J.; Yatsimirska, A. K. Selectivity in Supramolecular Host-Guest Complexes. *Chem. Soc. Rev.* **2008**, *37*, 263–277.
- (13) Biedermann, F. Water-Compatible Host Systems. In *Supramolecular Chemistry in Water*; Kubik, S., Ed. Wiley, 2020; pp 35–77.
- (14) Jordan, J. H.; Gibb, B. C. Molecular Containers Assembled Through the Hydrophobic Effect. *Chem. Soc. Rev.* **2015**, *44*, 547–585.
- (15) Oshovsky, G. V.; Reinhoudt, D. N.; Verboom, W. Supramolecular Chemistry in Water. *Angew. Chem., Int. Ed.* **2007**, *46*, 2366–2393.

- (16) Taylor, L. L. K.; Riddell, I. A.; Smulders, M. M. J. Self-Assembly of Functional Discrete Three-Dimensional Architectures in Water. *Angew. Chem., Int. Ed.* **2019**, *58*, 1280–1307.
- (17) Kataev, E. A.; Muller, C. Recent Advances in Molecular Recognition in Water: Artificial Receptors and Supramolecular Catalysis. *Tetrahedron* **2014**, *70*, 137–167.
- (18) Brown, C. J.; Toste, F. D.; Bergman, R. G.; Raymond, K. N. Supramolecular Catalysis in Metal-Ligand Cluster Hosts. *Chem. Rev. (Washington, DC, U. S.)* **2015**, *115*, 3012–3035.
- (19) Rizzi, A.; Murkli, S.; McNeill, J. N.; Yao, W.; Sullivan, M.; Gilson, M. K.; Chiu, M. W.; Isaacs, L.; Gibb, B. C.; Mobley, D. L.; Chodera, J. D. Overview of the SAMPL6 Host-Guest Binding Affinity Prediction Challenge. *J. Comput.-Aided Mol. Des.* **2018**, *32*, 937–963.
- (20) SAMPL Challenge. In *Wikipedia, The Free Encyclopedia*, 2020. https://en.wikipedia.org/wiki/SAMPL_Challenge.
- (21) Schneider, H. J. Comment on “HYDROPHOBE Challenge: A Joint Experimental and Computational Study on the Host-Guest Binding of Hydrocarbons to Cucurbiturils, Allowing Explicit Evaluation of Guest Hydration Free-Energy ‘Contributions’”. *J. Phys. Chem. B* **2018**, *122*, 2825–2826.
- (22) Snyder, P. W.; Mecinović, J.; Moustakas, D. T.; Thomas, S. W.; Harder, M.; Mack, E. T.; Lockett, M. R.; Héroux, A.; Sherman, W.; Whitesides, G. M. Mechanism of the Hydrophobic Effect in the Biomolecular Recognition of Arylsulfonamides by Carbonic Anhydrase. *Proc. Natl. Acad. Sci. U. S. A.* **2011**, *108*, 17889–17894.
- (23) Suating, P.; Nguyen, T. T.; Ernst, N. E.; Wang, Y.; Jordan, J. H.; Gibb, C. L. D.; Ashbaugh, H. S.; Gibb, B. C. Proximal Charge Effects on Guest Binding to a Non-Polar Pocket. *Chem. Sci.* **2020**, *11*, 3656–3663.
- (24) James, T. D.; Sandanayake, K.; Shinkai, S. Saccharide Sensing with Molecular Receptors Based on Boronic Acid. *Angew. Chem., Int. Ed. Engl.* **1996**, *35*, 1910–1922.
- (25) Striegler, S. Selective Carbohydrate Recognition by Synthetic Receptors in Aqueous Solution. *Curr. Org. Chem.* **2003**, *7*, 81–102.
- (26) Wu, X.; Li, Z.; Chen, X.-X.; Fossey, J. S.; James, T. D.; Jiang, Y.-B. Selective Sensing of Saccharides Using Simple Boronic Acids and Their Aggregates. *Chem. Soc. Rev.* **2013**, *42*, 8032–8048.
- (27) Rekharsky, M. V.; Inoue, Y. Complexation Thermodynamics of Cyclodextrins. *Chem. Rev. (Washington, DC, U. S.)* **1998**, *98*, 1875–1917.
- (28) Chen, G.; Jiang, M. Cyclodextrin-Based Inclusion Complexation Bridging Supramolecular Chemistry and Macromolecular Self-Assembly. *Chem. Soc. Rev.* **2011**, *40*, 2254–2266.
- (29) Kubik, S. Anion Recognition in Aqueous Media by Cyclopeptides and Other Synthetic Receptors. *Acc. Chem. Res.* **2017**, *50*, 2870–2878.
- (30) Uhlenheuer, D. A.; Petkau, K.; Brunsved, L. Combining Supramolecular Chemistry with Biology. *Chem. Soc. Rev.* **2010**, *39*, 2817–2826.
- (31) Rizzuto, F. J.; von Krbek, L. K. S.; Nitschke, J. R. Strategies for Binding Multiple Guests in Metal-Organic Cages. *Nat. Rev. Chem.* **2019**, *3*, 204–222.
- (32) Schneider, H. J. Mechanisms of Molecular Recognition: Investigations of Organic Host-Guest Complexes. *Angew. Chem., Int. Ed. Engl.* **1991**, *30*, 1417–1436.
- (33) Wang, L.; Berne, B. J.; Friesner, R. A. Ligand Binding to Protein-Binding Pockets with Wet and Dry Regions. *Proc. Natl. Acad. Sci. U. S. A.* **2011**, *108*, 1326–1330.
- (34) Schneider, H. J. Dispersive Interactions in Solution Complexes. *Acc. Chem. Res.* **2015**, *48*, 1815–1822.
- (35) White, A. D.; Keefe, A. J.; Ella-Menyé, J.-R.; Nowinski, A. K.; Shao, Q.; Pfaendtner, J.; Jiang, S. Free Energy of Solvated Salt Bridges: A Simulation and Experimental Study. *J. Phys. Chem. B* **2013**, *117*, 7254–7259.
- (36) Marcus, Y.; Hefta, G. Ion Pairing. *Chem. Rev. (Washington, DC, U. S.)* **2006**, *106*, 4585–4621.
- (37) Blondeau, P.; Segura, M.; Perez-Fernandez, R.; de Mendoza, J. Molecular Recognition of Oxoanions Based on Guanidinium Receptors. *Chem. Soc. Rev.* **2007**, *36*, 198–210.
- (38) Worm, K.; Schmidtchen, F. P. Molecular Recognition of Anions by Zwitterionic Host Molecules in Water. *Angew. Chem., Int. Ed. Engl.* **1995**, *34*, 65–66.
- (39) Schmidtchen, F. P.; Berger, M. Artificial Organic Host Molecules for Anions. *Chem. Rev. (Washington, DC, U. S.)* **1997**, *97*, 1609–1646.
- (40) Langton, M. J.; Serpell, C. J.; Beer, P. D. Anion Recognition in Water: Recent Advances from a Supramolecular and Macromolecular Perspective. *Angew. Chem., Int. Ed.* **2016**, *55*, 1974–1987.
- (41) Ballester, P. Anion Binding in Covalent and Self-Assembled Molecular Capsules. *Chem. Soc. Rev.* **2010**, *39*, 3810–3830.
- (42) Kubik, S. Anion Recognition in Water. *Chem. Soc. Rev.* **2010**, *39*, 3648–3663.
- (43) Zayed, J. M.; Nouvel, N.; Rauwald, U.; Scherman, O. A. Chemical Complexity-Supramolecular Self-Assembly of Synthetic and Biological Building Blocks in Water. *Chem. Soc. Rev.* **2010**, *39*, 2806–2816.
- (44) Persch, E.; Dumele, O.; Diederich, F. Molecular Recognition in Chemical and Biological Systems. *Angew. Chem., Int. Ed.* **2015**, *54*, 3290–3327.
- (45) Pascoe, D. J.; Ling, K. B.; Cockcroft, S. L. The Origin of Chalcogen-Bonding Interactions. *J. Am. Chem. Soc.* **2017**, *139*, 15160–15167.
- (46) Vogel, L.; Wonner, P.; Huber, S. M. Chalcogen Bonding: An Overview. *Angew. Chem., Int. Ed.* **2019**, *58*, 1880–1891.
- (47) Meyer, E. A.; Castellano, R. K.; Diederich, F. Interactions with Aromatic Rings in Chemical and Biological Recognition. *Angew. Chem., Int. Ed.* **2003**, *42*, 1210–1250.
- (48) Salonen, L. M.; Ellermann, M.; Diederich, F. Aromatic Rings in Chemical and Biological Recognition: Energetics and Structures. *Angew. Chem., Int. Ed.* **2011**, *50*, 4808–4842.
- (49) Izatt, R. M.; Pawlak, K.; Bradshaw, J. S.; Bruening, R. L. Thermodynamic and Kinetic Data for Macrocycle Interaction with Cations, Anions, and Neutral Molecules. *Chem. Rev. (Washington, DC, U. S.)* **1995**, *95*, 2529–2586.
- (50) Dougherty, D. A. The Cation- π Interaction. *Acc. Chem. Res.* **2013**, *46*, 885–893.
- (51) Arranz-Mascaros, P.; Bazzicalupi, C.; Bianchi, A.; Giorgi, C.; Godino-Salido, M. L.; Gutierrez-Valero, M. D.; Lopez-Garzon, R.; Savastano, M. Thermodynamics of Anion- π Interactions in Aqueous Solution. *J. Am. Chem. Soc.* **2013**, *135*, 102–105.
- (52) Adriaenssens, L.; Gil-Ramírez, G.; Frontera, A.; Quiñonero, D.; Escudero-Adán, E. C.; Ballester, P. Thermodynamic Characterization of Halide- π Interactions in Solution Using “Two-Wall” Aryl Extended Calix[4]pyrroles as Model System. *J. Am. Chem. Soc.* **2014**, *136*, 3208–3218.
- (53) Nishio, M. The CH/ π Hydrogen Bond in Chemistry. Conformation, Supramolecules, Optical Resolution and Interactions Involving Carbohydrates. *Phys. Chem. Chem. Phys.* **2011**, *13*, 13873–13900.
- (54) Asensio, J. L.; Arda, A.; Canada, F. J.; Jimenez-Barbero, J. Carbohydrate-Aromatic Interactions. *Acc. Chem. Res.* **2013**, *46*, 946–954.
- (55) Jimenez-Moreno, E.; Jimenez-Oses, G.; Gomez, A. M.; Santana, A. G.; Corzana, F.; Bastida, A.; Jimenez-Barbero, J.; Asensio, J. L. A Thorough Experimental Study of CH/ π Interactions in Water: Quantitative Structure-Stability Relationships for Carbohydrate/Aromatic Complexes. *Chem. Sci.* **2015**, *6*, 6076–6085.
- (56) Walker, D. B.; Joshi, G.; Davis, A. P. Progress in Biomimetic Carbohydrate Recognition. *Cell. Mol. Life Sci.* **2009**, *66*, 3177–3191.
- (57) Cox, J. P. L.; Nicholls, I. A.; Williams, D. H. Molecular Recognition in Aqueous Solution: An Estimate of the Intrinsic Binding Energy of an Amide-Hydroxy Hydrogen Bond. *J. Chem. Soc., Chem. Commun.* **1991**, 1295–1297.
- (58) Wang, H.; Wang, W.; Jin, W. J. σ -Hole Bond vs π -Hole Bond: A Comparison Based on Halogen Bond. *Chem. Rev. (Washington, DC, U. S.)* **2016**, *116*, 5072–5104.
- (59) Blokzijl, W.; Engberts, J. Hydrophobic Effects - Opinions and Facts. *Angew. Chem., Int. Ed. Engl.* **1993**, *32*, 1545–1579.

- (60) Bakker, H. J. Water's Response to the Fear of Water. *Nature* **2012**, *491*, 533–535.
- (61) Chandler, D. Interfaces and the Driving Force of Hydrophobic Assembly. *Nature* **2005**, *437*, 640–647.
- (62) Diederich, F. Apolar Complexation in Organic Solvents. In *Cyclophanes*; The Royal Society of Chemistry, 1991; pp 106–139.
- (63) Diederich, F. Solvent Effects in Molecular Recognition. In *Cyclophanes*; The Royal Society of Chemistry, 1991; pp 246–263.
- (64) Frank, H. S.; Evans, M. W. Free Volume and Entropy in Condensed Systems III. Entropy in Binary Liquid Mixtures; Partial Molal Entropy in Dilute Solutions; Structure and Thermodynamics in Aqueous Electrolytes. *J. Chem. Phys.* **1945**, *13*, 507–532.
- (65) Kauzmann, W. Some Factors in the Interpretation of Protein Denaturation. In *Advances in Protein Chemistry*; Anfinsen, C. B., Anson, M. L., Bailey, K., Edsall, J. T., Eds.; Academic Press, 1959; Vol. 14, pp 1–63.
- (66) Meyer, E. E.; Rosenberg, K. J.; Israelachvili, J. Recent Progress in Understanding Hydrophobic Interactions. *Proc. Natl. Acad. Sci. U. S. A.* **2006**, *103*, 15739–15746.
- (67) Ben-Amotz, D. Water-Mediated Hydrophobic Interactions. *Annu. Rev. Phys. Chem.* **2016**, *67*, 617–638.
- (68) Biedermann, F.; Uzunova, V. D.; Scherman, O. A.; Nau, W. M.; De Simone, A. Release of High-Energy Water as an Essential Driving Force for the High-Affinity Binding of Cucurbit[n]urils. *J. Am. Chem. Soc.* **2012**, *134*, 15318–15323.
- (69) Biedermann, F.; Nau, W. M.; Schneider, H. J. The Hydrophobic Effect Revisited—Studies with Supramolecular Complexes Imply High-Energy Water as a Noncovalent Driving Force. *Angew. Chem., Int. Ed.* **2014**, *53*, 11158–11171.
- (70) Prabhu, N. V.; Sharp, K. A. Heat Capacity in Proteins. *Annu. Rev. Phys. Chem.* **2005**, *56*, 521–548.
- (71) Cooper, A. Heat Capacity Effects in Protein Folding and Ligand Binding: A Re-Evaluation of the Role of Water in Biomolecular Thermodynamics. *Biophys. Chem.* **2005**, *115*, 89–97.
- (72) Leko, K.; Hanževački, M.; Brkljača, Z.; Pičuljan, K.; Ribić, R.; Požar, J. Solvophobically Driven Complexation of Adamantyl Mannoside with β -Cyclodextrin in Water and Structured Organic Solvents. *Chem. - Eur. J.* **2020**, *26*, 5208–5219.
- (73) Lemieux, R. U. How Water Provides the Impetus for Molecular Recognition in Aqueous Solution. *Acc. Chem. Res.* **1996**, *29*, 373–380.
- (74) Leung, D. H.; Bergman, R. G.; Raymond, K. N. Enthalpy-Entropy Compensation Reveals Solvent Reorganization as a Driving Force for Supramolecular Encapsulation in Water. *J. Am. Chem. Soc.* **2008**, *130*, 2798–2805.
- (75) Khrapunov, S. The Enthalpy-Entropy Compensation Phenomenon. Limitations for the Use of Some Basic Thermodynamic Equations. *Curr. Protein Pept. Sci.* **2018**, *19*, 1088–1091.
- (76) Dunitz, J. D. Win Some, Lose Some – Enthalpy-Entropy Compensation in Intermolecular Interactions. *Chem. Biol.* **1995**, *2*, 709–712.
- (77) Gibb, B. C. Supramolecular Assembly and Binding in Aqueous Solution: Useful Tips Regarding the Hofmeister and Hydrophobic Effects. *Isr. J. Chem.* **2011**, *51*, 798–806.
- (78) Biela, A.; Nasief, N. N.; Betz, M.; Heine, A.; Hangauer, D.; Klebe, G. Dissecting the Hydrophobic Effect on the Molecular Level: The Role of Water, Enthalpy, and Entropy in Ligand Binding to Thermolysin. *Angew. Chem., Int. Ed.* **2013**, *52*, 1822–1828.
- (79) Cremer, P. S.; Flood, A. H.; Gibb, B. C.; Mobley, D. L. Collaborative Routes to Clarifying the Murky Waters of Aqueous Supramolecular Chemistry. *Nat. Chem.* **2018**, *10*, 8–16.
- (80) Barnett, J. W.; Sullivan, M. R.; Long, J. A.; Tang, D.; Nguyen, T.; Ben-Amotz, D.; Gibb, B. C.; Ashbaugh, H. S. Spontaneous Drying of Non-Polar Deep-Cavity Cavitand Pockets in Aqueous Solution. *Nat. Chem.* **2020**, *12*, 589–594.
- (81) He, S.; Biedermann, F.; Vankova, N.; Zhechkov, L.; Heine, T.; Hoffman, R. E.; De Simone, A.; Duignan, T. T.; Nau, W. M. Cavitation Energies Can Outperform Dispersion Interactions. *Nat. Chem.* **2018**, *10*, 1252–1257.
- (82) Vaitheswaran, S.; Yin, H.; Rasaiah, J. C.; Hummer, G. Water Clusters in Nonpolar Cavities. *Proc. Natl. Acad. Sci. U. S. A.* **2004**, *101*, 17002–17005.
- (83) Diederich, F.; Smithrud, D. B.; Sanford, E. M.; Wyman, T. B.; Ferguson, S. B.; Carcanague, D. R.; Chao, I.; Houk, K. N. Solvent Effects in Molecular Recognition. *Acta Chem. Scand.* **1992**, *46*, 205–215.
- (84) Dong, J.; Davis, A. P. Molecular Recognition Mediated by Hydrogen Bonding in Aqueous Media. *Angew. Chem., Int. Ed.* **2020**, DOI: 10.1002/anie.202012315.
- (85) Assaf, K. I.; Nau, W. M. The Chaotropic Effect as an Assembly Motif in Chemistry. *Angew. Chem., Int. Ed.* **2018**, *57*, 13968–13981.
- (86) Ramaiah, D.; Neelakandan, P. P.; Nair, A. K.; Avirah, R. R. Functional Cyclophanes: Promising Hosts for Optical Biomolecular Recognition. *Chem. Soc. Rev.* **2010**, *39*, 4158–4168.
- (87) Odashima, K.; Itai, A.; Iitaka, Y.; Koga, K. Host-Guest Complex Formation Between a Water-Soluble Polyparacyclophe and a Hydrophobic Guest Molecule. *J. Am. Chem. Soc.* **1980**, *102*, 2504–2505.
- (88) Odashima, K.; Itai, A.; Iitaka, Y.; Arata, Y.; Koga, K. Inclusion Complex Formation in a Particular Geometry by a Water-Soluble Paracyclophe in Aqueous Solution - NMR Studies -. *Tetrahedron Lett.* **1980**, *21*, 4347–4350.
- (89) Odashima, K.; Soga, T.; Koga, K. Substrate Selective Inclusion by a Series of Water-Soluble Paracyclophanes - Host-Guest Recognition of Steric Structure and Charge -. *Tetrahedron Lett.* **1981**, *22*, 5311–5314.
- (90) Lai, C. F.; Odashima, K.; Koga, K. Synthesis and Properties of Water-Soluble Bis-Paracyclophanes. *Tetrahedron Lett.* **1985**, *26*, 5179–5182.
- (91) Lai, C. F.; Odashima, K.; Koga, K. Biomimetic Studies Using Artificial Systems. S. Design and Synthesis of Novel Water-Soluble Bis-Cyclophanes. *Chem. Pharm. Bull.* **1989**, *37*, 2351–2354.
- (92) Soga, T.; Odashima, K.; Koga, K. Modifications of Hydrophobic Cavity and their Effects on the Complex Formation with a Hydrophobic Substrate. *Tetrahedron Lett.* **1980**, *21*, 4351–4354.
- (93) Murakami, Y.; Kikuchi, J.; Ohno, T.; Hayashida, O.; Kojima, M. Synthesis of Macrocyclic Enzyme Models. 7. Octopus Cyclophanes Having L-Aspartate Residues as Novel Water-Soluble Hosts - Aggregation Behavior and Induced-Fit Molecular Recognition. *J. Am. Chem. Soc.* **1990**, *112*, 7672–7681.
- (94) Kikuchi, J.; Egami, K.; Suehiro, K.; Murakami, Y. pH-Response Molecular Recognition by a Water-Soluble Cyclophane Bearing L-Aspartate Moieties. *Chem. Lett.* **1992**, *21*, 1685–1688.
- (95) Schneider, H. J.; Blatter, T.; Palm, B.; Pfingstag, U.; Rudiger, V.; Theis, I. Complexation of Nucleosides, Nucleotides, and Analogs in an Azoniacyclophe - van der Waals and Electrostatic Binding Increments and NMR Shielding Effects. *J. Am. Chem. Soc.* **1992**, *114*, 7704–7708.
- (96) Schneider, H. J.; Kramer, R.; Simova, S.; Schneider, U. Solvent and Salt Effects on Binding Constants of Organic Substrates in Macrocyclic Host Compounds. A General Equation Measuring Hydrophobic Binding Contributions. *J. Am. Chem. Soc.* **1988**, *110*, 6442–6448.
- (97) Schneider, H. J.; Theis, I. Salt Effects on Supramolecular Complexation and Catalysis. *J. Org. Chem.* **1992**, *57*, 3066–3070.
- (98) Grawe, T.; Schrader, T.; Finocchiaro, P.; Consiglio, G.; Failla, S. A New Receptor Molecule for Lysine and Histidine in Water: Strong Binding of Basic Amino Acid Esters by a Macrocyclic Host. *Org. Lett.* **2001**, *3*, 1597–1600.
- (99) Diederich, F. Molecular Recognition in Aqueous Solution: Supramolecular Complexation and Catalysis. *J. Chem. Educ.* **1990**, *67*, 813–820.
- (100) Diederich, F.; Dick, K. A New Water-Soluble Macrocyclic Host of the Cyclophane Type: Host-Guest Complexation with Aromatic Guests in Aqueous Solution and Acceleration of the Transport of Arenes through an Aqueous Phase. *J. Am. Chem. Soc.* **1984**, *106*, 8024–8036.

- (101) Ferguson, S. B.; Seward, E. M.; Sanford, E. M.; Hester, M.; Uyeki, M.; Diederich, F. Molecular Recognition by Cyclophane Hosts. *Pure Appl. Chem.* **1989**, *61*, 1523–1528.
- (102) Ferguson, S. B.; Sanford, E. M.; Seward, E. M.; Diederich, F. Cyclophane Arene Inclusion Complexation in Protic Solvents – Solvent Effects Versus Electron-Donor Acceptor Interactions. *J. Am. Chem. Soc.* **1991**, *113*, 5410–5419.
- (103) Allott, C.; Adams, H.; Hunter, C. A.; Thomas, J. A.; Bernad, P. L., Jr.; Rotger, C. Hydrogen-Bond Recognition of Cyclic Dipeptides in Water. *Chem. Commun. (Cambridge, U. K.)* **1998**, 2449–2450.
- (104) Smithrud, D. B.; Wyman, T. B.; Diederich, F. Enthalpically Driven Cyclophane-Arene Inclusion Complexation: Solvent-Dependent Calorimetric Studies. *J. Am. Chem. Soc.* **1991**, *113*, 5420–5426.
- (105) Harrison, J. C.; Eftink, M. R. Cyclodextrin-Adamantanecarboxylate Inclusion Complexes: A Model System for the Hydrophobic Effect. *Biopolymers* **1982**, *21*, 1153–1166.
- (106) Cowart, M. D.; Sucholeiki, I.; Bukownik, R. R.; Wilcox, C. S. Molecular Recognition in Aqueous Media. Conformationally Restricted Water-Soluble Cyclophanes Derived from 6H,12H-5,11-Methanodibenzo[b, f][1,5]diazocine. *J. Am. Chem. Soc.* **1988**, *110*, 6204–6210.
- (107) Petti, M. A.; Sheppard, T. J.; Barrans, R. E.; Dougherty, D. A. “Hydrophobic” Binding of Water-Soluble Guests by High-Symmetry, Chiral Hosts. An Electron-Rich Receptor Site with a General Affinity for Quaternary Ammonium Compounds and Electron-Deficient π Systems. *J. Am. Chem. Soc.* **1988**, *110*, 6825–6840.
- (108) Ngola, S. M.; Kearney, P. C.; Mecozi, S.; Russell, K.; Dougherty, D. A. A Selective Receptor for Arginine Derivatives in Aqueous Media. Energetic Consequences of Salt Bridges That Are Highly Exposed to Water. *J. Am. Chem. Soc.* **1999**, *121*, 1192–1201.
- (109) Stauffer, D. A.; Barrans, R. E.; Dougherty, D. A. Concerning the Thermodynamics of Molecular Recognition in Aqueous and Organic Media. Evidence for Significant Heat Capacity Effects. *J. Org. Chem.* **1990**, *55*, 2762–2767.
- (110) Kearney, P. C.; Mizoue, L. S.; Kumpf, R. A.; Forman, J. E.; McCurdy, A.; Dougherty, D. A. Molecular Recognition in Aqueous Media. New Binding Studies Provide Further Insights into the Cation- π Interactions and Related Phenomena. *J. Am. Chem. Soc.* **1993**, *115*, 9907–9919.
- (111) Webb, T. H.; Suh, H. S.; Wilcox, C. S. Enantioselective and Diastereoselective Molecular Recognition of Alicyclic Substrates in Aqueous Media by a Chiral, Resolved Synthetic Receptor. *J. Am. Chem. Soc.* **1991**, *113*, 8554–8555.
- (112) Forman, J. E.; Barrans, R. E.; Dougherty, D. A. Circular Dichroism Studies of Molecular Recognition with Cyclophane Hosts in Aqueous Media. *J. Am. Chem. Soc.* **1995**, *117*, 9213–9228.
- (113) Zeng, F.; Chen, C. F. Synthesis of a Novel Water-Soluble Cylindrical Macrotricyclic Host and its Complexation with *N*-methylquinolinium and *N*-methylisoquinolinium Salts: Formation of 1:2 Complexes in Water. *Org. Biomol. Chem.* **2015**, *13*, 1988–1991.
- (114) Otto, S.; Furlan, R. L. E.; Sanders, J. K. M. Selection and Amplification of Hosts From Dynamic Combinatorial Libraries of Macrocyclic Disulfides. *Science* **2002**, *297*, 590–593.
- (115) Corbett, P. T.; Sanders, J. K. M.; Otto, S. Exploring the Relation Between Amplification and Binding in Dynamic Combinatorial Libraries of Macrocyclic Synthetic Receptors in Water. *Chem. - Eur. J.* **2008**, *14*, 2153–2166.
- (116) James, L. I.; Beaver, J. E.; Rice, N. W.; Waters, M. L. A Synthetic Receptor for Asymmetric Dimethyl Arginine. *J. Am. Chem. Soc.* **2013**, *135*, 6450–6455.
- (117) Ingerman, L. A.; Cuellar, M. E.; Waters, M. L. A Small Molecule Receptor that Selectively Recognizes Trimethyl Lysine in a Histone Peptide with Native Protein-Like Affinity. *Chem. Commun. (Cambridge, U. K.)* **2010**, *46*, 1839–1841.
- (118) Beaver, J. E.; Peacor, B. C.; Bain, J. V.; James, L. I.; Waters, M. L. Contributions of Pocket Depth and Electrostatic Interactions to Affinity and Selectivity of Receptors for Methylated Lysine in Water. *Org. Biomol. Chem.* **2015**, *13*, 3220–3226.
- (119) Dhaenens, M.; Lehn, J. M.; Vigneron, J. P. Molecular Recognition of Nucleosides, Nucleotides and Anionic Planar Substrates by a Water-Soluble Bis-Intercaland-Type Receptor Molecule. *J. Chem. Soc., Perkin Trans. 2* **1993**, 1379–1381.
- (120) Molt, O.; Rubeling, D.; Schafer, G.; Schrader, T. Adrenaline Recognition in Water. *Chem. - Eur. J.* **2004**, *10*, 4225–4232.
- (121) Carvalho, S.; Delgado, R.; Drew, M. G. B.; Calisto, V.; Felix, V. Binding Studies of a Protonated Dioxatetraazamacrocyclic with Carboxylate Substrates. *Tetrahedron* **2008**, *64*, 5392–5403.
- (122) Mendy, J. S.; Pilate, M. L.; Horne, T.; Day, V. W.; Hossain, M. A. Encapsulation and Selective Recognition of Sulfate Anion in an Azamacrocyclic in Water. *Chem. Commun. (Cambridge, U. K.)* **2010**, *46*, 6084–6086.
- (123) Mittapalli, R. R.; Namashivaya, S. S. R.; Oshchepkov, A. S.; Shumilova, T. A.; Ruffer, T.; Lang, H.; Kataev, E. A. Selective Recognition of Oxalate in Water: Effect of pH on Binding Strength and Sensing Mechanisms. *Chem. Commun. (Cambridge, U. K.)* **2017**, *53*, 11345–11348.
- (124) Odell, B.; Reddington, M. V.; Slawin, A. M. Z.; Spencer, N.; Stoddart, J. F.; Williams, D. J. Cyclobis(Paraquat-*p*-Phenylenes). A Tetracationic Multipurpose Receptor. *Angew. Chem., Int. Ed. Engl.* **1988**, *27*, 1547–1550.
- (125) Bria, M.; Cooke, G.; Cooper, A.; Garety, J. F.; Hewage, S. G.; Nutley, M.; Rabani, G.; Woisel, P. An Investigation of the Complexation Properties of Cyclobis(Paraquat-*p*-Phenylenes) in Water. *Tetrahedron Lett.* **2007**, *48*, 301–304.
- (126) Ryan, S. T. J.; Del Barrio, J.; Ghosh, I.; Biedermann, F.; Lazar, A. I.; Lan, Y.; Coulston, R. J.; Nau, W. M.; Scherman, O. A. Efficient Host-Guest Energy Transfer in Polycationic Cyclophane-Perylene Diimide Complexes in Water. *J. Am. Chem. Soc.* **2014**, *136*, 9053–9060.
- (127) Smithrud, D. B.; Diederich, F. Strength of Molecular Complexation of Apolar Solutes in Water and in Organic Solvents is Predictable by Linear Free Energy Relationships: A General Model for Solvation Effects on Apolar Binding. *J. Am. Chem. Soc.* **1990**, *112*, 339–343.
- (128) Ogoshi, T.; Kanai, S.; Fujinami, S.; Yamagishi, T.-a.; Nakamoto, Y. *para*-Bridged Symmetrical Pillar[5]arenes: Their Lewis Acid Catalyzed Synthesis and Host-Guest Property. *J. Am. Chem. Soc.* **2008**, *130*, 5022–5023.
- (129) Ogoshi, T.; Hashizume, M.; Yamagishi, T.-a.; Nakamoto, Y. Synthesis, Conformational and Host-Guest Properties of Water-Soluble Pillar[5]arene. *Chem. Commun. (Cambridge, U. K.)* **2010**, *46*, 3708–3710.
- (130) Li, C. J.; Shu, X. Y.; Li, J.; Chen, S. H.; Han, K.; Xu, M.; Hu, B. J.; Yu, Y. H.; Jia, X. S. Complexation of 1,4-Bis(pyridinium)butanes by Negatively Charged Carboxylatopillar[5]arene. *J. Org. Chem.* **2011**, *76*, 8458–8465.
- (131) Liu, Y.; Zhou, F.; Yang, F.; Ma, D. Carboxylated Pillar[n]arene ($n = 5 - 7$) Host Molecules: High Affinity and Selective Binding in Water. *Org. Biomol. Chem.* **2019**, *17*, 5106–5111.
- (132) Ma, Y.; Ji, X.; Xiang, F.; Chi, X.; Han, C.; He, J.; Abiliz, Z.; Chen, W.; Huang, F. A Cationic Water-Soluble Pillar[5]arene: Synthesis and Host-Guest Complexation with Sodium 1-Octanesulfonate. *Chem. Commun. (Cambridge, U. K.)* **2011**, *47*, 12340–12342.
- (133) Li, Z. T.; Yang, J.; Yu, G. C.; He, J. M.; Abiliz, Z.; Huang, F. H. Synthesis of a Water-Soluble Pillar[9]arene and its pH-Responsive Binding to Paraquat. *Chem. Commun. (Cambridge, U. K.)* **2014**, *50*, 2841–2843.
- (134) Dasgupta, S.; Chowdhury, A.; Mukherjee, P. S. Binding of Carboxylatopillar[5]arene with Alkyl and Aryl Ammonium Salts in Aqueous Medium. *RSC Adv.* **2015**, *5*, 85791–85798.
- (135) Li, C.; Ma, J.; Zhao, L.; Zhang, Y.; Yu, Y.; Shu, X.; Li, J.; Jia, X. Molecular Selective Binding of Basic Amino Acids by a Water-Soluble Pillar[5]arene. *Chem. Commun. (Cambridge, U. K.)* **2013**, *49*, 1924–1926.
- (136) Murray, J.; Kim, K.; Ogoshi, T.; Yao, W.; Gibb, B. C. The Aqueous Supramolecular Chemistry of Cucurbit[n]urils, Pillar[n]-

- arenes and Deep-Cavity Cavitands. *Chem. Soc. Rev.* **2017**, *46*, 2479–2496.
- (137) Gomez, B.; Francisco, V.; Fernandez-Nieto, F.; Garcia-Rio, L.; Martin-Pastor, M.; Paleo, M. R.; Sardina, F. J. Host-Guest Chemistry of a Water-Soluble Pillar[5]arene: Evidence for an Ionic-Exchange Recognition Process and Different Complexation Modes. *Chem. - Eur. J.* **2014**, *20*, 12123–12132.
- (138) Gomez-Gonzalez, B.; Francisco, V.; Montecinos, R.; Garcia-Rio, L. Investigation of the Binding Modes of a Positively Charged Pillar[5]arene: Internal and External Guest Complexation. *Org. Biomol. Chem.* **2017**, *15*, 911–919.
- (139) Hu, X.-B.; Chen, L.; Si, W.; Yu, Y.; Hou, J.-L. Pillar[5]arene Decaamine: Synthesis, Encapsulation of Very Long Linear Diacids and Formation of Ion Pair-Stopped [2]Rotaxanes. *Chem. Commun. (Cambridge, U. K.)* **2011**, *47*, 4694–4696.
- (140) Ma, Y. J.; Xue, M.; Zhang, Z. B.; Chi, X. D.; Huang, F. H. Neutral Guest Capture by a Cationic Water-Soluble Pillar[5]arene in Water. *Tetrahedron* **2013**, *69*, 4532–4535.
- (141) Yu, G. C.; Xue, M.; Zhang, Z. B.; Li, J. Y.; Han, C. Y.; Huang, F. H. A Water-Soluble Pillar[6]arene: Synthesis, Host-Guest Chemistry, and Its Application in Dispersion of Multiwalled Carbon Nanotubes in Water. *J. Am. Chem. Soc.* **2012**, *134*, 13248–13251.
- (142) Xia, D. Y.; Yu, G. C.; Li, J. Y.; Huang, F. H. Photo-Responsive Self-Assembly Based on a Water-Soluble Pillar[6]arene and an Azobenzene-Containing Amphiphile in Water. *Chem. Commun. (Cambridge, U. K.)* **2014**, *50*, 3606–3608.
- (143) Chen, W.; Zhang, Y. Y.; Li, J.; Lou, X. B.; Yu, Y. H.; Jia, X. S.; Li, C. J. Synthesis of a Cationic Water-Soluble Pillar[6]arene and its Effective Complexation towards Naphthalenesulfonate Guests. *Chem. Commun. (Cambridge, U. K.)* **2013**, *49*, 7956–7958.
- (144) Ma, Y. J.; Yang, J.; Li, J. Y.; Chi, X. D.; Xue, M. A Cationic Water-Soluble Pillar[6]arene: Synthesis, Host-Guest Properties, and Self-Assembly with Amphiphilic Guests in Water. *RSC Adv.* **2013**, *3*, 23953–23956.
- (145) Yao, Y.; Li, J. Y.; Dai, J.; Chi, X. D.; Xue, M. A Water-Soluble Pillar[6]arene: Synthesis, Host-Guest Chemistry, Controllable Self-Assembly, and Application in Controlled Release. *RSC Adv.* **2014**, *4*, 9039–9043.
- (146) Xue, W.; Zavalij, P. Y.; Isaacs, L. Pillar[n]MaxQ: A New High Affinity Host Family for Sequestration in Water. *Angew. Chem., Int. Ed.* **2020**, *59*, 13313–13319.
- (147) Xia, D. Y.; Wang, P.; Shi, B. B. Controlling the Photochemical Reaction of an Azastilbene Derivative in Water Using a Water-Soluble Pillar[6]arene. *Org. Biomol. Chem.* **2017**, *15*, 7618–7622.
- (148) Cintas, P. Cucurbituril: Supramolecular Perspectives for an Old Ligand. *J. Inclusion Phenom. Mol. Recognit. Chem.* **1994**, *17*, 205–220.
- (149) Lagona, J.; Mukhopadhyay, P.; Chakrabarti, S.; Isaacs, L. The Cucurbit[n]uril Family. *Angew. Chem., Int. Ed.* **2005**, *44*, 4844–4870.
- (150) Barrow, S. J.; Kasera, S.; Rowland, M. J.; del Barrio, J.; Scherman, O. A. Cucurbituril-Based Molecular Recognition. *Chem. Rev. (Washington, DC, U. S.)* **2015**, *115*, 12320–12406.
- (151) Burnett, C. A.; Witt, D.; Fettinger, J. C.; Isaacs, L. Acyclic Congener of Cucurbituril: Synthesis and Recognition Properties. *J. Org. Chem.* **2003**, *68*, 6184–6191.
- (152) Ma, D.; Zavalij, P. Y.; Isaacs, L. Acyclic Cucurbit[n]uril Congeners Are High Affinity Hosts. *J. Org. Chem.* **2010**, *75*, 4786–4795.
- (153) Lucas, D.; Isaacs, L. Recognition Properties of Acyclic Glycoluril Oligomers. *Org. Lett.* **2011**, *13*, 4112–4115.
- (154) Shen, C.; Ma, D.; Meany, B.; Isaacs, L.; Wang, Y. H. Acyclic Cucurbit[n]uril Molecular Containers Selectively Solubilize Single-Walled Carbon Nanotubes in Water. *J. Am. Chem. Soc.* **2012**, *134*, 7254–7257.
- (155) Lu, X. Y.; Isaacs, L. Synthesis and Recognition Properties of Enantiomerically Pure Acyclic Cucurbit[n]uril-Type Molecular Containers. *Org. Lett.* **2015**, *17*, 4038–4041.
- (156) Lu, X. Y.; Isaacs, L. Uptake of Hydrocarbons in Aqueous Solution by Encapsulation in Acyclic Cucurbit[n]uril-Type Molecular Containers. *Angew. Chem., Int. Ed.* **2016**, *55*, 8076–8080.
- (157) Nau, W. M.; Florea, M.; Assaf, K. I. Deep Inside Cucurbiturils: Physical Properties and Volumes of their Inner Cavity Determine the Hydrophobic Driving Force for Host-Guest Complexation. *Isr. J. Chem.* **2011**, *51*, 559–577.
- (158) Bardelang, D.; Udachin, K. A.; Leek, D. M.; Margeson, J. C.; Chan, G.; Ratcliffe, C. I.; Ripmeester, J. A. Cucurbit[n]urils ($n = 5–8$): A Comprehensive Solid State Study. *Cryst. Growth Des.* **2011**, *11*, 5598–5614.
- (159) Kaifer, A. E. Portal Effects on the Stability of Cucurbituril Complexes. *Isr. J. Chem.* **2018**, *58*, 244–249.
- (160) Mecozzi, S.; Rebek, J., Jr. The 55% Solution: A Formula for Molecular Recognition in the Liquid State. *Chem. - Eur. J.* **1998**, *4*, 1016–1022.
- (161) Mock, W. L.; Shih, N. Y. Host-guest Binding Capacity of Cucurbituril. *J. Org. Chem.* **1983**, *48*, 3618–3619.
- (162) Mock, W. L.; Shih, N. Y. Dynamics of Molecular Recognition Involving Cucurbituril. *J. Am. Chem. Soc.* **1989**, *111*, 2697–2699.
- (163) Kim, Y.; Kim, H.; Ko, Y. H.; Selvapalam, N.; Rekharsky, M. V.; Inoue, Y.; Kim, K. Complexation of Aliphatic Ammonium Ions with a Water-Soluble Cucurbit[6]uril Derivative in Pure Water: Isothermal Calorimetric, NMR, and X-ray Crystallographic Study. *Chem. - Eur. J.* **2009**, *15*, 6143–6151.
- (164) Jeon, Y.-M.; Kim, J.; Whang, D.; Kim, K. Molecular Container Assembly Capable of Controlling Binding and Release of Its Guest Molecules: Reversible Encapsulation of Organic Molecules in Sodium Ion Complexed Cucurbituril. *J. Am. Chem. Soc.* **1996**, *118*, 9790–9791.
- (165) Haouaj, M. E.; Ho Ko, Y.; Luhmer, M.; Kim, K.; Bartik, K. NMR Investigation of the Complexation of Neutral Guests by Cucurbituril. *J. Chem. Soc., Perkin Trans. 2* **2001**, 2104–2107.
- (166) El-Sheshawy, H. S.; Bassil, B. S.; Assaf, K. I.; Kortz, U.; Nau, W. M. Halogen Bonding inside a Molecular Container. *J. Am. Chem. Soc.* **2012**, *134*, 19935–19941.
- (167) Tuncel, D.; Katterle, M. pH-Triggered Dethreading-Rethreading and Switching of Cucurbit[6]uril on Bistable[3]-Pseudorotaxanes and [3]Rotaxanes. *Chem. - Eur. J.* **2008**, *14*, 4110–4116.
- (168) Hou, X.; Ke, C.; Fraser Stoddart, J. Cooperative Capture Synthesis: Yet Another Playground for Copper-Free Click Chemistry. *Chem. Soc. Rev.* **2016**, *45*, 3766–3780.
- (169) Mock, W. L.; Irra, T. A.; Wepsiec, J. P.; Manimaran, T. L. Cycloaddition Induced by Cucurbituril. A Case of Pauling Principle Catalysis. *J. Org. Chem.* **1983**, *48*, 3619–3620.
- (170) Goehry, C.; Besora, M.; Maseras, F. Computational Study on the Mechanism of the Acceleration of 1,3-Dipolar Cycloaddition inside Cucurbit[6]uril. *ACS Catal.* **2015**, *5*, 2445–2451.
- (171) Mock, W. L.; Irra, T. A.; Wepsiec, J. P.; Adhya, M. Catalysis by Cucurbituril. The Significance of Bound-Substrate Destabilization for Induced Triazole Formation. *J. Org. Chem.* **1989**, *54*, 5302–5308.
- (172) Rekharsky, M. V.; Mori, T.; Yang, C.; Ko, Y. H.; Selvapalam, N.; Kim, H.; Sobrarsingh, D.; Kaifer, A. E.; Liu, S.; Isaacs, L.; Chen, W.; Moghaddam, S.; Gilson, M. K.; Kim, K.; Inoue, Y. A Synthetic Host-Guest System Achieves Avidin-Biotin Affinity by Overcoming Enthalpy-Entropy Compensation. *Proc. Natl. Acad. Sci. U. S. A.* **2007**, *104*, 20737–20742.
- (173) Jeon, W. S.; Moon, K.; Park, S. H.; Chun, H.; Ko, Y. H.; Lee, J. Y.; Lee, E. S.; Samal, S.; Selvapalam, N.; Rekharsky, M. V.; Sindelar, V.; Sobrarsingh, D.; Inoue, Y.; Kaifer, A. E.; Kim, K. Complexation of Ferrocene Derivatives by the Cucurbit[7]uril Host: A Comparative Study of the Cucurbituril and Cyclodextrin Host Families. *J. Am. Chem. Soc.* **2005**, *127*, 12984–12989.
- (174) Gamal-Eldin, M. A.; Macartney, D. H. Cucurbit[7]uril Host-Guest Complexes and [2]Pseudorotaxanes with *N*-Methylpiperidinium, *N*-Methylpyrrolidinium, and *N*-Methylmorpholinium Cations in Aqueous Solution. *Org. Biomol. Chem.* **2013**, *11*, 1234–1241.

- (175) Liu, S.; Ruspic, C.; Mukhopadhyay, P.; Chakrabarti, S.; Zavalij, P. Y.; Isaacs, L. The Cucurbit[*n*]uril Family: Prime Components for Self-Sorting Systems. *J. Am. Chem. Soc.* **2005**, *127*, 15959–15967.
- (176) Cao, L.; Šekutor, M.; Zavalij, P. Y.; Mlinarić-Majerski, K.; Glaser, R.; Isaacs, L. Cucurbit[7]uril-Guest Pair with an Attomolar Dissociation Constant. *Angew. Chem., Int. Ed.* **2014**, *53*, 988–993.
- (177) Jang, Y.; Natarajan, R.; Ko, Y. H.; Kim, K. Cucurbit[7]uril: A High-Affinity Host for Encapsulation of Amino Saccharides and Supramolecular Stabilization of Their α -Anomers in Water. *Angew. Chem., Int. Ed.* **2014**, *53*, 1003–1007.
- (178) Lee, J. W.; Lee, H. H. L.; Ko, Y. H.; Kim, K.; Kim, H. I. Deciphering the Specific High-Affinity Binding of Cucurbit[7]uril to Amino Acids in Water. *J. Phys. Chem. B* **2015**, *119*, 4628–4636.
- (179) Palma, A.; Artelsmair, M.; Wu, G. L.; Lu, X. Y.; Barrow, S. J.; Uddin, N.; Rosta, E.; Masson, E.; Scherman, O. A. Cucurbit[7]uril as a Supramolecular Artificial Enzyme for Diels-Alder Reactions. *Angew. Chem., Int. Ed.* **2017**, *56*, 15688–15692.
- (180) Kim, H. J.; Heo, J.; Jeon, W. S.; Lee, E.; Kim, J.; Sakamoto, S.; Yamaguchi, K.; Kim, K. Selective Inclusion of a Hetero-Guest Pair in a Molecular Host: Formation of Stable Charge-Transfer Complexes in Cucurbit[8]uril. *Angew. Chem., Int. Ed.* **2001**, *40*, 1526–1529.
- (181) Jeon, W. S.; Kim, H.-J.; Lee, C.; Kim, K. Control of the Stoichiometry in Host-Guest Complexation by Redox Chemistry of Guests: Inclusion of Methylviologen in Cucurbit[8]uril. *Chem. Commun. (Cambridge, U. K.)* **2002**, 1828–1829.
- (182) Bush, M. E.; Bouley, N. D.; Urbach, A. R. Charge-Mediated Recognition of *N*-Terminal Tryptophan in Aqueous Solution by a Synthetic Host. *J. Am. Chem. Soc.* **2005**, *127*, 14511–14517.
- (183) Rauwald, U.; Biedermann, F.; Deroo, S.; Robinson, C. V.; Scherman, O. A. Correlating Solution Binding and ESI-MS Stabilities by Incorporating Solvation Effects in a Confined Cucurbit[8]uril System. *J. Phys. Chem. B* **2010**, *114*, 8606–8615.
- (184) Biedermann, F.; Scherman, O. A. Cucurbit[8]uril Mediated Donor-Acceptor Ternary Complexes: A Model System for Studying Charge-Transfer Interactions. *J. Phys. Chem. B* **2012**, *116*, 2842–2849.
- (185) Biedermann, F.; Vendruscolo, M.; Scherman, O. A.; De Simone, A.; Nau, W. M. Cucurbit[8]uril and Blue-Box: High-Energy Water Release Overwhelms Electrostatic Interactions. *J. Am. Chem. Soc.* **2013**, *135*, 14879–14888.
- (186) Heitmann, L. M.; Taylor, A. B.; Hart, P. J.; Urbach, A. R. Sequence-Specific Recognition and Cooperative Dimerization of *N*-Terminal Aromatic Peptides in Aqueous Solution by a Synthetic Host. *J. Am. Chem. Soc.* **2006**, *128*, 12574–12581.
- (187) Smith, L. C.; Leach, D. G.; Blaylock, B. E.; Ali, O. A.; Urbach, A. R. Sequence-Specific, Nanomolar Peptide Binding via Cucurbit-[8]uril-Induced Folding and Inclusion of Neighboring Side Chains. *J. Am. Chem. Soc.* **2015**, *137*, 3663–3669.
- (188) Biedermann, F.; Rauwald, U.; Cziferszky, M.; Williams, K. A.; Gann, L. D.; Guo, B. Y.; Urbach, A. R.; Bielawski, C. W.; Scherman, O. A. Benzobis(imidazolium)-Cucurbit[8]uril Complexes for Binding and Sensing Aromatic Compounds in Aqueous Solution. *Chem. - Eur. J.* **2010**, *16*, 13716–13722.
- (189) Jiao, D. Z.; Biedermann, F.; Scherman, O. A. Size Selective Supramolecular Cages from Aryl-Bisimidazolium Derivatives and Cucurbit[8]uril. *Org. Lett.* **2011**, *13*, 3044–3047.
- (190) Zheng, L. F.; Sonzini, S.; Ambarwati, M.; Rosta, E.; Scherman, O. A.; Herrmann, A. Turning Cucurbit[8]uril into a Supramolecular Nanoreactor for Asymmetric Catalysis. *Angew. Chem., Int. Ed.* **2015**, *54*, 13007–13011.
- (191) Ong, W.; Gómez-Kaifer, M.; Kaifer, A. E. Cucurbit[7]uril: A Very Effective Host for Viologens and Their Cation Radicals. *Org. Lett.* **2002**, *4*, 1791–1794.
- (192) Stancl, M.; Svec, J.; Sindelar, V. Novel Supramolecular Hosts Based on Linear and Cyclic Oligomers of Glycoluril. *Isr. J. Chem.* **2011**, *51*, 592–599.
- (193) Svec, J.; Necas, M.; Sindelar, V. Bambus[6]uril. *Angew. Chem., Int. Ed.* **2010**, *49*, 2378–2381.
- (194) Svec, J.; Dusek, M.; Fejfarova, K.; Stacko, P.; Klan, P.; Kaifer, A. E.; Li, W.; Hudeckova, E.; Sindelar, V. Anion-Free Bambus[6]uril and Its Supramolecular Properties. *Chem. - Eur. J.* **2011**, *17*, 5605–5612.
- (195) Yawer, M. A.; Havel, V.; Sindelar, V. A Bambusuril Macrocycle that Binds Anions in Water with High Affinity and Selectivity. *Angew. Chem., Int. Ed.* **2015**, *54*, 276–279.
- (196) Havel, V.; Babiak, M.; Sindelar, V. Modulation of Bambusuril Anion Affinity in Water. *Chem. - Eur. J.* **2017**, *23*, 8963–8968.
- (197) Fiala, T.; Slezáková, K.; Marsalek, K.; Salvadori, K.; Sindelar, V. Thermodynamics of Halide Binding to a Neutral Bambusuril in Water and Organic Solvents. *J. Org. Chem.* **2018**, *83*, 1903–1912.
- (198) Lisbjerg, M.; Jessen, B. M.; Rasmussen, B.; Nielsen, B. E.; Madsen, A. Ø.; Pittelkow, M. Discovery of a Cyclic 6 + 6 Hexamer of D-biotin and Formaldehyde. *Chem. Sci.* **2014**, *5*, 2647–2650.
- (199) Lisbjerg, M.; Nielsen, B. E.; Milhoj, B. O.; Sauer, S. P. A.; Pittelkow, M. Anion Binding by Biotin[6]uril in Water. *Org. Biomol. Chem.* **2015**, *13*, 369–373.
- (200) Atwood, J. L.; Hamada, F.; Robinson, K. D.; Orr, G. W.; Vincent, R. L. X-ray Diffraction Evidence for Aromatic π Hydrogen Bonding to Water. *Nature* **1991**, *349*, 683–684.
- (201) Fucke, K.; Anderson, K. M.; Filby, M. H.; Henry, M.; Wright, J.; Mason, S. A.; Gutmann, M. J.; Barbour, L. J.; Oliver, C.; Coleman, A. W.; Atwood, J. L.; Howard, J. A. K.; Steed, J. W. The Structure of Water in *p*-Sulfonatocalix[4]arene. *Chem. - Eur. J.* **2011**, *17*, 10259–10271.
- (202) Steed, J. W.; Johnson, C. P.; Barnes, C. L.; Juneja, R. K.; Atwood, J. L.; Reilly, S.; Hollis, R. L.; Smith, P. H.; Clark, D. L. Supramolecular Chemistry of *p*-Sulfonatocalix[5]arene: A Water-Soluble, Bowl-Shaped Host with a Large Molecular Cavity. *J. Am. Chem. Soc.* **1995**, *117*, 11426–11433.
- (203) Morel, J.-P.; Morel-Desrosiers, N. Binding of Monovalent Metal Cations by the *p*-Sulfonatocalix[4]arene: Experimental Evidence for Cation- π Interactions in Water. *Org. Biomol. Chem.* **2006**, *4*, 462–465.
- (204) Bonal, C.; Israëli, Y.; Morel, J.-P.; Morel-Desrosiers, N. Binding of Inorganic and Organic Cations by *p*-Sulfonatocalix[4]-arene in Water: A Thermodynamic Study. *J. Chem. Soc., Perkin Trans. 2* **2001**, 1075–1078.
- (205) Gutsche, C. D. Calixarenes. *Acc. Chem. Res.* **1983**, *16*, 161–170.
- (206) Arimura, T.; Kubota, M.; Araki, K.; Shinkai, S.; Matsuda, T. “Template Effects” on Calixarene Conformations Through Host-Guest-Type Interactions. *Tetrahedron Lett.* **1989**, *30*, 2563–2566.
- (207) Shinkai, S.; Araki, K.; Matsuda, T.; Manabe, O. NMR Determination of Association Constants for Aqueous Calixarene Complexes and Guest Template Effects on the Conformational Freedom. *Bull. Chem. Soc. Jpn.* **1989**, *62*, 3856–3862.
- (208) Shinkai, S.; Araki, K.; Kubota, M.; Arimura, T.; Matsuda, T. Ion Template Effects on the Conformation of Water-Soluble Calixarenes. *J. Org. Chem.* **1991**, *56*, 295–300.
- (209) Zhao, H.-X.; Guo, D.-S.; Liu, Y. Binding Behaviors of *p*-Sulfonatocalix[4]arene with Gemini Guests. *J. Phys. Chem. B* **2013**, *117*, 1978–1987.
- (210) Liu, Y.; Guo, D.-S.; Yang, E.-C.; Zhang, H.-Y.; Zhao, Y.-L. The Structures and Thermodynamics of Complexes between Water-Soluble Calix[4]arenes and Dipyridinium Ions. *Eur. J. Org. Chem.* **2005**, 162–170.
- (211) Guo, D.-S.; Zhang, H.-Q.; Ding, F.; Liu, Y. Thermodynamic Origins of Selective Binding Affinity Between *p*-Sulfonatocalix[4,5]-arenes with Biguanidiniums. *Org. Biomol. Chem.* **2012**, *10*, 1527–1536.
- (212) Arena, G.; Casnati, A.; Contino, A.; Lombardo, G. G.; Sciotto, D.; Ungaro, R. Water-Soluble Calixarene Hosts that Specifically Recognize the Trimethylammonium Group or the Benzene Ring of Aromatic Ammonium Cations: A Combined ^1H NMR, Calorimetric, and Molecular Mechanics Investigation. *Chem. - Eur. J.* **1999**, *5*, 738–744.

- (213) Arena, G.; Casnati, A.; Contino, A.; Gulino, F. G.; Sciotto, D.; Ungaro, R. Entropic Origin of the Sulfonate Groups' Electrostatic Assistance in the Complexation of Quaternary Ammonium Cations by Water Soluble Calix[4]arenes. *J. Chem. Soc., Perkin Trans. 2* **2000**, 419–423.
- (214) Douteau-Guevel, N.; Perret, F.; Coleman, A. W.; Morel, J. P.; Morel-Desrosiers, N. Binding of Dipeptides and Tripeptides Containing Lysine or Arginine by *p*-Sulfonatocalixarenes in Water: NMR and Microcalorimetric Studies. *J. Chem. Soc., Perkin Trans. 2* **2002**, 524–532.
- (215) Beshara, C. S.; Jones, C. E.; Daze, K. D.; Lilgert, B. J.; Hof, F. A Simple Calixarene Recognizes Post-translationally Methylated Lysine. *ChemBioChem* **2010**, 11, 63–66.
- (216) Daze, K. D.; Ma, M. C. F.; Pineux, F.; Hof, F. Synthesis of New Trisulfonated Calix[4]arenes Functionalized at the Upper Rim, and Their Complexation with the Trimethyllysine Epigenetic Mark. *Org. Lett.* **2012**, 14, 1512–1515.
- (217) Dziemidowicz, J.; Witt, D.; Rachon, J. Complexation of Amino Acids Derivatives in Water by Calix[4]arene Phosphonic Acids. *J. Inclusion Phenom. Mol. Recognit. Chem.* **2008**, 61, 381–391.
- (218) Shi, Y. H.; Schneider, H. J. Interactions Between Amino-calixarenes and Nucleotides or Nucleic Acids. *J. Chem. Soc., Perkin Trans. 2* **1999**, 1797–1803.
- (219) Arena, G.; Gentile, S.; Gulino, F. G.; Sciotto, D.; Sgarlata, C. Water-soluble Pentasulfonatocalix[5]arene: Selective Recognition of Ditopic Trimethylammonium Cations by a Triple Non-Covalent Interaction. *Tetrahedron Lett.* **2004**, 45, 7091–7094.
- (220) Bonaccorso, C.; Gentile, S.; Gulino, F. G.; Sciotto, D. Molecular Recognition of Alkylammonium, *N*-Methylpyridinium Cations and Native L- α -Amino Acids by Water Soluble Penta- and Tetra-Sulfonatocalixarenes. *Lett. Org. Chem.* **2009**, 6, 598–603.
- (221) Atwood, J. L.; Clark, D. L.; Juneja, R. K.; Orr, G. W.; Robinson, K. D.; Vincent, R. L. Double Partial Cone Conformation for $\text{Na}_8\{\text{Calix}[6]\text{arene sulfonate}\} \cdot 20.5\text{H}_2\text{O}$ and Its Parent Acid. *J. Am. Chem. Soc.* **1992**, 114, 7558–7559.
- (222) Zhang, L.; Macias, A.; Lu, T. B.; Gordon, J. I.; Gokel, G. W.; Kaifer, A. E. Calixarenes as Hosts in Aqueous Media: Inclusion Complexation of Ferrocene Derivatives by a Water-Soluble Calix[6]-arene. *J. Chem. Soc., Chem. Commun.* **1993**, 0, 1017–1019.
- (223) Gaeta, C.; Caruso, T.; Mincolelli, M.; Troisi, F.; Vasca, E.; Neri, P. *p*-Sulfonatocalix[7]arene: Synthesis, Protolysis, and Binding Ability. *Tetrahedron* **2008**, 64, 5370–5378.
- (224) Arimura, T.; Kawabata, H.; Matsuda, T.; Muramatsu, T.; Satoh, H.; Fujio, K.; Manabe, O.; Shinkai, S. New Water-Soluble Host Calixarenes Bearing Chiral Substituents. *J. Org. Chem.* **1991**, 56, 301–306.
- (225) Sansone, F.; Barboso, S.; Casnati, A.; Sciotto, D.; Ungaro, R. A New Chiral Rigid Cone Water Soluble Peptidocalix[4]arene and its Inclusion Complexes with α -Amino Acids and Aromatic Ammonium Cations. *Tetrahedron Lett.* **1999**, 40, 4741–4744.
- (226) Nimse, S. B.; Kim, J.; Ta, V. T.; Kim, H. S.; Song, K. S.; Jung, C. Y.; Nguyen, V. T.; Kim, T. New Water-Soluble Iminecalix[4]arene with a Deep Hydrophobic Cavity. *Tetrahedron Lett.* **2009**, 50, 7346–7350.
- (227) Nimse, S. B.; Kim, J.; Song, K.-S.; Kim, J.; Lee, J. T.; Nguyen, V.-T.; Ta, V.-T.; Kim, T. Selective Recognition of the Ditopic Trimethylammonium Cations by Water-Soluble Aminocalix[4]arene. *Tetrahedron Lett.* **2011**, 52, 3751–3755.
- (228) Tanaka, Y.; Aoyama, Y. ^1H NMR Characterization of the Hydrogen-Bond Network in the Water Complex of Resorcinol-Dodecanal Cyclotetramer. *Bull. Chem. Soc. Jpn.* **1990**, 63, 3343–3344.
- (229) Kobayashi, K.; Asakawa, Y.; Kato, Y.; Aoyama, Y. Complexation of Hydrophobic Sugars and Nucleosides in Water with Tetrasulfonate Derivatives of Resorcinol Cyclic Tetramer Having a Polyhydroxy Aromatic Cavity: Importance of Guest-Host CH- π Interaction. *J. Am. Chem. Soc.* **1992**, 114, 10307–10313.
- (230) Sebo, L.; Diederich, F.; Gramlich, V. Tetrakis-(phenylamidinium)-Substituted Resorcin[4]arene Receptors for the Complexation of Dicarboxylates and Phosphates in Protic Solvents. *Helv. Chim. Acta* **2000**, 83, 93–113.
- (231) Groppe, C.; Quigley, B. L.; Diederich, F. Molecular Recognition with Resorcin[4]arene Cavitands: Switching, Halogen-Bonded Capsules, and Enantioselective Complexation. *J. Am. Chem. Soc.* **2018**, 140, 2705–2717.
- (232) Biros, S. M.; Rebek, J., Jr. Structure and Binding Properties of Water-Soluble Cavitands and Capsules. *Chem. Soc. Rev.* **2007**, 36, 93–104.
- (233) Moran, J. R.; Karbach, S.; Cram, D. J. Cavitands: Synthetic Molecular Vessels. *J. Am. Chem. Soc.* **1982**, 104, 5826–5828.
- (234) Cram, D. J. Cavitands: Organic Hosts with Enforced Cavities. *Science* **1983**, 219, 1177–1183.
- (235) Haino, T.; Rudkevich, D. M.; Shivanyuk, A.; Rissanen, K.; Rebek, J., Jr. Induced-Fit Molecular Recognition with Water-Soluble Cavitands. *Chem. - Eur. J.* **2000**, 6, 3797–3805.
- (236) Hooley, R. J.; Van Anda, H. J.; Rebek, J. Extraction of Hydrophobic Species into a Water-Soluble Synthetic Receptor. *J. Am. Chem. Soc.* **2007**, 129, 13464–13473.
- (237) Biros, S. M.; Ullrich, E. C.; Hof, F.; Trembleau, L.; Rebek, J. Kinetically Stable Complexes in Water: The Role of Hydration and Hydrophobicity. *J. Am. Chem. Soc.* **2004**, 126, 2870–2876.
- (238) Lledo, A.; Rebek, J. Deep Cavitand Receptors with pH-Independent Water Solubility. *Chem. Commun. (Cambridge, U. K.)* **2010**, 46, 8630–8632.
- (239) Zhang, K. D.; Ajami, D.; Rebek, J. Hydrogen-Bonded Capsules in Water. *J. Am. Chem. Soc.* **2013**, 135, 18064–18066.
- (240) Mosca, S.; Yu, Y.; Gavette, J. V.; Zhang, K. D.; Rebek, J. A Deep Cavitand Templates Lactam Formation in Water. *J. Am. Chem. Soc.* **2015**, 137, 14582–14585.
- (241) Javor, S.; Rebek, J. Activation of a Water-Soluble Resorcinarene Cavitand at the Water-Phosphocholine Micelle Interface. *J. Am. Chem. Soc.* **2011**, 133, 17473–17478.
- (242) Haas, C. H.; Biros, S. M.; Rebek, J., Jr. Binding Properties of Cavitands in Aqueous Solution - The Influence of Charge on Guest Selectivity. *Chem. Commun. (Cambridge, U. K.)* **2005**, 6044–6045.
- (243) Trembleau, L.; Rebek, J. Helical Conformation of Alkanes in a Hydrophobic Cavitand. *Science* **2003**, 301, 1219–1220.
- (244) Hooley, R. J.; Biros, S. M.; Rebek, J., Jr. Normal Hydrocarbons Tumble Rapidly in a Deep, Water-Soluble Cavitand. *Chem. Commun. (Cambridge, U. K.)* **2006**, 509–510.
- (245) Schramm, M. P.; Rebek, J. Moving Targets: Recognition of Alkyl Groups. *Chem. - Eur. J.* **2006**, 12, 5924–5933.
- (246) Gibb, C. L. D.; Gibb, B. C. Well-Defined, Organic Nanoenvironments in Water: The Hydrophobic Effect Drives a Capsular Assembly. *J. Am. Chem. Soc.* **2004**, 126, 11408–11409.
- (247) Hillyer, M. B.; Gibb, C. L. D.; Sokkalingam, P.; Jordan, J. H.; Ioup, S. E.; Gibb, B. C. Synthesis of Water-Soluble Deep-Cavity Cavitands. *Org. Lett.* **2016**, 18, 4048–4051.
- (248) Gibb, C. L. D.; Gibb, B. C. Anion Binding to Hydrophobic Concavity Is Central to the Salting-in Effects of Hofmeister Chaotropes. *J. Am. Chem. Soc.* **2011**, 133, 7344–7347.
- (249) Pinalli, R.; Brancatelli, G.; Pedrini, A.; Menozzi, D.; Hernandez, D.; Ballester, P.; Geremia, S.; Dalcanale, E. The Origin of Selectivity in the Complexation of *N*-Methyl Amino Acids by Tetraphosphonate Cavitands. *J. Am. Chem. Soc.* **2016**, 138, 8569–8580.
- (250) Yu, Y.; Rebek, J. Reactions of Folded Molecules in Water. *Acc. Chem. Res.* **2018**, 51, 3031–3040.
- (251) Shi, Q. X.; Masseroni, D.; Rebek, J. Macrocyclization of Folded Diamines in Cavitands. *J. Am. Chem. Soc.* **2016**, 138, 10846–10848.
- (252) Wu, N.-W.; Petsalakis, I. D.; Theodorakopoulos, G.; Yu, Y.; Rebek, J., Jr. Cavitands as Containers for α,ω -Dienes and Chaperones for Olefin Metathesis. *Angew. Chem., Int. Ed.* **2018**, 57, 15091–15095.
- (253) Shi, Q.; Mower, M. P.; Blackmond, D. G.; Rebek, J. Water-Soluble Cavitands Promote Hydrolyses of Long-Chain Diesters. *Proc. Natl. Acad. Sci. U. S. A.* **2016**, 113, 9199–9203.

- (254) Masseroni, D.; Mosca, S.; Mower, M. P.; Blackmond, D. G.; Rebek, J. Cavitands as Reaction Vessels and Blocking Groups for Selective Reactions in Water. *Angew. Chem., Int. Ed.* **2016**, *55*, 8290–8293.
- (255) Angamuthu, V.; Rahman, F.-U.; Petroselli, M.; Li, Y.; Yu, Y.; Rebek, J. Mono Epoxidation of α,ω -Dienes Using NBS in a Water-Soluble Cavitand. *Org. Chem. Front.* **2019**, *6*, 3220–3223.
- (256) Petroselli, M.; Angamuthu, V.; Rahman, F.-U.; Zhao, X.; Yu, Y.; Rebek, J. Radical Reactions in Cavitands Unveil the Effects of Affinity on Dynamic Supramolecular Systems. *J. Am. Chem. Soc.* **2020**, *142*, 2396–2403.
- (257) Inouye, M.; Fujimoto, K.; Furusyo, M.; Nakazumi, H. Molecular Recognition Abilities of a New Class of Water-Soluble Cyclophanes Capable of Encompassing a Neutral Cavity. *J. Am. Chem. Soc.* **1999**, *121*, 1452–1458.
- (258) Kubik, S. Synthetic Lectins. *Angew. Chem., Int. Ed.* **2009**, *48*, 1722–1725.
- (259) Davis, A. P.; Wareham, R. S. Carbohydrate Recognition Through Noncovalent Interactions: A Challenge for Biomimetic and Supramolecular Chemistry. *Angew. Chem., Int. Ed.* **1999**, *38*, 2978–2996.
- (260) Davis, A. P. Biomimetic Carbohydrate Recognition. *Chem. Soc. Rev.* **2020**, *49*, 2531–2545.
- (261) Klein, E.; Crump, M. P.; Davis, A. P. Carbohydrate Recognition in Water by a Tricyclic Polyamide Receptor. *Angew. Chem., Int. Ed.* **2005**, *44*, 298–302.
- (262) Barwell, N. P.; Crump, M. P.; Davis, A. P. A Synthetic Lectin for β -Glucosyl. *Angew. Chem., Int. Ed.* **2009**, *48*, 7673–7676.
- (263) Barwell, N. P.; Davis, A. P. Substituent Effects in Synthetic Lectins - Exploring the Role of CH- π Interactions in Carbohydrate Recognition. *J. Org. Chem.* **2011**, *76*, 6548–6557.
- (264) Joshi, G.; Davis, A. P. New H-Bonding Patterns in Biphenyl-Based Synthetic Lectins; Pyrrolediamine Bridges Enhance Glucose-Selectivity. *Org. Biomol. Chem.* **2012**, *10*, 5760–5763.
- (265) Ferrand, Y.; Klein, E.; Barwell, N. P.; Crump, M. P.; Jimenez-Barbero, J.; Vicent, C.; Boons, G. J.; Ingale, S.; Davis, A. P. A Synthetic Lectin for O-Linked β -N-Acetylglucosamine. *Angew. Chem., Int. Ed.* **2009**, *48*, 1775–1779.
- (266) Rios, P.; Carter, T. S.; Mooibroek, T. J.; Crump, M. P.; Lisbjerg, M.; Pittelkow, M.; Supekar, N. T.; Boons, G. J.; Davis, A. P. Synthetic Receptors for the High-Affinity Recognition of O-GlcNAc Derivatives. *Angew. Chem., Int. Ed.* **2016**, *55*, 3387–3392.
- (267) Ferrand, Y.; Crump, M. P.; Davis, A. P. A Synthetic Lectin Analog for Biomimetic Disaccharide Recognition. *Science* **2007**, *318*, 619–622.
- (268) Sookcharoenpinyo, B.; Klein, E.; Ferrand, Y.; Walker, D. B.; Brotherhood, P. R.; Ke, C. F.; Crump, M. P.; Davis, A. P. High-Affinity Disaccharide Binding by Tricyclic Synthetic Lectins. *Angew. Chem., Int. Ed.* **2012**, *51*, 4586–4590.
- (269) Klein, E.; Ferrand, Y.; Barwell, N. P.; Davis, A. P. Solvent Effects in Carbohydrate Binding by Synthetic Receptors: Implications for the Role of Water in Natural Carbohydrate Recognition. *Angew. Chem., Int. Ed.* **2008**, *47*, 2693–2696.
- (270) Ke, C. F.; Destecroix, H.; Crump, M. P.; Davis, A. P. A Simple and Accessible Synthetic Lectin for Glucose Recognition and Sensing. *Nat. Chem.* **2012**, *4*, 718–723.
- (271) Tromans, R. A.; Carter, T. S.; Chabanne, L.; Crump, M. P.; Li, H.; Matlock, J. V.; Orchard, M. G.; Davis, A. P. A Biomimetic Receptor for Glucose. *Nat. Chem.* **2019**, *11*, 52–56.
- (272) Mooibroek, T. J.; Casas-Solvias, J. M.; Harniman, R. L.; Renney, C.; Carter, T. S.; Crump, M. P.; Davis, A. P. A Threading Receptor for Polysaccharides. *Nat. Chem.* **2016**, *8*, 69–74.
- (273) Shorthill, B. J.; Avetta, C. T.; Glass, T. E. Shape-Selective Sensing of Lipids in Aqueous Solution by a Designed Fluorescent Molecular Tube. *J. Am. Chem. Soc.* **2004**, *126*, 12732–12733.
- (274) Huang, G. B.; Wang, S. H.; Ke, H.; Yang, L. P.; Jiang, W. Selective Recognition of Highly Hydrophilic Molecules in Water by Endo-Functionalized Molecular Tubes. *J. Am. Chem. Soc.* **2016**, *138*, 14550–14553.
- (275) Yang, L.-P.; Wang, X.; Yao, H.; Jiang, W. Naphthotubes: Macrocyclic Hosts with a Biomimetic Cavity Feature. *Acc. Chem. Res.* **2020**, *53*, 198–208.
- (276) Yao, H.; Wang, X.; Xie, M.; Wang, Y.-M.; Quan, M.; Yang, L.-P.; Jiang, W. Mono-Functionalized Derivatives and Revised Configurational Assignment of Amide Naphthotubes. *Org. Biomol. Chem.* **2020**, *18*, 1900–1909.
- (277) Yao, H.; Ke, H.; Zhang, X.; Pan, S.-J.; Li, M.-S.; Yang, L.-P.; Schreckenbach, G.; Jiang, W. Molecular Recognition of Hydrophilic Molecules in Water by Combining the Hydrophobic Effect with Hydrogen Bonding. *J. Am. Chem. Soc.* **2018**, *140*, 13466–13477.
- (278) Wang, L. L.; Chen, Z.; Liu, W. E.; Ke, H.; Wang, S. H.; Jiang, W. Molecular Recognition and Chirality Sensing of Epoxides in Water Using Endo-Functionalized Molecular Tubes. *J. Am. Chem. Soc.* **2017**, *139*, 8436–8439.
- (279) Ke, H.; Yang, L.-P.; Xie, M.; Chen, Z.; Yao, H.; Jiang, W. Shear-Induced Assembly of a Transient Yet Highly Stretchable Hydrogel Based on Pseudopolyrotaxanes. *Nat. Chem.* **2019**, *11*, 470–477.
- (280) Kim, D. S.; Sessler, J. L. Calix[4]pyrroles: Versatile Molecular Containers with Ion Transport, Recognition, and Molecular Switching Functions. *Chem. Soc. Rev.* **2015**, *44*, 532–546.
- (281) Anzenbacher, P.; Jursiková, K.; Lynch, V. M.; Gale, P. A.; Sessler, J. L. Calix[4]pyrroles Containing Deep Cavities and Fixed Walls. Synthesis, Structural Studies, and Anion Binding Properties of the Isomeric Products Derived from the Condensation of *p*-Hydroxyacetophenone and Pyrrole. *J. Am. Chem. Soc.* **1999**, *121*, 11020–11021.
- (282) Verdejo, B.; Gil-Ramirez, G.; Ballester, P. Molecular Recognition of Pyridine N-Oxides in Water Using Calix[4]pyrrole Receptors. *J. Am. Chem. Soc.* **2009**, *131*, 3178–3179.
- (283) Hernandez-Alonso, D.; Zankowski, S.; Adriaenssens, L.; Ballester, P. Water-Soluble Aryl-Extended Calix[4]pyrroles with Unperturbed Aromatic Cavities: Synthesis and Binding Studies. *Org. Biomol. Chem.* **2015**, *13*, 1022–1029.
- (284) Diaz-Moscoso, A.; Hernández-Alonso, D.; Escobar, L.; Arroyave, F. A.; Ballester, P. Stereoselective Synthesis of Lower and Upper Rim Functionalized Tetra- α Isomers of Calix[4]pyrroles. *Org. Lett.* **2017**, *19*, 226–229.
- (285) Peñuelas-Haro, G.; Ballester, P. Efficient Hydrogen Bonding Recognition in Water Using Aryl-Extended Calix[4]pyrrole Receptors. *Chem. Sci.* **2019**, *10*, 2413–2423.
- (286) Escobar, L.; Diaz-Moscoso, A.; Ballester, P. Conformational Selectivity and High-Affinity Binding in the Complexation of N-Phenyl Amides in Water by a Phenyl Extended Calix[4]pyrrole. *Chem. Sci.* **2018**, *9*, 7186–7192.
- (287) Stewart, W. E.; Siddall, T. H. Nuclear Magnetic Resonance Studies of Amides. *Chem. Rev. (Washington, DC, U. S.)* **1970**, *70*, 517–551.
- (288) Escobar, L.; Aragay, G.; Ballester, P. Super Aryl-Extended Calix[4]pyrroles: Synthesis, Binding Studies, and Attempts To Gain Water Solubility. *Chem. - Eur. J.* **2016**, *22*, 13682–13689.
- (289) Escobar, L.; Ballester, P. Quantification of the Hydrophobic Effect Using Water-Soluble Super Aryl-Extended Calix[4]pyrroles. *Org. Chem. Front.* **2019**, *6*, 1738–1748.
- (290) Chi, X. D.; Zhang, H. C.; Vargas-Zuniga, G. I.; Peters, G. M.; Sessler, J. L. A Dual-Responsive Bola-Type Supra-amphiphile Constructed from a Water-Soluble Calix[4]pyrrole and a Tetraphenylethene-Containing Pyridine Bis-N-oxide. *J. Am. Chem. Soc.* **2016**, *138*, 5829–5832.
- (291) Laughrey, Z.; Gibb, B. C. Water-Soluble, Self-Assembling Container Molecules: An Update. *Chem. Soc. Rev.* **2011**, *40*, 363–386.
- (292) Fujita, M.; Tominaga, M.; Hori, A.; Therrien, B. Coordination Assemblies from a Pd(II)-Cornered Square Complex. *Acc. Chem. Res.* **2005**, *38*, 369–378.
- (293) Fujita, M.; Oguro, D.; Miyazawa, M.; Oka, H.; Yamaguchi, K.; Ogura, K. Self-Assembly of Ten Molecules into Nanometre-Sized Organic Host Frameworks. *Nature* **1995**, *378*, 469–471.

- (294) Ibukuro, F.; Kusukawa, T.; Fujita, M. A Thermally Switchable Molecular Lock. Guest-Templated Synthesis of a Kinetically Stable Nanosized Cage. *J. Am. Chem. Soc.* **1998**, *120*, 8561–8562.
- (295) Yoshizawa, M.; Kusukawa, T.; Kawano, M.; Ohhara, T.; Tanaka, I.; Kurihara, K.; Niimura, N.; Fujita, M. Endohedral Clusterization of Ten Water Molecules into a “Molecular Ice” within the Hydrophobic Pocket of a Self-Assembled Cage. *J. Am. Chem. Soc.* **2005**, *127*, 2798–2799.
- (296) Kusukawa, T.; Fujita, M. Encapsulation of Large, Neutral Molecules in a Self-Assembled Nanocage Incorporating Six Palladium(II) Ions. *Angew. Chem., Int. Ed.* **1998**, *37*, 3142–3144.
- (297) Takezawa, H.; Shitozawa, K.; Fujita, M. Enhanced Reactivity of Twisted Amides Inside a Molecular Cage. *Nat. Chem.* **2020**, *12*, 574–578.
- (298) Yoshizawa, M.; Tamura, M.; Fujita, M. Diels-Alder in Aqueous Molecular Hosts: Unusual Regioselectivity and Efficient Catalysis. *Science* **2006**, *312*, 251–254.
- (299) Murase, T.; Nishijima, Y.; Fujita, M. Cage-Catalyzed Knoevenagel Condensation under Neutral Conditions in Water. *J. Am. Chem. Soc.* **2012**, *134*, 162–164.
- (300) Sawada, T.; Yoshizawa, M.; Sato, S.; Fujita, M. Minimal Nucleotide Duplex Formation in Water Through Enclathration in Self-Assembled Hosts. *Nat. Chem.* **2009**, *1*, 53–56.
- (301) Caulder, D. L.; Brückner, C.; Powers, R. E.; König, S.; Parac, T. N.; Leary, J. A.; Raymond, K. N. Design, Formation and Properties of Tetrahedral M_4L_4 and M_4L_6 Supramolecular Clusters. *J. Am. Chem. Soc.* **2001**, *123*, 8923–8938.
- (302) Davis, A. V.; Fiedler, D.; Ziegler, M.; Terpin, A.; Raymond, K. N. Resolution of Chiral, Tetrahedral M_4L_6 Metal-Ligand Hosts. *J. Am. Chem. Soc.* **2007**, *129*, 15354–15363.
- (303) Pluth, M. D.; Bergman, R. G.; Raymond, K. N. Proton-Mediated Chemistry and Catalysis in a Self-Assembled Supramolecular Host. *Acc. Chem. Res.* **2009**, *42*, 1650–1659.
- (304) Pluth, M. D.; Johnson, D. W.; Szigethy, G.; Davis, A. V.; Teat, S. J.; Oliver, A. G.; Bergman, R. G.; Raymond, K. N. Structural Consequences of Anionic Host-Cationic Guest Interactions in a Supramolecular Assembly. *Inorg. Chem.* **2009**, *48*, 111–120.
- (305) Sgarlata, C.; Mugridge, J. S.; Pluth, M. D.; Tiedemann, B. E. F.; Zito, V.; Arena, G.; Raymond, K. N. External and Internal Guest Binding of a Highly Charged Supramolecular Host in Water: Deconvoluting the Very Different Thermodynamics. *J. Am. Chem. Soc.* **2010**, *132*, 1005–1009.
- (306) Sgarlata, C.; Mugridge, J. S.; Pluth, M. D.; Zito, V.; Arena, G.; Raymond, K. N. Different and Often Opposing Forces Drive the Encapsulation and Multiple Exterior Binding of Charged Guests to a M_4L_6 Supramolecular Vessel in Water. *Chem. - Eur. J.* **2017**, *23*, 16813–16818.
- (307) Davis, A. V.; Raymond, K. N. The Big Squeeze: Guest Exchange in an M_4L_6 Supramolecular Host. *J. Am. Chem. Soc.* **2005**, *127*, 7912–7919.
- (308) Pluth, M. D.; Bergman, R. G.; Raymond, K. N. Making Amines Strong Bases: Thermodynamic Stabilization of Protonated Guests in a Highly-Charged Supramolecular Host. *J. Am. Chem. Soc.* **2007**, *129*, 11459–11467.
- (309) Pluth, M. D.; Fiedler, D.; Mugridge, J. S.; Bergman, R. G.; Raymond, K. N. Encapsulation and Characterization of Proton-Bound Amine Homodimers in a Water-Soluble, Self-Assembled Supramolecular Host. *Proc. Natl. Acad. Sci. U. S. A.* **2009**, *106*, 10438–10443.
- (310) Dong, V. M.; Fiedler, D.; Carl, B.; Bergman, R. G.; Raymond, K. N. Molecular Recognition and Stabilization of Iminium Ions in Water. *J. Am. Chem. Soc.* **2006**, *128*, 14464–14465.
- (311) Hastings, C. J.; Pluth, M. D.; Biros, S. M.; Bergman, R. G.; Raymond, K. N. Simultaneously Bound Guests and Chiral Recognition: A Chiral Self-Assembled Supramolecular Host Encapsulates Hydrophobic Guests. *Tetrahedron* **2008**, *64*, 8362–8367.
- (312) Hong, C. M.; Bergman, R. G.; Raymond, K. N.; Toste, F. D. Self-Assembled Tetrahedral Hosts as Supramolecular Catalysts. *Acc. Chem. Res.* **2018**, *51*, 2447–2455.
- (313) Pluth, M. D.; Bergman, R. G.; Raymond, K. N. Acceleration of Amide Bond Rotation by Encapsulation in the Hydrophobic Interior of a Water-Soluble Supramolecular Assembly. *J. Org. Chem.* **2008**, *73*, 7132–7136.
- (314) Pluth, M. D.; Bergman, R. G.; Raymond, K. N. Encapsulation of Protonated Diamines in a Water-Soluble, Chiral, Supramolecular Assembly Allows for Measurement of Hydrogen-Bond Breaking Followed by Nitrogen Inversion/Rotation. *J. Am. Chem. Soc.* **2008**, *130*, 6362–6366.
- (315) Fiedler, D.; Bergman, R. G.; Raymond, K. N. Supramolecular Catalysis of a Unimolecular Transformation: Aza-Cope Rearrangement within a Self-Assembled Host. *Angew. Chem., Int. Ed.* **2004**, *43*, 6748–6751.
- (316) Hastings, C. J.; Fiedler, D.; Bergman, R. G.; Raymond, K. N. Aza Cope Rearrangement of Propargyl Enammonium Cations Catalyzed By a Self-Assembled “Nanozyme”. *J. Am. Chem. Soc.* **2008**, *130*, 10977–10983.
- (317) Hastings, C. J.; Pluth, M. D.; Bergman, R. G.; Raymond, K. N. Enzymelike Catalysis of the Nazarov Cyclization by Supramolecular Encapsulation. *J. Am. Chem. Soc.* **2010**, *132*, 6938–6940.
- (318) Hong, C. M.; Morimoto, M.; Kapustin, E. A.; Alzakhem, N.; Bergman, R. G.; Raymond, K. N.; Toste, F. D. Deconvoluting the Role of Charge in a Supramolecular Catalyst. *J. Am. Chem. Soc.* **2018**, *140*, 6591–6595.
- (319) Pluth, M. D.; Bergman, R. G.; Raymond, K. N. Acid Catalysis in Basic Solution: A Supramolecular Host Promotes Orthoformate Hydrolysis. *Science* **2007**, *316*, 85–88.
- (320) Pluth, M. D.; Bergman, R. G.; Raymond, K. N. Catalytic Deprotection of Acetals in Basic Solution with a Self-Assembled Supramolecular “Nanozyme”. *Angew. Chem., Int. Ed.* **2007**, *46*, 8587–8589.
- (321) Whitehead, M.; Turega, S.; Stephenson, A.; Hunter, C. A.; Ward, M. D. Quantification of Solvent Effects on Molecular Recognition in Polyhedral Coordination Cage Hosts. *Chem. Sci.* **2013**, *4*, 2744–2751.
- (322) Turega, S.; Whitehead, M.; Hall, B. R.; Haddow, M. F.; Hunter, C. A.; Ward, M. D. Selective Guest Recognition by a Self-Assembled Paramagnetic Cage Complex. *Chem. Commun. (Cambridge, U. K.)* **2012**, *48*, 2752–2754.
- (323) Metherell, A. J.; Cullen, W.; Williams, N. H.; Ward, M. D. Binding of Hydrophobic Guests in a Coordination Cage Cavity is Driven by Liberation of “High-Energy” Water. *Chem. - Eur. J.* **2018**, *24*, 1554–1560.
- (324) Turega, S.; Cullen, W.; Whitehead, M.; Hunter, C. A.; Ward, M. D. Mapping the Internal Recognition Surface of an Octanuclear Coordination Cage Using Guest Libraries. *J. Am. Chem. Soc.* **2014**, *136*, 8475–8483.
- (325) Taylor, C. G. P.; Cullen, W.; Collier, O. M.; Ward, M. D. A Quantitative Study of the Effects of Guest Flexibility on Binding Inside a Coordination Cage Host. *Chem. - Eur. J.* **2017**, *23*, 206–213.
- (326) Cullen, W.; Misuraca, M. C.; Hunter, C. A.; Williams, N. H.; Ward, M. D. Highly Efficient Catalysis of the Kemp Elimination in the Cavity of a Cubic Coordination Cage. *Nat. Chem.* **2016**, *8*, 231–236.
- (327) Cullen, W.; Turega, S.; Hunter, C. A.; Ward, M. D. Virtual Screening for High Affinity Guests for Synthetic Supramolecular Receptors. *Chem. Sci.* **2015**, *6*, 2790–2794.
- (328) Cullen, W.; Metherell, A. J.; Wragg, A. B.; Taylor, C. G. P.; Williams, N. H.; Ward, M. D. Catalysis in a Cationic Coordination Cage Using a Cavity-Bound Guest and Surface-Bound Anions: Inhibition, Activation, and Autocatalysis. *J. Am. Chem. Soc.* **2018**, *140*, 2821–2828.
- (329) Mal, P.; Schultz, D.; Beyeh, K.; Rissanen, K.; Nitschke, J. R. An Unlockable-Relockable Iron Cage by Subcomponent Self-Assembly. *Angew. Chem., Int. Ed.* **2008**, *47*, 8297–8301.
- (330) Ronson, T. K.; Giri, C.; Kodiah Beyeh, N.; Minkkinen, A.; Topic, F.; Holstein, J. J.; Rissanen, K.; Nitschke, J. R. Size-Selective Encapsulation of Hydrophobic Guests by Self-Assembled M_4L_6 Cobalt and Nickel Cages. *Chem. - Eur. J.* **2013**, *19*, 3374–3382.

- (331) Smulders, M. M. J.; Zarra, S.; Nitschke, J. R. Quantitative Understanding of Guest Binding Enables the Design of Complex Host-Guest Behavior. *J. Am. Chem. Soc.* **2013**, *135*, 7039–7046.
- (332) Zarra, S.; Smulders, M. M. J.; Lefebvre, Q.; Clegg, J. K.; Nitschke, J. R. Guanidinium Binding Modulates Guest Exchange within an $[M_4L_6]$ Capsule. *Angew. Chem., Int. Ed.* **2012**, *51*, 6882–6885.
- (333) Cram, D. J.; Tanner, M. E.; Thomas, R. The Taming of Cyclobutadiene. *Angew. Chem., Int. Ed. Engl.* **1991**, *30*, 1024–1027.
- (334) Galan, A.; Ballester, P. Stabilization of Reactive Species by Supramolecular Encapsulation. *Chem. Soc. Rev.* **2016**, *45*, 1720–1737.
- (335) Mal, P.; Breiner, B.; Rissanen, K.; Nitschke, J. R. White Phosphorus Is Air-Stable Within a Self-Assembled Tetrahedral Capsule. *Science* **2009**, *324*, 1697–1699.
- (336) Zhang, D.; Ronson, T. K.; Mosquera, J.; Martinez, A.; Guy, L.; Nitschke, J. R. Anion Binding in Water Drives Structural Adaptation in an Azaphosphatrane-Functionalized $FeII_4L_4$ Tetrahedron. *J. Am. Chem. Soc.* **2017**, *139*, 6574–6577.
- (337) Zhang, D.; Ronson, T. K.; Mosquera, J.; Martinez, A.; Nitschke, J. R. Selective Anion Extraction and Recovery Using a $FeII_4L_4$ Cage. *Angew. Chem., Int. Ed.* **2018**, *57*, 3717–3721.
- (338) Bogie, P. M.; Miller, T. F.; Hooley, R. J. Synthesis and Applications of Endohedrally Functionalized Metal-Ligand Cage Complexes. *Isr. J. Chem.* **2019**, *59*, 130–139.
- (339) Bolliger, J. L.; Belenguer, A. M.; Nitschke, J. R. Enantiopure Water-Soluble Fe_4L_6 Cages: Host-Guest Chemistry and Catalytic Activity. *Angew. Chem., Int. Ed.* **2013**, *52*, 7958–7962.
- (340) Custelcean, R.; Bonnesen, P. V.; Duncan, N. C.; Zhang, X.; Watson, L. A.; Van Berk, G.; Parson, W. B.; Hay, B. P. Urea-Functionalized M_4L_6 Cage Receptors: Anion-Templated Self-Assembly and Selective Guest Exchange in Aqueous Solutions. *J. Am. Chem. Soc.* **2012**, *134*, 8525–8534.
- (341) Yi, S.; Brega, V.; Captain, B.; Kaifer, A. E. Sulfate-Templated Self-Assembly of New M_4L_6 Tetrahedral Metal Organic Cages. *Chem. Commun. (Cambridge, U. K.)* **2012**, *48*, 10295–10297.
- (342) Percastegui, E. G.; Mosquera, J.; Nitschke, J. R. Anion Exchange Renders Hydrophobic Capsules and Cargoes Water-Soluble. *Angew. Chem., Int. Ed.* **2017**, *56*, 9136–9140.
- (343) Hof, F.; Craig, S. L.; Nuckolls, C.; Rebek, J. Molecular Encapsulation. *Angew. Chem., Int. Ed.* **2002**, *41*, 1488–1508.
- (344) Rebek, J. Molecular Behavior in Small Spaces. *Acc. Chem. Res.* **2009**, *42*, 1660–1668.
- (345) Corbellini, F.; Di Costanzo, L.; Crego-Calama, M.; Geremia, S.; Reinhoudt, D. N. Guest Encapsulation in a Water-Soluble Molecular Capsule Based on Ionic Interactions. *J. Am. Chem. Soc.* **2003**, *125*, 9946–9947.
- (346) Corbellini, F.; Knegtel, R. M. A.; Grootenhuis, P. D. J.; Crego-Calama, M.; Reinhoudt, D. N. Water-Soluble Molecular Capsules: Self-Assembly and Binding Properties. *Chem. - Eur. J.* **2005**, *11*, 298–307.
- (347) Gibb, C. L. D.; Gibb, B. C. Straight-Chain Alkanes Template the Assembly of Water-Soluble Nano-Capsules. *Chem. Commun. (Cambridge, U. K.)* **2007**, 1635–1637.
- (348) Liu, S.; Gibb, B. C. High-Definition Self-Assemblies Driven by the Hydrophobic Effect: Synthesis and Properties of a Supramolecular Nanocapsule. *Chem. Commun. (Cambridge, U. K.)* **2008**, 3709–3716.
- (349) Porel, M.; Jayaraj, N.; Raghothama, S.; Ramamurthy, V. Chemistry in Confined Spaces: High-Energy Conformer of a Piperidine Derivative is Favored Within a Water-Soluble Capsuleplex. *Org. Lett.* **2010**, *12*, 4544–4547.
- (350) Wang, K.; Cai, X.; Yao, W.; Tang, D.; Kataria, R.; Ashbaugh, H. S.; Byers, L. D.; Gibb, B. C. Electrostatic Control of Macrocyclization Reactions within Nanospaces. *J. Am. Chem. Soc.* **2019**, *141*, 6740–6747.
- (351) Choudhury, R.; Barman, A.; Prabhakar, R.; Ramamurthy, V. Hydrocarbons Depending on the Chain Length and Head Group Adopt Different Conformations within a Water-Soluble Nanocapsule: 1H NMR and Molecular Dynamics Studies. *J. Phys. Chem. B* **2013**, *117*, 398–407.
- (352) Kulasekharan, R.; Ramamurthy, V. New Water-Soluble Organic Capsules Are Effective in Controlling Excited-State Processes of Guest Molecules. *Org. Lett.* **2011**, *13*, 5092–5095.
- (353) Kaanumalle, L. S.; Gibb, C. L. D.; Gibb, B. C.; Ramamurthy, V. Controlling Photochemistry with Distinct Hydrophobic Nano-environments. *J. Am. Chem. Soc.* **2004**, *126*, 14366–14367.
- (354) Ramamurthy, V. Photochemistry within a Water-Soluble Organic Capsule. *Acc. Chem. Res.* **2015**, *48*, 2904–2917.
- (355) Kaanumalle, L. S.; Ramamurthy, V. Photodimerization of Acenaphthylene within a Nanocapsule: Excited State Lifetime Dependent Dimer Selectivity. *Chem. Commun. (Cambridge, U. K.)* **2007**, 1062–1064.
- (356) Mohan Raj, A.; Raymo, F. M.; Ramamurthy, V. Reversible Disassembly-Assembly of Octa Acid-Guest Capsule in Water Triggered by a Photochromic Process. *Org. Lett.* **2016**, *18*, 1566–1569.
- (357) Rahman, F.-U.; Tzeli, D.; Petsalakis, I. D.; Theodorakopoulos, G.; Ballester, P.; Rebek, J.; Yu, Y. Chalcogen Bonding and Hydrophobic Effects Force Molecules into Small Spaces. *J. Am. Chem. Soc.* **2020**, *142*, 5876–5883.